

**Vanadia Supported on Rice Husk Silica Promoted  
Rare Earth Oxides:-Characterization and Catalytic  
Application in Oxidation Reactions**

Thesis submitted to the  
Cochin University of Science and Technology

By

**Radhika T**

In partial fulfillment of the  
requirements for the award of the degree of

**DOCTOR OF PHILOSOPHY**

**In**

**Chemistry**

Under The Faculty of Science



Department of Applied Chemistry  
Cochin University of Science and Technology  
Cochin-682 022, Kerala, India.

November 2005



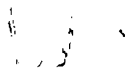
**DEPARTMENT OF APPLIED CHEMISTRY**  
COCHIN UNIVERSITY OF SCIENCE AND TECHNOLOGY  
COCHIN- 682 022, KERALA, INDIA.

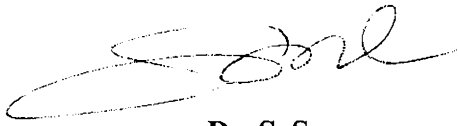
---

23-11-2005

**CERTIFICATE**

This is to certify that the research work presented in the thesis entitled **“Vanadia Supported on Rice Husk Silica Promoted Rare Earth Oxides:- Characterization and Catalytic Application in Oxidation Reactions”** is an authentic record of research work carried out by Ms. Radhika T under our supervision at the Department of Chemistry, Cochin University of Science and Technology, in partial fulfillment of the requirements for the degree of Doctor of Philosophy in Chemistry and that no part thereof has been included for the award of any other degree.

  
**Dr. P.V. Mohanan**  
Lecturer  
(Supervising Guide)


  
**Dr. S. Sugunan**  
Professor  
(Supervising Co-Guide)

## DECLARATION

I hereby declare that the thesis entitled “**Vanadia Supported on Rice Husk Silica Promoted Rare Earth Oxides:-Characterization and Catalytic Application in Oxidation Reactions**” is the bonafide report of the original work carried out by me under the combined supervision of Dr. P.V. Mohanan and Dr. S. Sugunan at the Department of Applied Chemistry, Cochin University of Science and Technology, and no part thereof has been included in any other thesis submitted previously for the award of any degree.

23-11-2005

Cochin-22

  
Radhika T

To

*Grandparents,*

*Parents and Brothers.*

## ACKNOWLEDGEMENT

*As days pass by, life convinces me more and more of the blessings and tender love Lord has showered upon me, strengthening and leading me through hardships and trials.*

*I am extremely grateful to my teacher Dr. S. Sugunan, for the excellent guidance throughout the entire course of this work. I express my earnest gratitude for his valuable advices and motivation ever since my M.Sc days in CUSAT.*

*I am very much thankful to Dr. P.V. Mohanan for all his support and cooperation during the period of this endeavour.*

*Also my gratitude to Dr.M.R. Prathapachandra Kurup, Head, Applied Chemistry, for his timely suggestions and advices, especially on EPR spectral elucidation. I relish the blessings and encouragement of Dr. Nalini and Dr. Mohammed Yusuff throughout my life in CUSAT. I am very much thankful to all teaching and non teaching staff specially Manoj chettan, Radhakrishnan chettan and Usha chechi of Applied Chemistry for all the help and support. The love and concern of Vatsala madam and family was a comfort and always memorable.*

*My heartfelt gratitude to Dr. K.V.R. Chary, IICT, Hyderabad, for his valuable discussions and also for the help with TPR analysis.*

*I thank Dr. Shibu, Prem and others of STIC (CUSAT), Mr. Kashmir (USIC, CUSAT), Mr. Suresh, Service Engineer, Chemito and SAIF, IITB and IISc, Bangalore for helping me with the analyses.*

*I acknowledge computerist Manoj and coworkers for their hardware assistance to play with all the software tricks applied in this thesis.*

*I memorize that this venture would not have materialized without the wholehearted help of my friend, Shylesh who was constantly there with valuable ideas and encouraging words from the beginning to the end.*

*Best friends are hard to find but I was fortunate enough to get someone like Mayagi. No words of gratitude are enough for all the moment of help she and her family had given in making my research life fruitful and memorable. My dear friend Iswarya, to whom I am indebted for being there through every seasons of my life since first day in cusat. A good friend like Sreekanth, who alone can make the world of friendship unique by just being there, a special thanks to him for helping me with literature collection. I am thankful to my friend Indraneel who rendered hours of unceasing help.*

*The fun filled moments shared with Shali and Binitha during day-night research in physical lab will be remembered at all time. I cherish the moments spend with Kochurani, Reshmi, Salini, Suraj, Renu, Reni and Joyes Miss, Rose Miss, George Sir and all friends who were and are in physical chemistry lab, for their goodwill and cooperation during this voyage. Ramu, who made the strenuous moments of research enjoyable with great pleasanry and is memorable for being a*

witty friend. Ajitha miss and family owe a special note of thanks for all their concern and love. I will always appreciate the love and support rendered by Sreejaranichechi, Smithachechi and Sunaja.

My friends Princy, Regi, Daly, Neena, Seema, Rekha, Sajichechi, Chandu, Suni, Mini, Roshini, Bessy, Mangala, Pearl, Santhi, Gleeja, Sini and Sheeba will always be treasured for the nice company they have given to make my cusat days brighter and happier.

The friendship of Kannan, Manoj, Sebastain, Aravind, Arun, John and Thomas are really a pleasure to know. The help and appreciation of a friend like Anoop is forever cherished. Words of thankfulness to all friends and well wishers in the applied chemistry department for their encouraging companionship. The care and support of friends from Physics, Biotech, Photonics and Hindi departments are especially remembered with gladness.

A special thanku gmail for wishes and regards of friends from all over the world. How can I not recall the enchanting/chatting friendship of each and every one of athulya yahoogroups.

Rehu as your dear roommate I enjoyed every moment in Room 30. Thank you for your tolerance. Nishu you are simply superb and hope we will meet again. Dear Ambus your 'anpu' took me into a world where dreams are nurtured. Dear friends Ginju, Smi, Bindu, Asha, Nisha, Beena, Sr. Ritty, Tenu, Manju, Prasi, Sreelu, Jisha, Rinkus, Deepa, Preethi with u I enjoy each and every moment as you make life so vibrant and grassful. Forever I am prayful to Sachidanandan for giving me these fantastic fantabulous friends.

My dears Premi, Sopu, Pravi, Jyots, Priyagi, Lax, Clove, Munch and Manjushachechi, friends like u are hard to find, harder to leave and impossible to forget. So special, with who reasons run short for celebrating life and forever a reason to smile.

Most people walk in and out of life but only dear friends like Rosemol, Suja, Sumi, Ushadevi, Anju, Rema, Juleena, Jisha, Jinsu, Ralph, Smitha, Lakshmi, Benita, Colleen, Jyothi, Neetha, Meethu and Ameer can leave footprints in heart. I am always thankful to them and family for their help, sustain and prayers.

Families of dear friends Surekha, Pankaj, Jaita, Poongodi and Pallavi are really siblings god forgot to give. Every moments of help received from them during my north Indian journeys are unforgettable.

Razia matron and Anu made my life in Athulya hostel for more than seven years a homely one and special thanks to Thressiamma chechi for help in collecting the rice husk. I am obliged to my school, college teachers, relatives and villagers for their best wishes and advices.

I dedicate this for the love, belief, hope, dreams and prayers of my Vallyachayi, Vallyammachi, Achan, Amma, Chekayi and Kunjumon; that could only make what I am today.

Radhika T

## PREFACE

---

Catalysis is primarily a molecular phenomenon, which involves well-defined surface intermediates and/or transition states. The design of better catalysts involves the construction of well-defined active sites, testing of its catalytic performance and assessing a structure-activity relationship. Selective catalytic oxidation especially of hydrocarbons is currently an area of tremendous research and industrial importance. For the protection of our Nature, the design and development of greener processes such as heterogeneous catalytic oxidation has become the motto of current catalytic research.

Vanadia based catalysts are used for the oxidation of alkanes at the industrial level. Supported vanadia catalysts behave superior in selective oxidation reactions. Rare earth oxide ceria is best known for its oxygen storage capacity. Few literature precedences of catalysis regarding rare earth praseodymia exist. The salient features of this work include utilization of high surface area amorphous rice husk silica to modify the surface and chemical properties of oxide supports such as ceria and praseodymia, which in turn produce highly active and selective supported vanadia catalysts. Oxidation of various aromatics was chosen to test the activity of the catalysts.

The thesis is an aggregate of 9 chapters, the first two deals with introduction to catalysis and catalytic oxidation respectively. The experimental techniques applied for the characterization of catalysts encompass Chapter 3. In chapter 4 the structural nature of catalysts is discussed with the information obtained from various techniques. Chapters 5 to 8 account and correlate the structural characteristics and oxidation activity of prepared catalysts. The last chapter comprehends the summary and conclusion of the results observed in the previous chapters. The present study envisages that these catalysts are better suitable for oxidation of aromatics and it is a stepping stone towards the usage of rice husk silica in sharpening the activity of various metal oxides in heterogeneous catalysis.

## CONTENTS

---

	Page No.
<b>CHAPTER 1 General Introduction</b>	
Abstract	1
1.1 The phenomenon catalysis	2
1.2 Supported catalysts	4
1.3 Promoters	6
1.4 Methods of preparation	7
1.5 Rare earth oxides as catalyst	11
1.6 Supported vanadium oxide as catalyst	14
1.7 Rice husk silica-composition, properties and applications	20
1.8 Scope and outline of the Thesis	23
References	25
<b>CHAPTER 2 Heterogeneous Catalytic Oxidation</b>	
Abstract	33
2.1 Catalytic oxidation	34
2.2 Kinetics of oxidation reactions	36
2.3 Selective oxidation of hydrocarbons	38
2.4 Redox behaviour of ceria, praseodymia and vanadia	41
2.5 Vanadia in oxidation catalysis	44
2.6 Leaching of catalysts	47
References	49
<b>CHAPTER 3 Materials and Methods</b>	
Abstract	54
3.1 Introduction	55
3.2 Chemicals for catalyst preparation	56
3.3 Catalyst preparation	56
3.4 Catalysts prepared	58
3.5 Characterization techniques	59
3.6 Surface and physico-chemical analysis	60
3.6.1 Energy dispersive X-ray analysis	60



3.6.2	Powder X-ray diffraction	61
3.6.3	BET surface area and pore volume	62
3.6.4	Thermal analysis	63
3.6.5	Scanning electron microscopy	64
3.7	Spectroscopic methods	65
3.7.1	UV-vis diffused reflectance spectroscopy	65
3.7.2	FT-Infrared spectroscopy	65
3.7.3	FT-Raman spectroscopy	66
3.7.4	Electron paramagnetic resonance spectroscopy	67
3.7.5	Nuclear magnetic resonance spectroscopy ( $^{29}\text{Si}$ and $^{51}\text{V}$ MAS NMR)	68
3.8	Reduction and acidity determination	71
3.8.1	Temperature programmed reduction	71
3.8.2	Temperature programmed desorption - $\text{NH}_3$	72
3.8.3	Cyclohexanol decomposition	73
3.9	Catalytic oxidation of aromatics	74
3.9.1	Liquid-phase oxidation of benzene, ethylbenzene and naphthalene	75
3.9.2	Oxidative dehydrogenation of ethylbenzene	75
	References	77
<b>CHAPTER 4 Surface Analysis and Chemical Characterization</b>		
	Abstract	79
4.1	Surface characterization	81
4.1.1	Energy dispersive X-ray analysis	82
4.1.2	Powder X-ray diffraction	86
4.1.3	BET surface area measurements	98
4.1.4	Thermal analysis	102
4.1.5	UV-vis diffused reflectance spectroscopy	111
4.1.6	FT-Infrared spectroscopy	116
4.1.7	FT-Raman spectroscopy	120
4.1.8	Electron paramagnetic resonance spectroscopy	126
4.1.9	$^{29}\text{Si}$ MAS NMR spectroscopy	139
4.1.10	$^{51}\text{V}$ MAS NMR spectroscopy	142

4.1.11	Scanning electron microscopy	150
4.1.12	Temperature programmed reduction	158
4.2	Acidity Measurements	166
4.2.1	Temperature programmed desorption-NH <sub>3</sub>	166
4.2.2	Cyclohexanol decomposition	170
4.2.2.1	Influence of reaction conditions	172
4.2.2.2	Cyclohexanol decomposition over catalysts	174
4.2.2.3	Cyclohexanol decomposition and acidity by TPD-NH <sub>3</sub>	177
4.3	Discussion	181
4.4	Conclusion	182
	References	186
<b>CHAPTER 5 Oxidation of Benzene</b>		
	Abstract	197
5.1	Introduction	198
5.2	Influence of reaction condition	202
5.2.1	Effect of Temperature	203
5.2.2	Effect of Solvent	204
5.2.3	Effect of Catalyst weight	205
5.2.4	Effect of Acetonitrile volume	206
5.2.5	Effect of Benzene volume	208
5.2.6	Effect of H <sub>2</sub> O <sub>2</sub> volume	208
5.2.7	Effect of Time	210
5.3	Benzene oxidation over prepared catalysts	211
5.4	Effect of Leaching	214
5.5	Regeneration and stability	216
5.6	Discussion	218
5.7	Conclusion	224
	References	225
<b>CHAPTER 6 Oxidation of Ethylbenzene</b>		
	Abstract	229
6.1	Introduction	230

6.2	Influence of Reaction condition	232
6.2.1	Effect of Temperature	232
6.2.2	Effect of Solvent	233
6.2.3	Effect of Catalyst weight	234
6.2.4	Effect of Acetonitrile volume	235
6.2.5	Effect of Ethylbenzene volume	236
6.2.6	Effect of H <sub>2</sub> O <sub>2</sub> volume	237
6.2.7	Effect of Time	237
6.3	Ethylbenzene oxidation over prepared catalysts	238
6.4	Effect of Leaching	242
6.5	Regeneration and stability	244
6.6	Discussion	245
6.7	Conclusion	249
	References	250

## **CHAPTER 7 Oxidation of Naphthalene**

	Abstract	252
7.1	Introduction	253
7.2	Influence of reaction condition	255
7.2.1	Effect of Temperature	255
7.2.2	Effect of Solvent	256
7.2.3	Effect of Catalyst weight	258
7.2.4	Effect of Acetonitrile volume	259
7.2.5	Effect of Naphthalene volume	260
7.2.6	Effect of H <sub>2</sub> O <sub>2</sub> volume	260
7.2.7	Effect of Time	261
7.3	Naphthalene oxidation over prepared catalysts	262
7.4	Effect of Leaching	266
7.5	Regeneration and stability	267
7.6	Discussion	267
7.7	Conclusion	270
	References	271

<b>CHAPTER 8</b>	<b>Oxidative Dehydrogenation of Ethylbenzene</b>	
	Abstract	273
8.1	Introduction	274
8.2	Influence of reaction condition	277
8.2.1	Effect of Temperature	277
8.2.2	Effect of Air flow	278
8.2.3	Effect of Feed flow rate	279
8.2.4	Effect of Time	280
8.3	Oxidative dehydrogenation over catalysts	281
8.4	Regeneration and stability	285
8.5	Discussion	286
8.6	Conclusion	292
	References	293
<b>CHAPTER 9</b>	<b>Summary and Conclusions</b>	
	Abstract	296
9.1	Summary	297
9.2	Conclusion	300
	Future Outlook	302
	List of publications	

# CHAPTER 1

## GENERAL INTRODUCTION

### Abstract

---

*Catalysis is a multidisciplinary area of chemistry, in particular, industrial chemistry and the catalyst is often, if not always, the heart of a chemical process. Catalysts have been used in the chemical industry for hundreds of years, and many large scale industrial processes can be carried out only with the aid of catalysis. Catalytic reactions often reduce energy requirements and decrease separations due to increased selectivity; they may permit the use of renewable feedstocks or minimize the quantities of reagents needed. Catalysis often permits the use of less toxic reagents, as in the case of oxidations using hydrogen peroxide in place of heavy metal catalysts. Heterogeneous catalysis is one of the most important processes in the petroleum and the chemical industries. The inherent advantages of heterogeneous catalysis, which affords interesting opportunities for environmentally benign production of fine chemicals and pharmaceuticals, as well as the ever-increasing demand for some of these products has been the driving force for the change to environmentally benign processes and technologies in chemical industry.*

---

## 1.1 THE PHENOMENON CATALYSIS

The term “catalysis” was introduced as early as 1836 by Berzelius in order to explain various decomposition and transformation reactions<sup>1</sup>. A definition that is still valid today is due to Ostwald (1895): “a catalyst accelerates a chemical reaction without affecting the position of the equilibrium”. Catalysis is the key to chemical transformations. Most industrial syntheses and nearly all biological reactions require catalysts. Numeric organic intermediate products required for the production of plastics, synthetic fibers, pharmaceuticals, dyes, crop-protection agents, resins and pigments can be produced only by catalytic processes. Most of the processes involved in crude oil processing and petrochemistry, such as purification stages, refining and chemical transformations require catalysts. Furthermore, catalysis is the most important technology in environmental protection, i.e., the prevention of emissions. A well-known example is the catalytic converter for automobiles. In theory, an ideal catalyst would not be consumed, but this is not the case in practice. While it was formerly assumed that the catalysts remained unchanged in the course of the reaction, it is known that the catalyst is involved in chemical bonding with the reactants during the catalytic process. Owing to competing reactions, the catalyst undergoes chemical changes, and its activity becomes lower. Thus catalysts must be regenerated or eventually replaced. Apart from accelerating reactions, they can influence the selectivity of chemical reactions. This means that completely different products can be obtained from a given starting material by using different catalyst systems. Industrially, this targeted reaction control is often even more important than the catalytic activity. Millions and millions of chemicals are produced all over

the world by catalytic reactions and various reactions require various catalysts. Thus catalyst design is a crucial aspect of chemistry and catalysts constitute an important class of materials. Catalysts have been successfully used in the chemical industry for more than 100 years, example being the synthesis of sulfuric acid, the conversion of ammonia to nitric acid, and catalytic hydrogenation. Later developments include new highly selective multicomponent oxide and metallic catalysts, zeolites, and the introduction of homogeneous transition metal complexes in the chemical industry<sup>2,3</sup>.

Catalysts can be gases, liquids, or solids. Most industrial catalysts are liquids or solids, where the latter react only via their surface. The importance of catalysis in the chemical industry is shown by the fact that 90 % of all chemicals are produced with the aid of catalysts; in newly developed processes. The numerous catalysts known today can be classified according to various criteria: structure, composition, area of application, or state of aggregation. According to the state of aggregation in which they act, there are two large groups: heterogeneous catalysts (solid-state catalysts) and homogeneous catalysts attached to solids (supported catalysts), also known as immobilized catalysts. By far the most important catalysts are the heterogeneous catalysts. Heterogeneous catalysis takes place between several phases. Generally the catalyst is a solid, and the reactants are gases or liquids. Heterogeneously catalyzed reactions are composed of purely chemical and purely physical reaction steps. For the catalytic process to take place, the starting materials must be transported to the catalyst. Thus apart from the actual chemical reaction, diffusion, adsorption, and desorption processes are of importance for the progress of the overall reaction. In heterogeneous catalysis

chemisorption of the reactants and products on the catalysts surface is of central importance, so that the actual chemical reaction cannot be considered independently. If a molecule is to enter a reactive state, it must undergo activated adsorption on the catalyst surface. Hence the catalyst must chemisorb at least one of the reactants. The strength of adsorption of the molecules is decisive for effective catalysis: neither too strong nor too weak binding of the reactants can induce the required reactivity; a certain medium binding strength is optimum. The active centers on the catalyst surface are probably the result of free valences or electron defects, which weaken the bonds in the adsorbed molecules to such an extent that a reaction can readily occur.

### **1.1 SUPPORTED CATALYSTS**

Metal oxides of one type supported by a metal oxide of another type in which the supported oxide is believed to be present in submonolayer to monolayer quantities comprise the largest group of heterogeneous catalysts and are of major economic importance, especially in refinery technology and the chemical industry. In supported catalysts small amounts of catalytically active materials, especially metals, are applied to the surface of porous, mostly inert solids-the so called supports. The main purpose of using a support is to achieve an optimal dispersion of the catalytically active components and to stabilize it against sintering. However, in a number of reactions, the support is not inert and the overall process is actually a combination of two catalytic functions: that of the active components and that of the support<sup>4</sup>. Traditionally a catalyst support is viewed as an inert material that not only provides a surface for the metal/metal oxide dispersion but also enhances thermal stability, thus



rendering it continuously useful even at elevated temperatures. However, the physical and chemical properties of the support have now been recognized as major contributors to resultant catalytic activity. While the physical properties of the support have been related to metal dispersion, the chemical properties were associated with both metal dispersion and electronic effects<sup>5</sup>. The supports can have forms such as pellets, rings, extrudates, and granules. Typical supports are porous solids such as  $\text{Al}_2\text{O}_3$ ,  $\text{SiO}_2$ ,  $\text{MgO}$ ,  $\text{TiO}_2$ ,  $\text{ZrO}_2$ , aluminosilicates, zeolites, activated carbon and ceramics<sup>6-8</sup>.

The main factors influencing these properties are the choice of the most suitable support material and the arrangement of the metal atoms in the pore structure of the support. The main function of the support is to increase the surface area of the active component. Generally catalytic activity increases with the increasing catalysts surface area, but a linear relationship cannot be expected since the reaction rate is often strongly dependent on the structure of the catalyst surface. The choice of the appropriate support for a particular active component is important because in many reactions the support can significantly influence the reaction rate and the course of the reaction. The nature of the reaction system largely determines the type of catalyst support. The pore structure of the support can also have an influence on the role of the active component, since the course of the reaction is often strongly dependent on the rate of diffusion of the reactants. In supported catalysts, the support does not only ensure high dispersion of the metal; there are also interactions between metal and support due to various physical and chemical effects such as electron transfer up to formation of chemical bonds, adhesive forces (van

der Waals forces) formation of reduced support species on the metal surface and formation of new phases at the boundary surface.

## 1.2 PROMOTERS

Promoters are substances that are themselves not catalytically active but increase the activity of catalysts<sup>1</sup>. The function of these, which are added to catalysts in amounts of a few percent, has not been fully elucidated. There are four types of promoters:

- **Structure promoters:** increase the selectivity by influencing the catalysts surface such that the number of possible reactions for the adsorbed molecules decreases and a favoured reaction path dominates.
- **Electronic promoters:** become dispersed in the active phase and influence its electronic character and therefore the chemical binding of the adsorbate.
- **Textural promoters:** inhibit the growth of catalyst particles to form larger, less active structures during the reaction. Thus prevent loss of active surface by sintering and increase the thermal stability of catalyst.
- **Catalyst-poison-resistant promoters:** protect the active phase against poisoning by impurities, either present in the starting materials or formed in side reactions.

A catalyst may contain one active component and one or more promoters. Since the above four effects tend to overlap in practice, it is sometimes difficult to precisely define the function of a promoter. Promoters are the subject of great interest in catalyst research due to their remarkable influence on the activity, selectivity, and stability of industrial catalysts.

Promoters can act in various ways. By means of the ensemble effect the promoters block active sites and thus suppress the dissociation of undesired products. Promoters can also influence catalytically active phases by stabilizing surface atoms in certain valence states. Besides these, the promoter can also form direct chemical bonds with the adsorbate. Promoters are also developed to strengthen the support or the active component. An important function is influencing the stability of support materials. These are often used to suppress undesired activity of support materials, such as coke formation.

### **1.3 METHODS OF PREPARATION**

The correct sampling, sample preparation, choice of the support and appropriate method are important in heterogeneous catalysis and are one of the major challenges in today's research<sup>9</sup>. According to Ardson, "catalyst preparation is the secret to achieving the desired activity, selectivity and life time"<sup>10</sup>. In recent years, major advances have been made on techniques for physically and chemically characterizing supported catalyst and on the quantitative and qualitative aspects of catalyst preparation, so that the design of supported catalysts has become a feasible activity<sup>11-15</sup>. The preparation methods of catalysts have been reported to directly affect the activity of the mixed oxide systems<sup>16-18</sup>. Some of the methods are discussed below.

#### **1. Precipitation and co-precipitation**

For support materials precipitation is the most frequently applied method of preparation. The main advantage of this method is the possibility of creating very pure materials and the flexibility of the process with respect to final product quality. It is generally desirable to precipitate the desired material

in such a form that the counter ions of the precursor salts and the precipitation agent, which can be occluded in the precipitate during the precipitation, can easily be removed by a calcination step. Favourable ions for precipitation are nitrates, carbonates, or ammonium, which decompose to volatile products during calcination. There are several ways to carry out the precipitation process. The simplest is the batch operation where the solution from which the salt is to be precipitated is usually present in the precipitating vessel and the precipitating agent is added.

Catalysts based on more than one component can be prepared by co-precipitation<sup>19</sup>. Co-precipitation is the simultaneous precipitation of a normally soluble component with a macrocomponent from the same solution by formation of mixed crystals, by adsorption, occlusion or mechanical entrapment. In other words, this method involves mixing aqueous solutions of precursors and precipitates the material at particular temperature and pH. Co-precipitation is very suitable for the generation of a homogeneous distribution of catalyst components or for the creation of precursors with a definite stoichiometry, which can be easily converted to the active catalyst. A good dispersion of catalyst components is difficult to achieve by other means of preparation, and thus co-precipitation will remain an important technique in the manufacture of heterogeneous catalysts in spite of its disadvantages like higher technological demands and the difficulties in following the quality of the precipitated product.

## **2. Impregnation**

One of the most frequently used methods to achieve deposition of the active component precursor over high surface area support is impregnation. This technique consists of introducing, into the pore space of a support, a solution of an inert precursor, i.e. one that does not interact with the solid surface. In principle, the precursor thus remains in the dissolved state in the solution and does not become fixed on the surface at this stage of preparation. Generally two cases can be distinguished, depending on whether the pore space of the support contains only ambient air at the start or whether it is already filled by the solvent from the impregnation solution or by another liquid. In the latter case, the second phase is generally an immersion phase that consists of plunging the solvent-saturated support into the impregnation solution. The precursor salt migrates progressively from the solution into the heart of the grains of the support. This is convenient to disperse a small amount of well-fine particles on the support. Incipient wetness impregnation is used for precious control of the amount of the deposition.

## **3. Deposition-precipitation**

This method is usually employed for the preparation of supported catalysts. To provide solid catalysts with the desired thermal stability, or highly porous, thermo stable material called support is dispersed into it. In this method we apply an active precursor onto a separately produced support with a solution of an active precursor and subsequent drying and calcination of the loaded support. One of the main advantages of this method is that we are able to apply the active component(s) uniformly and densely over the surface of the

support as particles of controlled size. This technique is highly promising for the preparation of synthetic clay materials.

In this method, hydroxide of the active components and support are co-precipitated together onto the support after drying and calcination the active components are surrounded by a thin layer of freshly formed support depositing on the original support surface. This method allows the preparation of catalyst with smaller particle sizes in better dispersion with large surface area and allows incorporation of higher loading of the active components<sup>20</sup>.

#### **4. Sol-gel process**

The preparation of supports and heterogeneous catalysts by sol-gel processing has attracted increasing interest in recent years. The sol-gel process involves first the formation of a sol followed by that of a gel. A sol, which is a liquid suspension of solid particles ranging in size from 1nm to 1 micron, can be obtained by the hydrolysis and partial condensation of molecular precursors, such as an inorganic salt or a metal alkoxide. The hydroxylation is achieved either by varying the pH or by hydrolyzing alkoxide precursors in an organic solvent. Further condensation of sol particles into a three-dimensional network produces a gel, which is a diphasic material with a solid encapsulating a solvent. The encapsulated liquid can be removed from a gel by either evaporative drying with supercritical extraction and the resulting solid products are known as a xerogel and an aerogel respectively. The most important characteristic of the sol-gel preparation is its ease of control giving the advantages such as high purity, homogeneity at a molecular level, different physical forms and the ability to change physical characteristics<sup>22-24</sup>.

## **4. Chemical vapour deposition**

In the heterogeneous catalysts preparation, gas phase techniques have also been gained interest in the recent years as a route of developing new catalysts<sup>25</sup>. In chemical vapour deposition (CVD), deposition is taking place by adsorption or reaction from the gas phase<sup>26,27</sup>. It is a very versatile process for the production of catalytic materials and is possible to deposit target species on the materials with almost any shape and size and it is also possible to produce almost any metal and nonmetallic material as well as compounds such as oxides, carbides, nitrides, intermetallics and many others<sup>28,29</sup>.

### **1.4 RARE EARTH OXIDES AS CATALYST**

During the last few years, much endeavour has been undertaken in order to understand the phenomenon that underlies the catalytic behaviour of multicomponent and multiphase oxide-based heterogeneous catalysts. Most have been especially interested in the systems containing lanthanide oxides, such as  $\text{La}_2\text{O}_3$ ,  $\text{Pr}_6\text{O}_{11}$ ,  $\text{CeO}_2$ ,  $\text{Tb}_4\text{O}_7$ ,  $\text{Nd}_2\text{O}_3$  and  $\text{Sm}_2\text{O}_3$ , because pertinent information on the real role played by these in partial as well as total oxidation is still rather scarce<sup>30-37</sup>.

Among the rare earth metal oxides that have been widely investigated in ceramics and industrial catalysis, cerium oxide ( $\text{CeO}_2$ ) certainly stands apart.  $\text{CeO}_2$ -based materials have been receiving tremendous attention recently because of their diverse uses in catalysis and materials science<sup>38</sup>. In a recent review, Trovarelli<sup>39</sup> summarized the catalytic properties and characterization studies reported for ceria in the last decades. Ceria is one of the most important components of fluid catalytic cracking (FCC) catalysts and three-way catalysts

(TWC)<sup>40,41</sup>. All desirable properties like high refractive index, good transmission in the visible and infrared regions, strong adhesion, and high stability against mechanical abrasion, chemical attack and high temperatures have rendered ceria as optical coatings, supports of metals for catalytic oxidation reactions, stable capacitors in silicon-on-insulator structures and as a buffer layer for high-temperature superconductor thin films. Other significant applications of cerium containing catalysts include removal of soot from diesel engine exhaust, removal of organics from wastewaters, as an additive for combustion catalysts, and in fuel cell processes<sup>42-45</sup>. The redox chemistry of ceria is a critical parameter in the efficiency of multifunctional components of three-way automotive catalysts. The main function of ceria is to promote oxygen buffering capacity during excursion of the air/fuel ratio into a rich or lean regime. This comes from the ability of CeO<sub>2</sub> to be easily reduced giving an extended range of possible stoichiometries CeO<sub>2-x</sub> with 0<x<0.5. The applications of these materials in various other catalytic processes such as oxygen permeation membrane systems, deNO<sub>x</sub> catalysis, exhaust combustion catalysts; oxidation of aromatics and catalytic wet oxidation are being extensively studied<sup>46-48</sup>. CeO<sub>2</sub> is frequently incorporated to the formulation of oxidation catalysts because it shows a considerable performance for the catalytic combustion of hydrocarbons and CO<sup>49</sup>. Pure CeO<sub>2</sub> alone is poorly thermostable. The redox and catalytic properties of CeO<sub>2</sub> are profoundly enhanced when used in combination with other transition metals or rare earth oxides<sup>50-54</sup>. Recent studies have suggested that formation of mixed oxides of CeO<sub>2</sub> with cations such as Zr<sup>4+</sup>, Al<sup>3+</sup>, and La<sup>3+</sup> enhance the catalytic, textural, redox, and oxygen storage properties of ceria and the so- formed mixed oxides



also exhibits good thermal stability<sup>55-58</sup>. Ceria deposited on  $\text{Al}_2\text{O}_3$  forms the basis of abatement of emissions and used also in hydrogen generation by steam methane reforming and  $\text{CO}_2$  reforming of methane<sup>59</sup>.  $\text{SiO}_2$  appears to be an ideal substrate for the growth of ceria and is also an effective surface area stabilizing agent for ceria<sup>60,61</sup>. Ceria supported gold catalysts increased the interest during last 15 years due to high temperature activity of these in CO oxidation at low temperature. In these, the ions  $\text{Au}^+$  or  $\text{Au}^{3+}$  would fill the vacant  $\text{Ce}^{4+}$  sites with consequent formation of oxygen vacancies and increased oxygen mobility and reducibility<sup>62,63</sup>. It is its oxygen storage capacity that gives ceria-based catalysts the unique ability to oxidize unburnt hydrocarbons or reduce nitrous oxides under fuel rich and lean conditions<sup>64</sup>.

There are other reducible oxides, which are not used, but would seem to have similar properties to that of ceria. Praseodymium is one of the possible “new” additives, which today attracts increasing attention<sup>65-69</sup>. Praseodymium is next to cerium in the periodic table and also has multiple stable oxidation states, yet praseodymia does not appear to be an effective replacement for ceria as an oxygen-storage component<sup>70,71</sup>. One major reason for this has to do with drastic difference in the reactivity of ceria and praseodymia. Praseodymia, due to its relatively low stability, can react with alumina at temperatures above  $600^\circ\text{C}$  in air and forms inert aluminates, whereas ceria remains stable to at least  $1100^\circ\text{C}$ <sup>72</sup>. Bunluesin et al.<sup>73</sup> did not find a zeroth order CO oxidation mechanism under reducing conditions on praseodymia-supported Pd and suggested that oxygen from praseodymia is not utilized under reaction conditions in the same way as that from ceria. In the behaviour of five lanthanide oxides as pure phases and mixed with other oxides, with respect to

the selective oxidation of isobutene to methacrolein only  $\text{CeO}_2$  and  $\text{Pr}_6\text{O}_{11}$  were found to give rise to pronounced co-operation effects when mixed with  $\text{MoO}_3$ <sup>74</sup>. The behaviour of  $\text{CeO}_2$  could be interpreted as co-operation effects occurred without apparent formation of new phases during the catalytic tests since ceria is a potential donor phase of spillover oxygen<sup>75</sup>. In the case of praseodymium oxide, the interpretation of the experimental data was much less straightforward. Smet et al.<sup>76</sup> concluded that the co-operative effects observed in the  $\text{MoO}_3$ - $\text{Pr}_6\text{O}_{11}$  mixtures cannot be attributed to the intrinsic catalytic properties of praseodymium molybdates and it does not seem that the observed synergic effects could be assigned to the simultaneous presence of ternary  $\text{Pr}_x\text{Mo}_y\text{O}_z$  phases and  $\text{Pr}_6\text{O}_{11}$ .  $\text{Pr}_6\text{O}_{11}$  changes to a composition with less oxygen at temperatures higher than 480°C. In benzylation of toluene, low weight percentage sulfate modified hexagonal phase praseodymia gave high conversion<sup>77</sup>. It is known that rare-earth oxides easily react with Si to form silicate like Si-O-metal configurations. Existence of two Pr-oxides,  $\text{Pr}_6\text{O}_{11}$  and  $\text{Pr}_2\text{O}_3$  was encountered during the deposition of thin  $\text{Pr}_x\text{O}_y$  films on  $\text{Si}(100)$ <sup>78</sup>. In the formation of  $\text{C}_2$  hydrocarbons from  $\text{CH}_4$  and  $\text{CO}_2$ , praseodymium oxide show high  $\text{C}_2$  yield and selectivity owing to a redox mechanism of unstable lattice oxygen atoms in Pr-oxides<sup>79</sup>.

### 1.5 SUPPORTED VANADIUM OXIDE AS CATALYST

Among group V elements, vanadium is one of the most important elements, widely used in solid-state chemistry, material science, catalysis and engineering<sup>80-83</sup>. Generally bulk vanadia cannot be used as a catalyst because of its poor thermal stability and mechanical strength. Therefore, vanadia is

normally supported on different carriers depending on the type of the reaction to be catalyzed<sup>84</sup>. Vanadium pentoxide and related phases have been used and studied in catalysis either as the neat oxides or deposited on inert and semiconducting oxide supports, such as SiO<sub>2</sub> and TiO<sub>2</sub><sup>85,86</sup>. The surface properties of a support are very important to the catalytic activity, because they affect the formation of the interfacial active sites. Supported vanadium oxide catalysts have been extensively used for catalyzing several oxidation reactions, e.g., the oxidation of methanol to formaldehyde and the oxidative dehydrogenation of light alkanes, partial oxidation of organic compounds and selective oxidation with rupture of the C-C bond<sup>87</sup>. Vanadium oxide catalysts have also been studied in dehydrogenation and oxidative dehydrogenation of alkanes, in selective catalytic reduction of nitrogen oxides by ammonia and synthesis of formaldehyde or phthalic anhydride. It has been demonstrated that the selectivity and activity of these catalysts depend on, among other factors, the vanadium loading, the method used to support vanadium species on a suitable support, calcination temperature, type of support and its surface acidity<sup>88-90</sup>.

The molecular structure of the vanadium oxide species on several supports have been examined with several techniques, such as Raman, <sup>51</sup>V NMR, UV-vis-NIR, DRS, TPR, NMR, HRTEM XPS and EXAFS<sup>91-93</sup>. The molecular structure of the supported vanadium oxide species was found to depend on several parameters, e.g., metal oxide loading, support oxide material, and degree of hydration. A number of vanadium species have been postulated on support surfaces, including, mono- and multilayer vanadium oxides islands, small vanadium oxide clusters, and isolated vanadate<sup>94,95</sup>. With increasing

loading, the vanadium oxide structure changes gradually from monomer to polymer and finally to crystalline  $V_2O_5$ . For low vanadium contents, vanadium oxide is molecularly dispersed on the surface of the carriers and its structure is quite unlike corresponding to the bulk oxide<sup>96,97</sup>. The catalytic properties of the active vanadia phase can be greatly influenced by the nature of supported oxide and the dispersion of active component<sup>98</sup>. Vanadium oxide remains as a highly dispersed amorphous monolayer phase containing isolated vanadium oxide species on the support surface at low vanadia loadings. However, at high loadings, the crystalline vanadia phase also co-exists with the monolayer phase.

The most widely used support in these catalysts is the low-temperature modification of  $TiO_2$ , anatase<sup>99</sup>. The optimal catalytic activity and selectivity are achieved when a one monolayer of vanadia is dispersed on anatase phase of  $TiO_2$ . However, due to the relatively low specific surface area and low thermal stability of  $TiO_2$ , other oxides have attracted attention as alternative supports<sup>100</sup>. Vanadium oxide supported on  $SiO_2$ ,  $TiO_2$ ,  $CeO_2$ , or  $ZrO_2$  is found to be an active catalyst for a variety of reactions including selective oxidations, such as methanol to formaldehyde, *o*-xylene to phthalicanhydride, the selective catalytic reduction of  $NO_x$  with ammonia and ammoxidation reactions<sup>101-113</sup>. Molybdenum is frequently added as a promoter in vanadia catalysts to impart strong acidity for selective oxidation reactions<sup>114,115</sup>. Hutchings et al.<sup>116-119</sup> have extensively studied vanadium phosphate catalysts for the synthesis of malicanhydride by the partial oxidation of *n*-butane. Recently much interest is focused on the synthesis and application of vanadium containing zeolites,

novel vanadium silicate molecular sieves and mesoporous materials for liquid-phase oxidation reactions of aromatics<sup>120-129</sup>.

Depending on the specific oxide support vanadia catalysts may show different catalytic activity and selectivity. The surface structure and dispersion of the active phase together with its redox and acid-base properties are influenced by the vanadium oxide support interaction. The interaction of  $\text{VO}_x$  species with the supporting material affects the dispersion of these species on the surface. In general, basic metal oxide supports, such as  $\text{MgO}$ , strongly interact with  $\text{VO}_x$ , resulting in the formation of a mixed metal oxide rather than a stable surface vanadia over layer<sup>130</sup>. Supports like  $\text{Al}_2\text{O}_3$ ,  $\text{ZrO}_2$ , and  $\text{TiO}_2$  allow good dispersion of surface vanadium oxide species<sup>131</sup>. Poorly dispersed  $\text{V}_2\text{O}_5$  crystals on  $\text{SiO}_2$ , due to the weak interaction with the acidic  $\text{V}_2\text{O}_5$  even at low surface coverage have been reported. The acid-base character of the support modifies the acid-base properties of the support-vanadia overlayer interface and therefore determines the distribution of the surface species, the metal-oxygen bond strength, and the mean distance between the vanadium active centers which are factors that appear to be of key importance for the catalytic performance. A distinguishing characteristic of these catalysts is that the active form of the vanadia consists of monolayer or submonolayer deposits on the support<sup>132-135</sup>. Three kinds of bonds observed between vanadium and oxygen in these are;  $\text{V}=\text{O}$ ,  $\text{V}-\text{O}-\text{V}$ , and  $\text{V}-\text{O}-\text{S}$  (S, support). It is generally accepted that the bridging  $\text{V}-\text{O}-\text{S}$  bond is critical for redox reactions catalyzed by supported  $\text{VO}_x$ <sup>136</sup>. Reports of Ferreira et al.<sup>137</sup> concluded that the nature of  $\text{VO}_x$  species depends on the composition of the support. At low vanadia loading,  $\text{SiO}_2$  surface is covered with V-monomers; for the case of  $\gamma\text{-Al}_2\text{O}_3$

and  $\text{TiO}_2$ , dimeric V-structures are predominant. The composition of the support also influences the  $\text{VO}_x$ -support interaction, since the strength of V-O<sub>s</sub> bond is altered by the nature of a given support. In general, supported vanadium oxide contains isolated monomeric species, polymeric species, and bulk  $\text{V}_2\text{O}_5$  in amorphous and crystalline states. In bulk  $\text{V}_2\text{O}_5$ , vanadium is octacoordinated (Figure 1.1), while in the monomeric and polymeric species, known as “monolayer vanadia,” vanadium is tetracoordinated<sup>138</sup>. In contrast to the monolayer phase, bulk vanadia has low activity for selective oxidation reactions<sup>139</sup>.

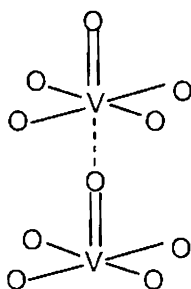


Figure 1.1

Under hydrous conditions, the  $\text{VO}_x$  species may be formulated as structures (b) or (c) in Figure 1.2. On heating in a dry atmosphere, dehydration take place to structure (a) and/or to an octahedral polyvanadate species, such as structure (d). In a review Wachs et al.<sup>140</sup> stated that dehydrated surface vanadia species on  $\text{Al}_2\text{O}_3$ ,  $\text{TiO}_2$ ,  $\text{ZrO}_2$ ,  $\text{Nb}_2\text{O}_5$ <sup>141</sup>, and  $\text{CeO}_2$  all possess identical molecular structures. On these supports isolated  $\text{VO}_4$  units would be mainly present. From  $^{18}\text{O}$  isotopic labeling experiments they have concluded that surface vanadia species possess only one terminal  $\text{V}=\text{O}$  bond. The molecular structures of these vanadia species consist of a terminal  $\text{V}=\text{O}$  bond and three

bridging V-O-support bonds for the isolated species by structure (e) in Figure 1.1. Polymerized species is also encountered, which consists of a terminal V=O bond with one bridging V-O-support bond and two bridging V-O-V bonds shown as (d).

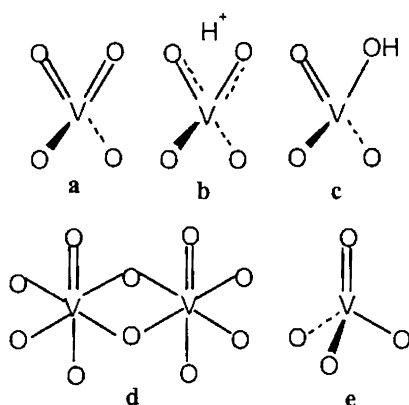


Figure 1.2

Reports reveal that  $V_2O_5$ - $CeO_2$  combination catalysts have been the subjects of numerous investigations in recent years because of its wide range of applications in catalysis and material science<sup>142-145</sup>. According to Wachs et al.<sup>146</sup> the surface vanadia structure and density of active vanadia surface sites is the same on all supports viz.  $CeO_2$ ,  $ZrO_2$ ,  $TiO_2$  and  $Al_2O_3$  studied at monolayer coverage. Structure of surface vanadia species over a support can be represented schematically as shown in Figure 1.3.

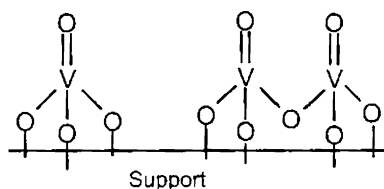


Figure 1.3

## 1.7 RICE HUSK SILICA-COMPOSITION, PROPERTIES AND APPLICATIONS

Rice husk is one of the by products of rice, a major food material of most of the developing countries including India. Rice husk, natural sheaths that form on rice grains during their growth are the predominant byproduct in the milling process of domestic agriculture is usually burned or discarded, resulting not only in resource wasting, but also in environmental pollution<sup>147</sup>. Rice husk contains organic matter such as sugars, lignin, cellulose, protein etc., and inorganic constituents as silica (20-25 %), and cellulose, which yields carbon when thermally decomposed under inert atmosphere<sup>148</sup>. Fundamental organic element analysis reveals that the average organic composition of rice husk was 38.01 wt % carbon, 5.28 wt % hydrogen, 36.10 wt % oxygen, and 1.94 wt % nitrogen. However, the reported compositions of rice husk differ widely, as affected by the type of paddy and climate.

The presence of silica in rice husk has been known since 1938<sup>149</sup>. The silica is in hydrated amorphous form, either opal or silica gel. Rice husk on burning gives ash containing 90 % silica, which is highly reactive due to its ultra fine size and high surface area<sup>150-152</sup>. Silica in these cases is at a nanoscale and scientists in India and abroad has been successful in harnessing this nanosized silica to manufacture silicon carbide that had hardness next only to diamond<sup>153</sup>. Silica is widely used in electronics, ceramic, and polymer material industries. Because the silicon atoms in the rice husk have been naturally and uniformly dispersed by molecular units, very fine particle size, with very high purity and surface area silica powder can be prepared under controlled conditions. The ash contains > 90 % silica by mass with minor amounts of metallic elements. Extensive research has been carried out on the preparation,



properties and applications of rice husk ash during the last three decades and many papers and patents have been published on this subject<sup>154,155</sup>.

Rice husk on burning gives ash, which contains a very high percentage of crystalline silica. However, if it is burnt under controlled conditions, amorphous silica is produced which is highly reactive in nature<sup>156</sup>. Amorphous silica of high purity, small particle size and high surface area can be of use as an adsorbent or catalyst support in fine chemical synthesis<sup>157</sup>. Sharma et al.<sup>158</sup> have shown that silica is concentrated primarily within the outer epidermis, although a small amount of silica was found within the inner epidermis adjacent to the rice kernel. Real et al.<sup>159</sup> found that a homogeneous size distribution of nanometric silica particles could be obtained by burning rice husk at 873-1073K in a pure oxygen atmosphere. Active silica with a high specific area could be produced from rice husk after heat-treating at 973K in air<sup>160</sup>. As a consequence, especially in the field of material science, it makes sense to prepare rice husk silica by a series of process including acid leaching, pyrolysis and carbon removing<sup>161</sup>.

Rice husk, which is an agro waste, can be a source for many silicon-based materials if burnt under controlled conditions. Rice husk ash got potential applications in every field of lifestyle. Mini power plants based on rice husk ash (RHA) technology can fulfill the electricity needs of rural areas<sup>162</sup>. Preparation of solar grade silicon at low cost and with low energy consumption has been published and patented by Banerjee et al.<sup>163</sup>. Novel applications of the rice husk silica include as filler in polymeric materials, substitute for condensed silica fume in high strength concrete and starting

materials for high performance silicon compounds<sup>164</sup>. A number of studies on converting rice husk into activated carbon have also been reported. It was reported that NaA zeolite could be synthesized from rice husk and carbonaceous rice husk ash<sup>165</sup>. Instead of the silica gel commonly used, rice husk ash has been first adopted as a catalyst support by Chang et al.<sup>166-168</sup> and found to exhibit a very high activity for the rice husk ash-supported nickel catalysts in CO<sub>2</sub> hydrogenation. When rice husk ash supported nickel catalysts were prepared by ion exchange and incipient wetness impregnation techniques, at low nickel content, the nickel spreads uniformly on the surface and the reduction of the NiO particles resulting from thermal decomposition of the layered nickel silicates is found to be unusually difficult<sup>168</sup>. Ni/RHA/Al<sub>2</sub>O<sub>3</sub> catalysts performed better than Ni/SiO<sub>2</sub>-Al<sub>2</sub>O<sub>3</sub> ones for CO<sub>2</sub> hydrogenation with maximum yield and CH<sub>4</sub> selectivity. In these, small nickel oxide crystallites were formed with good dispersion and more than one species, such as NiO or NiAl<sub>2</sub>O<sub>4</sub>-like ones were detected<sup>170,171</sup>. Chang et al.<sup>172</sup> studied Cr<sub>2</sub>O<sub>3</sub>-promoted copper catalysts on rice husk ash prepared by incipient wetness impregnation and found chromia promoter is well dispersed among CuO particles over RHA support. They could conclude that despite the lower BET surface area, RHA is superior to commercial silica gel as a candidate for the catalyst support since the majority of surface pores are unique ones while those on the silica gel are interconnected and can be clogged easily. Production of value added materials from rice husk with specific properties assumes importance at this juncture. This not only facilitates utilization of an abundantly available agro waste but also reduces the environmental pollution.

## **1.6 SCOPE AND OUTLINE OF THE THESIS**

The development of new catalytic materials and routes to replace environmentally unacceptable processes in the fine chemical industry is emerging due to stringent legislation. Replacement of currently applied hazardous acids and homogeneous catalysts in catalytic industry can result in diminishing of pollution, less corrosion and catalytic reuse. One of the better choices is supported vanadia catalyst, which shows promising results for selective oxidation of aromatics. The research work presented in this thesis aims at gaining more insight into the structural behaviour of vanadia with various supports (ceria, ceria-silica, praseodymia and praseodymia-silica) and its catalytic performance in liquid-phase oxidation of benzene, ethylbenzene and naphthalene and oxidative dehydrogenation of ethylbenzene. Our investigation on the scope of supported vanadia catalysts as solid oxide catalysts in the selective oxidation reactions of aromatics and correlation to structural variation will be described.

The relation between structure and catalytic activity and selectivity is of crucial importance for further improvement of supported and bulk vanadia-rare earth oxide catalysts. The study is based on various characterization techniques. Many of the adopted characterization techniques are X-ray diffraction, EDX, BET surface area analysis, FT-IR, FT-Raman, TGA/DTA, UV-vis DRS, EPR,  $^{29}\text{Si}$  and  $^{51}\text{V}$  MAS NMR, SEM, TPR and acidity by TPD and cyclohexanol decomposition. Oxidation of aromatics has been applied as the reaction to investigate the catalytic activity over supported vanadia catalysts. In short the thesis emphasizes the relation between catalyst structure, as studied by several instrumental techniques and catalytic activity.

Chapter 1 and 2 deals with a general introduction to catalysis and an insight into heterogeneous catalytic oxidation respectively.

In chapter 3, a detailed description of the various experimental techniques used to characterize the catalysts is presented.

Chapter 4 deals with the results of surface composition and bulk characterization of the various rare earth oxides supported vanadia catalysts by means of X-ray, spectroscopic and other techniques.

In chapter 5, the activity of the catalysts towards benzene oxidation in liquid phase is correlated with physico chemical characteristics.

The oxidation of ethylbenzene performed in liquid-phase using the prepared catalysts and its correlation with the catalyst structure is presented in chapter 6.

Chapter 7 involves a study of the liquid-phase naphthalene oxidation with the catalysts and its correlation to catalyst structure.

Oxidative dehydrogenation of ethylbenzene with the catalysts and its correlation to catalyst structure is presented in chapter 8.

In the final chapter, chapter 9, summary of the results from the previous chapters are briefly reviewed and the implications thereof for future research work is also discussed.



**REFERENCES**

- [1] G.C. Bond, *Heterogeneous Catalysis: Principles and Applications*, Clarendon Press, Oxford (1987).
- [2] B. Cornils, Wolfgang A. Hermann, Robert Schlogl, Chi-Huey Wang, *Catalysis from A to Z: A Concise Encyclopedia* (2000) 902.
- [3] Hampii, Hawley, *The Encyclopedia of Chemistry*, 3<sup>rd</sup> Edn. (1973) 209.
- [4] J. Hagen, *Industrial Catalysis: A Practical Approach*, New York, Wiley-VCH (1999).
- [5] X. Gao, S.R. Bare, J.L.G. Fierro, I.E. Wachs, *J. Phys. Chem. B* 103 (1999) 618.
- [6] A. Carati, G. Ferraris, M. Guidotti, G. Moretti, R. Psaro, C. Rizzo, *Catal. Today* 77 (2003) 315.
- [7] V. Parvulescu, C. Constantin, B.L. Su, *J. Mol. Catal. A: Chem.* 202 (2003) 171.
- [8] J. Jia, K.S. Pillai, W.M.H. Sachtler, *J. Catal.* 221 (2004) 119.
- [9] J.G. Goodwin, Jr. Koranre, M.M. Marcelin G, *J. Catal.* 148 (1994) 369.
- [10] J.T. Richardson, *Principles of Catalyst Development*, Plenum Press, New York (1989) 134.
- [11] B. Imelik, J.C. Vedrine (Eds), *Catalyst Characterization: Physical Techniques for Solid Materials*, Plenum Press, New York (1994).
- [12] K. Morikawa, T. Shirsaki, M. Okada, *Adv. Catal.* 20 (1969) 97.
- [13] J.J. Burton, R.L. Garten (Eds.) L.L. Murrell in *Advanced Materials in Catalysis*, Chap. 8, Academic Press, New York (1977).
- [14] D.L. Trimm, *Design of Industrial Catalysts*, Elsevier, New York (1980).
- [15] K. Foger, *Catalysis, Science and Technology*, JR. Anderson, M. Boudart (Eds.) Springer, New York 6 (1984) 227.
- [16] Q. Fu, A. Weber, M. Flytzani-Stephanopoulos, *Catal. Lett.* 77 1-3 (2001) 87.
- [17] P. Moriceau, B. Grzybowska, Y. Barboux, G. Wrobel, G. Hecquet, *Appl. Catal. A: Gen.* 168 (1998) 269.
- [18] M.J. Holgado, S. San Roman, P. Malet, V. Rives, *Mater. Chem. Phys.* 89 (2005) 49.
- [19] D.M. Whittle, A.A. Mirzaei, J.S.J. Hargreaves, R.W. Joyner, C. J. Kiely, S.H. Taylor, G.J. Hutchings, *Phys. Chem. Chem. Phys.* 4 (2002) 5915.
- [20] F. Pinna, *Catal. Today* 41 (1998) 129.

- [21] B.M. Reddy, P. Lakshmanan, A. Khan, C. Lopez-Cartes, T.C. Rojas, A. Fernandez, *J. Phys. Chem. B* 109 (2005) 1781.
- [22] V. Lafond, P.H. Mutin, A. Vioux, *J. Mol. Catal. A: Chem.* 182-183 (2002) 81.
- [23] C. Palazzo, L. Olivia, M. Signoretto, G. Strukul, *J. Catal.* 194 (2000) 286.
- [24] M. Gotic, S. Popovic, M. Ivanda, S. Music, *Mater. Lett.* 57 (2003) 3186.
- [25] J. Keranen, A. Auroux, S. Ek, L. Niinisto, *Appl. Catal. A: Gen.* 228 (2002) 213.
- [26] J. Haber, *Pure Appl. Chem.* 63 (1991) 1227.
- [27] C.F. Powell, J.H. Oxley, J.M. Blocher Jr, (Eds.) *Vapour Deposition*, Wiley, New York (1996).
- [28] H.O. Pierson, *Handbook of Chemical Vapour Deposition—Principles, Technology and Applications*, Noyes Publications, New Jersey (1992).
- [29] L. Torrison, J. Tolle, J. Kouvetakis, S.K. Dey, D. Gu, I.S.T. Tsong, P.A. Crozier, *Mater. Sci. Eng. B* 97 (2003) 54.
- [30] A. Burrows, C.J. Kiely, J.S.J. Hargreaves, R.W. Joyner, G.J. Hutchings, M.Y. Sinev, Y.P. Tulenin, *J. Catal.* 173 (1998) 383.
- [31] J.S.J. Hargreaves, G.J. Hutchings, R.W. Joyner, S.H. Taylor, *Appl. Catal. A: Gen.* 227 (2002) 191.
- [32] B.M. Reddy, P. Lakshmanan, A. Khan, *J. Phy. Chem. B* 108 43 (2004) 16863.
- [33] Friebe, O. Nuyken, H. Windisch, W. Obrecht, *Macromol. Chem. Phys.* 203 8 (2002) 1055.
- [34] S. Sugunan, N.K. Renuka, *Bull. Chem. Soc. Jpn.* 75 (2002) 463.
- [35] D.H. Tsai, T.J. Huang, *Appl. Catal. A: Gen.* 223 (2002) 1.
- [36] A.G. Dedov, A.S. Loktev, I.I. Moiseev, A. Aboukais, J.F. Lamonier, I.N. Filimonov, *Appl. Catal. A: Gen.* 245 (2003) 209.
- [37] S. Shylesh, T. Radhika, K. Sreejarani, S. Sugunan, *J. Mol. Catal. A: Chem.* 236 (2005) 253.
- [38] A. Trovarelli, *Catalysis by Ceria and Related Materials*, Imperial College Press, London (2002).
- [39] A. Trovarelli, *Catal. Rev.* 38 (1996) 439.

- [40] B.M. Reddy, A. Khan, Y. Yamada, T. Kobayashi, S. Loridant, J.C. Volta, J. Phys. Chem. B. 106 (2002) 10964.
- [41] J. Matta, D. Courcot, E. Abi-Aad, A. Aboukais, Chem. Mater. 14 (2002) 4118.
- [42] R.G. Toro, G. Malandrino, I.L. Fragala, R.L. Nigro, M. Losurdo, G. Bruno, J. Phys. Chem. B 108 (2004) 16357.
- [43] S. Logothetidis, P. Patsalas, C. Charitidis, Mater. Sci. Eng. C 23 (2003) 803.
- [44] V. Briois, D.L. Hecht, F. Villain, E. Fonda, S. Belin, B. Griesebock, R. Frahm, J. Phys. Chem. A. 109 (2005) 320.
- [45] K. Nagaveni, M.S. Hedge, G. Madras, J. Phys. Chem. B 108 (2004) 20204.
- [46] C.S. Yao, H.S. Weno, Chem. Eng. Sci. 47 9-11 (1992) 2745.
- [47] A.M. Shahin, F. Grandjean, G.J. Long, T.P. Schuman, Chem. Mater. 17 (2005) 315.
- [48] H. Chen, A. Aleksandrov, Y. Chen, S. Zha, M. Liu, T. M. Orlando, J. Phys. Chem. B. 109 (2005) 11257.
- [49] J.M. Coronado, A.J. Maria, A.M. Arias, J.C. Conesa, J. Soria, J. Photochem. Photobiol. A: Chem. 150 (2002) 213.
- [50] M.M. Mohamed, S.M.A. Katib, Appl. Catal. A: Gen. 287 (2005) 236.
- [51] R. Niewa, Z. Hu, C. Grazioli, U. Robler, M.S. Golden, M. Knupfer, J. Fink, H. Giefers, G. Wortmann, F.M.F. de Groot, F.J.D. Salvo, J. Alloys Comp. 346 (2002) 129.
- [52] F. Zhang, S.W. Chan, J.E. Spanier, E. Apak, Q. Jin, Appl. Phys. Lett. 80 (2002) 127.
- [53] M.V.M. Huerta, J.M. Coronado, M.F. Garcia, A.I. Juaz, G. Deao, J.L.G. Fierro, M.A. Banares, J. Catal. 225 (2004) 240.
- [54] B. Murugan, A.V. Ramaswamy, Chem. Mater. 17 (15) (2005) 3983.
- [55] T. Mimani, K.C. Patil, Mater. Phys. Mech. 4 (2001) 134.
- [56] S. Sugunan, B. Varghese, Ind. J. Chem. A 37: 9 (1998) 806.
- [57] R. Sasikala, N.M. Gupta, S.K. Kulshreshtha, Catal. Lett. 71 1-2 (2001) 69.
- [58] M. Ponzi, C. Duschatzky, A. Carrascull, E. Ponzi, Appl. Catal. A: Gen. 169 (1998) 373.

- [59] A. Piras, S. Colussi, A. Trovarelli, V. Sergo, J. Liorca, R. Psaro, L. Sordelli, *J. Phys. Chem. B* 109 (2005) 11110.
- [60] E. Rocchini, M. Vicario, J. Llorca, C. de Leitenburg, G. Dolcetti, A. Trovarelli, *J. Catal.* 211 (2002) 407.
- [61] J.Z. Colina, R.M. Nix, H. Weiss, *J. Phys. Chem. B* 109 (2005) 10978.
- [62] A.M. Venezia, G. Pantaleo, A. Longo, G.D. Carlo, M.P. Casaletto, F.L. Liotta, G. Deganello, *J. Phys. Chem. B* 109 (2005) 2821.
- [63] G. Munteanu, L. Ilieva, R. Nedyalkova, D. Andreeva, *Appl. Catal. A: Gen.* 277 (2004) 31.
- [64] D.M. Lyons, K.M. Ryan, M.A. Morris, *J. Mater. Chem.* 12 (2002) 1207.
- [65] R. Long, H. Wan, *J. Catal.* 172 (1997) 471.
- [66] Z.C. Kang, L. Eyring, *J. Alloys and Comp.* 275-277 (1998) 721.
- [67] G. De, A. Licciulli, M. Nacucchi, *J. Non-Crystalline Solids* 201 (1996) 153.
- [68] Y. Kaneko, S. Mori, J. Yamanaka, *Solid State Ionics* 151 (2002) 35.
- [69] M.C. Caracoche, J.A. Martinez, P.C. Rivas, A.M. Rodriguez, F. Bondioli, T. Manfredini, A.M. Ferrari, S. Conconi, *Chem. Mater.* 16 (2004) 4319.
- [70] S. Rossignol, C. Descorme, C. Kappenstein, D. Duprez, *J. Mater. Chem.* 11 (2001) 2587.
- [71] S. Rossignol, F. Gerard, D. Mesnard, C. Kappenstein, D. Duprez, *J. Mater. Chem.* 13 (2003) 3017.
- [72] E.S. Putna, J.M. Vohs, R.J. Gorte, G.W. Graham, *Catal. Lett.* 54 (1998) 17.
- [73] T. Bunluesin, G.W. Graham, R.J. Gorte, *Appl. Catal. B* 14 (1997) 105.
- [74] F. De Smet, P. Ruiz, B. Delmon, M. Devillers, *Appl. Catal. A: Chem.* 172 (1998) 333.
- [75] F.D. Smet, P. Ruiz, B. Delmon, M. Devillers, *Catal. Lett.* 41 (1996) 203.
- [76] F.D. Smet, M. Devillers, C. Poleunis, P. Bertrand, *J. Chem. Soc., Faraday Trans.* 94 7 (1998) 941.
- [77] S. Sugunan, K. Sreejarani, C.S. Deepa, H. Suja, *React. Kinet. Catal. Lett.* 71 2 (2000) 307.
- [78] D. Wolfframm, M. Ratzke, M. Kappa, M.J. Montenegro, M. Dobeli, T. Lippert, J. Reif, *Mater. Sci. Eng. B* 109 (2004) 24.
- [79] K. Asami, K.I. Kusakabe, N. Ashi, Y. Ohtsuka, *Appl. Catal. A: Gen.* 156 (1997) 43.
- [80] E.J. Baran, *Bol. Soc. Chil. Quim.* 42 (1997) 247; *Chem. Abstr.* 127 (1997) 174046a.



- [81] J.C. Badot, A. Mantoux, N. Baffier, O. Dubrunfaut, D. Lincot, *J. Mater. Chem.* 14 (2004) 3411.
- [82] O.B. Lapina, A.A. Shubin, D.F. Khabibulin, V.V. Terskikh, P.R. Bodart, J. P. Amoureux, *Catal. Today* 78 (2003) 91.
- [83] E.P. Reddy, R.S. Varma, *J. Catal.* 221 (2004) 93.
- [84] K.L. Furdala, T.D. Tilly, *Chem. Mater.* 14 (2002) 1376.
- [85] V. Luca, D.J. MacLachlan, R. Bramley, *Phys. Chem. Chem. Phys.* 1 (1999) 2597.
- [86] N.N. Nair, T. Bredow, K. Jug, *J. Phys. Chem. B* 109 (2005) 12115.
- [87] C. Martin, D. Klissurski, J. Rocha, V. Rives, *Phys. Chem. Chem. Phys.* 2 (2000) 1543.
- [88] V.P. Vislovskiy, J.S. Chang, M.S. Park, S.E. Park, *Catal. Commun.* 3 (2002) 227.
- [89] D.A. Bulushev, L.K. Minsker, F. Rainone, A. Renken, *J. Catal.* 205 (2002) 115.
- [90] W. Reichl, K. Hayek, *Surf. Sci.* 537 (2003) 247.
- [91] F. Prinetto, G. Ghiotti, M. Occhiuzzi, V. Indovina, *J. Phys. Chem. B* 102 (1998) 10316.
- [92] J. Antonio, L. Sanchez, J.K. Bartley, R.P.K. Wells, C. Rhodes, G.J. Hutchings, *New J. Chem.* 26 (2002) 1613.
- [93] A.M. Shahin, F. Grandjean, G.J. Long, T.P. Schuman, *Chem. Mater.* 17 (2005) 315.
- [94] D.E. Keller, F.M.F. de Groot, D.C. Koningsberger, S. Bert, M. Weckhuysen, *J. Phys. Chem. B* 109 (2005) 20.
- [95] J. Haber, M. Witko, R. Tokarz, *Appl. Catal. A: Gen.* 157 (1997) 3.
- [96] M.L. Ferreira, M. Volpe, *J. Mol. Catal. A: Chem.* 184 (2002) 349.
- [97] M.A. Larrubia, G. Busca, *Mater. Chem. Phys.* 72 (2001) 337.
- [98] K.V.R Chary, *Bull. Catal. Soc. India.* 3 (2004) 10.
- [99] S. Besselmann, C. Freitag, O. Hinrichsen, M. Muhler, *Phys. Chem. Chem. Phys.* 3 (2001) 4633.
- [100] M. Kantcheva, *Phys. Chem. Chem. Phys.* 2 (2000) 3043.
- [101] D.C.M. Dutoit, M. Schneider, P. Fabrizioli, A. Baiker, *J. Mater. Chem.* 7 2 (1997) 271.
- [102] C.B. Wang, G. Deo, I.E. Wachs, *J. Catal.* 178 (1998) 640.
- [103] X. Gao, J.M. Jehng, I.E. Wachs, *J. Catal.* 209 (2002) 43.

- [104] R. Neumann, M.L. Elad, *Appl. Catal. A: Gen.* 122 (1995) 85.
- [105] G. Vivekanandan, V. Krishnaswamy, *Catalysis: Present and Future* (1995) 269.
- [106] G.S. Wong, M.R. Concepcion, J.M. Vohs, *J. Phys. Chem. B* 106 (2002) 6451.
- [107] U.G. Nielsen, H.J. Jakobsen, J. Skibsted, *J. Phys. Chem. B* 105 (2001) 420.
- [108] K.P. Rao, R.S. Beniwal, *Catalysis: Present and Future*, Wiley Eastern Ltd., New Delhi (1995).
- [109] Y.H. Kim, H.I. Lee, *Bull. Korean Chem. Soc.* 20 12 (1999) 1457.
- [110] K.V. Narayana, A. Venugopal, K.S.R. Rao, S.K. Masthan, V.V. Rao, P.K. Rao, *Appl. Catal. A: Gen.* 167 (1998) 11.
- [111] X. Yin, H. Han, A. Miyamoto, *Phys. Chem. Chem. Phys.* 2 (2000) 4243.
- [112] T. Garcia, B. Solsona, D.M. Murphy, K.L. Antcliff, S.H. Taylor, *J. Catal.* 229 (2005) 1.
- [113] P. Ciambelli, L. Lisi, G. Russo, J.C. Volta, *Appl. Catal. B: Environ.* 7 (1995) 1.
- [114] J.R. Sohn, K.C. Seo, Y. Il Pae, *Bull. Korean Chem. Soc.* 24 3 (2003) 311.
- [115] K.V.R. Chary, C.P. Kumar, K.R. Reddy, T. Bhaskar, T. Rajiah, *Catal. Commun.* 3 (2002) 7.
- [116] G.J. Hutchings, J.A.L. Sanchez, J.K. Bartley, J.M. Webster, A. Burrows, C.J. Kiely, A.F. Carley, C. Rhodes, M. Havecker, A.K. Gericke, R.W. Mayer, R. Schlogl, J.C. Volta, M. Poliakoff, *J. Catal.* 208 (2002) 197.
- [117] J.K. Bartley, C.J. Kiely, R.P.K. Wells, G.J. Hutchings, *Catal. Lett.* 72 1-2 (2001) 99.
- [118] G.J. Hutchings, J.K. Bartley, J.M. Webster, J.A.L. Sanchez, D.J. Gilbert, C.J. Kiely, A.F. Carley, S.M. Howdle, S. Sajip, S. Caldarelli, C. Rhodes, J.C. Volta, M. Poliakoff, *J. Catal.* 197 (2001) 232.
- [119] R. Tanner, P. Gill, R. Wells, J.E. Bailie, G. Kelly, S.D. Jackson, G.J. Hutchings, *Phys. Chem. Chem. Phys.* 4 (2002) 688.
- [120] P. Brandao, A. Philippou, N. Hanif, P.R. Claro, A. Ferreira, M. W. Anderson, J. Rocha, *Chem. Mater.* 14 (2002) 1053.
- [121] O.A. Anunziata, L.B. Pierella, A.R. Beltramone, *Catal. Lett.* 75 1-2 (2001) 87.
- [122] T. Selvam, A.P. Singh *J. Chem. Soc., Chem. Commun.* (1995) 883.
- [123] O.A. Anunziata, L.B. Pierella, M.G. Costa, A.R. Beltramone, *Catal. Lett.* 71 1-2 (2001) 127.
- [124] B. Solsona, T. Blasco, J.M. Lopez Nieto, M.L. Pena, F. Rey, A. Vidal Moya, *J. Catal.* 203 (2001) 443.

- [125] S. Shylesh, A.P. Singh, *J. Catal.* 228 2 (2004) 333.
- [126] S. Shylesh, S.P. Mirajkar, A.P. Singh, *J. Mol. Catal. A: Chem.* 239 (2005) 57.
- [127] S. Shylesh, A.P. Singh, *J. Catal.* 233 2 (2005) 359.
- [128] J. George, S. Shylesh, A.P. Singh, *Appl. Catal. A: Gen.* 290 1-2 (2005) 148.
- [129] C.W. Lee, W.J. Lee, Y.K. Park, S.E. Park, *Catal. Today* 61 (2000) 137.
- [130] A. Christodoulakis, M. Machli, A.A. Lemonidou, S. Boghosian, *J. Catal.* 222 2 (2004) 293.
- [131] K.V.R. Chary, G. Kishan, C.P. Kumar, G.V. Sagar, *Appl. Catal. A: Gen.* 246 (2003) 335.
- [132] S. Sugunan, N.K. Renuka, A.R. Koshy, S.M. Varghese, C.G. Ramankutty, *React. Kinet. Catal. Lett.* 67 2 (2002) 267.
- [133] E.H. Park, M.H. Lee, J. R. Sohn, *Bull. Korean Chem. Soc.* 21 9 (2000) 913.
- [134] Z. Zhao, Y. Yamada, A. Ueda, H. Sakurai, T. Kobayashi, *Catal. Today* 93-95 (2004) 163.
- [135] I.L. Botto, M. Vassallo, G. Fierro, D. Cordischi, M. Inversi, G. Minelli, *J. Mater. Chem.* 7 11 (1997) 2279.
- [136] Z. Wu, H.S. Kim, P.C. Stair, S. Rugmini, S.D. Jackson, *J. Phys. Chem. B* 109 (2005) 2793.
- [137] M.L. Ferreira, M. Volpe, *J. Mol. Catal. A: Chem.* 164 (2000) 281.
- [138] D.A. Bulushev, L.K. Minsker, F. Rainone, A. Renken, *J. Catal.* 205 (2002) 115.
- [139] T. Feng, J.M. Vohs, *J. Phys. Chem. B* 109 (2005) 2120.
- [140] M. Ruitenbeek, A.J. van Dillen, F.M.F. de Groot, I.E. Wachs, J.W. Geus, D.C. Koningsberger, *Topics in Catal.* 10 (2000) 241.
- [141] K.V.R. Chary, C.P. Kumar, A. Murali, A. Tripathi, A. Clearfield, *J. Mol. Catal. A: Chem.* 216 (2004) 139.
- [142] R. Cousin, M. Dourdin, E. Abi-Aad, D. Courcot, S. Capelle, M. Guelton, A. Aboukais, *J. Chem. Soc., Faraday Trans.* 93 21 (1997) 3863.
- [143] U. Opara Krasovec, B. Orel, A. Surca, N. Bukovec, R. Reisfeld, *Solid State Ionics* 118 (1999) 195.
- [144] G. S. Wong, J. M. Vohs, *Surf. Sci.* 498 (2002) 266.
- [145] J.M. Vohs, T. Feng, G.S. Wong, *Catal. Today* 85 (2003) 303.
- [146] L.J. Burcham, I.E. Wachs, *Catal. Today* 49 (1999) 467.
- [147] J. Paya, J. Monzo, M.V. Borrachero, A. Mellado, L.M. Ordonez, *Cem. Concr. Res.* 31 (2001) 227.

- [148] L.J. Kennedy, J.J. Vijaya, G. Sekaran, *Ind. Eng. Chem. Res.* 43 (2004) 1832.
- [149] C.S. Prasad, K.N. Maiti, R. Venugopal, *Ceram. Int.* 29 (2003) 907.
- [150] N. Yalcin, V. Sevinc, *Ceram. Int.* 27 (2001) 219.
- [151] P. Mishra, A. Chakraverty, H.D. Banerjee, *J. Mater. Sci.* 20 (1985) 4387.
- [152] A. Chakraverty, P. Mishra, H.D. Banerjee, *J. Mater. Sci.* 23 (1988) 21.
- [153] R. Prasad, *Science and Technology, The Hindu*, January 15 (2004).
- [154] J. James, M.S. Rao, *Thermochim. Acta*, 97 (1986) 329.
- [155] B.C. Saha, L.B. Iten, M.A. Cotta, Y.V. Wu, *Biotechnol. Prog.* 21 (2005) 816.
- [156] R. Chander, K. Rohatgi, B.N. Johri, *J. Sci. Indust. Res.* 44 (1985) 607.
- [157] S. Chandrasekhar, K.G. Satyanarayana, P.N. Pramada, P. Raghavan, *J. Mater. Sci.* 38 (2003) 3159.
- [158] N.K. Sharma, W.S. Williams, A. Zanguil, *J. Am. Ceram. Soc.* 67 (1984) 715.
- [159] C. Real, M.D. Alcalá, J.M. Criado, *J. Am. Ceram. Soc.* 79 8 (1996) 2012.
- [160] T.H. Liou, *Mater. Sci. Eng.* 1-2 (2004) 364.
- [161] I.A. Rahman, J. Ismail, H. Osman, *J. Mater. Chem.* 7 8 (1997) 1505.
- [162] R. Sampath, *Sci. Tech. The Hindu*, January 19 (2003).
- [163] H.D. Banerjee, S.Sen, H.N. Acharya, *Mater. Sci. Engg.* 52 2 (1982) 173.
- [164] M.Y.A. Fuad, M. Jamludin, Z.A.M. Ishak, A.K.M. Omar, *Int. J. Polym. Mater.* 19 1-2 (1993) 75.
- [165] H. Nur, *Indonesian J. Agric. Sci.* 1 (2001) 40.
- [166] F.W. Chang, W.Y. Kuo, K. Lee, *Appl. Catal. A: Gen.* 8517 (2003) 1.
- [167] F.W. Chang, T.J. Hsiao, S.W. Chung, J.J. Lo, *Appl. Catal. A: Gen.* 164 (1997) 225.
- [168] F.W. Chang, T.J. Hsiao, J.D. Shih, *J. Ind. Eng. Chem. Res.* 37 (1998) 3838.
- [169] M.T. Tsay, F.W. Chang, *Appl. Catal. A: Gen.* 203 (2000) 15.
- [170] F.W. Chang, M.S. Kuo, M.T. Tsay, M.C. Hsieh, *Appl. Catal. A: Gen.* 247 (2003) 309.
- [171] F.W. Chang, M.S. Kuo, M.T. Tsay, M.S. Kuo, C.M. Yang, *Appl. Catal. A: Gen.* 226 (2002) 213.
- [172] F.W. Chang, W.Y. Kuo, H.C. Yang, *Appl. Catal. A: Gen.* 288 (2005) 53.

## CHAPTER 2

### HETEROGENEOUS CATALYTIC OXIDATION

#### Abstract

---

*Oxidation is a fundamental transformation in organic synthesis, and numerous methods are reported in the literature. It is a core technology for concerting petroleum based materials to useful chemicals of a higher oxidation state. In industrial chemistry, heterogeneous catalyst systems are preferred over homogeneous system due to easy recyclability and separability. Due to the increasing environmental concerns; oxidation using environmentally friendly oxidants such as molecular oxygen and hydrogen peroxide are more desirable these days. Catalytic oxidation offers the advantage that volatile organic compounds can be removed from aerial effluents to very low levels. Studies of catalytic volatile organic compound oxidation have shown that short-chain aromatic hydrocarbons are among the most difficult to destroy. The nuclear oxidation of non-activated aromatics is noteworthy in terms of both its mechanistic study and practical applications.*

---

## 2.1 CATALYTIC OXIDATION

Catalytic oxidation is the largest class of catalytic organic reactions in the petrochemical industry; since hydrocarbon derivatives containing oxygen and other heteroatom are intermediate to practically all important plastics, synthetic rubber, chemical fibers, products of household industry etc.<sup>1</sup>. Simple aromatic hydrocarbons, mainly methylated benzenes, are emitted to the atmosphere through solvent use or from automobiles. These compounds contribute significantly to the formation of ozone and other photo-oxidants in industrial regions. The degradation of benzene and other simple aromatic hydrocarbons in the lower atmosphere is therefore a prerequisite for good environmental concerns<sup>2-5</sup>. Oxidation is one of the most important methods of adding functionalities to an organic molecule and is most important for hydrocarbons where low molecular weight starting materials are converted into valuable acids, ketones and alcohols<sup>6,7</sup>. There is a growing interest in the oxidation of saturated hydrocarbons especially under mild conditions due to the wide ranging utility of the ensuing functionalized compounds as raw materials and intermediates in industrial and pharmaceutical industry<sup>8-10</sup>. The oxidation products of cyclohexane, viz., cyclohexanol and cyclohexanone, are key intermediates in the production of caprolactam (a monomer in the manufacture of nylon-6) and adipic acid (a building block of polyamides viz. nylon-66 and polyurethane resins)<sup>11-13</sup>. While the oxidation of olefin into  $\alpha,\beta$ -unsaturated ketone has been utilized in the synthesis and transformations of several natural products, the oxidation products of ethylbenzene and cyclohexene are widely employed as intermediates in organic, steroid, and resin synthesis. Hence, the development of catalytic methods involving clean

oxidants for the selective oxidation of hydrocarbons is of great practical interest, besides the intrinsic importance of C-H activation chemistry<sup>14</sup>.

Nowadays, large scale industrial chemical processes, which generally involve several steps afflicted with the generation of by products and waste are subject to continuously increasing environmental concerns and suffer from severe regulations. Molecular oxygen is obviously an ideal oxidant, but aerobic oxidation is often difficult to control and sometimes results in combustion and the reaction is performed with a low conversion to avoid over-oxidation. In the last decade  $N_2O$  has also attracted growing attention as a selective oxygen donor for oxidation reactions<sup>15-18</sup>. Among commonly used oxidants such as dioxygen,  $H_2O_2$  and alkyl hydroperoxide,  $H_2O_2$  is an attractive one since it is easy to handle, have high content of active oxygen, cheap availability, non-toxicity, and non-polluting property and produces only water as the co-product<sup>19-24</sup>.  $H_2O_2$  is an adduct of  $H_2$  and  $O_2$  and it also viewed as an adduct of an O atom and an  $H_2O$  molecule. It can oxidize organic compounds with an atom efficiency of 47 % and  $H_2O_2$  can be an ideal, waste-avoiding oxidant only when it is used in a controlled manner without organic solvents and other toxic compounds. The  $H_2O_2$  oxidation is particularly useful for the synthesis of high-value fine chemical, pharmaceuticals or agrochemicals, and electronic materials, which require high chemical purity. In fact, there is a trend to use  $H_2O_2$  as an oxidant for large volume processes such as caprolactam synthesis and propylene oxidation. One of the major advantages of the  $H_2O_2$  oxidation is the high tenability of the reaction parameters<sup>25-27</sup>. However, the activation of  $H_2O_2$  requires the use of catalysts<sup>28</sup>. Several studies have been conducted using

environmentally benign supercritical fluids such as CO<sub>2</sub> and water as the solvents in order to replace hazardous organic solvents. Metal-containing aluminophosphate molecular sieves and rare earth exchanged zeolite Y offer tremendous potential as catalysts in the oxidation reactions to transform hydrocarbons into valuable products<sup>29,30</sup>. Corma et al.<sup>31</sup> reported that properly coupling catalyst design and reaction conditions could give very high turnover numbers for Baeyer-Villiger oxidation using Sn-Beta/H<sub>2</sub>O<sub>2</sub> and Al-Beta/H<sub>2</sub>O<sub>2</sub> as catalysts in acetonitrile solvent. V-containing xerogels are active catalysts for a variety of oxidation reactions with H<sub>2</sub>O<sub>2</sub>, including epoxidation of alkanes, oxidation of secondary alcohol and hydroxylation of phenol<sup>32-35</sup>.

Heterogeneous catalytic oxidation, both in the vapour and liquid phase, is an important technological area in the field of processes for the production of bulk organic chemicals, the production of fine chemicals and for pollution abatement<sup>36</sup>. Oxidation processes that are driven by the heterogeneous catalysts can be divided into two groups, namely selective oxidation, ammoxidation and oxychlorination where the desired reaction product is not the most thermodynamically stable and total oxidation reactions where the desired reaction products are the most stable thermodynamically. In general, the former type of reaction is for the production of bulk organic chemicals whereas the latter is for energy conservation and pollution abatement<sup>37</sup>.

## 2.2 KINETICS OF OXIDATION REACTIONS

There are five basic types of kinetic rate laws commonly used to describe heterogeneous oxidations<sup>38,39</sup>. Important ones are discussed below.



### **1. Mars -van Krevelen mechanism**

In 1954 Mars and van Krevelen published the study of oxidation of benzene, toluene, naphthalene and anthracene over vanadium oxide catalysts. It is stated that contact oxidation is performed by a redox cycle of metal oxide catalysts and, as a result, the oxidation activity is dependent on the redox action, that is, a pair of reducibility and reoxidizability. The rate-determining step in this mechanism is the diffusion of oxygen in the catalyst bulk. The mechanism proposed was that the hydrocarbon extracts lattice oxygen from the surface layer of the catalyst, thereby generating a reduced catalyst. An important part of the Mars and van Krevelen mechanism is that the lattice oxygen is replenished by gas phase oxygen in a reoxidation process. This mechanism has come to be the most widely applied in heterogeneous oxidation catalysis.

### **2. The Eley-Rideal mechanism**

In this mechanism a simple reaction between an adsorbed species and a second species reacting without adsorbing is considered. The gas phase reactant such a carbon monoxide molecule, does not reside on the catalysts surface for less than the time required to define physisorbed state. In that time a simple reaction with an adsorbed species,  $O_2$  or  $O$  appropriately charged in the case of oxidations, can occur according to this mechanism. A feature is that the adsorbing species must be in equilibrium with the species from which it is derived in the gas phase. The overall reaction rate increases as the surface coverage by oxygen increases and as the gas phase pressure of carbon monoxide increases. The simplest Eley-Rideal reaction mechanism predicts a

first order dependence on hydrocarbon partial pressure; first order in oxygen partial pressure at low partial pressures changing progressively to zero order at high pressures.

### 3. The Langmuir-Hinshelwood mechanism

This envisages that the slowest of the five steps involved in a catalyzed reaction is the reaction between two adsorbed species on a uniform catalyst surface. Adsorption can be on a single type of surface site, or each adsorbing species can adsorb on its own type of surface site, but each adsorbed species is in thermodynamic equilibrium with the corresponding gas phase species, according to the appropriate Langmuir adsorption isotherm. The kinetic expression predicts reaction orders in both reactants varying from one to zero as the partial pressures increases.

#### 2.3 SELECTIVE OXIDATION OF HYDROCARBONS

Processes involving the oxidation of hydrocarbons in the liquid phase, using air or oxygen, are of great importance to industrialized economies because of its role in converting petroleum hydrocarbon feedstocks such as alkanes, olefins, and aromatics into industrial organic chemicals important in the polymer and petro-chemical industries. Because oxidation of hydrocarbons ultimately gives carbon dioxide and water, it is clear that it is partial oxidations that are of greatest interest to the industry, and the success of an industrial oxidation process depends on proper control of the reaction to yield the desired intermediates with reasonable selectivities<sup>40</sup>. The complex chemistry of hydrocarbon oxidations leads to a multiplicity of products even at fairly early stages in the conversion. In modern heterogeneous catalysis, in-situ

characterization and catalytic design have not only added to our understanding of catalytic phenomena, but also have led to new solid catalysts capable of remarkably selective oxidation of hydrocarbons<sup>41</sup>. The selective catalytic oxidation of organic molecules continues to be a very important method for the preparation of primary and specialty chemicals in the chemical industry world wide<sup>42</sup>. Catalytic oxidation reactions using metal complexes are valuable for development of 'no-waste' chemical technology based on the 'atom economy principle'. However, catalytic oxidation of unactivated hydrocarbons remains as a challenging topic. The main driving force for the development of new efficient oxygenation catalysts is the necessity to functionalize feedstock alkanes to raw oxygen-containing chemicals and the ability to selectively hydroxylate non-activated C-H bonds in elaborate chemicals in order to save many steps in the preparation of fine chemicals. In addition, for environmental constraints, classical stoichiometric oxidants, such as dichromate or permanganate, should be replaced by new environment friendly catalytic processes using clean oxidants like molecular oxygen or hydrogen peroxide<sup>43,44</sup>. The objective of the selective oxidation is to oxidize the organic molecule while keeping its skeleton. The catalysts used are solids, most often mixed oxides with elements with different oxidation states, which present redox properties. They can be continuously reduced by hydrocarbons and oxidized by the oxygen present in the reaction mixture. The lattice oxygen is inserted in the hydrocarbon molecule while the reduced solid is reoxidized by gaseous oxygen. The insertion of lattice oxygen in the hydrocarbon and the incorporation of gaseous oxygen as lattice oxygen commonly take place at

different cation sites. Then, the catalyst should allow electrons, lattice oxygen  $O^{2-}$  and anion vacancies to move between those sites<sup>45</sup>.

The most studied mechanism is the Mars-van Krevelen mechanism or redox mechanism, which demonstrated first to have a two-step consecutive mechanism for the oxidation of naphthalene and is operative at moderate temperatures<sup>46-48</sup>. It is schematically represented in Figure 2.3.

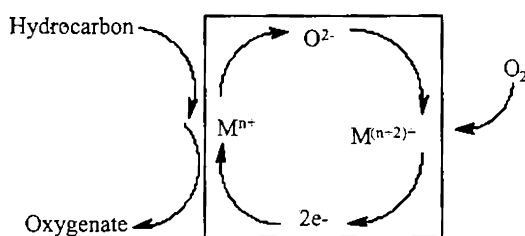


Figure 2.3

The mechanism can best be defined as a mechanism in which one of the products leaves the surface, containing one of the constituents of the lattice. With this mechanism oxidation, reduction, de-oxygenation and oxidative dehydrogenation can be described. In general, the Mars-van Krevelen mechanism is assumed to be operative for selective oxidation reactions. First, the reactant to be oxidized is adsorbed on the surface of the catalyst resulting in the formation of an adsorbed complex. Subsequently a reaction takes place between the adsorbate and oxygen from the lattice of the catalyst, resulting in the formation of a partially oxidized product, which after desorption leaves an oxygen vacancy at the surface. Re-oxidation of this vacancy takes place via gas phase oxygen, as represented in Figure 2.3. If diffusion of lattice oxygen is sufficiently fast, the  $O^{2-}$  surface species will migrate into the lattice. This

process can continuously take place as long as reactants are present to reduce the catalyst and oxygen to re-oxidize the surface. The presence of metal ions of which the lower oxidation state is relatively stable is a prerequisite for the development of this mechanism. The surface of a metal oxide catalyst is likely to contain an amount of metal ions of a lower oxidation state. Up to a certain concentration, these metal sites can be considered as defects in the metal oxide matrix. However, when the oxygen vacancy concentration becomes too high, a new solid phase can form. Formation of a new solid phase generally calls for a nucleation step, which usually proceeds too slowly to give rise to a marked catalytic activity. If the redox mechanism is to be operative, it is undesirable that the catalyst becomes crystalline. Catalysts exhibiting the Mars-van Krevelen mechanism therefore should be able to contain a certain amount of lattice defects without recrystallizing into a metal suboxide<sup>49</sup>.

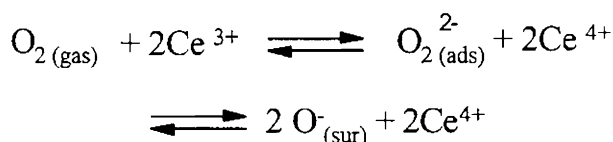
#### **2.4 REDOX BEHAVIOUR OF CERIA, PRASEODYMIA AND VANADIA**

The redox property of small metal particles differs from their bulk value and depends on the size and structure of the modified particle. The redox properties of ceria and the high lability of its lattice oxygen are among the most important factors that contribute to the catalytic reactivity of  $\text{CeO}_2$  in oxidation reactions; in particular for total oxidation reactions<sup>50</sup>. Generally the oxidation rate is limited by the oxygen transfer from the liquid phase to the metal active sites, while  $\text{CeO}_2$ , able to enhance this oxygen transfer to efficiently catalyze oxidations<sup>51</sup>. The promotional oxidation activity of ceria-containing catalysts clearly assigned to role of ceria in creating  $\text{Ce}^{3+}/\text{Ce}^{4+}$  redox couple<sup>52-54</sup>. The  $\text{Ce}^{3+}/\text{Ce}^{4+}$  redox couple present in ceria-containing

catalysts is known to be responsible for the intrinsic property of  $\text{CeO}_2$  forms in TWC formulations because it acts as an oxygen buffer by storing and releasing oxygen under controlled conditions<sup>55-57</sup>. According to Bueno-Lopez et al.<sup>58</sup> the performance of  $\text{CeO}_2$  in the soot oxidation is related to the oxygen storage capacity and the redox cycle created during the oxidation process through the formation of new highly reactive “active oxygen”. The promoting effect of ceria on lanthana in oxidative methane coupling is correlated to the presence of oxygen vacancies since the concentration of oxygen vacancies is high in crystals with a cubic lattice. Presence of transition metal impurity ions in the crystal lattice also affects the efficiency through oxidative transformations. These ions can present the lacking electrons required for dioxygen activation, during which the catalyst donates and an oxygen molecule accepts at least one electron.

Cerium is the most abundant of the rare earths and is characterized chemically by having two valence states, the 3+ cerous and 4+ ceric states. The ceric state is the only non-trivalent rare earth ion stable in aqueous solutions and is also a strong oxidizer. Variable valency of the ions especially  $\text{Ce}^{3+/4+}$  usually lead to nonstoichiometric  $\text{CeO}_{2-x}$ . This aspect and the defect structure on ceria were due to oxygen vacancies accompanied by triply and/or quadruply ionized Ce interstitial to maintain electrical neutrality. Later these oxygen vacancies have been affirmed as the prevailing defects neglecting the negligible effect of Ce interstitials in such a fluorite structure oxide system. The availability of these defect sites at the surface is related to its high bulk concentration. Variable-valence cerium ions can favour the formation of oxygen active sites  $\text{O}_{(\text{sur})}^-$ , which are stabilized near cation vacancies through

the reaction shown in scheme 2.3 and this additional dioxygen activation pathway lead to an increase in the activity of the catalyst<sup>59,60</sup>.



**Scheme 2.3**

Praseodymium is next to cerium in the Periodic Table and also has multiple stable oxidation states of 3+ and 4+. It possesses several oxide forms such as PrO<sub>2</sub>, hexagonal Pr<sub>2</sub>O<sub>3</sub> and cubic Pr<sub>6</sub>O<sub>11</sub>. Partially reduced ceria is relatively easy to reoxidize than praseodymia, even though it undergoes similar structural changes upon oxidation and reduction. One possible explanation is that the structural changes from cubic to hexagonal do not occur upon reduction of the active form of ceria like praseodymia. Oxidation from hexagonal Pr<sub>2</sub>O<sub>3</sub> (Pr<sup>3+</sup>) to the cubic Pr<sub>6</sub>O<sub>11</sub> (Pr<sup>4+</sup>) is a highly activated process after complete reduction while incomplete reduction of ceria to CeO<sub>2-x</sub> having the cubic form is known and reduction to the hexagonal form does not occur in this case. The ΔH for the reaction 4PrO<sub>2</sub> → 2Pr<sub>2</sub>O<sub>3</sub> + O<sub>2</sub> is 45 kcal/mol and for 4CeO<sub>2</sub> → 2Ce<sub>2</sub>O<sub>3</sub> + O<sub>2</sub> is 178 kcal/mol at 800 K, latter is too large compared to former one for O<sub>2</sub> desorption to occur. This energy difference may well be that required for the structural change to the hexagonal form and possibly, praseodymia does not form the same types of intermediate structure, as does ceria<sup>61-64</sup>. Moreover, praseodymium has been chosen being one of the materials under investigation in the field of oxygen-storage materials because it

undergoes oxygen exchange at a lower temperature than cerium oxide and its oxygen storage capacity is not diminished by high temperature of sintering<sup>65-67</sup>.

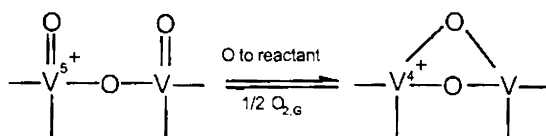
There are many reports concerning the redox property and the relation between it and catalytic performance of vanadium-supported oxide catalysts in the past two decades<sup>68-76</sup>. During chemical reactions,  $V^{5+}$  can be reduced to  $V^{4+}$  or  $V^{3+}$ . According to Haber et al.<sup>77</sup> and Erdohelyi et al.<sup>78</sup>  $V^{5+}$  was reduced to  $V^{3+}$  on  $TiO_2$ , while  $V^{5+}$  was only reduced to  $V^{4+}$  on  $SiO_2$  and  $Al_2O_3$ . Recently, Arena et al.<sup>79</sup> studied the structure and dispersion of supported-vanadia catalyst by  $H_2$ -TPR and indicated the reduction sequence: defective coordinatively unsaturated surface V ion > Td isolated vanadyls > bidimensional polymeric vanadyls > three-dimensional cluster or crystalline  $V_2O_5$ . The presence of other transition metals can enhance the extent of reduction.

## 2.5 VANADIA IN OXIDATION CATALYSIS

Special chemistry of vanadium oxides and vanadium oxide based catalysts results from a number of different interrelated electronic and structural factors. Vanadium oxide is a well-known catalyst among various metal oxides, and so many fundamental studies have been developed wide-spreadingly centering on catalytic oxidation. This has partially filled d-orbitals ( $V^{5+}$ ,  $3d^0$ ), which are responsible for a wide variety of electronic, magnetic and catalytic properties. Metals in its higher oxidation states readily release lattice oxygen, formally as  $O^{2-}$ . Vanadium atoms exist in different formal oxidation states, which vary from two to five. The ability of vanadium atoms to possess multiple oxidation states results in the easy conversion between oxides of different stoichiometry and is believed to be an important factor for the oxide



to function as catalyst in selective oxidation<sup>80</sup>. Reactions of partial oxidation on vanadium oxides were considered to base on the redox mechanism, Mars-van Krevelen cycle. The active sites were reported to be the  $V^{5+}=O$  species and it was found that the rate of oxidation depends on the number of  $V=O$  bonds on the surface. The decisive step is the transition of  $V^{5+}$  into the lower oxidation state  $V^{4+}$ . Monolayer vanadia is found to be more active than bulk  $V_2O_5$  in several reactions. However, the reasons for its high catalytic activity and high selectivity toward partial oxidation products are still not clear<sup>81-83</sup>.



**Scheme 2.4**

Many vanadium compounds are known to have interesting catalytic properties: Thus,  $V^{5+}$  complexes are catalysts in the synthesis of polymers like polyethylene, and vanadium oxide is one of the most important oxidation catalysts in industrial production, e.g. for the synthesis of sulphuric acid<sup>85</sup>. The first use of a vanadium compound for the catalytic oxidation of hydrocarbons was reported in 1937 by Milas<sup>86</sup>, who was studied the hydroxylation of alkenes by  $V_2O_5$  and hydrogen peroxide. As a commercial catalyst for selective oxidation of benzene, naphthalene, *o*-xylene or methanol, vanadium oxide has been watched for a long time<sup>87</sup>. Recently it is also used in the preparation of malicanhydride from 1-butene or *n*-butane<sup>88</sup>. Since this date, many  $V^{5+}$  and  $V^{4+}$  compounds have been used to catalyze the oxidation of alcohols, alkenes, aromatics and thioethers with hydrogen peroxide<sup>89</sup>. Vanadium containing

catalysts were found to be active in a number of oxidation reactions, while the activity depends strongly on the preparation methods, supports as well as the vanadium sources<sup>90,91</sup>. Vanadium phosphate catalysts represent a class of materials that are amongst the most well studied and characterized heterogeneous catalysts and have been used extensively as commercial heterogeneous catalyst for the oxidation of alkanes<sup>92-101</sup>. Supported vanadium oxide catalysts have attracted much attention in recent years as promising model catalysts for the oxidation and oxidative dehydrogenation of C<sub>2</sub>-C<sub>4</sub> alkanes. Various factors such as reducibility, acidity-basicity, support effect, coordination geometry and aggregation state (polymerization degree or VO<sub>x</sub> domain size) of the surface vanadium oxide species have been associated with the catalytic activity and selectivity of the supported vanadia catalysts. It is generally accepted that during oxidation reactions, the active surface V sites undergo a redox cycle. The degree of reduction of the catalyst under steady-state reaction conditions is thus associated with the equilibrium of reduction and reoxidation of the active sites. The degree of reduction of the catalysts, which has been associated with the increase in the binding strength of surface lattice oxygen, was proposed to be the major factor determining the reaction rates of butane oxidation and the selectivity to partial oxidation products. For well-dispersed vanadium oxide species on oxide supports, two types of vanadium oxide species are generally identified: isolated and polymeric vanadium oxide species. The ratio of polymerized to isolated surface vanadia species depends on the vanadia loading, the support surface area, and the specific nature of the support<sup>102</sup>.

In general, supported vanadia catalysts are one of the most active and attractive catalyst for light alkane ODH. Several studies address the structure and the oxidation state of supported vanadia catalysts during hydrocarbon oxidation reactions<sup>103,104</sup>. Studies under reaction conditions provide new insights into the behaviour of surface vanadia species during hydrocarbon oxidation reactions: (i) the hydrated surface  $V^{5+}$  species appears to be the predominant surface species, and (ii) the extent of reduction of the surface vanadia species depends on the reducing power of the hydrocarbon, the specific oxide support, and the ratio of polymeric to isolated surface vanadia species<sup>105</sup>.

## 2.6 LEACHING OF CATALYSTS

Most new redox catalysts belong to the class of porous mixed oxides of crystalline or amorphous nature. An ever-popular subject of concern associated with these materials is the stability of the active sites in the catalysts under reaction conditions. The oxidation in the liquid phase with organic hydroperoxides or even  $H_2O_2$  are very often subject of leaching phenomena and the question about true nature of the catalytic reaction is a serious one. Leaching can occur during a catalyzed reaction without an induction period and the nature of a reaction may gradually change from heterogeneous to homogeneous<sup>106</sup>. Leaching is much more rapid than the catalysis itself, in which case there would be exclusively homogeneous catalysis<sup>107</sup>. On the leaching of V from various V-HMS-catalysts during oxidation with  $H_2O_2$  it was reported that leaching occurs only in the presence of substrate under experimental conditions. Leaching also detected with the use of TBHP as

oxidant. In supported vanadium catalysts, the stability of vanadium during liquid phase reactions is found to depend on the nature of the substrate, the solvent and the oxidant. None of the vanadium containing aerogels or xerogels tested was found to resistant towards dilute  $\text{H}_2\text{O}_2$ . According to Rohan et al.<sup>108</sup> none of the titania supported vanadia catalysts are stable to leaching in the reaction conditions, but there are strong evidence to show that the reactivity originates from the heterogeneous form of vanadium oxide present. Leaching of vanadium oxide catalysts during the oxidation of 2-butanol has been reported to depend solely on the presence of  $\text{H}_2\text{O}_2$  even though most of the catalytic activity observed has to be attributed to heterogeneous catalysis<sup>109</sup>. In the literature we found no evidence for vanadium oxide containing catalysts, which have been documented not to leach under liquid phase oxidation conditions. However, leaching is less of a problem with Ti-Si mixed oxides, such as xerogels, aerogels or TS-1 and related Ti-zeolites. Under nonpolar reaction conditions with organic hydroperoxides as oxidants these mixed oxide catalysts show little to no leaching effects<sup>110</sup>. However, suitable choice of the dispersing medium and careful tuning of the preparation procedure help to disperse the active metal form without undesired crystalline oxide species, thus leaching can be minimized.



REFERENCES

- [1] J.R. Kosak, T.A. Johnson, *Catalysis of Organic Reactions*, Marcel Dekker Inc, New York (1994).
- [2] B. Klortz, I. Barnes, B.T. Golding, K.H. Becker, *Phys. Chem. Chem. Phys.* 2 (2000) 227.
- [3] A. Mellouki, F. Oussar, X. Lun, A. Chakir, *Phys. Chem. Chem. Phys.* 6 (2004) 2951.
- [4] J. Peng, F. Shi, Y. Gu, Y. Deng, *Green Chem.* 5 (2003) 224.
- [5] T. Ataloglou, J. Vakkas, K. Bourikas, C. Fountzoula, C. Kordulis, A. Lycourghiotis, *Appl. Catal. B: Environ.* 57 (2005) 299.
- [6] Z. Hou, B. Han, L. Gao, Z. Liu, G. Yang, *Green Chem.* 4 (2002) 426.
- [7] F. Shirini, M.A. Zolfigol, M. Khaleghi, *Bull. Korean Chem. Soc.* 24 7 (2003) 1021.
- [8] V. Kesavan, D. Dhar, Y. Koltypin, N. Perkas, O. Palchik, A. Gedanken, S. Chandrasekaran, *Pure Appl. Chem.* 73 1 (2001) 85.
- [9] U.R. Pillai, E.S. Demessie, *New J. Chem.* 27 (2003) 525.
- [10] M. Hayashi, K. Yamada, S. Nakayama, H. Hayashi, S. Yamazaki, *Green Chem.* 2 (2000) 257.
- [11] I. Belkhir, A. Germain, F. Fajula, E. Fache, *J. Chem. Soc., Faraday Trans.* 94 12 (1998) 1761.
- [12] C.M. Ho, T.C. Lau, *New J. Chem.* 24 (2000) 587.
- [13] U.R. Pillai, Endalkachew, *Chem. Commun.* 18 (2002) 2142.
- [14] S.E. Dapurkar, A. Sakthivel, P. Selvam, *New J. Chem.* 27 (2003) 1184.
- [15] V.I. Avdeev, S.P. Ruzankin, G.M. Zhidomirov, *Chem. Commun.* (2003) 42.
- [16] E. Selli, A. Isernia, L. Forni, *Phys. Chem. Chem. Phys.* 2 (2000) 3301.
- [17] E.J.M. Hensen, Q. Zhu, R.A. van Santen, *J. Catal.* 233 (2005) 136.
- [18] J. Jia, K.S. Pillai, W.M.H. Sachtler, *J. Catal.* 221 (2004) 119.
- [19] G.D. Vulpescu, M. Ruitenbeek, L.L. van Lieshout, L.A. Correia, D. Meyer, Paul P.A.C. Pex, *Catal. Commun.* 5 (2004) 347.
- [20] K.M. Choi, S. Ikeda, S. Ishino, K. Ikeue, M. Matsumura, B. Ohtani, *Appl. Catal. A: Gen.* 278 (2005) 269.
- [21] N. Ma, Z. Ma, Y. Yue, Z. Gao, *J. Mol. Catal. A: Chem.* 184 (2002) 361.
- [22] C. Palazzi, L. Olivia, M. Signoretto, G. Strukul, *J. Catal.* 194 (2004) 286.
- [23] S. Biella, M. Rossi, *Chem. Commun.* (2003) 378.

- [24] J.E. Remias, T.A. Pavlosky, Ayusman, J. Mol. Catal. A: Chem. 203 (2003) 179.
- [25] R. Noyori, M. Aoki, K. Sato, Chem. Commun. (2003) 1977.
- [26] U.R. Pillai, E.S. Demessie, Green Chem. 6 (2004) 161.
- [27] T. Iwahama, G. Hatta, S. Sakaguchi, Y. Ishii, Chem. Commun. (2000) 163.
- [28] J.M. Fraile, J.I. Garcia, J.A. Mayoral, E. Vispe, Appl. Catal. A: 245 (2003) 363.
- [29] E.L. Pires, M. Wallau, U. Schuchardt, J. Mol. Catal. A: Chem. 144 1 (1999) 91.
- [30] J. Chisem, I.C. Chisem, J.S. Rafelt, D.J. Macquarrie, J.H. Clark, Chem. Commun. (1997) 2203.
- [31] A. Corma, V. Fornes, S. Iborra, M. Mifsud, M. Renz, J. Catal. 221 (2004) 67.
- [32] J. Zhang, Y. Tang, G. Li, C. Hu, Appl. Catal. A: Gen. 278 (2005) 251.
- [33] K. Nomiya, K. Yagishita, Y. Nemoto, T.A.K. Matakai, J. Mol. Catal. A: Chem. 126 (1997) 43.
- [34] C.W. Lee, W.J. Lee, Y.K. Park, S.E. Park, Catal. Today 61 (2003) 137.
- [35] R.S. da Cruz, J.M. de Silva, U. Arnold, M.S. Sercheli, U. Schuchardt, J. Braz. Chem. Soc. 13 2 (2002) 170.
- [36] P. Brandao, A. Valente, A. Ferreira, V.S. Amaral, J. Rocha, Microp. Mesop. Mater. 69 (2004) 209.
- [37] A. Sakthivel, P. Selvam. J. Catal. 211 (2002) 13438.
- [38] B.K. Hodnett, Heterogeneous Catalytic Oxidation: Fundamental and Technological Aspects of the selective and Total Oxidation of Organic Compounds, John Wiley, New York (2000).
- [39] J. Hagen, Industrial Catalysis: A Practical Approach, New York, Wiley-VCH, (1999).
- [40] A.K. Suresh, M.M. Sharma, T. Sridhar, Ind. Eng. Chem. Res. 39 (2000) 3958.
- [41] S. Mohebbi, D.M. Boghaei, A.H. Sarvestani, A. Salimi, Appl. Catal. A: Gen. 278 (2005) 263.
- [42] S.I. Murahashi, N. Komiya, Y. Hayashi, T. Kumano, Pure Appl. Chem. 73 2 (2001) 311.
- [43] F. Gao, R. Hua, Appl. Catal. A: Gen. 270 (2003) 223.
- [44] H.H. Monfared, Z. Amouei, J. Mol. Catal. 217 1-2 (2004) 161.
- [45] S. Larrondo, B. Irigoyen, G. Baronetti, N. Amadeo, Appl. Catal. A: Gen. 250 (2003) 279.
- [46] P. Mars, D.W. van Krevelen, Chem. Eng. Sci. 3 (1954) 41.

- [47] M. Ruitenbeek, A.J. van Dillen, F.M.F. de Groot, I.E. Wachs, J.W. Geus, D.C. Koningsberger, *Topics in Catalysis* 10 (2000) 241.
- [48] G.I. Golodets, *Stud. Surf. Sci. Catal.* 55 (1990) 693.
- [49] K.V.R Chary, K.R. Reddy, T. Bhaskar, G.V. Sagar, *Green Chem.* 4 (2002) 206.
- [50] A. Piras, S. Colussi, A. Trovarelli, V. Sergo, J. Llorca, R. Psaro, L. Sordelli, *J. Phys. Chem. B* 109 (2005) 11110.
- [51] B. Renard, J. Barbier Jr, D. Duprez, S. Durecu, *Appl. Catal. B: Environ.* 55 (2005) 1.
- [52] M.M. Mohamed, S.M.A. Katib, *Appl. Catal. A: Gen.* 287 (2005) 236.
- [53] R. Niewa, Z. Hu, C. Grazioli, U. Robler, M. S Golden, M. Knupfer, J. Fink, H. Giefers, G. Wortmann, F.M.F. de Groot, F.J.D. Salvo, *J. Alloys Comp.* 346 (2002) 129.
- [54] F. Zhang, S.W. Chan, J.E. Spanier, E. Apak, Q. Jin, *Appl. Phys. Lett.* 80 1 7 (2002) 127.
- [55] E. Abi-Aad, R. Bechara, J. Grimblot, A. Aboukais, *Chem. Mater.* 5 (1993) 793.
- [56] B.M. Reddy, A. Khan, Y. Yamada, T. Kobayashi, S. Loridant, J.C. Volta, *J. Phys. Chem. B.* 106 (2002) 10964.
- [57] J. Matta, D. Courcot, E. Abi-Aad, A. Aboukais, *Chem. Mater.* 14 (2002) 4118.
- [58] A.B. Lopez, K. Krishna, M. Makke, J.A. Moulijn, *J. Catal.* 230 1 (2005) 237.
- [59] A.G. Dedov, A.S. Loktev, V.A. Menshchikov, M.N. Kartasheva, K.V. Parkhomenko, Academician I.I. Moiseev, *Doklady Chem.* 380 4-6 (2001).
- [60] D.M. Lyons, K.M. Ryan, M.A. Morris, *J. Mater. Chem.* 12 (2002) 1207.
- [62] E.S. Putna, J.M. Vohs, R.J. Gorte, G.W. Graham, *Catal. Lett.* 54 (1998) 17.  
S. Rossignol, C. Descorme, C. Kappenstein, D. Duprez, *J. Mater. Chem.* 11 (2001) 2587.
- [63] Y. Kaneko, S. Mori, J. Yamanaka, *Solid State Ionics* 151 (2002) 35.
- [64] D. Wolfframm, M. Ratzke, M. Kappa, M.J. Montenegro, M. Dobeli, T. Lippert, J. Reif, *Mater. Sci. Eng. B* 109 (2004) 24.
- [65] A.B. Corradi, F. Bondioli, A.M. Ferrari, *Chem. Mater.* 13 (2001) 4550.
- [66] C.K. Narula, J.E. Allison, D.R. Bauer, H.S. Gandhi, *Chem. Mater.* 8 (1996) 984.

- [67] A.D. Logan, M. Shelef, *J. Mater. Res.* 9 (1994) 468.
- [68] I.L. Botto, M. Vassallo, G. Fierro, D. Cordischi, M. Inversi, G. Minelli, *J. Mater. Chem.* 7 11 (1997) 2279.
- [69] P. Kornelak, F. Mizukami, A.W. Birczynska, L. Proniewicz, G.D. Mariadassou, A. Bialas, M. Najbar, *Catal. Today* 90 (2004) 103.
- [70] S. Besselmann, C. Freitag, O. Hinrichsen, M. Muhler, *Phys. Chem. Chem. Phys.* 3 (2001) 4633.
- [71] M. Kantcheva, *Phys. Chem. Chem. Phys.* 2 (2000) 3043.
- [72] F. Prinetto, G. Ghiotti, M. Occhiuzzi, V. Indovina, *J. Phys. Chem. B* 102 (1998) 10316.
- [73] L.J. Burcham, I.E. Wachs, *Catal. Today* 49 (1999) 467.
- [74] R. Neumann, M.L. Elad, *Appl. Catal. A: Gen.* 122 (1995) 85.
- [75] D. Andreeva, R. Nedyalkova, L. Ilieva, M.V. Abrashev, *Appl. Catal. A: Gen.* 246 (2003) 29.
- [76] Z. Zhao, Y. Yamada, A. Ueda, H. Sakurai, T. Kobayashi, *Catal. Today* 93-95 (2004) 163.
- [77] Harber, A.J. Kozłowska, R. Kozłowski, *J. Catal.* 102 (1986) 52.
- [78] A. Erdohely, F. Solymosi, *J. Catal.* 123 (1990) 31.
- [79] F. Arena, F. Frusteri, A. Parmaliana, *Appl. Catal. A* 176 (1999) 189.
- [80] M. Ishida, Y. Masumoto, R. Hamada, S. Nishiyama, S. Tsuruya, M. Masai, *J. Chem. Soc., Perkin Trans. 2* (1999) 847.
- [81] R. Dziembaj, J. Lojewska, T. Lojewski, *Solid State Ionics* 117 (1999) 87.
- [82] C.T. Au, W.D. Zhang, *J. Chem. Soc., Faraday Trans.* 93 6 (1997) 1195.
- [83] N. R. Shiju, M. Anilkumar, S.P. Mirajkar, C.S. Gopinath, B.S. Rao, C.V. Satyanarayana, *J. Catal.* 230 (2005) 493.
- [84] J. Haber, M. Witko, R. Tokarz, *Appl. Catal. A: Gen.* 157 (1997) 3.
- [85] N.N. Greenwood, A. Earnshaw, (Eds.), *Chemistry of the Elements*, Butterworth-Heinemann, Oxford (1997).
- [86] N.A. Milas, *J. Am. Chem. Soc.* 59 (1937) 2342.
- [87] F. Javier C. Sanchez, J.A.L. Sanchez, R.P.K. Wells, C. Rhodes, A.Z. Isfahani, G.J. Hutchings, *Catal. Lett.* 77 4 (2001) 189.
- [88] V. Conte, F.D. Furia, G. Licini, *Appl. Catal. A: Gen.* 157 (1997) 335.
- [89] P. Selvam, S.E. Dapurkar, *J. Catal.* 229 (2005) 64.
- [90] A.T. Radosevich, C. Musich, F.D. Toste, *J. Am. Chem. Soc.* 127 (2005) 1090.
- [91] G.J. Hutchings, J.A.L. Sanchez, J.K. Bartley, J.M. Webster, A. Burrows, C.J. Kiely, A.F. Carley, C. Rhodes, M. Havecker, A.K. Gericke, R.W. Mayer, R.



- Schlogl, J.C. Volta, M. Poliakoff, *J. Catal.* 208 (2002) 197.
- [92] J.K. Bartley, C.J. Kiely, R.P.K. Wells, G.J. Hutchings, *Catal. Lett.* 72 12 (2001) 99.
- [93] G.J. Hutchings, J.K. Bartley, J.M. Webster, J.A.L. Sanchez, D.J. Gilbert, C.J. Kiely, A.F. Carley, S.M. Howdle, S. Sajip, S. Caldarelli, C. Rhodes, J.C. Volta, M. Poliakoff, *J. Catal.* 197 (2001) 232.
- [94] R. Tanner, P. Gill, R. Wells, J.E. Bailie, G. Kelly, S.D. Jackson, G.J. Hutchings, *Phys. Chem. Chem. Phys.* 4 (2002) 688.
- [95] J.A.L. Sanchez, R. Tanner, P. Collier, R.P.K. Wells, C. Rhodes, G.J. Hutchings, *New J. Chem.* 26 (2002) 1613.
- [96] J.A.L. Sanchez, J.K. Bartley, R.P.K. Wells, C. Rhodes, G.J. Hutchings, *Appl. Catal. A: Gen.* 326 (2002) 323.
- [97] L. Thomas, R. Tanner, P. Gill, R. Wells, J.E. Bailie, G. Kelly, S.D. Jackson, G. Hutchings, *Phys. Chem. Chem. Phys.* 4 (2002) 4555.
- [98] X. Gao, M.A. Banares, I.E. Wachs, *J. Catal.* 188 (1999) 325.
- [99] Y.H. Kim, H.I. Lee, *Bull. Korean Chem. Soc.* 20 12 (1999) 1457.
- [100] D.A. Bulushev, L.K. Minsker, F. Rainone, A. Renken, *J. Catal.* 205 (2002) 115.
- [101] T. Garcia, B. Solsona, D.M. Murphy, K.L. Antcliff, S.H. Taylor, *J. Catal.* 229 (2005) 1.
- [102] M.D. Argyle, K. Chen, E. Iglesia, A.T. Bell, *J. Phys. Chem. B* 109 (2005) 2414.
- [103] C.L. Pieck, S. del Val, M.L. Granados, M.A. Banares, J.L.G. Fierro, *Langmuir* 18 (2002) 2642.
- [104] S. Shylesh, A.P. Singh, *J. Catal.* 228 (2004) 333.
- [105] M.V.M. Huerta, J.M. Coronado, M.F. Garcia, A.I. Juez, G. Deo, J.L.G. Fierro, M.A. Banares, *J. Catal.* 225 (2004) 240.
- [106] Y. Deng, C. Lettmann, W.F. Maier, *Appl. Catal. A: Gen.* 214 (2001) 31.
- [107] R.A. Sheldon, M. Wallau, I.W.C.E. Arends, U. Schuchardt, *Acc. Chem. Res.* 31 (1998) 485.
- [108] D. Rohan, B. K. Hodnett, *Appl. Catal. A: Gen.* 151 (1997) 409.
- [109] J.S. Reddy, P. Liu, A. Sayari, *Appl. Catal. A: Gen.* 148 (1996) 7.
- [110] C. H. Lee, T. S. Lin, C.Y. Mou, *J. Phys. Chem. B* 107 (2003) 2543.

## CHAPTER 3

### MATERIALS AND METHODS

#### Abstract

---

*Since heterogeneous catalysts are often highly non-uniform solids, correct sampling, sample preparation, choice of the support and of the /appropriate method are important if meaningful results are to be obtained. Both physical and chemical structure of a catalyst must be known if relationships between the material structure of the catalyst and activity, selectivity, and lifetime are to be revealed. The modern methods include classical procedures and state-of-art techniques for studying the physics and chemistry of surfaces. The physical properties of pore volume, BET surface area etc are nowadays routinely monitored in the production and use of industrial catalysts. The upper atomic layers often have a different composition to that in the catalyst bulk. Therefore, in order to understand heterogeneous catalysis, information about the nature and structure of the upper atomic layers is required. In this chapter we will encounter different chemicals used, methods of preparation and various techniques adopted for structural characterization of catalysts and discuss its capabilities and limitations.*

---

### 3.1 INTRODUCTION

Catalyst development and synthesis is located at the interface of chemistry, chemical reaction engineering and material science. Developing new green processes for the catalyst synthesis of industrially important chemicals is relevant in order to minimize the production of highly hazardous wastes. Efficient and simple preparation methods for heterogeneous catalysts are essential in the application of industrial processes. The surface properties, nature of adsorption sites and active sites were expected to vary over a wide range with nature of oxide supports and the supported phase. The catalytic properties of a surface are determined by its composition and structure on the atomic scale. Establishing empirical relations between the factors that govern catalyst composition, particle size and shape, and pore dimensions on one side, and catalytic performance on the other are extremely useful in the process of catalyst development. Thus, catalyst characterization is a lively and highly relevant discipline in catalysis. Information regarding the nature of surface as well as bulk active sites can be derived by the application of instrumental and chemical techniques. Numerous instrumental techniques are known today for the characterization of solid acid catalysts named a few viz. EDX, XRD, TGA/DTA, UV-vis DRS, EPR, FT-IR, FT-Raman, MAS NMR, SEM, TPD and TPR. The physical characterization provides an insight into the structure of different species and its interaction while chemical characterization leads to an insight into reactivity for the application of the catalysts in an industrial point of view.

### 3.2 CHEMICALS FOR CATALYST PREPARATION

The chemicals used for the preparation of catalysts are listed below in Table 3.1.

**Table 3.1**

Sl. No.	Chemicals	Company
1.	Cerium nitrate	Indian Rare Earths Ltd., Udyogamandal, Kerala (99.9%).
2.	Praseodymium nitrate	Indian Rare Earths Ltd., Udyogamandal, Kerala (99.9%).
3.	Rice husk	Rice Mill, Aluva, Kerala.
4.	Ammonium metavanadate	Central Drug House P. Ltd.
5.	Ammonia solution	Qualigens Fine Chemicals (25 %).
6.	Conc. HCl	s.d Fine Chem. Ltd.
7.	Oxalic acid	s.d Fine Chem. Ltd.

### 3.3 CATALYST PREPARATION

#### 1. Rare earth oxides:- Hydroxide method

Rare earth oxides were prepared by precipitation of hydroxides<sup>1</sup> from  $\text{RE}(\text{NO}_3)_3 \cdot 6\text{H}_2\text{O}$  (0.05 M) with 1:1 ammonia solution at  $\text{pH} = 10.3$ . The resulting hydroxide was filtered, washed and dried for about 12 h in a drying oven (~383 K). Calcination of hydroxides conducted at 773 K for 5 h under a flow of dried air in a muffle furnace to get oxides.

#### 2. Rice husk silica:- Incineration before acid leaching

Rice husk was obtained from a Rice Mill. The husk was first washed with distilled water to remove adhering materials, dried and followed an acid

leaching process<sup>2</sup>. The husk was treated with 10% solution of conc. HCl at its boiling point for 3 h. The digested husk was then washed with distilled water and dried in an oven at 383 K for 12 h. Pure amorphous white silica was obtained by burning this rice husk at 873 K in a muffle furnace for 6 h.

### **3. Silica promoted rare earth oxides:- Deposition precipitation**

Rice husk silica promoted rare earth oxides were prepared by a deposition precipitation method<sup>3</sup>. In this method, the requisite quantities of RE (NO<sub>3</sub>)<sub>3</sub>.6H<sub>2</sub>O, dissolved separately in distilled water, and colloidal silica were mixed together. Dilute 1:1 ammonia solution was added dropwise to this mixture with vigorous stirring until the precipitation was complete at pH=10.3. The resulting product was filtered off, washed with distilled water, oven dried at 383 K for 12 h and then calcined at 773 K for 5 h in air.

### **4. Supported vanadia catalysts:- Wet impregnation method**

To impregnate vanadium oxide, the requisite quantity of ammonium metavanadate (0.001 M) was dissolved in aqueous oxalic acid solution (0.1 M). To this clear solution, the finely powdered dried support was added, stirred for 6 h at room temperature and kept overnight<sup>4</sup>. The excess water was evaporated with stirring, and the resulting material was oven dried at 383 K for 12 h and subsequently calcined at 773 K for 5 h in a muffle furnace in air atmosphere. Some portions of the finished catalyst were again heated at different temperatures for 5 h in air atmosphere.

Vanadium pentoxide was prepared from ammonium metavanadate by heating at 773 K for 5 h in a muffle furnace<sup>5</sup>.

## 3.4 CATALYSTS PREPARED

The catalysts prepared for the present work with its symbols are listed in Table 3.2.

Table 3.2

Sl. No.	Catalyst	Symbol
1.	CeO <sub>2</sub>	Ce
2.	Rice husk SiO <sub>2</sub>	RS
3.	CeO <sub>2</sub> -SiO <sub>2</sub>	CRS
4.	2 V <sub>2</sub> O <sub>5</sub> /CeO <sub>2</sub>	2VC
5.	4 V <sub>2</sub> O <sub>5</sub> /CeO <sub>2</sub>	4VC
6.	6 V <sub>2</sub> O <sub>5</sub> /CeO <sub>2</sub>	6VC
7.	8 V <sub>2</sub> O <sub>5</sub> /CeO <sub>2</sub>	8VC
8.	10V <sub>2</sub> O <sub>5</sub> /CeO <sub>2</sub>	10VC
9.	2 V <sub>2</sub> O <sub>5</sub> / CeO <sub>2</sub> -SiO <sub>2</sub>	2VCRS
10.	4 V <sub>2</sub> O <sub>5</sub> / CeO <sub>2</sub> -SiO <sub>2</sub>	4VCRS
11.	6 V <sub>2</sub> O <sub>5</sub> / CeO <sub>2</sub> -SiO <sub>2</sub>	6VCRS
12.	8 V <sub>2</sub> O <sub>5</sub> / CeO <sub>2</sub> -SiO <sub>2</sub>	8VCRS
13.	10 V <sub>2</sub> O <sub>5</sub> / CeO <sub>2</sub> -SiO <sub>2</sub>	10VCRS
14.	V <sub>2</sub> O <sub>5</sub>	V
15.	6 V <sub>2</sub> O <sub>5</sub> / SiO <sub>2</sub>	6VRS
16.	6 V <sub>2</sub> O <sub>5</sub> / SiGel	6VSG
17.	Pr <sub>2</sub> O <sub>3</sub>	Pr
18.	Pr <sub>2</sub> O <sub>3</sub> -SiO <sub>2</sub>	PRS
19.	2 V <sub>2</sub> O <sub>5</sub> /Pr <sub>2</sub> O <sub>3</sub>	2VP
20.	6 V <sub>2</sub> O <sub>5</sub> /Pr <sub>2</sub> O <sub>3</sub>	6VP
21.	10 V <sub>2</sub> O <sub>5</sub> /Pr <sub>2</sub> O <sub>3</sub>	10VP
22.	2 V <sub>2</sub> O <sub>5</sub> /Pr <sub>2</sub> O <sub>3</sub> -SiO <sub>2</sub>	2VPRS
23.	6 V <sub>2</sub> O <sub>5</sub> /Pr <sub>2</sub> O <sub>3</sub> -SiO <sub>2</sub>	6VPRS
24.	10 V <sub>2</sub> O <sub>5</sub> /Pr <sub>2</sub> O <sub>3</sub> -SiO <sub>2</sub>	10VPRS

### 3.5 CHARACTERIZATION TECHNIQUES

Several approaches can be adopted to investigate fundamental relations between the state of a catalyst and its catalytic properties. By using the appropriate combination of analysis techniques, the desired characterization on the atomic as well as bulk scale is certainly possible<sup>9</sup>. Various techniques are presented in Table 3.3.

**Table 3.3**

Technique	In	Out	Information
X-ray Diffraction	X-ray	X-ray	Bulk structure, Particle Size
Energy Dispersive X-Ray	e-	X-ray	Composition
Infrared Spectroscopy Diffused Reflectance	Photon	Photon	Molecular Vibrations
Spectroscopy	UV	e-	Chemical bonding
Raman Spectroscopy	Light	Light	Molecular Vibrations
Scanning Electron Microscopy	e-	e-	Morphology
Temperature Programmed Reduction	Heat + Gas	Gas	Mechanism of Surface and Bulk Reactions
Temperature Programmed Desorption	Heat + Gas	Gas	Mechanism of Surface and Bulk Reactions

Chemicals used for the physico-chemical characterization of catalysts are listed in Table 3.4.

Table 3.4

Sl. No.	Chemicals	Company
1.	Conc. H <sub>2</sub> SO <sub>4</sub>	s.d Fine Chem. Ltd.
2.	Sodium carbonate	Merck
2.	Cyclohexanol	Central Drug House P. Ltd.
3.	Liquid Nitrogen	Sterling Gases Pvt. Ltd.
4.	Magnesium oxide	Merck

### 3.6 SURFACE AND PHYSICO-CHEMICAL ANALYSIS

#### 3.6.1 Energy dispersive X-ray analysis

The chemical compositions of catalysts were determined using energy dispersive X-ray analyzer (EDX). This technique is used in conjunction with SEM. An electron beam strikes the surface of a conducting sample. The energy of the beam is typically in the range 10-20 k eV. This causes X-rays to be emitted from the point of the material. The energy of the X-rays emitted depends on the material under examination. The X-rays are generated in a region about 2 microns in depth. By moving the electron beam across the material an image of each element in the sample can be acquired. The detector used in EDX is the Lithium drifted Silicon detector. This detector must be operated at liquid nitrogen temperature. When an X-ray strikes the detector, it will generate a photoelectron within the body of the Si, as this photoelectron travels through the Si, it generates electron-hole pairs. The electrons and holes are attracted to opposite ends of the detector with the aid of a strong electric field. The size of the current pulse thus generated depends on the number of electron-hole pairs created, which in turn depends on the energy of the incoming X-ray. Thus, an X-ray spectrum can be acquired giving information



on the elemental composition of the material under examination. The Si-Li detector is often protected by a Beryllium window. The absorption of the soft X-rays by Be precludes the detection of elements below an atomic number of 11 (Na). In windowless systems, elements with as low atomic number as 4 (Be) have been detected, but the problems involved get progressively worse as the atomic number is reduced<sup>4</sup>. The chemical compositions of catalysts were obtained from Stereoscan 440 Cambridge, UK energy dispersive X-ray analyzer used in conjunction with SEM.

### **3.6.2 Powder X-ray diffraction**

Powder X-ray diffraction (XRD) is a standard method for the characterization of catalysts and generally has been used to determine the crystalline phases, including solid solutions, that are present and to measure the particle size and shape. Monochromatic X-rays, incident on a crystalline solid, are diffracted owing to the crystal structure of the solid<sup>6</sup>. For a maximum to occur in the diffraction pattern at a particular angle of incidence  $\theta$  (with respect to lattice planes (hkl)), the Bragg equation must be satisfied:

$$n\lambda = 2 d_{hkl} \sin \theta_{hkl}$$

where;

$d_{hkl}$  -interplanar distance between (hkl) planes, n-order of diffraction and  $\lambda$  = wavelength of incident X-rays

Crystallite size was calculated using the Scherrer equation,

$$L = (0.9\lambda 180)/(\pi \text{ FWHM}_{hkl} \cos \theta)$$

where;

$\text{FWHM}_{hkl}$  is the full width at half-maximum of an  $hkl$  peak at  $\theta$  value.

Powder X-ray diffraction data were recorded using Rigaku D-Max Ni filtered Cu K $\alpha$  radiation ( $\lambda = 1.5418 \text{ \AA}$ ) diffractometer equipped with a diffracted beam monochromator at a scan rate of 4°/min. Peak width at half-height was used to assess the relative crystallinity of the materials.

### 3.6.3 BET surface area and pore volume

Brunauer Emmett and Teller developed the famous BET equation for the determination of the surface area of a solid<sup>7</sup>. The method is based on non-specific physisorption of a gas (N<sub>2</sub> or Ar) onto a solid close to the condensation temperature of the adsorbing gas. Adsorption is characterized by an isotherm, which represents the equilibrium amount of gas adsorbed on a solid at a given temperature as a function of pressure. The BET equation extends the Langmuir isotherm to multilayer adsorption,

$$p/V (p_0 - p) = 1/V_m C + (C-1)p/CV_m p_0$$

where;

V: the volume, reduced standard conditions (STP) of gas adsorbed per unit mass of adsorbent at a given pressure, p and constant temperature, p<sub>0</sub>: the saturation pressure at the measurement temperature, V<sub>m</sub>: volume of gas adsorbed at STP per unit mass of adsorbent, when the surface is covered by a unimolecular layer of adsorbate, and C: a constant, related to the free energy of adsorption.

According to this equation, a plot of p/V (p<sub>0</sub> - p) versus p/p<sub>0</sub> should yield a straight line. The surface area is then calculated using:

$$S_{\text{BET}} = V_m A_m N_a / V_{\text{mol}}$$

where;

$N_a$ : Avogadro's number ( $6.0238 \times 10^{23}$ ),  $V_{mol}$ : molar volume of adsorbate gas at STP ( $22.41 \text{ mol}^{-1}$ ) and  $A_m$ : Cross sectional area of adsorbed gas,  $A_m (N_2) = 0.162 \text{ nm}^2$ .

When nitrogen is the adsorbing gas this reduces to:

$$S_{BET} = 4.353 V_m$$

BET surface areas and pore volume values of the catalysts were acquired by nitrogen adsorption and subsequent desorption at liquid nitrogen temperature (77 K) with a Micromeritics Flow Prep-060 Gemini 2360 instrument. After 1 h activation, the catalyst was degassed at 623 K for 3 h prior to analysis.

### **3.6.4 Thermal analysis**

Thermal analysis (TG/DTA/DTG) includes a group of techniques in which specific physical properties of a material are measured as a function of temperature. Thermogravimetric analysis (TGA) provides a quantitative measurement of any weight changes associated with thermally induced transitions. It can record directly the loss in weight as a function of temperature or time<sup>8</sup>. In TGA, the weight of sample is continuously recorded as the temperature is increased. Samples are placed in a crucible that is positioned in a furnace on a quartz beam attached to an automatic recording balance. The horizontal quartz beam is maintained in the null position by the current flowing through the transducer coil of an electromagnetic balance. Any change in the weight of the sample causes a deflection of the beam, which is sensed by one of the photodiodes connected to act as a position sensor to determine the movement of the beam. The beam is then restored to the original null position by a feedback current sent from the photodiodes to the coil of the balance and

the current is proportional to the change in weight of the sample. In differential thermal analysis (DTA), the difference in temperature between the sample and a thermally inert reference material is measured as a function of temperature usually the sample temperature. Any transition that the sample undergoes results in liberation or absorption of energy by the sample with a corresponding deviation of its temperature from that of the reference. A plot of the differential temperature,  $\Delta T$ , versus the programmed temperature,  $T$ , indicates the transition temperatures and whether the transition is exothermic or endothermic. When an endothermic change occurs, the sample temperature lags behind the reference temperature because of the heat in the sample. Exothermic behaviour is associated with the decrease in enthalpy of a phase or a chemical system. DTA and thermogravimetric analyses are often run simultaneously on a single sample.

TGA/DTG were collected on a *METTLER TOLEDO STARSYSTEM* TGA Q50 thermal analysis instrument under nitrogen atmosphere at heating rate of 20°C/ min from room temperature to 800°C. TGA/DTA were done on a Perkin Elmer Pyris Diamond thermogravimetric/differential thermal analyzer instrument under nitrogen atmosphere at heating rate of 20°C/ min from room temperature to 800°C with samples mounted on an alumina sample holder.

### 3.6.5 Scanning electron microscopy

Scanning electron microscopy (SEM) is a very widely used technique to study surface topography. High energy (typically 10 keV) electron beam is scanned across the surface. The incident electrons cause low energy secondary electrons to be generated, and some escape from the surface. The secondary

electrons emitted from the sample are detected by attracting them onto a phosphor screen. This screen will glow and the intensity of the light is measured with a photomultiplier<sup>9</sup>.

Secondary electron images were obtained on Cambridge Oxford 7060 scanning electron microscope connected to a 4-quadrant backscattered electron detector under a resolution of 1.38 eV coated with a layer of gold to minimum charge effects.

### **3.7 SPECTROSCOPIC METHODS**

#### **3.7.1 UV-vis Diffused reflectance spectroscopy**

The UV-vis-diffused reflectance spectroscopy (UV-vis DRS) is a suitable technique to study solids, particularly dispersed oxides and metal ions in constrained environment such as MCM, zeolites and clay materials to obtain information on the coordination, oxidation state etc. of the metal ions<sup>10</sup>. It can also provide the electronic structure of dispersed metal oxides. In situ UV-vis spectroscopy can probe the extent of reduction under steady state catalysis.

UV-vis DR spectra were taken in the range 200-800 nm on an Ocean Optics, Inc. SD 2000, Fiber Optic Spectrometer with a charged coupled device detector. The spectra were recorded at room temperature using MgO as a reference. Prior to measurement, the samples were pretreated for 1h at the calcination temperature.

#### **3.7.2 FT-Infrared spectroscopy**

Infrared spectroscopy (FT-IR) can be considered as the first and the most important of the modern spectroscopic techniques that has found general

acceptance in catalysis. Vibrations in molecules or in solid lattices are excited by the absorption of photons in infrared spectroscopy. Infrared spectroscopic investigations can be used to characterize active centers on catalysts surfaces and chemisorbed molecules. It involves examination of the twisting, bending, rotating and vibrational motions of atoms in a molecule. Upon interaction with infrared radiation, portions of the incident radiation are absorbed at specific wavelengths. The infrared spectrum of a compound is essentially the superposition of absorption bands of specific functional groups, yet subtle interactions with the surrounding atom of the molecule impose the stamp individually on the spectrum of each compound<sup>11</sup>.

Infrared spectra were recorded with KBr pellets on an ABB BOMEM (MB Series) FT-IR spectrometer model in the range 400-4000  $\text{cm}^{-1}$ .

### 3.7.3 FT-Raman spectroscopy

Raman spectroscopy (FT-Raman) is based on the inelastic scattering of photons, which lose energy by exciting vibrations in the sample. When monochromatic radiation is scattered by molecules, a small fraction of the scattered radiation is observed to have a different frequency from that of the incident radiation; this is known as the Raman effect (1928)<sup>12-14</sup>. Raman effect arises when a beam of intense monochromatic radiation passes through a sample contains molecules that undergo a change in molecular polarizability as they vibrate. Polarizability is the value of the induced dipole moment divided by the strength of the field that causes the induced dipole moment. Monochromatic light of frequency  $\nu_0$  falls on a sample, where the majority of the photons undergo Rayleigh scattering, i.e. scattering without energy

exchange. However, the excited molecule decays to the first vibrational level with frequency  $\nu_{\text{vib}}$ , it effectively takes an amount of energy equal to  $h\nu_{\text{vib}}$ , away from the photon. Scattered light exhibits change in intensity at frequency  $\nu_0 - \nu_{\text{vib}}$  and give rise to Stokes bands. If the collision with a photon brings a vibrationally excited molecule to the unstable state of energy  $h\nu_0 + h\nu_{\text{vib}}$  it may decay to the ground state, transferring a net amount of energy  $h\nu_{\text{vib}}$  to the photon, which leaves the sample with a higher frequency equal to  $\nu_0 + \nu_{\text{vib}}$ . This anti-Stokes bands, has much lower intensity than the Stokes band. A vibration is Raman active if it changes the polarizability of the molecule. This technique is highly suitable for *in situ* studies since the spectra of adsorbed species interfere weakly with signals from the gas phase, enabling studies under reaction conditions. Another advantage is that typical supports such as silica and alumina are weak Raman scatterers. This makes Raman spectroscopy a powerful tool to study catalytically active phases on a support<sup>15</sup>.

For the Raman spectra measurements the catalysts calcined at 773 K were introduced into a metallic sample holder. FT-Raman spectra were collected on Bruker FRA 106 FT-Raman Accessory and the RES 100 FT-Raman spectrometer.

#### 3.7.4 Electron paramagnetic resonance spectroscopy

Electron paramagnetic resonance (EPR) and electron spin resonance (ESR) can be viewed as two alternative names in a family of electron magnetic resonance (EMR) techniques. The measurements owe their origin to the magnetic properties of the electron, which since it has a magnetic moment (associated with the electron spin), will interact with an external magnetic field. Simply, the electron can behave like a small bar magnet when placed in a

magnetic field, trying to align itself with the external field. It is then possible to cause the electron to 'flip' from alignment with the external field, to alignment against the field by irradiation with suitable microwave radiation (Gigahertz,  $10^9$  Hz). Resonance techniques are generally used to measure this intriguing phenomenon<sup>16,17</sup>.

When the molecules of a solid exhibit paramagnetism as a result of unpaired electron spins, transitions can be induced between spin states by applying a magnetic field and then supplying electromagnetic energy, usually in the microwave range of frequencies. The resulting absorption spectra are described as electron spin resonance or electron paramagnetic resonance. Electron spin resonance has been used as an investigative tool for the study of radicals formed in solid materials, since the radicals typically produce an unpaired spin on the molecule from which an electron is removed. Particularly fruitful has been the study of the ESR spectra of radicals produced as radiation damage from ionizing radiation. Study of the radicals produced by such radiation gives information about the locations and mechanisms of radiation damage. EMR techniques are widely used to study paramagnetic centers on various solid surfaces and these centers may be surface defects, inorganic or organic radicals, metal cations or supported metal complexes and clusters.

The EPR spectra were acquired on a VARIAN E-line century series instrument at X-band. Analysis was conducted both at room and liquid nitrogen temperature.

### 3.7.5 Nuclear magnetic resonance spectroscopy ( $^{29}\text{Si}$ and $^{51}\text{V}$ MAS NMR)

Of the important spectroscopic aids that are at the disposal of the chemist for use in structure elucidation, nuclear magnetic resonance



spectroscopy ( $^{29}\text{Si}$  and  $^{51}\text{V}$  MAS NMR) is relatively recent. Nuclear magnetic resonance spectroscopy lies in the magnetic properties of atomic nuclei. The interaction of the nuclear magnetic moment of a nucleus with an external magnetic field  $B_0$ , leads, according to the rules of quantum mechanics, to a nuclear energy level diagram, because the magnetic energy of the nucleus is restricted to certain discrete values  $E_i$ , the so-called eigen values. Associated with the eigen values are the eigen states, which are the only states in which an particle can exist. Through a high frequency transmitter, transitions between eigen states within the energy level diagram can be stimulated. The absorption of energy can be detected, amplified and recorded as a spectral line, the so-called resonance signal. In this way a spectrum can be generated for a compound containing atoms whose nuclei have non-zero magnetic moments. Several resonance signals are found for various atoms in a molecule because the atoms reside in different chemical environments. The resonance signals are separated by a so-called chemical shift. Empirically determined correlation between the spectral parameters, chemical shift and spin-spin coupling and the structure of chemical compounds forms the basis for the application of nuclear magnetic resonance to the structural determination of unknown samples. In this respect the nuclear magnetic moment has proved itself to be a very sensitive probe with which one can gather extensive information<sup>18,19</sup>.

Nowadays  $^{51}\text{V}$  solid-state nuclear magnetic resonance spectroscopy ( $^{51}\text{V}$  MAS NMR) became a keystone technique for characterization of local structure of vanadium sites in different vanadium systems<sup>20,21</sup>. Modern NMR techniques such as ultra-high-speed MAS, MQMAS, SATRAS allow to obtain direct and precise information on the local structure of vanadium sites: (i) the

number of nonequivalent vanadium sites, (ii) coordination numbers, (iii) the nature of the atoms in the first coordination sphere, (iv) the distortion of this coordination sphere, (v) association of vanadium-oxygen polyhedron.  $^{51}\text{V}$  nucleus (natural abundance 99.76 %) has a spin quantum number of  $7/2$  and an electric quadrupole moment of  $0.05\text{b}$ , the relative intensity of  $^{51}\text{V}$  NMR signal is 0.38 compared to an equal number of protons. In presence of a magnetic field, each vanadium nucleus of solid diamagnetic samples experiences, in general, three different types of interaction: (i) dipole interaction of its magnetic moment with magnetic moments of other nuclei, (ii) quadrupole interaction of its electric quadrupole moment with the electric field gradient, (iii) chemical shielding anisotropy interaction. The extensive applicability of NMR to solids relies heavily on magic angle spinning (MAS) technique. This is able to narrow the lines by successful averaging dipolar, anisotropic chemical shielding and first order quadrupolar effects. In the case of vanadium, the small value of electric quadrupole moment moderates the quadrupolar interaction and simple MAS technique, has proven to be a very convenient technique for vanadium characterization.

The solid-state ( $^{29}\text{Si}$  and  $^{51}\text{V}$ ) MAS NMR experiments were performed at 78.9 MHz on a Bruker DSX-300 spectrometer (300 MHz) with a standard 4 mm double bearing Bruker MAS probe at room temperature. Experimental conditions employed are time domain points of 1024, line broadening parameter is 200-400 Hz, number of scans of about 1024-3600 and spinning speeds in the range of 5-10 kHz. The pulse lengths for the experiments were 15 ms whereas pulse delay was 1 s. The reference used for  $^{29}\text{Si}$  MAS NMR is tetra methyl silane whose chemical shift is 0 ppm. Isotropic chemical shifts for

$^{51}\text{V}$  MAS NMR are reported relative to neat  $\text{NH}_4\text{VO}_3$  ( $\delta_{\text{iso}} = -570.4$  ppm) as the reference.

### **3.8 REDUCTION AND ACIDITY DETERMINATION**

The reduction and acidic properties were measured with the use of temperature programmed techniques.

#### **3.8.1 Temperature programmed reduction**

Temperature programmed reduction (TPR- $\text{H}_2$ ) is a technique used for the chemical characterization of solids and has proved to be a powerful tool to analyze the reduction kinetics of oxide catalyst precursors<sup>22</sup>. It is highly sensitive and does not depend on any specific property of the solid under investigation other than its reducibility. The technique based on the reducibility of species in solids, enables one to obtain information not of a purely analytical nature and the condition of solids present in and on solids. This consists of heating the catalyst with a linear temperature ramp in a flow of hydrogen while monitoring the hydrogen consumption. In this way, fingerprint profiles are obtained which allow one to study the influence of the support and of promoters on the reducibility. Furthermore, the amount of reducible species in the catalyst and their degree of reduction can be derived from the integrated hydrogen consumption, and lumped kinetic parameters can be estimated if an adequate model of the reduction process exists. In a temperature programmed method, for a linear increase in temperature, the concentration of the reacting/desorbing particles is recorded as a function of temperature<sup>23,24</sup>.

Reduction is an inevitable step in the preparation of metallic catalysts. The reduction of a metal oxide  $\text{MO}_x$  by  $\text{H}_2$  is described by the equation,



As with every reaction, the reduction will proceed when the change in Gibbs free energy,  $\Delta G$ , has a negative value. Expression below shows how  $\Delta G$  depends on pressures and temperature,

$$\Delta G = \Delta G^\circ + n RT \ln [P_{\text{H}_2\text{O}}/P_{\text{H}_2}] \quad (\text{b})$$

where;  $\Delta G$ -change in Gibbs free energy for the reduction,  $\Delta G^\circ$ -same under standard conditions,  $n$ -stoichiometric coefficient,  $R$ -gas constant,  $T$ -temperature and  $P$ -partial pressure. If reduction of catalyst occurs under flowing hydrogen, the reaction product water is removed effectively and the second term in equation (b) is always negative.

TPR experiments were carried out on an Auto Chem 2910 (Micromeritics, USA) instrument. In a typical experiment, catalyst was taken in a U-shaped quartz sample tube. Prior to TPR studies, the catalyst sample was pretreated at 573 K for 1 h in argon (50 ml/min) in order to eliminate any impurities present. After pretreatment the sample was cooled to room temperature. The carrier gas that consists of 5% hydrogen balance argon (50 ml/min), which is purified by passing through oxy-trap and molecular sieves, was allowed to pass over the sample. The temperature was increased from ambient to 1173 K at a heating rate of 15 K/min and the data was recorded simultaneously<sup>25</sup>.

### 3.8.2 Temperature programmed desorption-NH<sub>3</sub>

Temperature programmed desorption (TPD) of probe molecules like ammonia or pyridine is a well-known method for the determination of acidity of solid heterogeneous catalysts as well as acid strength since it is easy and reproducible. In this, an inert gas is passed over a catalyst bed, while the

temperature is increased. A TPD profile is obtained by monitoring the gases, which are desorbed from the surface as the temperature is increased. The temperature of desorption is an indication of the strength of binding of the adsorbate<sup>26</sup>.

Acidity measurements were performed by temperature programmed desorption (TPD-NH<sub>3</sub>) of ammonia using a conventional flow apparatus. In a typical experiment, about 500 mg of catalyst was activated at 773 K for 1 h and kept in a tube. The sample was pretreated by passage of nitrogen at 573 K for 1 h. Subsequently catalyst was saturated with pure anhydrous ammonia gas and the system was allowed to attain equilibrium. After 30 min, the excess and physisorbed ammonia was subsequently flushed with flowing nitrogen. TPD analysis was then carried out by desorption of ammonia from 373 to 873 (K) at a heating rate of 293 K/min in nitrogen atmosphere and trapped in H<sub>2</sub>SO<sub>4</sub>. The amount of ammonia desorbed is calculated by titrating against NaOH.

### **3.8.3 Cyclohexanol decomposition**

This reaction is considered as a test reaction for acid-base properties of solid catalysts as well as a model reaction to determine the catalytic activity of metal oxides. It is generally accepted that the dehydration of cyclohexanol to cyclohexene occur on acid sites, while dehydrogenation to cyclohexanone is associated with both acid/base and redox sites<sup>27,28</sup>. However, recent reports indicated that both acid and basic sites were responsible for the dehydration processes in the gas-phase conversion of alcohols<sup>29</sup>. Acid-base properties of metal oxides were dependent on a number of variables such as metal salt, method of preparation, precipitation agent, calcination temperature and the effect of promoters. Stronger acid sites are found to be responsible for the

formation of methylcyclopentenes through the secondary reaction of cyclohexene and aromatization of cyclohexanol produced phenol in small quantities<sup>30</sup>.

The vapour phase cyclohexanol decomposition reaction was carried out at atmospheric pressure in a fixed bed down flow glass reactor at a temperature of 350 °C using nitrogen as the carrier gas. About 500 mg of the activated catalyst was packed between silica beads in the reactor with glass wool. The liquid reactant was fed into the reactor with the help of an injection pump at different flow rates. The products were analyzed by Chemito 8610 gas chromatography with FID detector by comparison with authentic standards. Analysis conditions are given in Table 3.4.

### 3.9 CATALYTIC OXIDATION OF AROMATICS

The chemicals used for the catalytic activity studies of prepared catalysts are listed below in Table 3.5 along with the company supplied.

**Table 3.5**

Sl. No.	Chemicals	Company
1.	Benzene	s.d Fine Chem. Ltd.
2.	Ethylbenzene	s.d Fine Chem. Ltd.
3.	Naphthalene	s.d Fine Chem .Ltd.
4.	Hydrogen peroxide (30%)	s.d Fine Chem. Ltd.
5.	Acetonitrile	Qualigens Fine Chemicals (99%).
6.	Acetone	Qualigens Fine Chemicals (99%).
7.	Acetic acid	Qualigens Fine Chemicals (99%).
8.	Dichloromethane	Qualigens Fine Chemicals (99%).

### **3.9.1 Liquid-phase oxidation of benzene, ethylbenzene and naphthalene**

The liquid-phase oxidation of aromatics was carried out in a 50 ml round bottom flask. The flask was immersed in an oil bath in order to make the working temperature constant, which was connected with a condenser. In a typical run, catalyst, and substrate were added to the solvent. The oxidant, 30%  $\text{H}_2\text{O}_2$  was added to the system after attaining the reaction temperature. The reaction mixture was stirred using a magnetic stirrer for the indicated reaction time. Then, the reaction products were analyzed by gas chromatograph equipped with flame ionization detector and BP-1 capillary column. Conversion rate and selectivity were calculated based on the relative area of each of authentic samples with standard ones. The reaction system consisted of two liquid phases: an organic phase containing substrate and solvent, and an aqueous layer containing solvent and  $\text{H}_2\text{O}_2$ . In quantitative analysis of products, the amounts contained in the organic phase are much more than in the aqueous layer; the latter amount was negligible<sup>31,32</sup>.

### **3.9.2 Oxidative dehydrogenation of ethylbenzene**

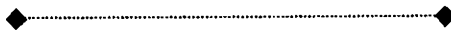
Oxidative dehydrogenation of ethylbenzene in vapour phase was conducted in a tubular, down flow reactor at atmospheric pressure. Reaction was performed in presence of air as oxidant. About 500 mg of the activated catalyst is placed in between a glass wool bed packed with silica beads in a glass reactor<sup>33</sup>. The temperature was controlled using a temperature controller. The reaction mixture was fed from the top of a syringe pump at controlled flow rate. Prior to the reaction, the catalyst was pretreated at 773 K for 2 h. The mass balance was noted wherever necessary. The hydrocarbon products were

collected to ice traps and analyzed with a gas chromatograph equipped with a flame ionization detector.

Analysis conditions of various reactions are presented in Table 3.6.

Table 3.6

Reaction	Capillary Column	Temperature (°C)		
		Injector	Detector	Programme of analysis
Cyclohexanol	BP-1	200	200	100 °C –Isothermal
Benzene	BP-1	200	200	60°C-3 min-20°/min-280 °C
Ethylbenzene	BP-1	250	250	60°C-3 min-20°/min-280 °C
Naphthalene	BP-1	250	250	60°C-3 min-20°/min-280 °C
ODH of Ethylbenzene	BP-1	230	230	60°C-3 min-20°/min-230 °C





**REFERENCES**

- [1] E. Abi-Aad, R. Bechara, J. Grimblot, A. Aboukais, *Chem. Mater.* 5 (1993) 793.
- [2] C. Real, M.D. Alcala, J.M. Criado, *J. Am. Ceram. Soc.* 79 8 (1996) 2012.
- [3] B.M. Reddy, A. Khan, Y. Yamada, T. Kobayashi, S. Loidant, J.C. Volta, *J. Phys. Chem. B.* 106 (2002) 10964.
- [4] J. Matta, D. Courcot, E. Abi-Aad, A. Aboukais, *Chem. Mater.* 14 (2002) 4118.
- [5] Y.H. Kim, H.I. Lee, *Bull. Korean Chem. Soc.* 20 12 (1999) 1457.
- [6] C. Suryanarayana, M.G. Norton, *X-ray Diffraction A Practical Approach*, New York (1998).
- [7] B.K. Hodnett, *Heterogeneous Catalytic Oxidation: Fundamental and Technological Aspects of the Selective and Total Oxidation of Organic Compounds*, John Wiley, New York (2000).
- [8] H.H. Willared, L.L. Merrit Jr., J.A. Dean, F.A. Settle Jr., *Instrumental Methods of Analysis 7<sup>th</sup> edn.*, CBS Publishers, New Delhi (1986).
- [9] J.W. Niemansverdriet, *Spectroscopy in Catalysis: An Introduction*, VCH Publisher, New York (1995) 165.
- [10] M.A. Larrubia, G. Busca, *Mater. Chem. Phys.* 72 (2001) 337.
- [11] J.W. Niemansverdriet, *Spectroscopy in Catalysis: An Introduction*, VCH Publisher, New York (1995) 200.
- [12] D.C.M. Dutoit, M. Schneider, P. Fabrizioli, A. Baiker, *J. Mater. Chem.* 7 2 (1997) 271.
- [13] V. Briois, D.L. Hecht, F. Villain, E. Fonda, S. Belin, B. Griesebock, R. Frahm, *J. Phys. Chem. A.* 109 (2005) 320.
- [14] A.G.S. Filho, O.P. Ferreira, E.J.G. Santos, J.M. Filho, O.L. Alves, *Nano Lett.* 14 11 (2004) 2099.
- [15] J.W. Niemansverdriet, *Spectroscopy in Catalysis: An Introduction*, VCH, New York (1995).
- [16] J.M. Coronado, A.J. Maria, A. Arias, J.C. Conesa, J. Soria, *J. Photochem. Photobio. A: Chem.* 150 (2002) 213.
- [17] J.W. Wiench, C.J. Fontenot, J.F. Woodworth, G.L. Schrader, M. Pruski, S.C. Larsen, *J. Phys. Chem. B* 109 (2005) 1756.

- [18] H. Gunther, *NMR Spectroscopy; Basic Principles, Concepts and Applications in Chemistry*, 2<sup>nd</sup> edn. John Wiley and Sons, New York (1998).
- [19] X. Yu, S. Cai, Z. Chen, *Spectrochimica Acta Part A* 60 (2004) 391.
- [20] O.B. Lapina, A.A. Shubin, D.F. Khabibulin, V.V. Terskikh, P.R. Bodart, J. P. Amoureux, *Catal. Today* 78 (2003) 91.
- [21] U.G. Nielsen, H.J. Jakobsen, J. Skibsted, *J. Phys. Chem. B* 105 (2001) 420.
- [22] A. Jones, B. McNicol (Eds.), *Temperature-Programmed Reduction for Solid Materials Characterization*, Marcel Dekker, New York (1986).
- [23] S. Besselmann, C. Freitag, O. Hinrichsen, M. Muhler, *Phys. Chem. Chem. Phys.* 3 (2001) 4633.
- [24] M. Boaro, M. Vicario, C. de Leitenburg, G. Dolceti, A. Trovarelli, *Catal. Today* 77 (2003) 407.
- [25] K.V.R. Chary, C.P. Kumar, A. Murali, A. Tripathi, A. Clearfield, *J. Mol. Catal. A: Chem.* 216 (2004) 139.
- [26] M. Bhaiyalakshmi, K. Shanmugapriya, M. Palanichamy, B. Arabindoo, V. Murugesan, *Appl. Catal. A: Gen.* 267 1-2 (2004) 77.
- [27] H.J.M. Bosman, E.C. Kruissink, J. van der Spoel, F. van den Brink, *J. Catal.* 148 (1994) 660.
- [28] B.M. Reddy, I. Ganesh, *J. Mol. Catal. A* 169 (2001) 207.
- [29] M.A. Aramendia, V. Borau, C. Jimenez, J.M. Marinas, A. Porras, F.J. Urbano, *J. Mater. Chem.* 9 (1999) 819.
- [30] V.Z. Fridman, A.A. Davydov, *J. Catal.* 195 (2000) 20.
- [31] K. Nomiya, K. Yagishita, Y. Nemoto, T. Kamataki, *J. Mol. Catal. A: Chem.* 126 (1997) 43.
- [32] E.P. Reddy, R.S. Varma, *J. Catal.* 221 (2004) 93.
- [33] S. Sugunan, N.K. Renuka, *Bull. Chem. Soc. Jpn.* 75 (2002) 463.

## CHAPTER 4

### SURFACE AND CHEMICAL CHARACTERIZATION

#### Abstract

---

---

*Characterization of surfaces is of major importance in modern catalyst research since the solid surfaces plays the decisive role in the heterogeneous catalysis. Of particular importance are the composition, i.e., the distribution of elements in the catalyst, and the detection of phases and surface compounds. Also of interest are differences in composition between catalyst volume and catalyst surface, as well as interactions between active components and support materials and between the active components themselves. Relationships between the structures of material and the catalyst activity require high-resolution investigation of the microstructure of the catalyst. Catalyst surfaces, surface compounds, metals dispersed on supports and adsorbed molecules are investigated by X-ray techniques, electron and nuclear spectrosopes, analytical tools and other methods. Since vanadia-based catalysts are active at low temperatures where the reactions take place on the surface, the functionality of vanadia species on the catalysts surface is of great importance.*

---

---

#### 4.1 SURFACE CHARACTERIZATION

During the past days, much endeavour has been undertaken in order to understand the phenomenon that underlines the catalytic behaviour of multicomponent and multiphase oxide-based heterogeneous catalysts. In the present study we have been especially interested in the catalysts containing rare earth oxides such as ceria and praseodymia, since pertinent information on the real roles played by these in partial as well as total oxidation is still rather scarce.

In numerous works, it was shown that when  $\text{Ce}(\text{OH})_3$  is prepared at room temperature by precipitation from  $\text{Ce}(\text{NO}_3)_3 \cdot 6\text{H}_2\text{O}$  and  $\text{NaOH}$ ,  $\text{CeO}_2$  is partially formed with  $\text{Ce}^{3+}$  and  $\text{Ce}^{4+}$  hydroxides whereas it is mainly produced when calcined under air at high temperatures  $>673$  K. This product exhibits a large deviation from its  $\text{CeO}_2$  stoichiometric composition by the creation of oxygen vacancies<sup>1,2</sup>.  $\text{Pr}_x\text{O}_y$  systems might exist in different non-stoichiometric phases by solid state reactions occurring under catalytic conditions<sup>3-5</sup>.

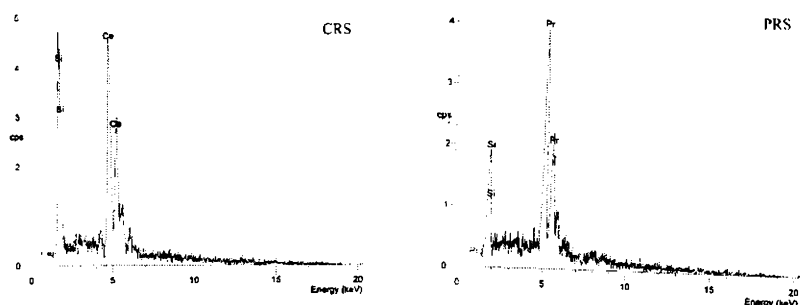
The molecular structures of vanadia catalysts evolve from isolated monovanadates (a terminal  $\text{V}=\text{O}$  bond and three  $\text{V}-\text{O}-\text{M}$  ( $\text{M}=\text{metal atom of the oxide support}$ ) in a distorted tetrahedral configuration,  $\text{O}=\text{V}-(\text{O}-\text{M})_3$  and larger polyvanadates ( $\text{V}$  atoms has one terminal  $\text{V}=\text{O}$  bond, one, two, or three  $\text{V}-\text{O}-\text{V}$  bonds and two, one, or zero  $\text{V}-\text{O}-\text{M}$  bonds) where vanadium appears tetraordinated, to bulk  $\text{V}_2\text{O}_5$  crystals when vanadia loading exceeds the monolayer coverage of the support. In bulk  $\text{V}_2\text{O}_5$ , vanadium is octacoordinated, while in the monomeric and polymeric species; known as “monolayer vanadia” vanadium is tetraordinated<sup>6-12</sup>.

The molecular structure of the supported vanadium oxide species was found to depend upon several parameters, e.g. metal oxide loading, support oxide material, and degree of hydration. With increasing loading, the vanadium oxide structure changes gradually from monomer to polymer and finally to crystalline  $V_2O_5$ . There will be clear differences between the surface and bulk compositions. Therefore the understanding of the molecular structure of vanadia on the support and the basic processes that underline the synergetic effect observed between modified vanadia based catalytic systems and industrially important selective oxidation reactions remains a matter of intensive debate.

This chapter deals with the results of various instrumental techniques used to characterize the rare earth oxides, silica promoted rare earth oxides and different weight percentage of vanadia supported on these oxides.

#### 4.1.1 Energy dispersive X-ray analysis

A detailed analysis of all catalysts after calcination has been performed by energy dispersive X-ray analysis (EDX) to get the amount of each species consists with prepared catalysts. The EDX spectra obtained for representative catalysts are shown in Figure 4.1.



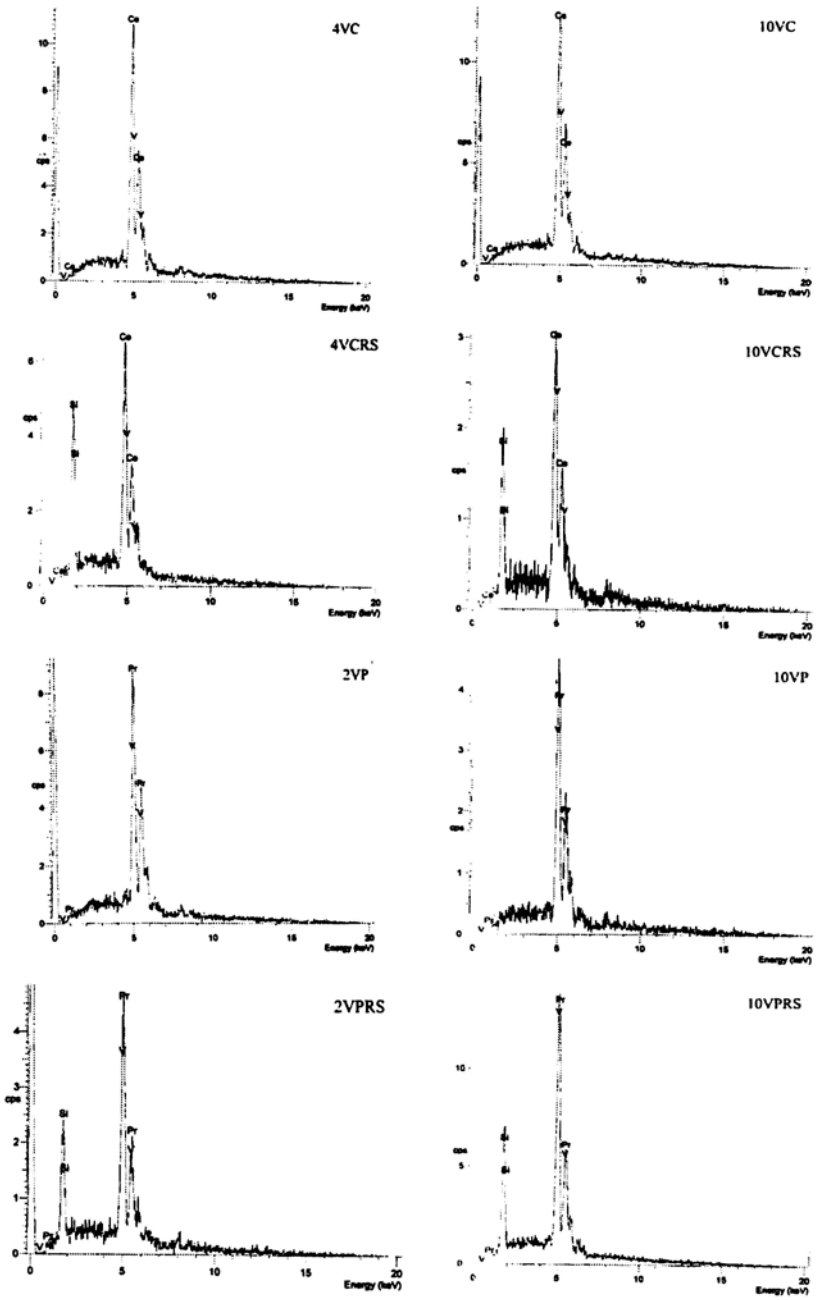


Figure 4.1

The EDX analysis performed on the catalysts clearly reveals the occurrence of various elements. Intensity of the spectra correlates to the amount of element (%) present.

The elemental composition as atom % of ceria catalysts is presented in Table 4.1.

Table 4.1

Catalyst	Composition (atom %)					
	Ce		Si		V	
	Theo.	Calc.	Theo.	Calc.	Theo.	Calc.
Ce	100	100	-	-	-	-
RS	-	-	100	98.81	-	-
CRS	50	55.18	50	44.82	-	-
2VC	96.35	93.23	-	-	3.64	6.77
4VC	92.96	90.44	-	-	7.03	9.56
6VC	89.80	89.60	-	-	10.19	10.40
8VC	86.85	86.84	-	-	13.14	13.16
10VC	84.09	83.47	-	-	15.90	16.53
2VCRS	48.75	39.06	48.75	54.88	2.48	6.09
4VCRS	47.57	41.32	47.57	52.34	4.85	6.34
6VCRS	46.44	38.29	46.44	53.43	7.11	8.28
8VCRS	45.37	43.67	45.37	44.79	9.26	11.25
10VCRS	44.34	43.02	44.34	40.29	11.31	16.70

Energy dispersive X-ray analysis confirms the occurrence of Ce, V and Si for the supported catalysts. From the values it is seen that both theoretical and experimental values are found to agree with each other. It is evident that

atom % of Si and Ce in CRS decreases with increase in vanadium loading. The results indicate that effective loading of vanadium oxide is taking place on ceria and silica promoted ceria.

The rice husk silica has Si content of 98 %, indicating that the impurity contents are significantly reduced by acid-leaching before thermal decomposition process<sup>12</sup>. Analysis conducted to measure the silica content from rice husk has shown that, after acid leaching process the weight of the rice husk is reduced by 60 % and on further high temperature treatment about 24.6 % SiO<sub>2</sub> could be obtained. Elemental analysis of CRS showed a content of 55.1 (atom %) Ce and 44.8 (atom %) Si. Vanadia impregnation could maintain the amount of Si as theoretically calculated.

The elemental composition as atom % of praseodymia supports and supported vanadia catalysts are presented in Table 4.2.

**Table 4.2**

Catalyst	Composition (atom %)					
	Pr		Si		V	
	Theo.	Calc.	Theo.	Calc.	Theo.	Calc.
Pr	100	100	-	-	-	-
PRS	50	54.73	50	45.27	-	-
2VP	89.09	87.31	-	-	10.90	12.69
6VP	73.13	87.43	-	-	26.86	12.57
10VP	62.03	78.35	-	-	37.96	21.65
2VPRS	46.62	35.29	46.62	53.12	6.74	11.59
6VPRS	41.08	43.81	41.08	40.37	17.83	15.83
10VPRS	36.71	40.27	36.71	36.79	26.56	22.11



Data show that effective promotion of  $\text{SiO}_2$  has been occurred on  $\text{Pr}_x\text{O}_y$  surface. Composition of Si and Pr (atom %) in PRS decreases with increase in vanadium loading. Atom % of V obtained suggest that amount of vanadium is remarkably higher in these catalysts compared to ceria catalysts.

Table 4.3 gives the Ce/Si and Pr/Si atomic ratios determined by EDX.

**Table 4.3**

Catalyst	Composition atom (%)		Ratio
	Ce/Pr	Si	(Ce/Pr)/Si
CRS	55.18	44.82	1.23
2VCRS	39.06	54.88	0.73
4VCRS	41.32	52.34	0.78
6VCRS	38.29	53.43	0.71
8VCRS	43.67	44.79	0.69
10VCRS	43.02	40.29	1.06
PRS	54.73	45.27	1.21
2VPRS	35.29	53.12	0.66
6VPRS	43.81	40.37	1.08
10VPRS	40.27	36.79	1.09

As seen in the table, the Ce/Si atomic ratio is higher for CRS and PRS supports than for the vanadia containing catalysts. It indicates that the surfaces of the support CRS and PRS are covered by the vanadium oxide overlayer. The decrease of the Ce/Si atomic ratio with increasing vanadia loading is due to the formation of  $\text{CeVO}_4$  on the surface of the support. The Pr/Si ratio is found to be higher than Ce/Si for the same vanadia loading indicating more silica is

present on the catalyst surface. The present results indicate the formation of dispersed vanadium oxide layer on CRS support at lower loading and  $\text{CeVO}_4$  formation as the vanadia loading increases. Relatively large ratio of Pr/Si in 6 and 10VPRS suggest the formation of agglomerated bigger particles thereby uncovering the part of the silica surface<sup>13</sup>.

#### 4.1.2 Powder X-ray diffraction

Powder X-ray diffraction patterns were collected for all catalysts after calcination at the temperature of 773 K unless otherwise specified.

The corresponding diffraction patterns of the support oxides are presented in Figure 4.2.

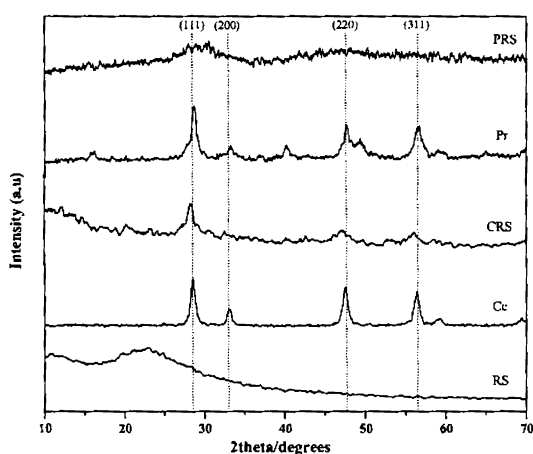


**Figure 4.2**

The X-ray reflections of ceria are observed at  $2\theta/\text{degrees} \sim 28.32, 32.86, 47.34$  and  $56.12$  corresponding to 111, 200, 220 and 311 planes respectively. This shows a typical cubic crystal structure of fluorite type  $\text{CeO}_2$

with a space group  $Fm3m$ <sup>14</sup>. Silica obtained from rice husk is found to be completely X-ray amorphous with a broad diffraction peak centered on  $2\theta/\text{degrees} \sim 22$ <sup>15</sup>. As shown in figure, the X-ray powder diffraction of CRS calcined at 773 K exhibits poor crystallinity with only the diffraction lines due to cubic CeO<sub>2</sub>. The characteristic features due to SiO<sub>2</sub> are absent, indicating that it is in the amorphous state. A dispersion effect is operated by hydrogen when ceria is promoted with silica<sup>16</sup>.

X-ray diffraction analysis suggests cubic phase of praseodymia. The diffraction pattern of praseodymia indicates a fluorite type Pr<sub>x</sub>O<sub>y</sub> structure. Generally several praseodymia phases observed by X-ray diffractometry are PrO<sub>2</sub>, Pr<sub>2</sub>O<sub>3</sub> and Pr<sub>6</sub>O<sub>11</sub><sup>17</sup>. Two types of species observed in the Pr-ion are Pr<sup>+3</sup> in Pr<sub>2</sub>O<sub>3</sub> and Pr<sup>+4</sup> in PrO<sub>2</sub> and Pr<sub>6</sub>O<sub>11</sub><sup>18,19</sup>. Praseodymia containing catalysts changed from light green to black after treatment at calcination temperature of 773 K. The origin of light green shades is due to the Pr<sup>3+</sup> oxide while Pr<sup>4+</sup> appeared black<sup>20</sup>. Thus Pr<sub>x</sub>O<sub>y</sub> exhibits presence of only Pr<sup>4+</sup> in catalysts. The cubic Pr<sub>x</sub>O<sub>y</sub> changes to a composition with less oxygen at temperature higher than 753 K according to the reaction,  $4 \text{PrO}_2 \longrightarrow 2 \text{Pr}_2\text{O}_3 + \text{O}_2$  (45 kcal/mol). This temperature is attained during the calcination treatment of catalysts<sup>21</sup>. Diffraction pattern exhibited very low intensity after promotion of praseodymia by silica suggesting the influence of amorphous nature of rice husk silica.

The XRD patterns of VC series of catalysts along with that of V<sub>2</sub>O<sub>5</sub> are presented in Figure 4.3.

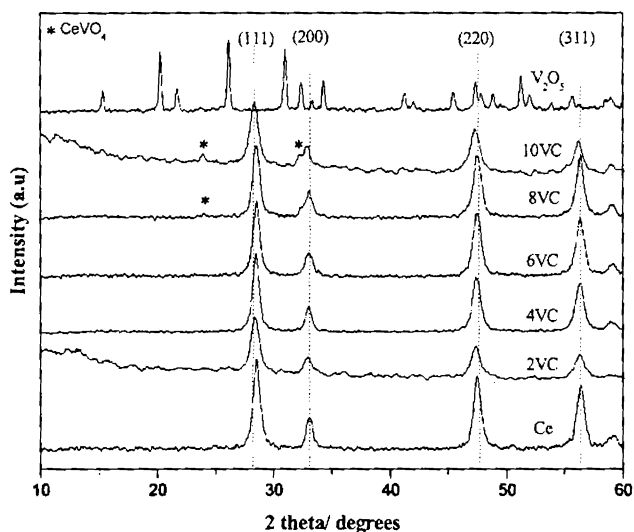


Figure 4.3

The diffraction pattern of VC series catalysts shows typical lines due to ceria in the low vanadia loading and lines of orthovanadate type as the loading increases with the absence of any characteristic lines due to  $V_2O_5$ <sup>22</sup>. This indicates that vanadia seems to be finely dispersed state on the support surface. Thus vanadia particles are under limit to be detected by XRD technique (<2 nm) for low  $V_2O_5$  loading. For 2, 4 and 6 wt. %  $V_2O_5$  loading, vanadia seems to be finely dispersed over the support with no other peak except of ceria. While for loading above 6 wt. %, in addition to sharp ceria lines, new lines with less intensity can be seen at  $2\theta/\text{degrees} = 24.0$  and  $32.5$  respectively. These lines are attributed to the formation of the mixed phase cerium orthovanadate,  $CeVO_4$ . It was reported that  $CeO_2$  and  $V_2O_5$  could react together in the solid state in the temperature range 773-1073 K to form

$\text{CeVO}_4$ <sup>23-25</sup>. The intensity of these lines increases steadily with increasing the vanadia content.

The X-ray diffraction patterns of VCRS series of catalysts are presented in Figure 4.4.

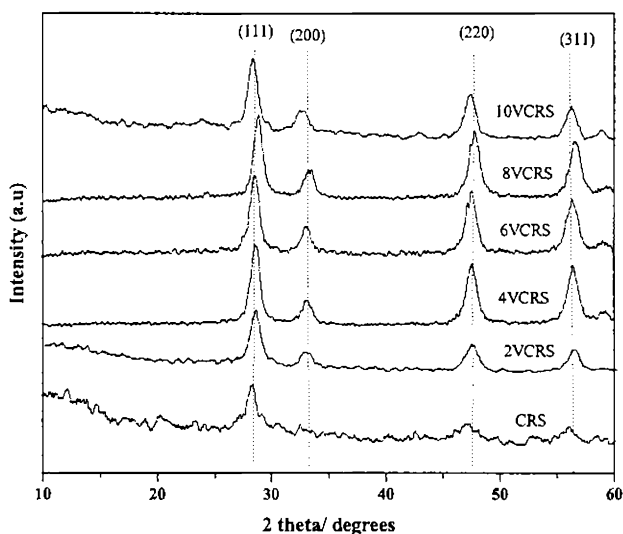


Figure 4.4

For VCRS catalysts, the intensity of diffraction peaks is found to be low confirming the amorphous nature of CRS support with no appreciable changes in the shape and position of the peaks up to 10 wt. %  $\text{V}_2\text{O}_5$  loading. As crystalline vanadia features are not apparent, it can be inferred that vanadium oxide is in a highly dispersed or amorphous form on the surface of the support<sup>26</sup>. Peaks due to orthovanadate formation did not appear even with 10 wt. %  $\text{V}_2\text{O}_5$ . It suggests that amorphous nature of silica helps to

form highly dispersed vanadia on the surface.

The various parameters calculated from XRD data for ceria catalysts are summarized in Table 4.4.

**Table 4.4**

Catalyst	Crystallite size (nm)	Lattice parameter (Å°)	Unit cell volume
Ce	12.13	5.45	161.8
2VC	9	5.44	160.9
4VC	19	5.42	159.2
6VC	13	5.41	158.3
8VC	15	5.40	157.4
10VC	10	5.46	162.7

The lattice parameter value of CeO<sub>2</sub> (5.45 Å°) suggests cubic structure with space group *Fm3m* is in good agreement with the experimental value  $a = 5.41$  Å°. The unit cell is Ce<sub>4</sub>O<sub>8</sub> with 8-coordinate anions (O in tetrahedral sites), in which the ionic radius ratio of Ce<sup>4+</sup> to O<sup>2-</sup> is equal to 0.782, whereas, in the perfect fluorite structure, this ratio is 0.82 Å°<sup>27</sup>. As can be noted from the table, an increase in the crystallite size is observed with increasing vanadia loading. The crystallite size of VC catalysts is larger, which indicates that the impregnated vanadium oxide accelerates the grain growth of ceria in supported catalysts. There is a theoretical monolayer capacity of vanadium oxide over the support material. Above which the impregnated vanadium oxide accelerates the grain growth of ceria in supported catalysts thus increasing the crystallite size upon vanadia loading<sup>28</sup>. A decrease in the lattice parameter from 5.45 Å° (CeO<sub>2</sub>) is observed after vanadia impregnation, confirming that the

impregnated vanadia ions are incorporated in the ceria lattice forming homogeneous solid solutions without substitution in the cubic lattice of ceria<sup>29</sup>. This suggests that impregnated vanadia can be incorporated into the defect sites or occupies the lattice sites possibly at the outer layers of crystallites.

The various parameters calculated from XRD data for VCRS series catalysts are summarized in Table 4.5.

Table 4.5

Catalyst	Crystallite size (nm)	Lattice parameter (Å°)	Unit cell volume
CRS	10	5.51	167.2
2VCRS	8	5.43	160.1
4VCRS	11	5.40	157.4
6VCRS	9	5.41	158.3
8VCRS	10	5.35	153.1
10VCRS	11	5.43	160.0
2VCRS*	27	-	-
6VCRS*	27	-	-
10VCRS*	29	-	-

\* Catalysts calcined at 923 K

The crystallite size of CRS is found to reduce with an increase in lattice parameter. Promotion of CeO<sub>2</sub> with SiO<sub>2</sub> can insert Si without any compound formation, thus stabilizing fluorite structure. Lattice parameters of these oxides are very similar to each other; for silica (*Fd3m*)  $a = 5.431 \text{ Å}^\circ$  and for CeO<sub>2</sub> (*Fm3m*)  $a = 5.411 \text{ Å}^\circ$ <sup>30</sup>. The diffraction pattern of CRS support indicated an amorphous character. Thus crystallite size of CRS supported catalyst is

little influenced by the vanadia addition. Another observation to be noted is that for supported VCERS catalysts, no appreciable changes occurred in crystallite size of ceria as the weight percentage of vanadia loading increases. The result shows that  $V_2O_5$  can be fairly easily dispersed on the high surface area support for 2-10 wt. (%) of loading.

Eventhough, the formation of orthovanadate structure is not visible in the XRD pattern, it cannot be ruled out since ceria surface can strongly interact with vanadia species as the  $V_2O_5$  density increases<sup>31</sup>.

Powder X-ray diffraction of VCERS catalysts collected after calcination at 923 K are shown in Figure 4.5 and the crystallite size values are reported in Table 4.5.

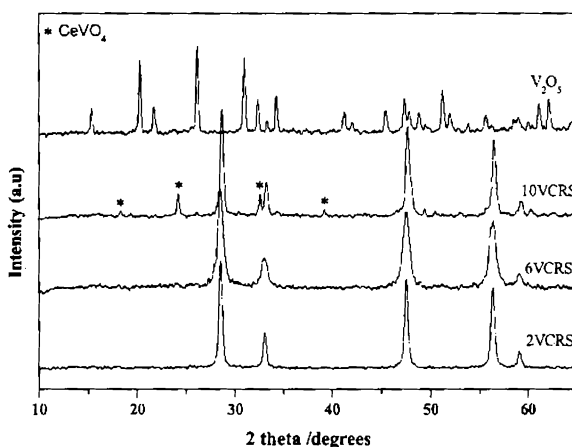


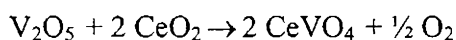
**Figure 4.5**

A ceria phase is evidenced in all the catalysts. For 2VCERS and 6VCERS, only this phase is present, whereas for 10VCERS, numerous lines with weak



intensities are superposed on those corresponding to ceria phase<sup>32</sup>. For 10VCRS calcined at 923 K in addition to sharp CeO<sub>2</sub> lines, new lines at 2θ/degrees = 18.5, 24.0 and 32.5 with less intensity also appeared. The lines observed can be attributed to the formation of CeVO<sub>4</sub>. The silica features are not observed since this is in amorphous form and the preferential formation of CeVO<sub>4</sub> indicates that supported vanadia interacts selectively with the ceria portion of the promoted support. Similar studies with low surface area metal oxides supports suggest the formation of CeVO<sub>4</sub> and further crystallization even at 773 K<sup>27</sup>. X-ray analysis of vanadia impregnation on ceria suggests the formation of CeVO<sub>4</sub> (Figure 4.2) even after 6 wt. % V<sub>2</sub>O<sub>5</sub> loading at calcination temperature of 773 K. However, CeVO<sub>4</sub> formation on CRS exhibits diffraction pattern only after calcination temperature of 923 K and vanadia loading of 10 wt. % V<sub>2</sub>O<sub>5</sub>. The presence of V<sub>2</sub>O<sub>5</sub> was not detected even at this high temperature indicating that the vanadia species are present in a highly dispersed state. An interesting observation to be noted from Table 4.5 is that the impregnated vanadia appears to increase the crystallite size of ceria after calcination at higher temperature. Increasing vanadia loading also seems to increase the size of ceria crystallites.

In CeVO<sub>4</sub>, vanadium possesses a valence of 5+ whereas that of cerium is 3+. Formation of CeVO<sub>4</sub> phase at higher calcination temperature is probably due to the following reaction:



During the formation of CeVO<sub>4</sub>, cerium is reduced from Ce<sup>4+</sup> to Ce<sup>3+</sup>, whereas the vanadium reactant remains in the 5+ oxidation state. The reduction

of  $Ce^{4+}$  in preference  $V^{5+}$  can be explained by the fact that cerium frequently exhibits a valence of 3+. This is due to the electronic configuration of  $Ce^0$  ( $4f^15d^16s^2$ ). In this arrangement, the volumes of the 6s and 5d orbitals are greater than that of the 4f orbital; consequently, only the three electrons in the 6s and 5d shells contribute to the valence<sup>33</sup>.

Powder X-ray diffraction pattern obtained for VP catalysts are presented in Figure 4.6.

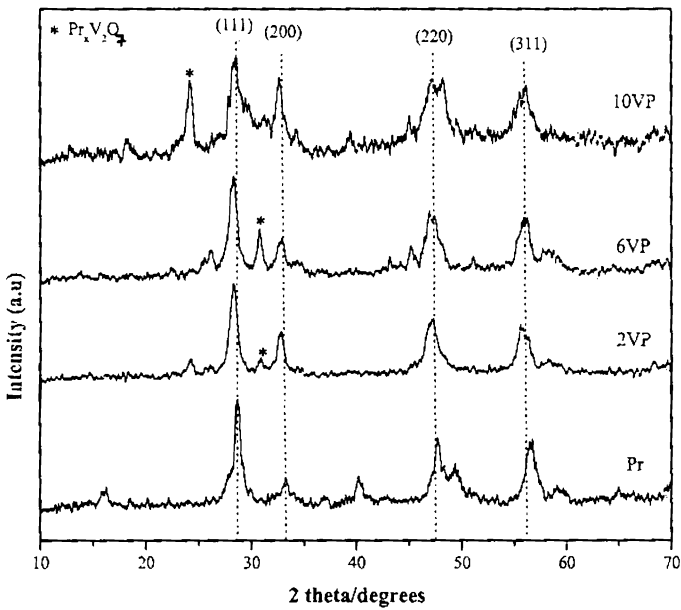


**Figure 4.6**

Vanadia impregnation causes formation of new phases giving rise to various diffraction peaks in the supported catalysts depending upon the amount

of vanadia loaded. In supported vanadia catalysts we can observe formation of Pr-VO<sub>x</sub> due to solid state reaction between the support and supported vanadia. For 2VP, new peaks appeared at 2θ/degrees of 24.2 and 30.9. However, in 6VP a peak observed at 26.1° along with one at 30.7. In 10VP this peak is highly intense. All these suggest formation of various structures depending upon the amount of vanadia loaded over the support. According to Guilia et al.<sup>34</sup> a peak observed at 26.4 ° for Pr-zircon could not be assigned to any known compound while two peaks at 29.0 and 32.3 could be ascertained to structure of the Pr<sub>2</sub>Zr<sub>2</sub>O<sub>7</sub> type. Ocana et al.<sup>35</sup> also could not attribute the former peak to any specific Pr containing phase.

According to the report by Smet et al.<sup>36</sup> new phases obtained for Pr<sub>6</sub>O<sub>11</sub>-MoO<sub>3</sub> catalysts are Pr<sub>2</sub>Mo<sub>3</sub>O<sub>12</sub>, Pr<sub>6</sub>MoO<sub>12</sub> and Pr<sub>2</sub>MoO<sub>6</sub>. New peaks observed for supported vanadia catalysts are attributed to Pr<sub>x</sub>V<sub>2</sub>O<sub>7</sub> formed from the interaction of Pr<sub>6</sub>O<sub>11</sub> with V<sub>2</sub>O<sub>5</sub> loaded. The 4f<sup>n-1</sup> 5d states (Pr<sup>4+</sup>) strongly interact with the crystalline environment contrary to 4f<sup>n</sup> (Pr<sup>3+</sup>) states and appear in different lattice forms. Diffraction analysis of Mg-V-O catalysts suggested the presence of ortho- [(Mg<sub>3</sub>(VO<sub>3</sub>)<sub>2</sub>), pyro- [(Mg<sub>2</sub>(V<sub>2</sub>O<sub>7</sub>)], and meta- [(Mg(VO<sub>3</sub>)<sub>2</sub>] vanadates similarly with Co<sub>2</sub>V<sub>2</sub>O<sub>7</sub> and Ni<sub>2</sub>V<sub>2</sub>O<sub>7</sub><sup>37</sup>. Pyrovanadates contain two tetrahedrally coordinated vanadium atoms connected by bridging oxygen in a V<sub>2</sub>O<sub>7</sub><sup>4-</sup> unit, which consists mainly V-O-V bonds<sup>38,39</sup>.

Powder X-ray diffraction pattern obtained for VPRS series catalysts is presented in Figure 4.7.

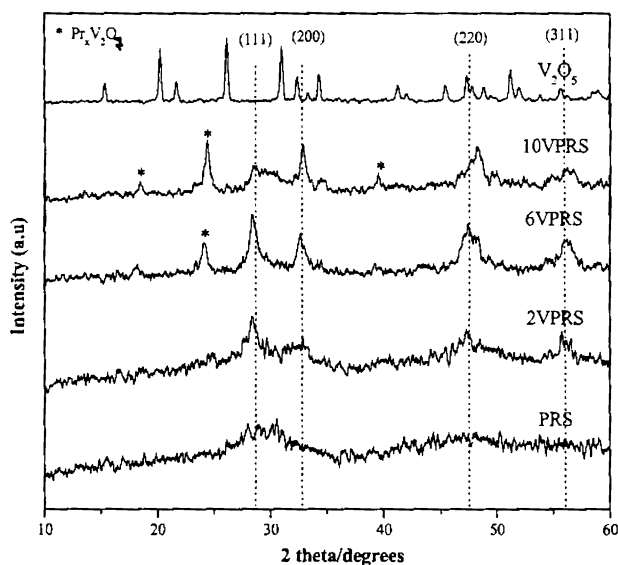


Figure 4.7

All PRS supported vanadia exhibit low crystallinity due to the presence of amorphous nature of silica. 6VPRS exhibits a new peak at  $24.1^\circ$  along with all peaks of praseodymia. This pattern is assigned to  $\text{Pr}_x\text{V}_2\text{O}_7$  type structure formation similar to VP catalysts as the vanadia loading increases. When  $\text{Pr}_x\text{O}_y$  is promoted with silica it can interact with Si to form compounds with  $\text{Pr}^{4+}$ . It is reported that rare earth oxides easily react with Si to form silicate like Si-O-metal configurations<sup>40,41</sup>. EDX analysis show that amount of vanadium in these catalysts is higher compared to ceria catalysts. This results solid state reaction with 6 wt. %  $\text{V}_2\text{O}_5$  loading.

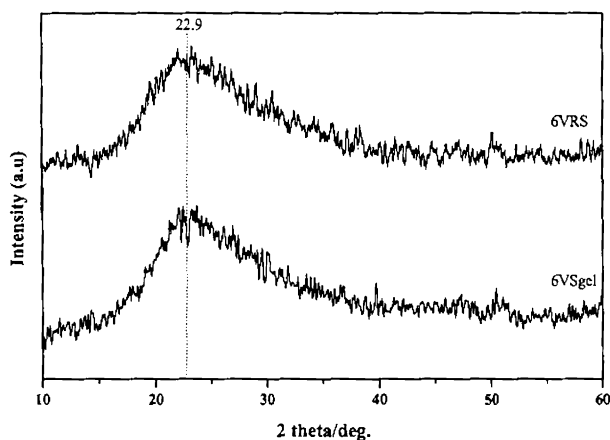
The various parameters calculated from XRD data for praseodymia catalysts are listed in Table 4.6.

Table 4.6

Catalyst	Crystallite size (nm)	Lattice parameter (Å°)	Unit cell volume
Pr	26	5.40	157.4
PRS	-	5.35	153.1
2VP	13	5.45	161.8
6VP	12	5.46	162.7
10VP	2	5.41	158.3
2VPRS	-	5.44	160.9
6VPRS	19	5.43	160.1
10VPRS	45	6.32	252.4

Lattice parameter value (5.40 Å°) gives additional evidence for cubic praseodymia. A decrease in lattice parameter is observed for PRS support. This change can occur by two opposite effects such as a decrease in ionic radii when going from  $\text{Pr}^{3+}$  to  $\text{Pr}^{4+}$  cations and a concomitant increase of oxygen anions into the oxygen vacancies<sup>42</sup>. The lattice parameter values causes an expansion according to the difference in the ionic radii of  $\text{Pr}^{4+}/\text{Pr}^{3+}$  as 0.90/1.126 Å°<sup>43</sup>. Among supported vanadia catalysts, 10VP exhibits higher crystallite size than 10VPRS. Thus silica promotion seems to be helpful in reducing the crystallite size of particles due to its amorphous nature. Lattice parameter value of 10VPRS suggests some kind of compound formation between the support and supported vanadia leading to a different coordination environment.

X-ray diffraction pattern of various silica supported vanadia (6 wt. %  $\text{V}_2\text{O}_5$ ) catalysts are presented in Figure 4.8.

**Figure 4.8**

The XRD pattern of rice husk silica and silica gel supported (6 wt. %  $V_2O_5$ ) vanadia showed only a broad peak characteristic of amorphous silica, indicating that vanadia is highly dispersed state or the vanadia crystals are too small ( $< 4$  nm) to be detected by X-ray diffraction<sup>44</sup>. This suggests that vanadia supported on rice husk silica is similar to that on silica gel. Silica supported vanadia catalysts can contain isolated and distorted  $V^{5+}$  species with the bridging V-O-Si bonds that are active functionality in selective oxidation reactions<sup>45</sup>.

#### 4.1.3 BET surface area measurements

The Brunauer-Emmett-Teller (BET) method was used for the analysis of surface area at liquid nitrogen temperature of all catalysts calcined at 773 K.

The specific surface area and pore volumes of ceria containing catalysts are presented in Table 4.7.

**Table 4.7**

Catalyst	BET surface area ( $\text{m}^2\text{g}^{-1}$ )	Pore volume ( $\text{ccg}^{-1}$ )	Mean pore diameter (nm)
Ce	67	0.11	6.31
2VC	64	0.10	6.30
4VC	36	0.06	7.06
6VC	46	0.11	9.20
8VC	49	0.05	3.84
10VC	44	0.03	2.97

The BET surface area of ceria prepared was  $67 \text{ m}^2\text{g}^{-1}$ . A substantial decrease in BET surface area can be observed after impregnation of the supports with  $\text{V}_2\text{O}_5$ . This is a general phenomenon observed in the case of supported catalysts when an active component is impregnated over its surface<sup>46</sup>. The observed decrease is mainly due to penetration of the dispersed vanadium oxide into the pores of the support, thereby narrowing its pore diameter and blocking some of the pores. Additionally, solid-state reactions between the dispersed vanadium oxide and the support may also contribute to the observed decrease in the BET surface areas and pore volumes. The decrease is more severe with increase in vanadia loading, especially with metal oxide support, caused by the progressive formation of orthovanadate crystals, which block the pores of the support<sup>47</sup>. The decrease of the specific area of ceria containing solids can be related to the formation of  $\text{CeVO}_4$  phase as the

vanadia loading increases. The formation of  $CeVO_4$  at relatively low temperature could be probably favoured by the preparation method, since the vanadium oxide precursor was impregnated on the support material. There is a theoretical monolayer capacity of vanadium oxide over the support material. From the unit cell dimensions of  $V_2O_5$  an average value for a loading corresponding to a monolayer can be calculated as  $1.2 \text{ mg } V_2O_5 / \text{m}^2$  of the support. Bond et al.<sup>48</sup> reported the concentration of  $V_2O_5$  necessary to form a monolayer was  $0.09 \text{ mg/m}^2$ . Above which,  $V_2O_5$  interacts with the support material and forms compounds or multilayer species.

The specific surface areas and pore volumes of VCRS catalysts are presented in Table 4.8.

**Table 4.8**

Catalyst	BET surface area ( $\text{m}^2 \text{g}^{-1}$ )	Pore volume ( $\text{ccg}^{-1}$ )	Mean pore diameter (nm)
RS	224	0.28	5.03
CRS	102	0.27	10.80
2VCRS	94	0.26	11.11
4VCRS	90	0.25	11.03
6VCRS	76	0.18	9.22
8VCRS	66	0.14	8.51
10VCRS	52	0.15	9.79
V	3	0.01	10.95
6VRS	163	0.24	5.85
6VSG	360	0.44	4.92



Rice silica exhibits surface area of  $224 \text{ m}^2\text{g}^{-1}$  with pore volume of  $0.28 \text{ ccg}^{-1}$ . The silica is highly porous material, which has a larger internal surface area since the organic matter has been broken up during the thermal decomposition of rice husk, thus leaving a highly porous structure<sup>49</sup>. Upon silica promotion the surface area of ceria has been increased from 67 to  $102 \text{ m}^2\text{g}^{-1}$ . Increase in pore volume is also observed with corresponding reduction in crystallite size. However, surface area of silica has been reduced. This decrease can be attributed to the fraction of the pores having been destroyed upon promotion. Incorporation of  $\text{V}_2\text{O}_5$  leads to a consistent decrease in the specific surface area and such a decrease is more pronounced as the vanadium content is increased. This is a general phenomenon of supported catalysts, where the surface area of the support decreases with increasing quantity of the active component up to monolayer coverage of the impregnated one<sup>50</sup>. Results suggest that during impregnation and further calcination, strong interaction with the support is developed, leading to phase interaction of the two metal oxides. However, the extent of decrease in surface area is lower in CRS supported vanadia systems, suggesting that the degree of sintering can be reduced with high surface area supports in amorphous form. The presence of high surface area support does stabilize small particles and their growth is inhibited usually in a purely mechanical fashion<sup>51</sup>.

Table 4.9 shows the BET surface area and pore volume of supports and vanadium containing praseodymia catalysts.

**Table 4.9**

Catalyst	BET surface area (m <sup>2</sup> g <sup>-1</sup> )	Pore volume (ccg <sup>-1</sup> )	Mean pore diameter (nm)
Pr	44	0.17	15.24
PRS	73	0.18	9.92
2VP	24	0.02	3.93
6VP	22	0.02	4.02
10VP	19	0.06	11.73
2VPRS	45	0.06	3.41
6VPRS	109	0.17	6.42
10VPRS	30	0.04	5.05

Compared to ceria catalysts, these exhibits low surface area. For supported vanadia catalysts, the specific area decreased upon increasing the vanadium content. Surface area decrease is more pronounced in the case of VP series than with VPRS catalysts. It can be noted that the surface area of 6VPRS is very high while it reduces with 10VPRS. This variation can be attributed the different coordination environment for the supported catalysts as the vanadia content increases. Variation in BET surface area is in agreement with the crystallite size obtained from XRD analysis.

#### **4.1.4 Thermal analysis**

The thermal analysis (TGA/DTG/DTA) of prepared catalysts was done to understand the thermal stability of the catalysts.

Figure 4.9 illustrates the TGA/DTG curves obtained for dried rice husk silica, ceria and silica promoted ceria along with that of NH<sub>4</sub>VO<sub>3</sub>.

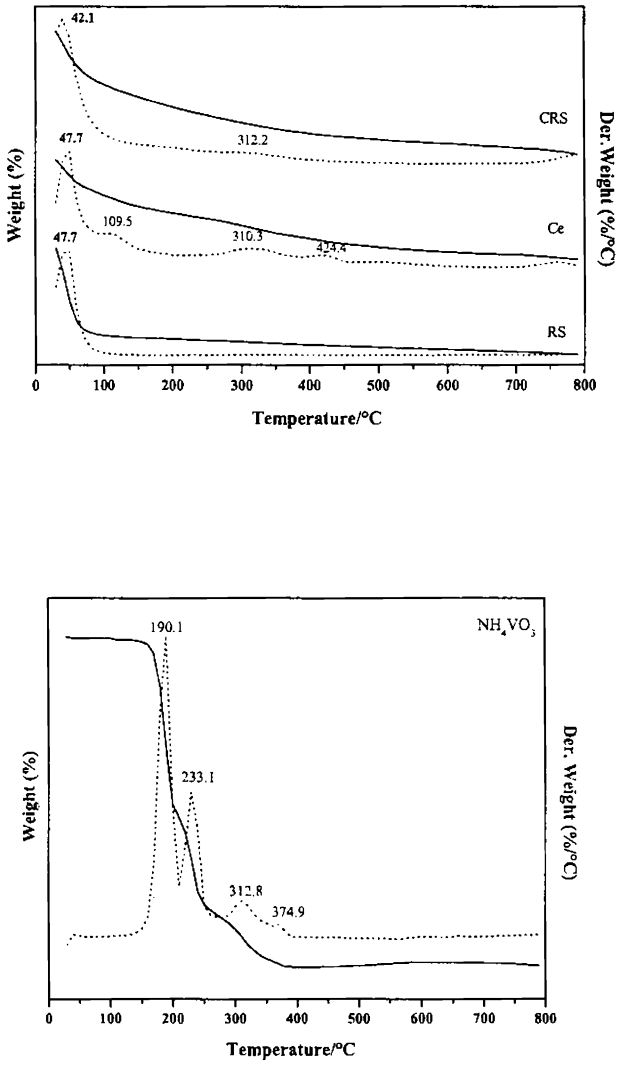


Figure 4.9

In RS, the initial weight loss below 100 °C is owing to evaporation of hydrated water. Absence of any other decomposition peaks suggests the

presence of only water without any organic materials in rice husk silica<sup>52</sup>. A 4.75 % total loss in weight was recorded for Ce from 40- 450 °C. The cerium hydroxide has been prepared from a Ce<sup>3+</sup> salt, Ce(NO<sub>3</sub>)<sub>3</sub>. It is known that Ce(OH)<sub>3</sub> changes to Ce(OH)<sub>4</sub> during its preparation under air and at room temperature which gives the yellow colour to the oxide. During drying in oven at 110 °C, partial dehydration of the hydroxide is possible into CeO<sub>2</sub> with a small quantity of Ce(OH)<sub>3</sub>. Consequently, Ce(OH)<sub>4</sub> and CeO<sub>2</sub> are the major constituents of the solid with a small quantity of Ce(OH)<sub>3</sub> and the loss is effectively due to the dehydration<sup>53</sup>. As can be noted from the figure, the CRS exhibits one major and one minor weight loss peaks with total weight loss of 6.71%. The major low temperature peak in the range 35-100 °C is primarily due to the loss of nondissociative adsorbed water as well as water held on the surface by hydrogen bonding. The minor weight loss peak in the 275-320 °C range could be due to loss of water held in the pores of the promoted oxides. No weight loss was observed at higher temperature<sup>54</sup>.

In TGA/DTG pattern of ammonium metavanadate (NH<sub>4</sub>VO<sub>3</sub>), the thermogram exhibits four weight losses at 190, 233, 312 and 374 (°C). Two major losses appear in the temperature ranges 150-250 and 300-380 (°C)<sup>55</sup>. The total loss value of 23.6 % corresponds to the transformation, 2NH<sub>4</sub>VO<sub>3</sub> → V<sub>2</sub>O<sub>5</sub> + 2NH<sub>3</sub> + H<sub>2</sub>O. The first temperature range (150-250 °C) is ascribed to the desorption of volatile components, water and ammonia, giving rise to (NH<sub>4</sub>)<sub>2</sub>O(V<sub>2</sub>O<sub>5</sub>)<sub>3</sub>, an intermediate product. The second transition (300-380 °C) is assigned to the transformation of this intermediate into V<sub>2</sub>O<sub>5</sub> and no more loss is observed<sup>56,57</sup>. From this, the conversion of NH<sub>4</sub>VO<sub>3</sub> to V<sub>2</sub>O<sub>5</sub> can be characterized from framework rearrangement and formation of intermediates

such as  $(\text{NH}_4)_2\text{V}_4\text{O}_{11}$ , and  $\text{NH}_4\text{V}_3\text{O}_8$ . This supports the formation of  $\text{V}_2\text{O}_5$  by heating  $\text{NH}_4\text{VO}_3$  at 773 K.

The TGA/DTG/DTA pattern obtained for VC series of catalysts are presented in Figure 4.10.

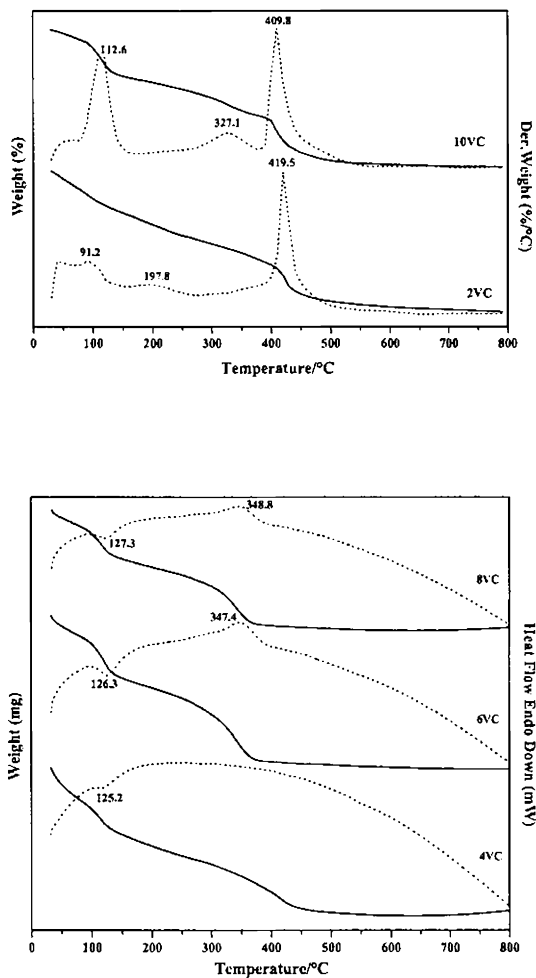


Figure 4.10

In TGA/DTG of 2VC and 10VC, the first weight loss obtained from room temperature to 160 °C corresponds to the loss of physisorbed water. A second weight loss starts from 175 °C and achieved between weight loss in the region of 150-250 and 300-350 °C in 10VC are attributed to the water held in the pores and the decomposition of oxalate species formed during the impregnation of vanadia using ammonium metavanadate. A progressive loss of weight around 405-415 °C is observed for 10VC. It can be attributed to the increased formation of CeVO<sub>4</sub> phase from CeO<sub>2</sub> and V<sub>2</sub>O<sub>5</sub> as the amount of vanadia increases. This vanadate formation reduces the Ce<sup>4+</sup> (CeO<sub>2</sub>) species into Ce<sup>3+</sup> (CeVO<sub>4</sub>) following the reaction:  $2\text{CeO}_2 + \text{V}_2\text{O}_5 \rightarrow 2\text{CeVO}_4 + \frac{1}{2}\text{O}_2$ . The TGA/DTA of VC series exhibits endotherms and exotherms associated with various weight losses. Broad endothermic peak is observed due to removal of water, desorption of volatile components and ammonia, giving rise to (NH<sub>4</sub>)<sub>2</sub>O(V<sub>2</sub>O<sub>5</sub>)<sub>3</sub>, an intermediate. Exothermic peaks are attributed to decomposition of oxalate species formed during impregnation of vanadia using ammonium metavanadate in oxalic acid. Loss around 310-350 °C is attributed to the transformation,  $2\text{VOC}_2\text{O}_4/\text{CeO}_2 \rightarrow \text{V}_2\text{O}_5/\text{CeO}_2 + 2\text{CO}_2 + \frac{1}{2}\text{O}_2$ <sup>58</sup>.

Figure 4.11 illustrates the TGA/DTG/DTA analysis of VCRS series of catalysts conducted before calcination.

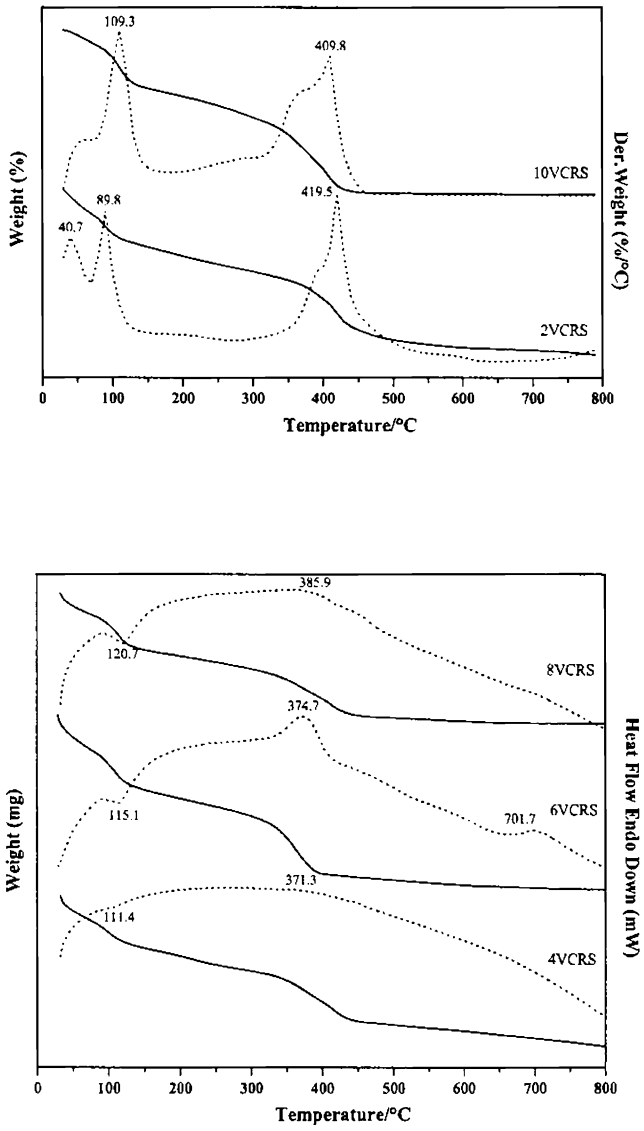


Figure 4.11

An intense endothermic peak appears at 111 °C for 4VCRS. This peak is shifted to higher temperatures (115 °C-8VCRS and 120 °C-10VCRS) as the vanadia loading increases and is attributed to the loss of interlayer water. The exothermic peak in the range of 300-400 °C for supported catalysts must be attributed to the decomposition of oxalates formed by the reaction of oxalate ions with vanadia during the preparation of supported catalysts. Complete decomposition of  $\text{VOC}_2\text{O}_4$  is confirmed when a temperature of 420 °C is reached. The TGA results are in agreement with the DTA curves discussed with weight losses corresponding to water molecules and oxalate species. Weight loss obtained from room temperature until 200 °C is due to the removal of undissociative adsorbed water as well as water held on the surface by hydrogen bonding<sup>59</sup>. Differential thermogram around 400 °C suggests complete removal of oxalate species formed during vanadia impregnation.

Figure 4.12 depicts the TGA/DTA obtained for  $\text{Pr}_x\text{O}_y$  and PRS.

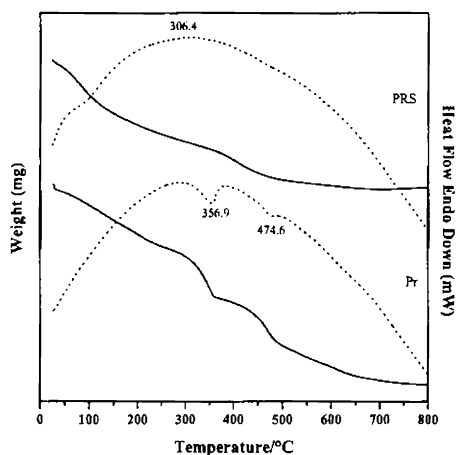


Figure 4.12



Thermograms consist of an endothermic peak at 330 °C due to removal of water molecules. For praseodymia, endotherm in the range 400-500 °C, corresponds to the departure of oxygen from the ligand. This endotherm suggests transformation of  $\text{PrO}_2$  to  $\text{Pr}_6\text{O}_{11}$  in this temperature range<sup>60</sup>. It is reported that the  $\text{PrO}_2$  formed will begin to lose oxygen at 350 °C producing some  $\text{Pr}^{3+}$  ions and oxygen vacancies within the fluorite lattice<sup>61</sup>. This is in agreement with the X-ray diffraction pattern obtained after calcination at 773 K. However, only water removal is associated with PRS.

Figure 4.13 depicts the TGA/DTA curves for VP series of catalysts.

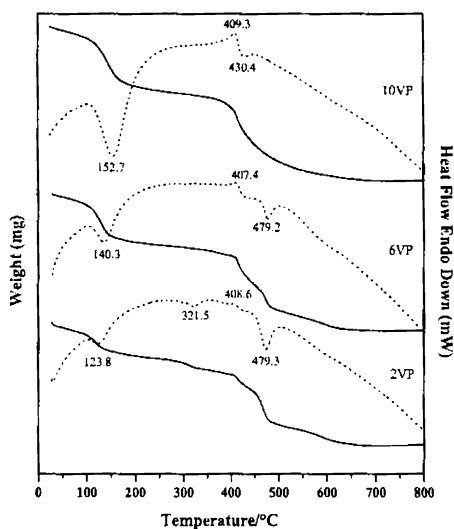


Figure 4.13

Thermogram of VP catalysts consists of endotherms and exotherms that are different from ceria catalysts. In VP catalysts, the thermal analysis curves showed only a weak weight loss, coinciding with a weak endothermic effect,

around 120-155 °C, corresponding to removal of physisorbed water, and weak exothermic peaks, assigned to crystallization of Pr vanadates. Endotherm at ~400 °C suggests departure of oxalate species formed during impregnation process. An exothermic feature recorded immediately after this probably due to oxidation  $V^{3+}$  to  $V^{5+}$ , as species is observed after calcination of the catalysts. It was reported for decomposition of Mg-V-O catalysts that two opposite processes, relating weight changes occur: weight is lost because of  $CO_2$  and  $H_2O$  removal, but simultaneously, weight increases because oxidation from  $V^{3+}$  to  $V^{5+}$ . The second process can be formally envisaged as  $V_2O_3 \rightarrow V_2O_5$ <sup>62</sup>. Otherwise it can be due to the complete conversion of  $Pr^{3+}$  to  $Pr^{4+}$  occurring at a temperature of about 450 °C is already reported<sup>63</sup>. Crystallization process is completed above 400 °C as indicated in the DTA curve and TGA results are in agreement with the DTA curves obtained.

Figure 4.14 depicts the TGA/DTA curves for VPRS series of catalysts.

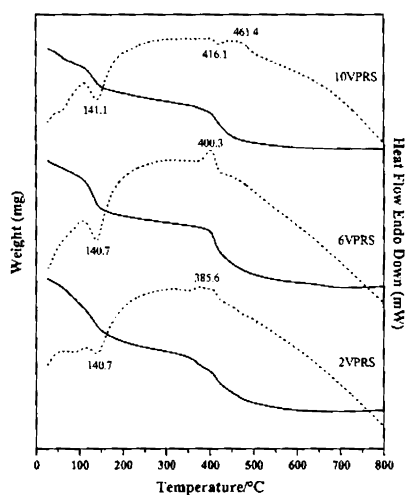


Figure 4.14

The TGA/DTA curves of VPRS catalysts exhibited a different pattern from that of VP catalysts. The first endotherm observed at 140 °C coincides with the removal of water molecules. An exotherm corresponding to oxalate species removal from 380-420 °C is shown depending upon the vanadia loading. From corresponding TGA, it can be seen that as the vanadia loading increases the temperature at which this loss occurs is lowered. Supported catalysts presents endotherm corresponding to orthovanadate type formation,  $\text{Pr}_6\text{V}_2\text{O}_7$  depending upon the vanadia loaded<sup>64</sup>. A second endotherm could be observed only for 10VPRS suggesting the crystallization of the species as the vanadia loading increases. Extent of transformation is lower due to the presence of silica.

#### 4.1.5 UV-vis diffused reflectance spectroscopy

The UV-vis diffused reflectance spectroscopy (UV-vis DRS) can provide information regarding the coordination, oxidation state of the transition and rare earth metal ions<sup>65,66</sup>. In general, the UV-vis spectra of vanadium ions are characterized by charge transfer (CT) transitions between central vanadium atoms and oxygen ligands. The energy of these transitions is influenced strongly by the number and nature of ligands surrounding the central vanadium ion, and thus provides information on the local structure of vanadium. Isolated species generally give rise to CT transitions in a higher energy range (higher frequencies) than polymeric species<sup>67</sup>. The intensities of d-d transitions are generally 10 times lower than those of CT transitions. The absorption bands at 600 and 420-430 nm are assigned to the d-d transitions of  $\text{V}^{4+}$ , which are not observed for any catalysts<sup>68</sup>.

The UV-vis DR spectra of VC series of catalysts are shown in Figure 4.15.

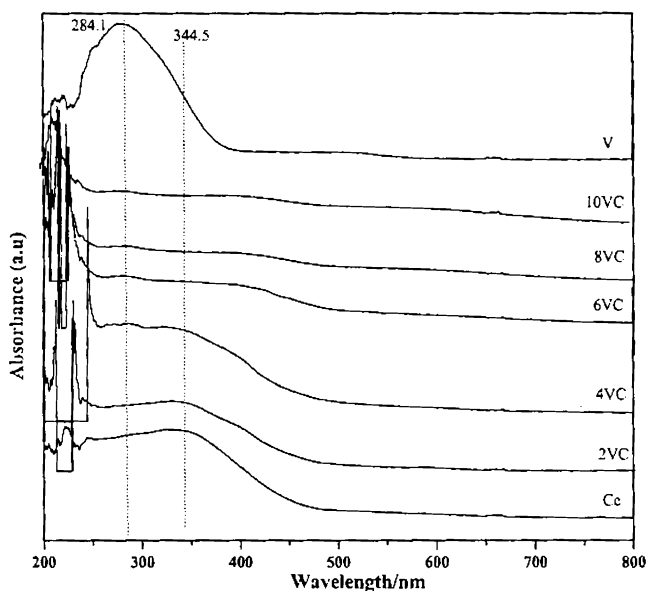


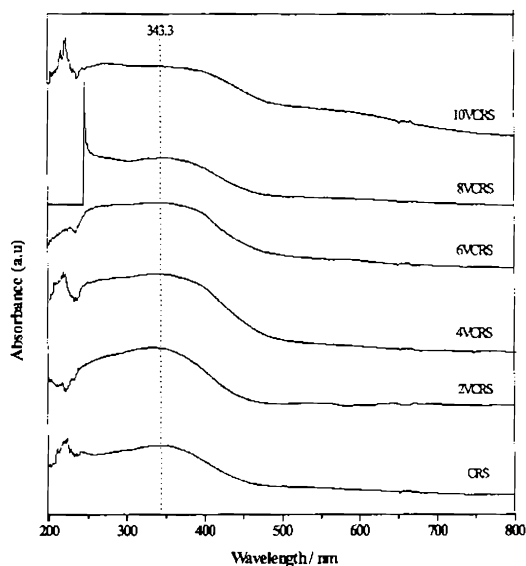
Figure 4.15

The two main transitions involved in the absorption of  $\text{CeO}_2$  in the visible-UV range are from the highest occupied valence 2p oxygen band into empty 4f states of cerium ( $\text{O } 2p \rightarrow \text{Ce } 4f$ ) and from the 2p band into the d conduction band ( $\text{O } 2p \rightarrow \text{Ce } 5d$ )<sup>69</sup>. The DRS spectra of  $\text{CeO}_2$  indicate the existence of  $\text{O}^{2-} \rightarrow \text{Ce}^{4+}$  charge transfer transitions in the range 200-400 with maxima at  $\sim 250$  and 344 nm. The former is a specular reflectance band arising from the surface sites while the latter is a diffuse reflectance band originating from the bulk  $\text{CeO}_2$ <sup>70</sup>. This spectral profile indicates that the charge-transfer

transition of  $\text{Ce}^{4+}$  overlaps with the  $4f^1 \rightarrow 5d^1$  transition of  $\text{Ce}^{3+}$ . No absorption was detected above  $500 \text{ nm}^{71}$ . The DRS spectra of vanadium oxides are characterized by charge-transfer transitions of the type  $\text{O}-\text{V}^{n+}$  and d-d transitions of  $\text{V}^{n+}$ , and their energies are dependent on the oxidation state and coordination environment<sup>72</sup>. The absence of absorption in the 600-800 nm suggests that catalysts contain only  $\text{V}^{5+}$ .

In the UV-vis spectra of the bulk  $\text{V}_2\text{O}_5$ , strong absorption is observed in the UV region with maxima at 284 nm, which is deep orange in colour. This absorption is associated to charge transfer transitions (LMCT) from the O 2p valence band of the oxide to the empty V 3d ( $\text{O}^{2-} \rightarrow \text{V}^{5+}$ ) orbital. Thus oxide has a coordination of 6 for the cation in bulk  $\text{V}_2\text{O}_5$ <sup>73</sup>. However, supported metal oxides can have lower coordination, such as 4 or 5 depending on the support material and weight % of  $\text{V}_2\text{O}_5$  supported<sup>74</sup>. The impregnation of  $\text{V}_2\text{O}_5$  onto the ceria surface causes a decrease of the main absorption intensity and also forms a tail at higher wavelengths. The absorption band at 384 nm can be assigned to  $\text{V}^{5+}$  species characterized by a  $\text{V}=\text{O}$  bond. This indicates the presence of  $\text{V}^{5+}$  species in a tetrahedral environment<sup>75</sup>. For 2 and 4VC, not much difference is obtained from ceria absorption pattern. On the other hand, for higher  $\text{V}_2\text{O}_5$  weight % loading, the spectra obtained shows low absorption intensity. This evidences that the vanadium oxide centers in 6, 8, and 10VC differ from  $\text{V}_2\text{O}_5$ , which in contrast, shows a strong absorption in the UV region<sup>76</sup>.

The UV-vis DR spectra of VCRS series of catalysts are shown in Figure 4.16.

**Figure 4.16**

The UV-vis spectra of VCERS series catalysts exhibit the broad band due to the charge transfer transition between oxygen ligands and vanadium metal centers. Slight broadening of the electronic absorption band compared to VC series, indicates some changes in coordination of the surface  $\text{VO}_x$  species. Broadening increases with increase in vanadia loading and the absorption tail extends into visible region for 10VCERS. Supported vanadia catalysts have been extensively studied using UV-vis DRS, and the spectra were usually very broad<sup>77,78</sup>. By comparison with known data, absorption bands around 250-300 nm were assigned to tetrahedrally coordinated monovanadate. The bands at 300-400 nm range have been ascribed to polyvanadate in either tetrahedral or pentahedral coordination<sup>79,80</sup>. Thus the UV-vis spectra in Figure 4.16 imply that tetrahedral monovanadate  $\text{VO}_x$  species are present on the support surface

at low vanadia loading while polyvanadate species in a tetrahedral environment exist to a large extent on the support with higher loading since absence of pentahedral polyvanadate species are evidenced from EPR and NMR spectroscopic studies.

Figure 4.17 depicts the UV-vis DR spectra obtained for VP series catalysts.

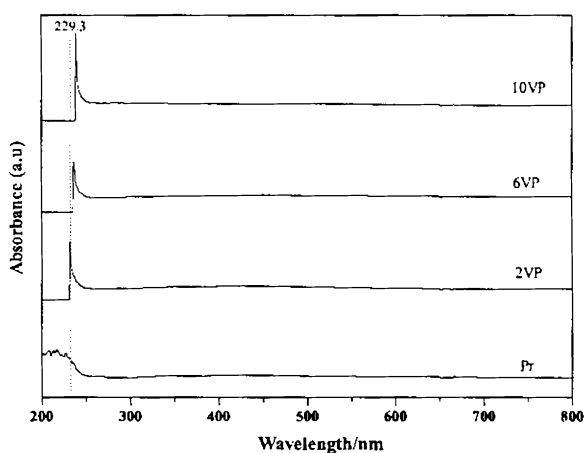
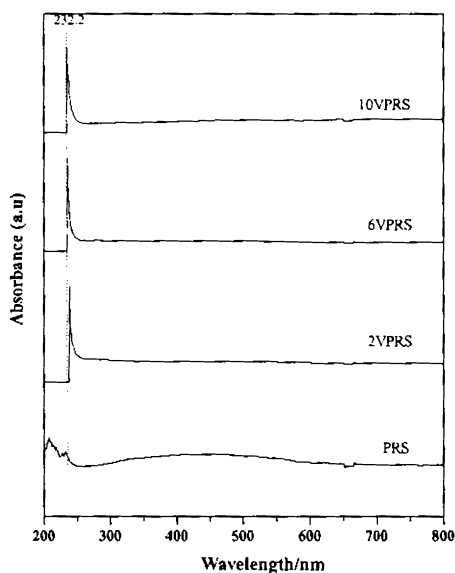


Figure 4.17

The bands are visible only within the range of 200-300 nm attributed to the Pr and charge-transfer transitions of vanadium<sup>81</sup>. The Pr<sup>4+</sup> does not show absorption in the visible region. Since 4f orbital of praseodymium are shielded from the surroundings it is not possible to obtain information related to its geometry of coordination sphere from absorption measurement studies<sup>82,83</sup>. Absence of absorption bands at 500-600 nm range due to Pr<sup>3+</sup> transitions evidenced that catalyst is not containing these ions<sup>84</sup>.

Figure 4.18 depicts the UV-vis DR spectra obtained for VPRS series of catalysts.



**Figure 4.18**

UV-vis DR spectra of VPRS series catalysts also exhibit the similar behaviour as that of VP series. All catalysts appeared black after calcination at 773 K, which gave no absorption in the visible region.

#### **4.1.6 FT-infrared spectroscopy**

In general the FT-IR spectroscopy is used to confirm the structure assignments, since the V-O stretching vibrations are usually characterized as “strong” whereas the bending vibrations get the “weak-medium” range.

Figure 4.19 shows FT-IR spectra of CRS obtained by the KBr method.



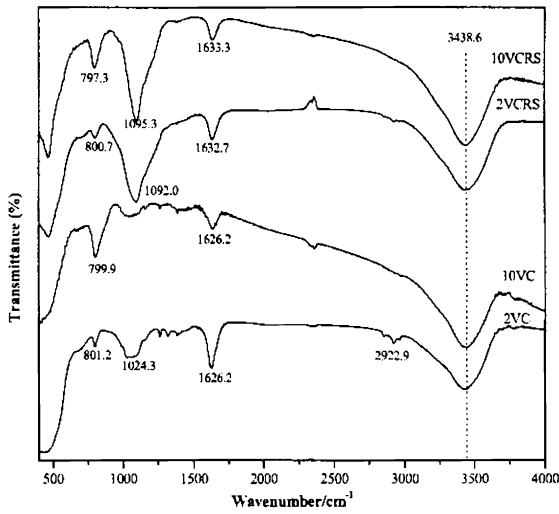
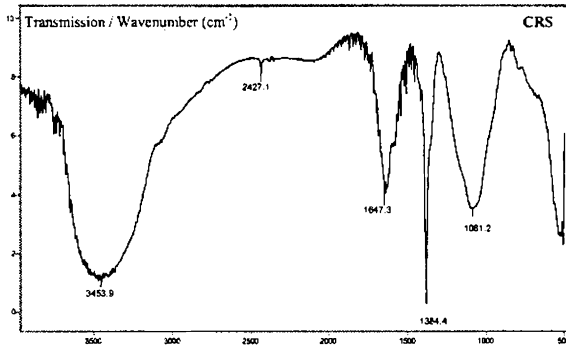


Figure 4.19

Ceria is only weakly absorbed in the infrared region. The absorption band at 465 and 1384 cm<sup>-1</sup> is the characteristics of CeO<sub>2</sub><sup>85</sup>. FT-IR spectrum of CRS in the 1000-4000 cm<sup>-1</sup> region exhibits a broad absorption band at 3760-3000 cm<sup>-1</sup> and a sharp band at ~1645 cm<sup>-1</sup>, due to surface hydroxyls and

coordinated water. The band around  $1081\text{ cm}^{-1}$  corresponds to the asymmetric  $\nu_{\text{as}}$  (Si-O-Si) stretching vibrations. In the hydroxyl region ( $3200\text{-}3600\text{ cm}^{-1}$ ), a very broad IR absorption band centered at  $3463\text{ cm}^{-1}$  is observed, which is ascribed to the silanol groups occurring with strong hydrogen bonding<sup>86</sup>.

For VC catalysts the absorption bands are visible in the range  $795\text{-}805$  and  $1000\text{-}1100\text{ cm}^{-1}$  regions in addition to those observed for ceria. The band at  $1022\text{ cm}^{-1}$  was reported to the V=O stretching vibration, while that at  $818\text{ cm}^{-1}$  was attributed to the coupled vibrations between V=O and V-O-V<sup>87,88</sup>. In general, the sharp band with a maximum at  $1022\text{ cm}^{-1}$  is attributed to the fundamental V=O stretching mode of surface  $\text{VO}_x$  species and bands in the range  $1065\text{-}980\text{ cm}^{-1}$  contains contributing peaks from the stretching modes of isolated  $\text{VO}_4$  species directly bonded to the support<sup>89</sup>. A band is observed at  $1024\text{ cm}^{-1}$  for 2VC corresponding to surface V=O species and at  $801.2\text{ cm}^{-1}$  due to coupled vibration. The intensity of the V=O absorption decreased and more intense band at  $799\text{ cm}^{-1}$  is observed with increasing vanadia to 10VC and is arises from the  $\text{VO}_4^{3-}$  species of orthovanadate structure<sup>90</sup>. Sohn et al.<sup>91</sup> reported a similar observation for  $\text{V}_2\text{O}_5/\text{ZrO}_2$  in which at  $973\text{ K}$  all  $\text{V}_2\text{O}_5$  reacted with  $\text{ZrO}_2$  and changed to  $\text{ZrV}_2\text{O}_7$  so that V=O stretching at  $1022\text{ cm}^{-1}$  disappeared completely. However, at  $1073\text{ K}$  some of the  $\text{ZrV}_2\text{O}_7$  decomposed into  $\text{V}_2\text{O}_5$  and  $\text{ZrO}_2$  and then V=O stretching band due to the crystalline  $\text{V}_2\text{O}_5$  was again observed at  $1022\text{ cm}^{-1}$ . These are in good agreement with those of  $^{51}\text{V}$  MASNMR described later.

In 2 and 10VCRS, the peak intensities of hydroxyl absorption are large and the presence of Si-O-Si vibration is retained at  $\sim 1093\text{ cm}^{-1}$ . IR spectrum of 2VCRS show a less intense band at  $800\text{ cm}^{-1}$  attributes to highly dispersed

$\text{VO}_x$  species compared to 10VCRS in which corresponding vibration is observed at  $797\text{ cm}^{-1}$  with more intensity. The structure of vanadia on CRS for low weight loadings is similar to that on other oxides with an isolated  $\text{VO}_4$  species<sup>92,93</sup>. In 10VCRS intense peak suggests more number of  $\text{V}=\text{O}$  species than 2VCRS. No band observed around  $1022\text{ cm}^{-1}$  suggests that vanadium oxide is in a highly dispersed state on CRS support. Formation of vanadium crystallites on silica occurs well below monolayer coverage compared to other oxides while two-dimensional polyvanadate species are not readily formed<sup>94-96</sup>. This confirms the results obtained from XRD analysis are in good agreement with those of FT-Raman and  $^{51}\text{V}$  solid state NMR which will be observed later.

Figure 4.20 depicts the FT-IR spectra of VP and VPRS catalysts.

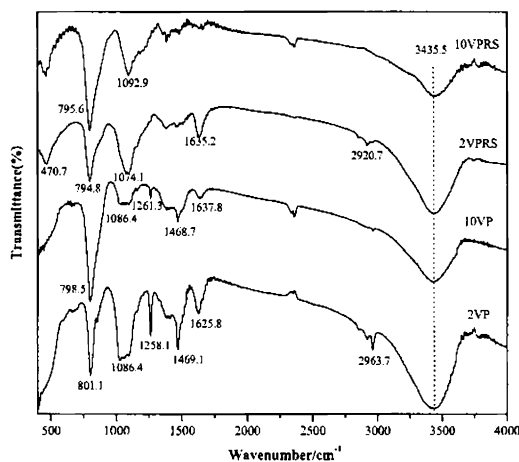


**Figure 4.20**

The spectra of 2VP shows sharp peaks at 801, 1032, 1086, 1258, 1469, 1625,  $2963\text{ cm}^{-1}$  and in the region  $3500\text{--}3200\text{ cm}^{-1}$  while 10VP shows a strong band at  $798\text{ cm}^{-1}$  with low intense bands at 1086, 1261, 1468, 1637 and 2962

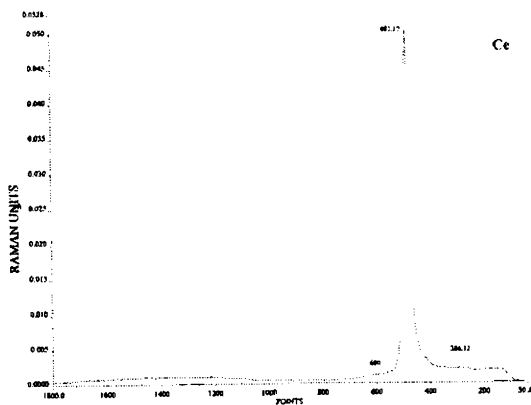
$\text{cm}^{-1}$ . The peak observed at  $1032 \text{ cm}^{-1}$  for 2VP results from the V=O stretching of the vanadia species<sup>97</sup>. The prominent band observed of 10VP at  $798 \text{ cm}^{-1}$  can be accounted for the presence of higher vanadate species<sup>98</sup>. In general it is due to the asymmetric stretching of  $\text{VO}_4^{3-}$  entity. The formation of higher vanadates species depends on the nature of acid-base properties of supports and on the vanadia concentration<sup>99</sup>. In acidic supports V-O-V polymers and on basic supports pyro or orthovanadates are preferentially formed. The bands in the region  $3200\text{-}3600$  and  $1500\text{-}1600 \text{ cm}^{-1}$ s correspond to surface hydroxyls and coordinated water. A broad band centered on  $3435 \text{ cm}^{-1}$  is accounted for the presence of surface hydroxyl groups and a slight decrease in intensity of this band with 10VP shows some sort of interaction of the surface hydroxyls with vanadia. FT-IR analysis of  $\text{V}_2\text{O}_5/\text{Nd}_2\text{O}_3$  catalyst suggests the formation of higher vanadates with increase in vanadia loading after monolayer capacity<sup>100</sup>. For 2 and 10 VPRS, absorption corresponding to the presence of Si-O-Si vibration is retained at  $\sim 1092 \text{ cm}^{-1}$  with all other absorptions similar to that of VP catalysts. Absence of crystalline  $\text{V}_2\text{O}_5$  as evidenced from XRD technique is confirmed since formation of any polyvanadyl surface species with stretching frequencies in  $1000\text{-}950 \text{ cm}^{-1}$  is not observed<sup>101</sup>.

#### **4.1.7 FT-Raman spectroscopy**

Raman spectroscopy directly probes structures and bonds by its vibrational spectrum. Therefore this technique has been extensively used to discriminate between different structures on oxide surfaces<sup>102,103</sup>. The distinction between highly dispersed surface phases and otherwise crystalline species may be discerned on the basis of whether hydration-dehydration

produces shifts in the terminal metal=O stretching mode. Raman spectroscopy was used to identify changes in the structure of dispersed  $V_2O_5$  in dependence on its loading and the nature of the support<sup>104</sup>. By the nature of the reflected radiation Raman spectroscopy is more sensitive to the catalyst surface<sup>105-108</sup>. For supported vanadia, however, Raman spectra can appear to be essentially similar to bulk  $V_2O_5$  but without the  $V_2O_5$  having a reducibility that is similar to bulk  $V_2O_5$ . This difference is a result of relatively large Raman scattering cross section for  $V_2O_5$  as compared to the scattering cross section for supported vanadia species. A decrease in reducibility may suggest a significant distortion of  $V_2O_5$  bonding and/or some interaction of a  $V_2O_5$ -like species with the support. Hence a close examination of vanadia should be needed to ascertain whether broadening and peak splitting have occurred<sup>109-111</sup>.

Figure 4.21 illustrates the FT-Raman spectra of  $CeO_2$  and CRS.



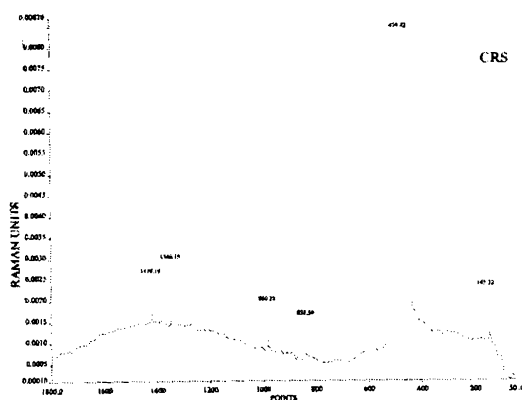


Figure 4.21

As shown in Figure 4.21, the spectrum of ceria exhibits a prominent peak at 475-485  $\text{cm}^{-1}$ , a weak band at 286  $\text{cm}^{-1}$  and a shoulder at 600  $\text{cm}^{-1}$ . According to the literature, only one mode ( $F_{2g}$ ) is Raman active for the fluorite structure of ceria with space group  $Fm\bar{3}m$ <sup>112</sup>. This band is characteristic of the presence of a cubic  $\text{CeO}_2$  phase<sup>113</sup>. In general, the spectrum of ceria is characterized by a strong band at 462  $\text{cm}^{-1}$  due to the triply degenerate  $F_{2g}$  Raman active mode regarded as symmetric O-Ce-O stretching of the fluorite structure<sup>114,115</sup>. The strong band observed at 482  $\text{cm}^{-1}$  can be attributed to the triply degenerate  $F_{2g}$  Raman active mode of the fluorite structure of ceria and can be viewed as a symmetric breathing mode of oxygen atoms around cerium ions. It also exhibits a weak band at  $\sim 286 \text{ cm}^{-1}$  and a shoulder at  $\sim 600 \text{ cm}^{-1}$ , which have been attributed to the normal Raman inactive (IR active) transverse and longitudinal optical phonon modes, respectively, at the Brillouin zone center. Generally not observed in Raman but some defects can involve the relaxation of selection rules, in particular, has been linked to oxygen vacancies in the  $\text{CeO}_2$  lattice. In CRS, the weak Raman

bands observed at 838 and 980  $\text{cm}^{-1}$  are due to the Si-OH stretching mode of isolated surface hydroxyl groups and the bending modes of the support<sup>116</sup>. It has been reported that, silica gel gives vibrations at 975  $\text{cm}^{-1}$  (Si-O stretching of Si-OH group), 820-800, 605 and in the range 350-550  $\text{cm}^{-1}$  vibrational mode of Si-O-Si bridges<sup>117</sup>.

The FT-Raman spectra of 6VC and 6VCRS are shown in Figure 4.22.

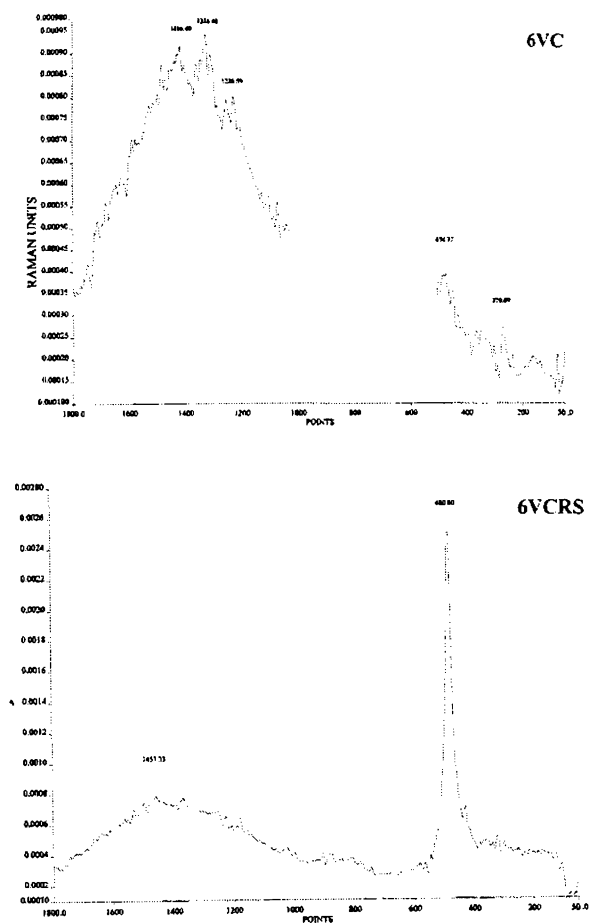


Figure 4.22

The spectrum of the 6VC exhibits Raman bands at  $\sim 270$ ,  $\sim 474$ ,  $\sim 1226$ ,  $\sim 1326$ , and  $\sim 1416$   $\text{cm}^{-1}$  and few broad bands in the region of  $1000$ - $1500$   $\text{cm}^{-1}$ . A band observed at  $\sim 270$   $\text{cm}^{-1}$  is assigned to surface vanadia species<sup>118-120</sup>. The other bands are due to the formation of  $\text{CeVO}_4$ . The band at  $474$   $\text{cm}^{-1}$  already observed in ceria is slightly shifted in this case. It can be assigned due to the presence of  $\text{VO}_4^{3-}$  tetrahedra. Bands in the region  $1000$ - $1200$   $\text{cm}^{-1}$  can be assigned to the stretching mode of surface  $\text{VO}_x$  species. Raman spectrum shows a strong band at  $995$   $\text{cm}^{-1}$  is usually attributed to microcrystalline  $\text{V}_2\text{O}_5$ , no such bands could be observed for vanadia loading up to 6 wt. %  $\text{V}_2\text{O}_5$ <sup>121</sup>.

In 6VCRS, the bands above  $1000$   $\text{cm}^{-1}$  due to  $\text{V}=\text{O}$  vibration are not much observed since the presence of amorphous  $\text{SiO}_2$  make the species more hydrated. The molecular structure of the supported vanadia species depends on the loading. Raman bands are usually attributed to the  $\text{V}=\text{O}$  vibration of  $\text{VO}_x$  species in either octahedral or tetrahedral environment. Generally, monovanadate or tetrahedral vanadia species have been assigned for low loading and two-dimensional polyvanadates or octahedral species with characteristic band around  $950$ - $990$   $\text{cm}^{-1}$ , for high vanadia loading<sup>122-126</sup>.

FT-Raman spectra of VP series of catalysts are depicted in Figure 4.23.



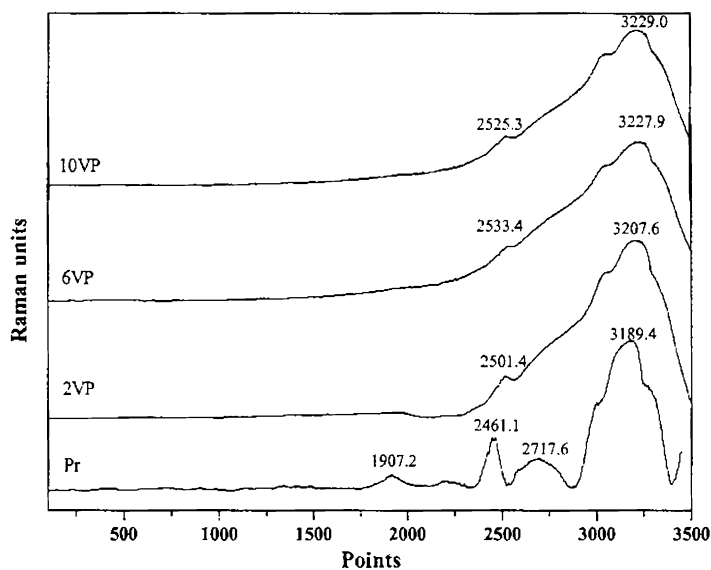


Figure 4.23

The peaks observed at 2717 and 3139 and 3590  $\text{cm}^{-1}$  are related to the  $\text{Pr}_x\text{O}_y$  and the peaks are identified as Pr-Raman peaks<sup>127</sup>. In VP catalysts, no peaks corresponding to 2717  $\text{cm}^{-1}$  appeared and the intensity of peak at 2461 decreases very much.

FT-Raman spectra of VPRS catalysts are depicted in Figures 4.24.

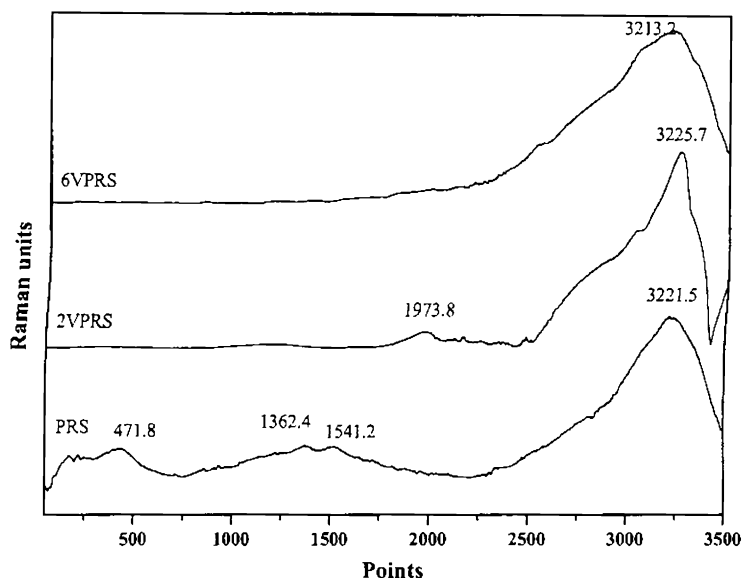


Figure 4.24

Raman spectra of VPRS catalysts appeared similar to VP catalysts. For PRS, the Si Raman peaks appear at  $471.3 \text{ cm}^{-1}$ <sup>128</sup>. The appearance of peak at  $3221.5 \text{ cm}^{-1}$  is related to the  $\text{Pr}_x\text{O}_y$ . The lack of detection of bands in the V-O-V bending region ( $200\text{-}300 \text{ cm}^{-1}$ ) for Zr-V catalysts suggests the species existing as isolated, tetrahedral or five-coordinated, mono-oxo species<sup>129</sup>. The highly broadened spectra suggest an amorphous nature for these catalysts<sup>130</sup>.

#### 4.1.8 Electron paramagnetic resonance spectroscopy

Electron magnetic resonance (EPR) techniques are widely used to study paramagnetic centers on various solid surfaces. These centers may be surface defects, inorganic or organic radicals, metal cations or supported metal

complexes and clusters. Each of these paramagnetic species will produce a characteristic EPR profile with well defined spin-hamiltonian parameters. However, the magnetic properties, stability and reactivity of these centers can vary dramatically depending on the nature of the support. In the present case, electron paramagnetic resonance measurements were carried out to investigate the influence of vanadia loading on the coordination geometry of vanadium oxide structures and the electron delocalization of rare earths supported vanadia catalysts under room and liquid nitrogen temperatures. Ceria, a well-known component of modern three-way exhaust-gas catalyst, can act as an oxygen reservoir, releasing oxygen under fuel-rich conditions, and absorbing oxygen under lean conditions. This is achieved via the facile  $\text{Ce}^{3+}$ - $\text{Ce}^{4+}$  redox couple with consequent formation/annihilation of surface defects or oxygen vacancies. All aspects of the catalysts such as redox sites, surface defect sites, metal dopants and dispersed metal particles have been investigated using EPR<sup>131-135</sup>.

The EPR spectra of the ceria and CRS supports collected at room temperature are shown in Figure 4.25.

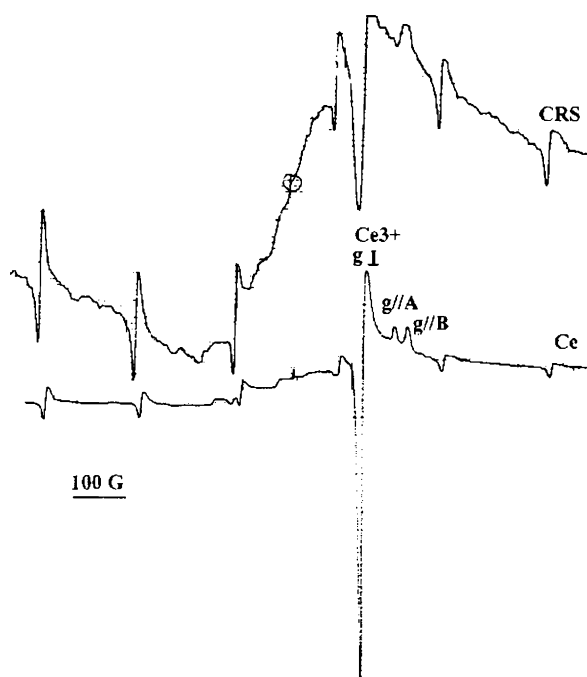


Figure 4.25

The spectrum of ceria is composed of two superimposed signals with  $g < 2$  denoted by A and B. These signals can be attributed to the presence of  $\text{Ce}^{3+}$  ions located at two different sites<sup>136-138</sup>. Signal A has been assigned to unpaired electrons trapped at oxygen vacancies, where these vacancies are stabilized by structural defects or impurities and the B signal to  $\text{Ce}^{3+}$  ions stabilized by some lattice defects ( $\text{CeO}_{2-x}$ )<sup>139</sup>. It has been also proposed that the unpaired electrons might be localized as  $\text{Ce}^{3+}$  ions in particularly low symmetry positions or delocalized among ions at the vacancy environment<sup>140,141</sup>. Ceria contains always a small percentage (about 6 %) of  $\text{Ce}^{3+}$  and the presence of  $\text{Ce}^{3+}$  related surface defects can leads to corresponding signals<sup>142</sup>. The  $\text{Ce}^{3+}$  ion has two isotopes  $^{140}\text{Ce}$  and  $^{142}\text{Ce}$  with natural abundances of 88.48 and 11.08 (%),

respectively. They do not possess any nuclear magnetic moment; thus, in their case, only one fine-structure EPR line corresponding to the electronic spin  $S = \frac{1}{2}$  is observed<sup>143</sup>. The nuclear spin of  $^{51}\text{V}$  is  $I = 7/2$  and natural abundance of 99.75 %<sup>144</sup>. In contrast to the closed shell  $\text{Ce}^{4+}$  ion,  $\text{Ce}^{3+}$  possesses a single electron, which in the ground state configuration lies in the  $4f^1$  orbital. Within this configuration the transitions between levels are formally parity forbidden. However, relative to other trivalent rare earth ions,  $\text{Ce}^{3+}$  has a first state configuration  $5d^1$  that is close in energy. Thus parity-allowed electric dipole transitions  $4f^1 \rightarrow 5d^1$  can easily occur in the UV range as evidenced from UV-vis DR spectra<sup>145</sup>. The spectra suggest presence of  $\text{Ce}^{3+}$  that can be detected by EPR. Spectra obtained also at 77 K in order to justify its detection in spite of the low spin relaxation time expected for these ions. When ceria is promoted with silica, the intensity of the A signal decreased whereas, the B signal intensity remained stable. Since the A signal is disappeared after silica introduction into ceria, it is believed that the  $\text{Ce}^{3+}$  ions corresponding to that signal can be located on the ceria surface, whereas those corresponding to the B signal are in the ceria bulk. Thus promoted species are located on the surface rather than in the bulk of ceria.

The EPR spectra of VC series catalysts collected at room and liquid nitrogen (77 K) temperature are shown in Figure 4.26.

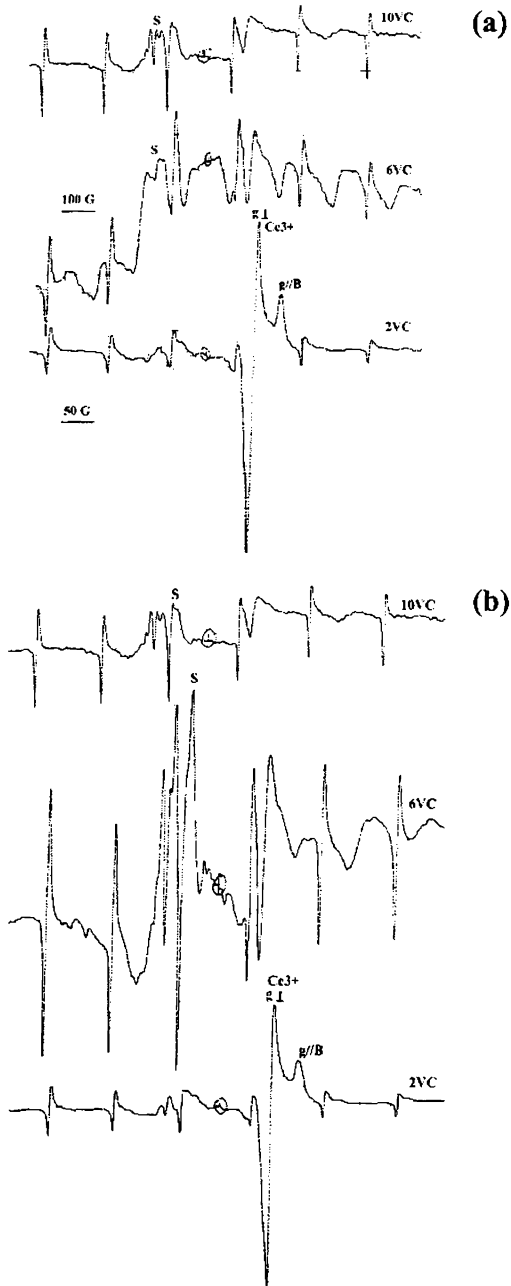


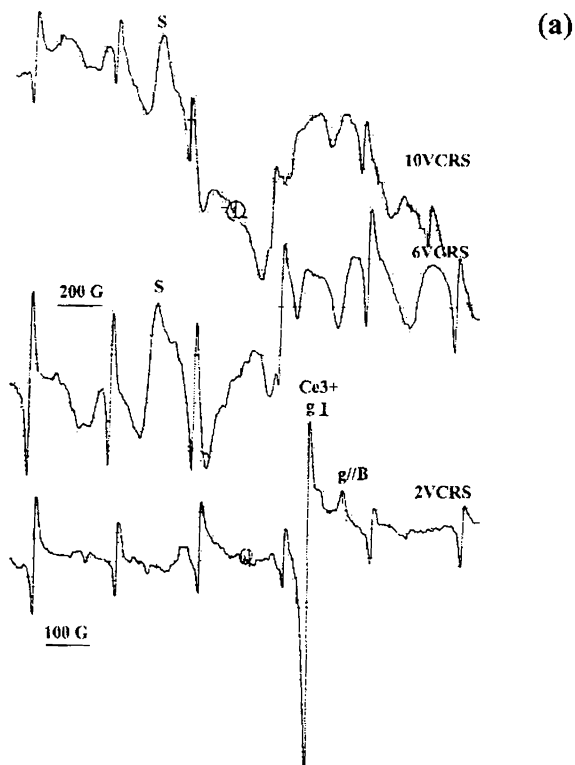
Figure 4. 26

In comparison with pure ceria, it is observed that the presence of vanadium ions in VC catalysts stabilized the  $Ce^{3+}$  species, leading to B signal for all vanadia loading. However, intensity of signal corresponding to  $Ce^{3+}$  is reduced for high vanadia loading suggesting reduced concentration of paramagnetic centre. It provides an evidence for the ability of ceria to lose its lattice oxygen and form  $Ce^{3+}$  ions thereby modifying redox process. Similar behaviour was reported in yttria stabilized ceria<sup>146</sup>. The oxygen vacancies are created in reduced ceria according to the equation,  $2Ce^{4+} + O^{2-} \leftrightarrow 1/2 O_{2(g)} + 2Ce^{3+} + V_o \dots$ , where  $V_o \dots$  is a doubly positively charged oxygen vacancy. The incorporation of reduced metal oxide is believed to increase the concentration of these  $V_o \dots$  vacancies, and so shift the above equilibrium to the left (decreasing the paramagnetic  $Ce^{3+}$  content). During this transformation the electron from  $Ce^{3+}$  is transferred to the oxygen vacancy centre according to:  $Ce^{3+} + V_o \dots \leftrightarrow Ce^{4+} + F^+$ . This  $F^+$  centers are the consequence of the spin-orbit coupling arising from the interaction of the trapped electron with the f orbital of the surrounding  $Ce^{4+}$  cations<sup>147</sup>. Thus redox behaviour gets enhanced upon vanadia impregnation.

No signal relative to  $V^{4+}$  species has been observed, whatever be the weight percentage of vanadia loading, demonstrating that the totality of the vanadium species is in the  $V^{5+}$  oxidation state after the complete decomposition of vanadyl oxalate on the ceria support. This confirms the corresponding remarks obtained from TGA/DTA and NMR studies. For high vanadia loading, a new signal denoted by S is appeared. This signal is attributed to trapped electron in oxygen vacancies<sup>148</sup>. To have a better

resolution of the signal, the recording of the spectrum has been performed also at 77 K. The intensity of the S signal increases with the decrease of the recording temperature following  $(I_1/I_2 = T_1/T_2)$ . Increase in intensity is much more with 6VC and such phenomenon can arise from the paramagnetic species with short spin relaxation time. The similar behaviour was reported for  $\text{TeO}_2$  crystals and is attributed to trapped electron in oxygen vacancies<sup>149</sup>. The appearance of the S signal can be correlated to the formation of the  $\text{CeVO}_4$  already observed from other techniques.

The EPR spectra of VCRS series catalysts collected at room and liquid nitrogen (77 K) temperature are shown in Figure 4.27.





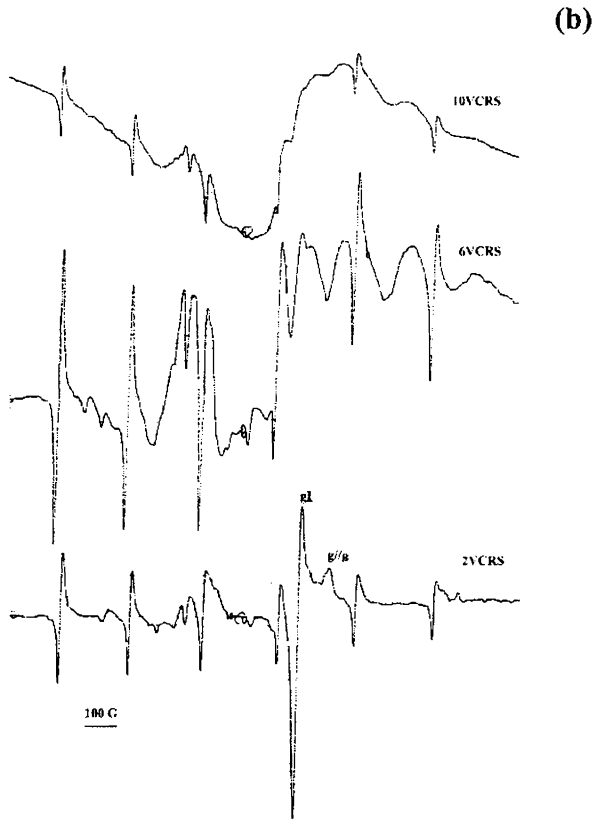


Figure 4. 27

The EPR spectra of VCERS catalysts also show the same pattern as that of VC catalysts. Signal A vanished after vanadia impregnation. The intensity of signal corresponding to  $\text{Ce}^{3+}$  is reduced as the vanadia loading increases suggesting  $\text{CeO}_2$  consumption to form  $\text{CeVO}_4$  phase. The spectra obtained at 77 K shows an enhancement of S signal for 6VCERS. Intensity of S signal is more for 10VCERS compared to 10VC for spectra obtained at room temperature.

The EPR parameters of ceria catalysts obtained at room

temperature are presented in Table 4.10.

**Table 4.10**

Catalyst	EPR parameters		
	$g_{\perp}$	$g_{//A}$	$g_{//B}$
CeO <sub>2</sub>	1.966	1.943	1.934
CRS	1.960		1.931
2VC	1.964	-	1.939
6VC	1.984	-	1.966
10VC	1.978	-	1.966
2VCRS	1.966	-	1.939
6VCRS	1.984	-	1.949
10VCRS	1.978	-	1.948

The A and B signals are apparently characterized as  $g_{\perp(A)} = 1.966$  and  $g_{//A} = 1.943$  and  $g_{//B} = 1.934$  respectively. These hamiltonian parameters observed for ceria can be attributed to the presence of two different types of Ce<sup>3+</sup> [ $f^1$  ions:  $g_e > g_{\perp} > g_{//}$ ] sites either in the bulk or surface states. Similar results were reported in the literature and assigned to Ce<sup>3+</sup> ions or, more precisely, to an interaction between conduction electrons and 4f orbitals of Ce<sup>4+</sup> ions in the CeO<sub>2</sub> matrix<sup>150</sup>. For 2VC and VCRS the  $g_{\perp}$  value is =  $\sim 1.964$  and  $g_{//B} = 1.939$ . These values are close to Hamiltonian parameters of ceria. The effective  $g$  values that are deduced from the spectra, are  $g_{\perp(A)} = 1.984, 1.978, g_{//B} = 1.949$  and  $1.948$  for 6, 10VC and VCRS respectively. These are due to the presence of Ce<sup>3+</sup> in the matrix and to the lattice defect centers<sup>151</sup>.

The EPR spectra obtained at room temperature for praseodymia and PRS supports are presented in Figure 4.28.

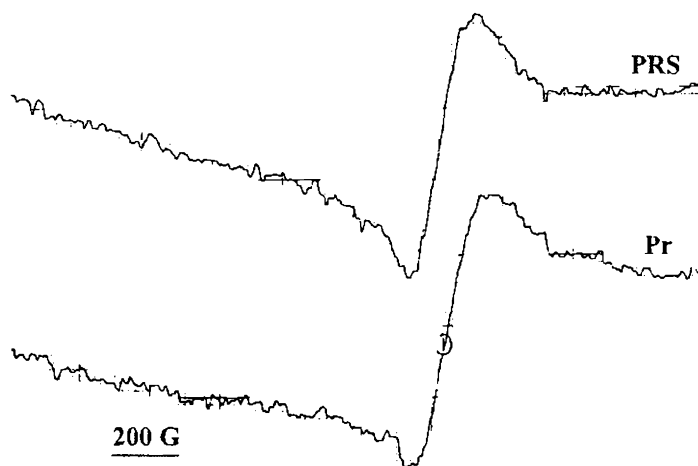
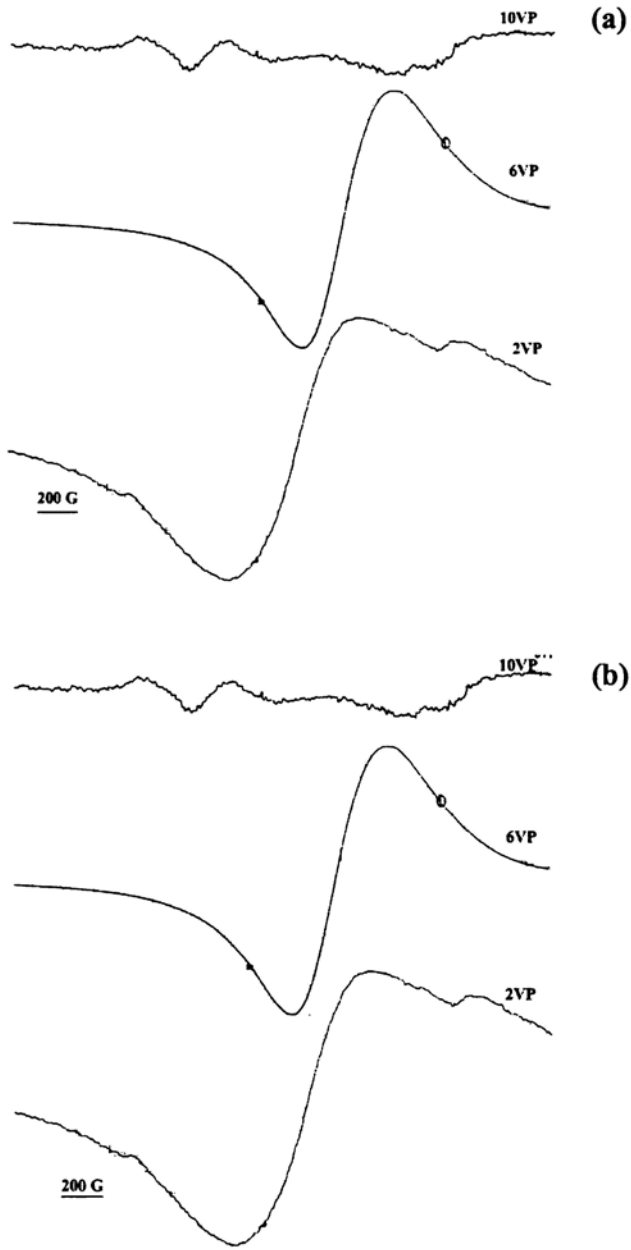


Figure 4. 28

No specific features corresponding to  $\text{Pr}^{3+}$  could be observed from the spectra suggesting the complete formation of  $\text{Pr}^{4+}$  ions at the calcination temperature of 773 K.

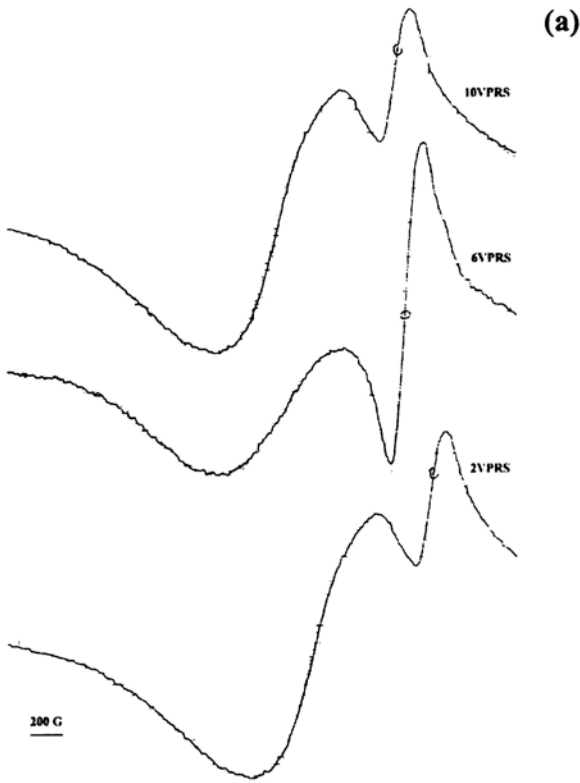
The EPR spectra obtained for VP series of catalysts at room temperature and 77 K are presented in Figure 4.29.



**Figure 4. 29**

The spectra of 2 and 6 VP have similar pattern while that of 10 VP is different. Spectra do not show any features of  $\text{Pr}^{3+}$  or  $\text{V}^{4+}$ . A different pattern of 10 VP suggests structure different from others as indicated by XRD analysis.

The EPR spectra obtained for VPRS series of catalysts at room temperature and 77 K are presented in Figure 4.30.



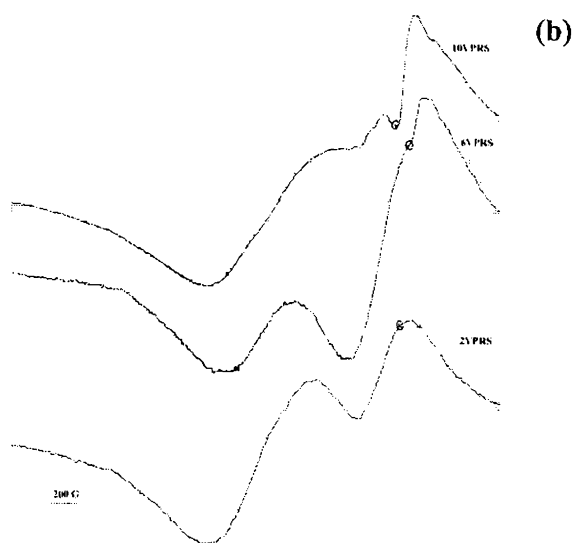


Figure 4.30

The EPR parameters of praseodymia catalysts calculated at room temperature are presented in Table 4.11.

Table 4.11

Catalyst	g value
Pr	1.996
PRS	2.003
2VP	2.574
6VP	2.465
10VP	1.978
2VPRS	2.015
6VPRS	1.999
10VPRS	1.978

The calculated g values show an increase upon silica promotion and vanadia loading.

### 4.1.9 $^{29}\text{Si}$ MAS NMR spectroscopy

In order to characterize the nature of the silica species in the catalysts, solid-state  $^{29}\text{Si}$  NMR spectroscopy was used. Figure 4.31 shows  $^{29}\text{Si}$  MAS NMR spectra obtained for RS and CRS supports with chemical shifts relative to that of TMS.

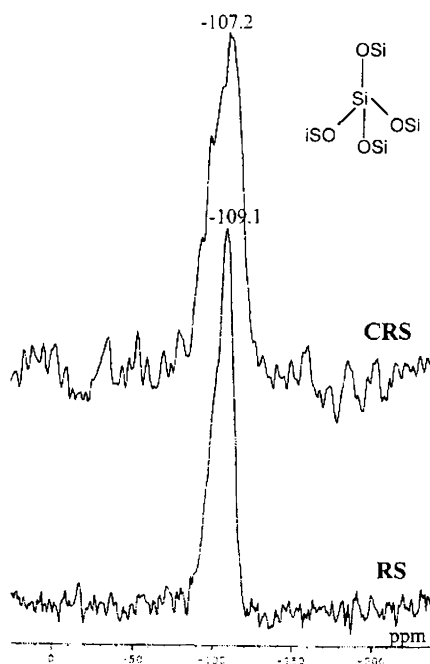


Figure 4.31

As a result of a wide range of Si-O-Si bond angles, amorphous silica related materials show broad peaks in the  $-90$  to  $110$  ppm regions. The silicate species can be assigned to  $Q^1$ ,  $Q^2$  (geminal silanol groups),  $Q^3$  (single silanol groups) and  $Q^4$  ( $\text{Si}(\text{OSi})_4$ ) units<sup>152</sup>. The  $^{29}\text{Si}$  MAS NMR spectra of RS and CRS showed a signal at  $\sim -109$  ppm. This signal obtained is assigned to

the presence of  $\text{Si}(\text{OSi})_4$  units<sup>153</sup>. This single composite signal centered near -109 ppm for RS arises from nuclei that are incompletely relaxed. The spectra also confirmed the presence of large number of internal silanol groups ( $\text{Q}^3$  sites) with a small shoulder around  $\sim -100$  ppm<sup>154</sup>.

The  $^{29}\text{Si}$  MAS NMR spectra obtained for 2 and 6VCRS are presented in Figure 4.32.

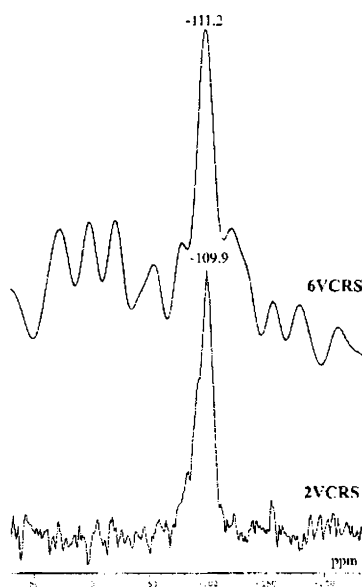


Figure 4. 32

The  $^{29}\text{Si}$  MAS NMR spectra evidenced  $\text{Q}^4$  units for VCRS catalysts. However, as the vanadium content increases (6VCRS), a highly symmetric shift centered at  $-111$  ppm was observed. For VMCM-41 a similar observation suggested that during the synthesis, vanadyl species ( $\text{VO}_2^{2+}$ ) may bind to the surface terminate groups ( $\equiv\text{Si}-\text{OH}$ ) in the MCM-41 matrix via condensation to



form  $(\text{SiO})_3 \text{V}=\text{O}$  type units thereby intensity of  $\text{Q}^3$  sites decreases or the intensity ratio of  $\text{Q}^4/\text{Q}^3$  sites increases<sup>155,156</sup>.

Figure 4.33 show  $^{29}\text{Si}$  MAS NMR spectra obtained for VPRS catalysts.

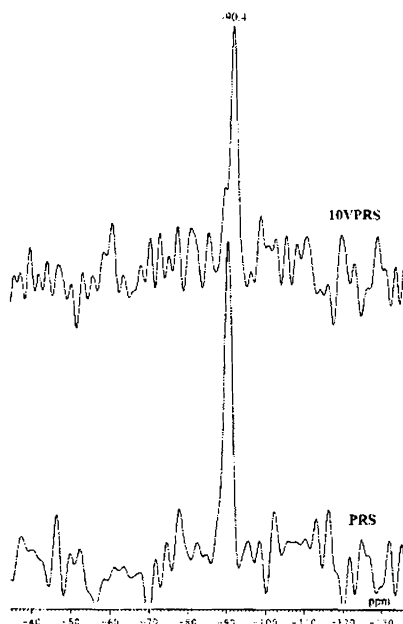


Figure 4. 33

In contrary to spectra of ceria catalysts, PRS and 10VPRS shows chemical shifts at  $\sim -90$  ppm. It suggests an interaction between Pr and Si atoms in the silica promoted catalysts. The formation of silicate like Si-O-Pr configuration was reported already for rare earth oxides  $\text{La}_2\text{O}_3$  and  $\text{Y}_2\text{O}_3$  on Si and  $\text{SiO}_2$ <sup>157,158</sup>. According to Shoyama et al.  $\text{Pr}^{4+}$  may substitute easily for both  $\text{Zr}^{4+}$  and  $\text{Si}^{4+}$  in a zircon lattice<sup>159</sup>.

#### 4.1.10 $^{51}\text{V}$ MAS NMR spectroscopy

Solid-state nuclear magnetic resonance (NMR) methods represent a novel and promising approach to vanadium oxide catalytic materials.  $\text{V}^{5+}$  containing phases can be easily characterized by conventional  $^{51}\text{V}$  MAS NMR<sup>160</sup>.  $^{51}\text{V}$  nucleus (natural abundance 99.76 %) has a spin quantum number of 7/2 and an electric quadrupole moment of 0.05 b<sup>161</sup>.  $^{51}\text{V}$  is a nucleus unusually with small quadrupole moment, relatively large gyromagnetic ratio and high natural abundance. So far  $^{51}\text{V}$  is one of the most popular nuclei in NMR study<sup>162</sup>. The small quadrupolar spin of  $^{51}\text{V}$  nucleus can lead to singularities in the NMR signals and it is usually admitted that the line shapes of the nonspinning spectra are dominated by the anisotropy of the chemical shift<sup>163</sup>. Indeed, the extensive applicability of NMR to solids relies heavily on magic angle spinning (MAS). This technique is able to narrow the lines by successful averaging dipolar, anisotropic chemical shielding and first order quadrupolar effects. However limitation of MAS remains due to residual line broadening from the quadrupolar interaction at second order. Nevertheless, in the case of vanadium, the small value of electric quadrupole moment moderates the quadrupolar interaction and simple MAS technique has proven to be a very convenient technique for vanadium characterization.

Last decade, numerous papers devoted to  $^{51}\text{V}$  NMR studies of solid vanadia based catalysts have been published, demonstrating NMR importance and self-descriptiveness for so complex systems as catalysts<sup>164-166</sup>. Structure and other physicochemical properties of the supported metal oxides are considered to be in different states compared with bulk metal oxides because

of their interaction with the supports. Since only the local environment of a nucleus under study is probed by NMR, this method is well suited for the structural analysis of disordered systems such as the two-dimensional surface vanadium oxide phases.

The solid-state  $^{51}\text{V}$  MAS NMR spectra of catalysts calcined at 773 K is recorded with a spinning frequency  $\nu_{\text{R}} = 7.0$  kHz. Figure 4.34 depicts the  $^{51}\text{V}$  MAS NMR spectra of  $\text{NH}_4\text{VO}_3$ , the reference compound for further investigation.

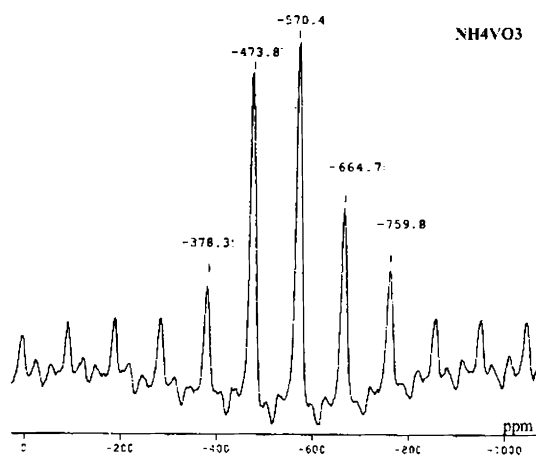
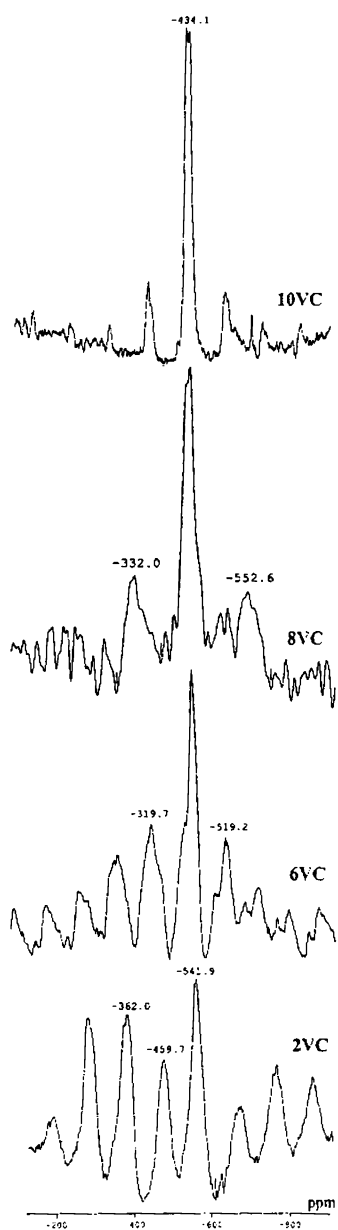


Figure 4.34

The spectrum displays a single broad peak centered at -572 ppm and several associated spinning bands. The peak around -572 ppm of ammonium metavanadate identified is related to the vanadyl oxygen with one water molecule coordinated and shift at -664 ppm is vanadium dimer with one water molecule coordinated to each V site suggesting an octahedral coordination environment<sup>167</sup>. The chemical shift at about -750 ppm indicates an octahedral oxygen coordination of vanadium atoms<sup>168</sup>.

The  $^{51}\text{V}$  MAS NMR spectra of VC catalysts are shown in Figure 4.35.



**Figure 4.35**

The surface vanadium oxide structure is remarkably dependent on the metal oxide support material. In general, it is known that low surface coverage favour a tetrahedral coordination of vanadium oxide, while at higher surface coverage vanadium oxide becomes increasingly octahedral coordinated. There are different types of signals in the spectra of catalysts with varying intensities depending on  $V_2O_5$  content. For low vanadium content catalyst 2VC, the peaks observed are at  $\sim -260$ ,  $\sim -360$ ,  $\sim -459$ ,  $\sim -495$ ,  $\sim -541$ ,  $\sim -545$ ,  $\sim -748$  and  $\sim -760$  ppm. This presents a species characterized by isotropic component and several associated spinning bands. The shape of the sideband pattern of species evidenced a distortion of the vanadium site. The broad line pattern associated with this species could be correlated with an absence of regular ordering of these vanadia sites. The peak at  $-260$  ppm is assigned to the surface vanadium-oxygen structures surrounded by a distorted octahedron of oxygen atoms<sup>169</sup>. The band at  $\sim -360$  ppm can be assigned to pseudo-octahedrally coordinated  $V^{5+}$  species as a consequence of the interaction of tetrahedral sites. The resonances at  $\sim -459$  and  $\sim -495$  ppm can be attributed to distorted isolated tetrahedral  $V^{5+}$  sites. The peaks at  $\sim -545$  and  $\sim -750$  ppm are attributed to the tetrahedral vanadium-oxygen structures. Hence, in this low vanadia supported catalysts, the species are consistent with surface  $V=O$  and polymeric species  $V-O-V$ , highly dispersed on the ceria surface<sup>170</sup>. For samples with higher vanadium content (6VC, 8VC, 10VC) a highly symmetric signal centered at  $\delta_{iso} = -432$  ppm has been obtained. Recently, it has been reported that the signal with  $\delta_{iso} = -432$  ppm corresponds to the tetragonal structure of cerium orthovanadate ( $CeVO_4$ ), in which vanadium atoms are located at the center of isolated tetrahedral<sup>171</sup>. The only peak of 10VC observed at  $-432$  ppm due to the

CeVO<sub>4</sub> compound saying that most of the V<sub>2</sub>O<sub>5</sub> on the surface of ceria was consumed to form the CeVO<sub>4</sub> compound. These observations are in good agreement with the results of the IR spectra. Different peak positions normally indicate the differences of the spectral parameters and are observed due to different local environments of vanadium nuclei.

The <sup>51</sup>V MAS NMR spectra of VCRS series of catalysts are shown in Figure 4.36.

At low vanadium content, the spectrum consists of intense bands at -260, -379, -761 (ppm) associated with several spinning side bands. It reveals the presence of tetrahedral vanadium species for 2 (%) vanadia loading on the support material. In the spectra of 6VCRS, a signal centered at -432 ppm has been obtained along with -264, -371, -573 and -776 (ppm) signals. The intensity of this signal is increased for 8 and 10VCRS. The chemical shift value around -432 ppm corresponds to the tetragonal structure of CeVO<sub>4</sub>, in which vanadium atoms are located at the center of isolated tetrahedra. The resonance around -260 is corresponds to that of the distorted octahedral environment present in the catalyst.

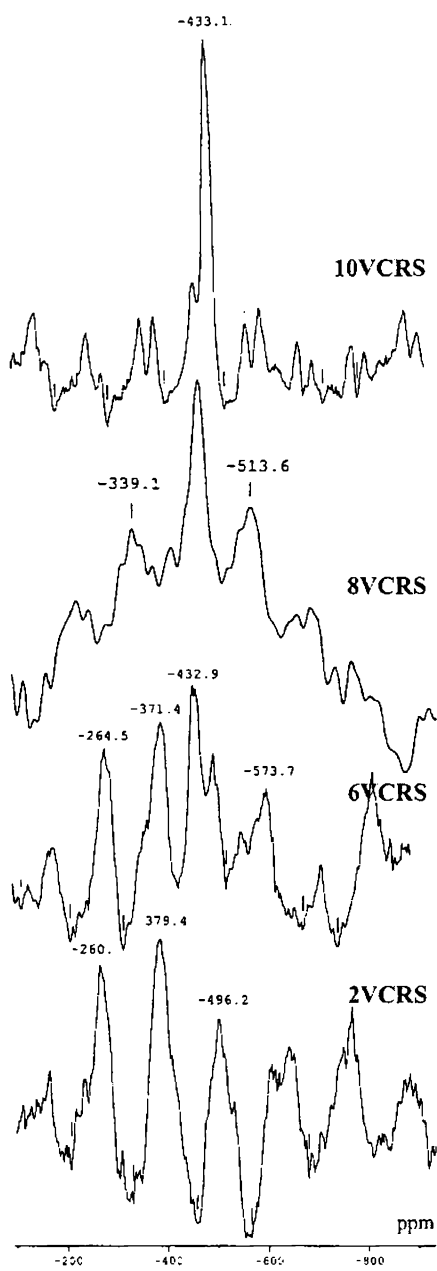
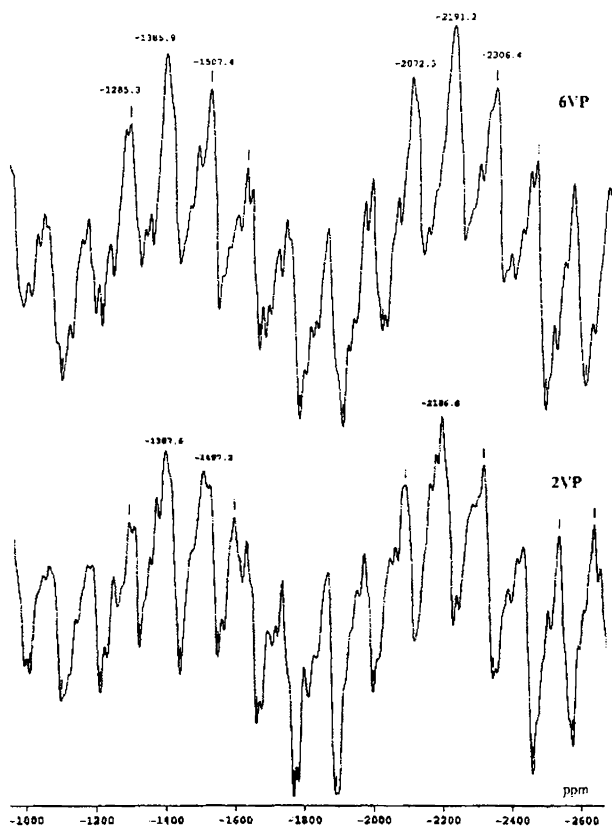


Figure 4.36

The  $^{51}\text{V}$  MAS NMR spectra of VP series of catalysts are shown in Figure 4.37.



**Figure 4.37**

The  $^{51}\text{V}$  MAS NMR spectra of VPRS catalysts recorded with 9 kHz spinning frequency are shown in Figure 4.38.



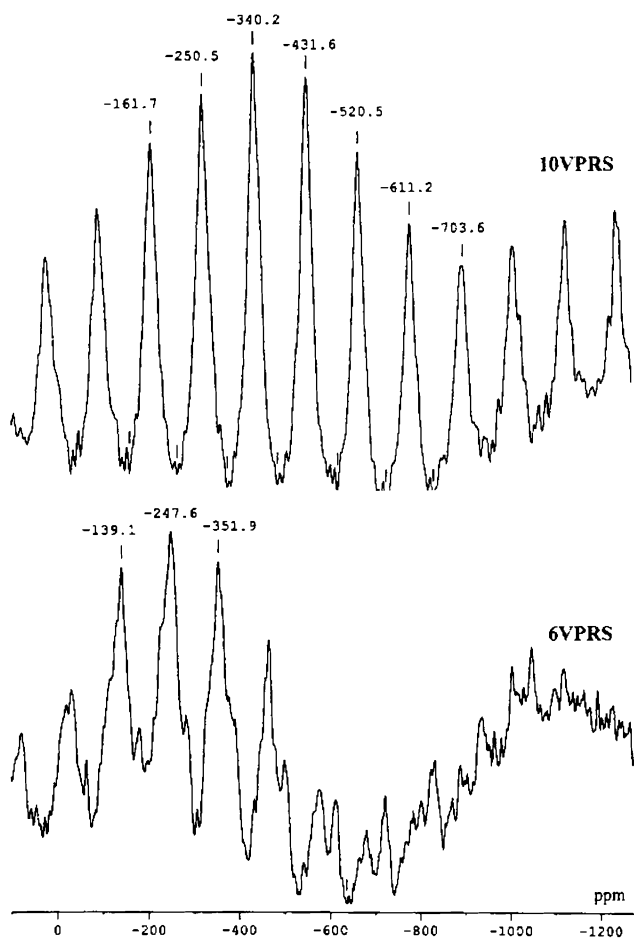


**Figure 4.38**

The  $^{51}\text{V}$  MAS NMR spectra of praseodymia containing vanadia catalysts exhibit a different pattern from that of ceria catalysts. A pyrovanadate type structure is evidenced from XRD analysis. Spectra exhibit several overlapping bands. In 6VPRS, the chemical shifts parameters are observed around  $\sim -139$ ,  $-247$ ,  $-351$ ,  $-490$  and  $-635$  ppm. These values are in agreement

with those reported for  $\beta$ - $\text{Mg}_2\text{V}_2\text{O}_7$ <sup>172</sup>. A well defined spectra observed for 10VPRS with an additional shift at  $\sim$ -432 ppm suggests presence of orthovanadate along with pyrovanadates upon 10 wt. %  $\text{V}_2\text{O}_5$  loading. The chemical shift anisotropy parameter increases with an increasing degree of polymerization and specific chemical shift values have been suggested for the different types of tetrahedrally coordinated V-O species and for vanadium in octahedral environments. Jorgen et al.<sup>173</sup> investigated  $^{51}\text{V}$  quadrupole coupling and chemical shift anisotropy for divalent metal pyrovanadates:  $\text{Mg}_2\text{V}_2\text{O}_7$ ,  $\text{Ca}_2\text{V}_2\text{O}_7$ ,  $\text{Zn}_2\text{V}_2\text{O}_7$ ,  $\text{Cd}_2\text{V}_2\text{O}_7$ ,  $\text{BaCaV}_2\text{O}_7$  and concluded that pyrovanadates can be distinguished as “thortveitite” and “dichromate” by the sign of the chemical shift anisotropy parameter.

#### **4.1.12 Scanning electron microscopy**

Scanning electron micrographs (SEM) are recorded to get the surface morphology of the supports and supported catalysts. SEM studies on supported vanadia catalysts are few in the literature<sup>174,175</sup>. SEM images of vanadium oxide made by different calcination temperatures showed structural differences varying from agglomerated small grains giving to needle like crystal and multilayer structure of sheets<sup>176</sup>. The stoichiometric  $\text{V}_2\text{O}_5$  is built up from distorted trigonal bipyramids,  $\text{VO}_5$  unit cell, so the 2-dimensional sheets, which are weakly linked each other via oxygen atoms.

Figure 4.39-4.41 envisages the scanning electron micrographs obtained for rice husk silica and ceria containing catalysts.

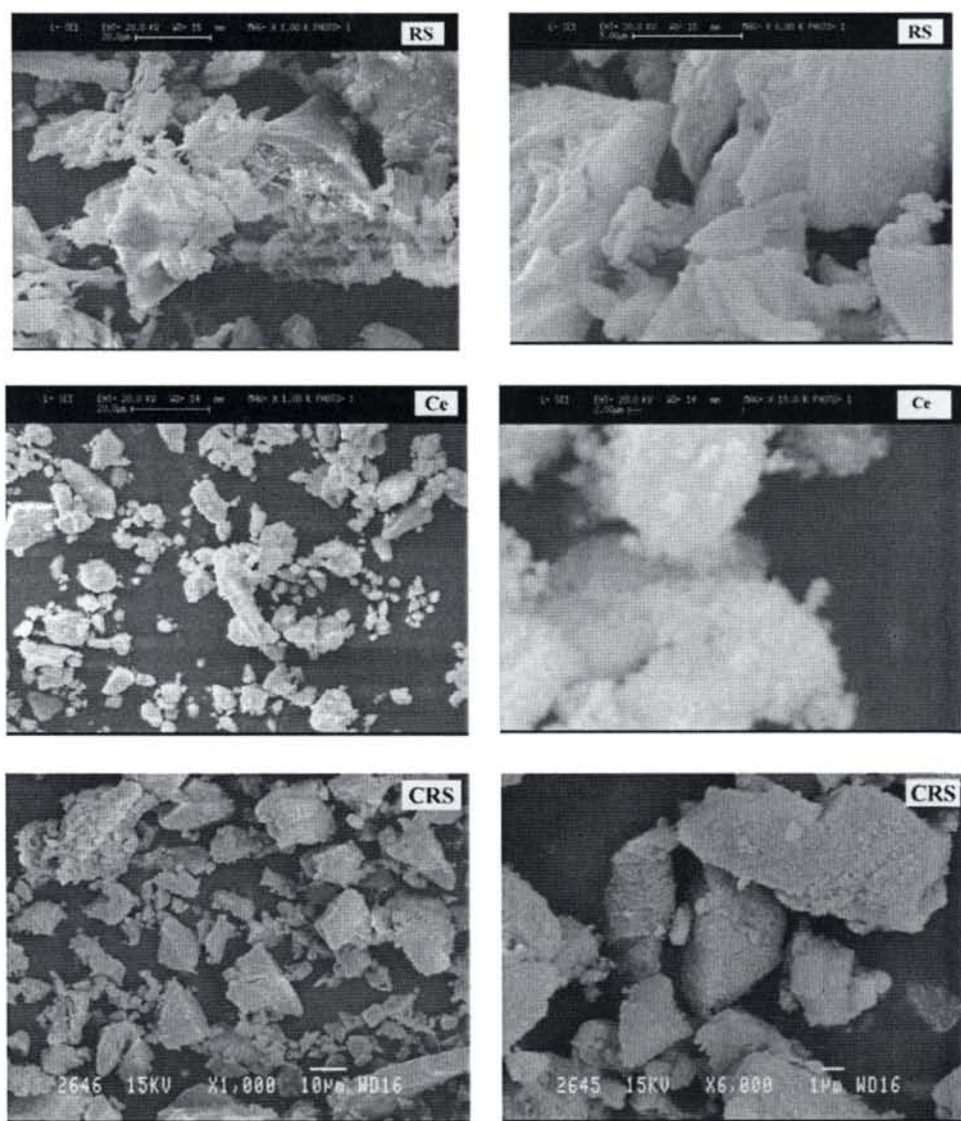
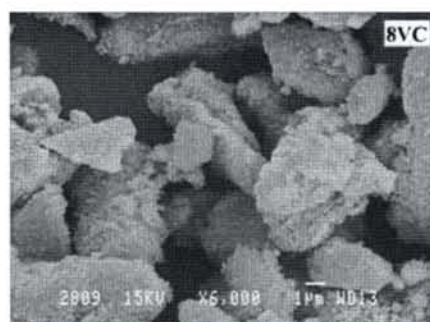
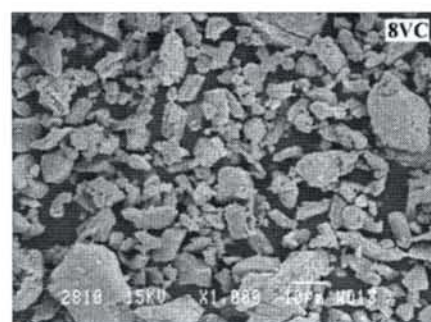
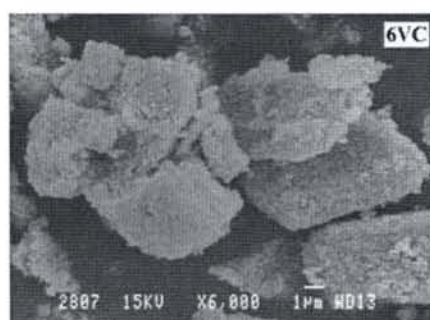
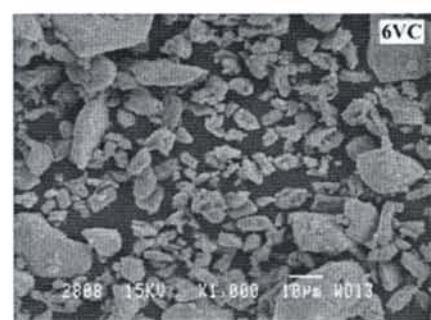
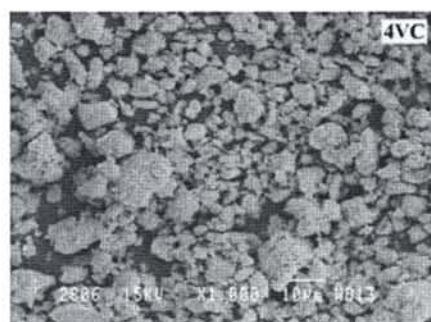
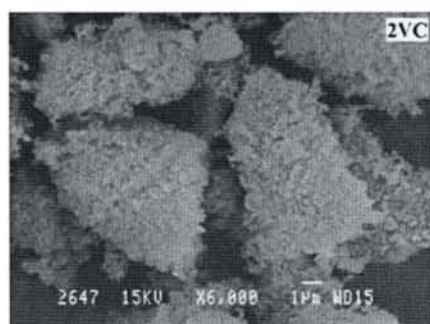
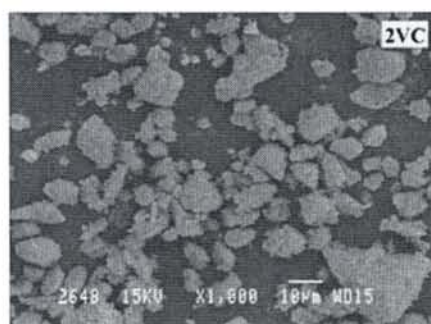


Figure 4.39



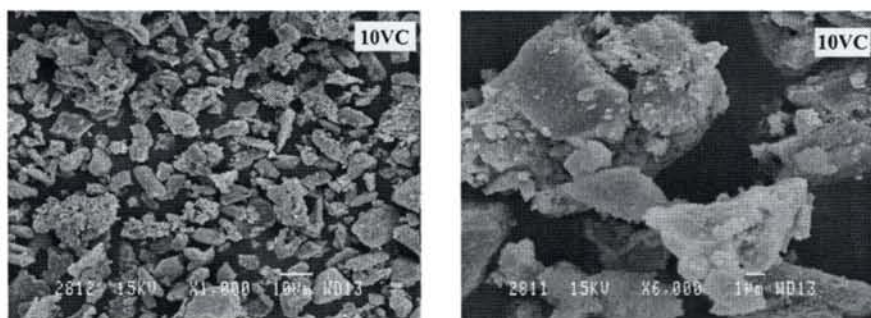
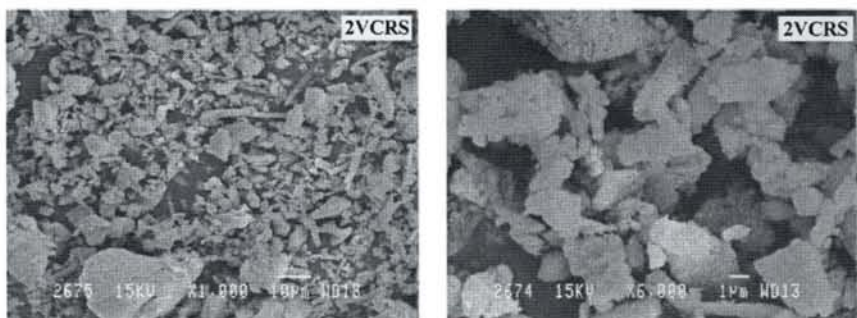
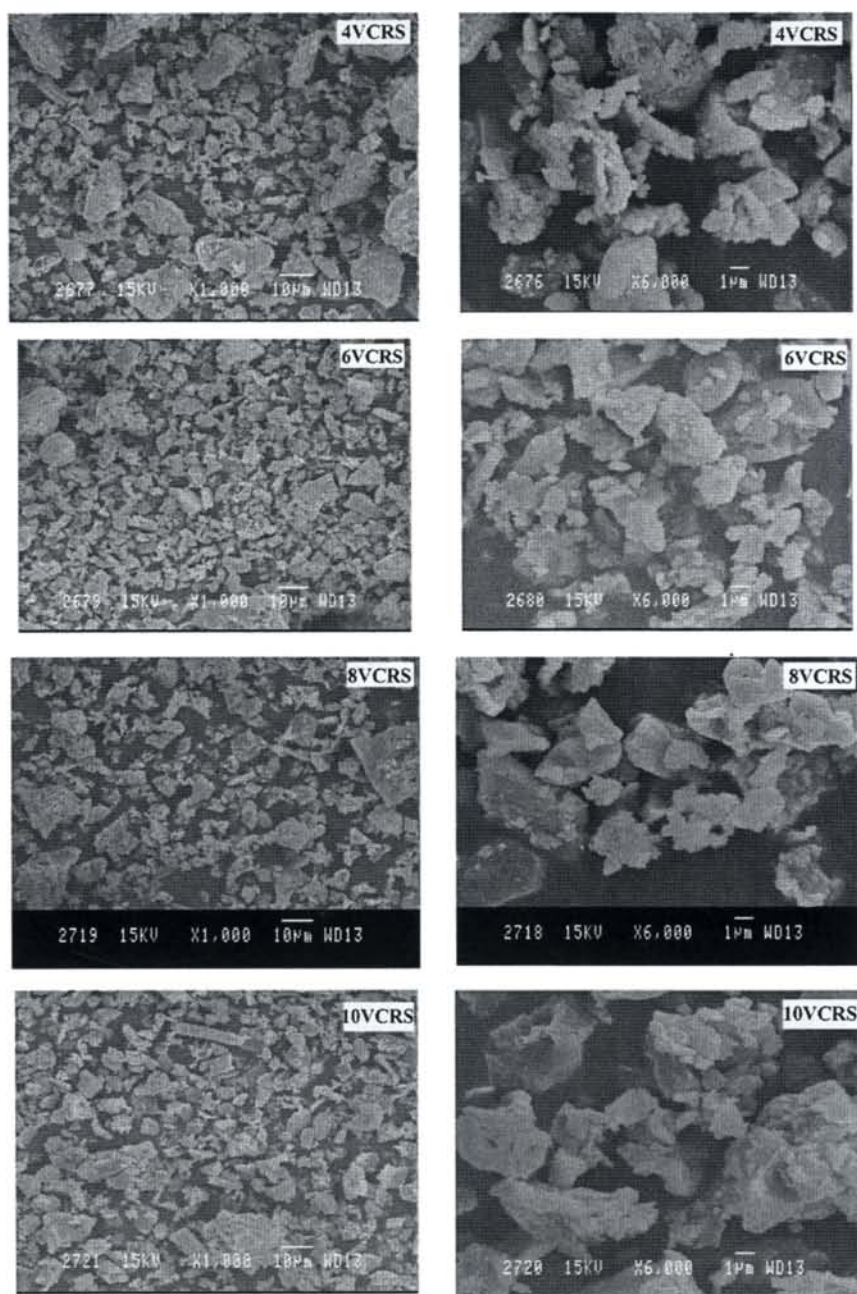


Figure 4.40

These micrographs show the morphology of the catalysts and its changes occurring at various wt. % of  $V_2O_5$  loading and with different supports. The electron micrographs of the catalysts with lower loading (2 to 6VC) show that the catalysts have a very fine dispersion of vanadia on ceria. However, for higher vanadia loading the particles are agglomerated into crystallites. The morphology is consistent with the observation of powder X-ray reflections.





**Figure 4.41**

In VCRS series of catalysts, comparatively smaller particles are observed and the increase of particle size is not that much with VC catalysts. Structure appeared like sheets up to 10VCRS.

Figure 4.42 envisages the scanning electron micrographs of  $\text{Pr}_x\text{O}_y$  and PRS.

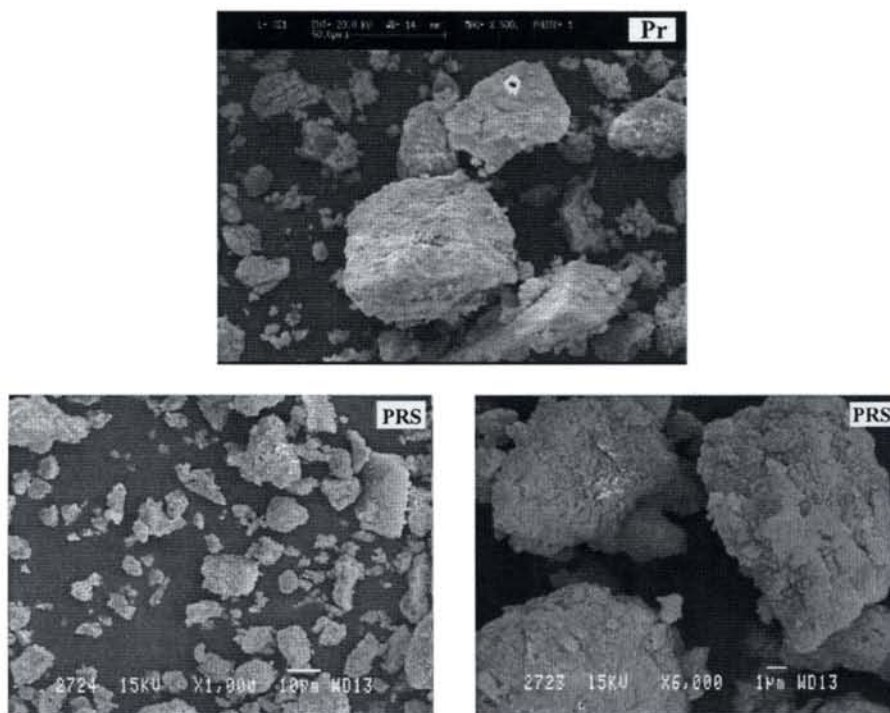
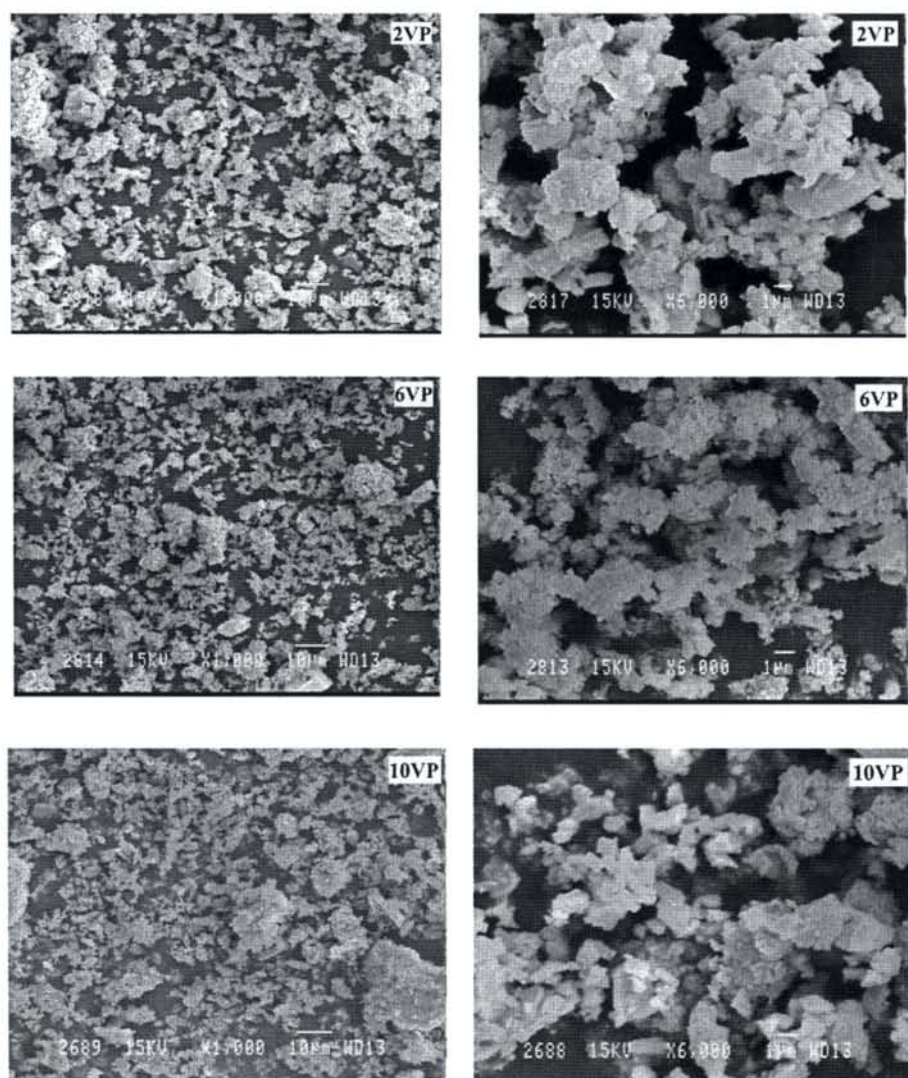


Figure 4.42

The micrographs of  $\text{Pr}_x\text{O}_y$  and PRS show comparatively larger particles than ceria supporting the low BET surface area shown by these supports.

Figure 4.43 and 4.44 envisage scanning electron micrographs of VP

and VPRS series of catalysts.



**Figure 4.43**



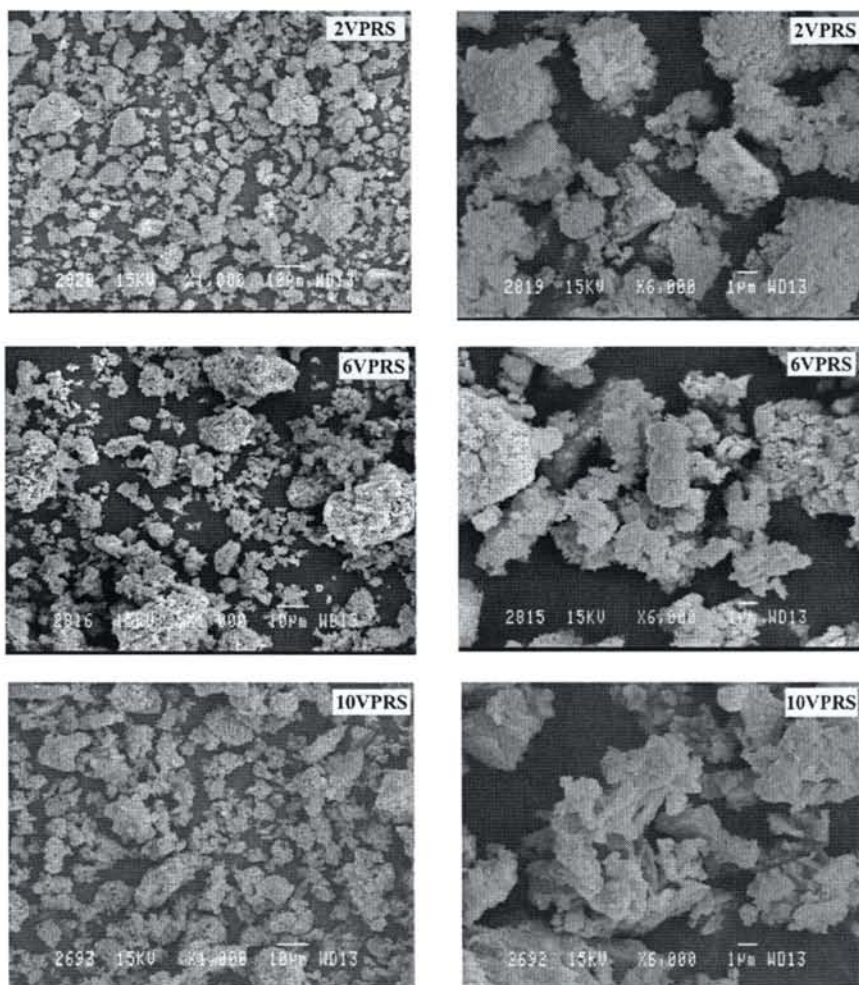


**Figure 4.44**

The scanning electron micrographs of VP and VPRS series of catalysts investigated by SEM show different morphology compared to ceria catalysts.

Figure 4.45 envisages the scanning electron micrographs obtained for various silica supported vanadia.

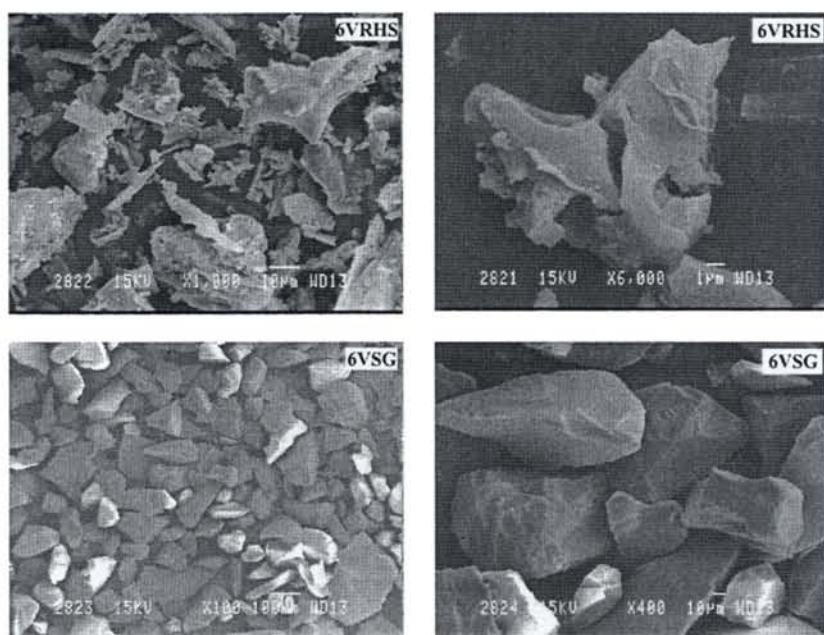


Figure 4. 45

#### 4.1.12 Temperature programmed reduction

Temperature programmed reduction (TPR) by  $H_2$  is a technique extensively studied in the literature to characterize the oxygen reducibility of doped oxide catalysts<sup>177-179</sup>. The interaction of reactants with the catalysts surface is a key parameter in heterogeneous reaction systems; the temperature at which species are desorbed from a surface is indicative of the strength of the surface bond: the higher the temperature, the stronger the bond. Therefore the adsorption of a probe molecule at low temperature, and subsequent monitoring of its desorption/reaction characteristics with temperature, is a simple way to characterize surface properties of catalysts and adsorbents<sup>180</sup>. The study of reduction of ceria and its interaction with  $H_2$  under more or less severe

conditions have represented a major effort in the last decade. Ceria is reduced by  $H_2$  at temperatures higher than 600 K and reduction is strongly affected by pretreatments, precursor salts, and presence of noble metals.

Often a correlation is observed between the reducibility of vanadia determined by temperature programmed reduction (TPR) in hydrogen and the catalytic activity. In spite of similar coordination of the vanadium atom in the monomeric and polymeric species, their structure differs strongly due to the different length of the V-O bonds. Moreover, contrary to the monomeric species, the polymeric species contain V-O-V oxygen bridges. Hence, different reducibility could be expected in hydrogen i.e., different pre-exponential factors and/or activation energies. However, the TPR profile of the catalysts containing these two species usually consists of one peak. This shows that a differentiation between monomeric and polymeric vanadia by this method is difficult<sup>181,182</sup>. It is appropriate to study the catalytic systems by TPR since the reduction behaviour is related to the strength of the V-O support bridging bond, which is a factor controlling both the reducibility and the redox activity of supported metal oxide catalysts<sup>183-189</sup>.

Temperature programmed reduction profile of ceria recorded in the range 0-900 °C is depicted in Figure 4.46.

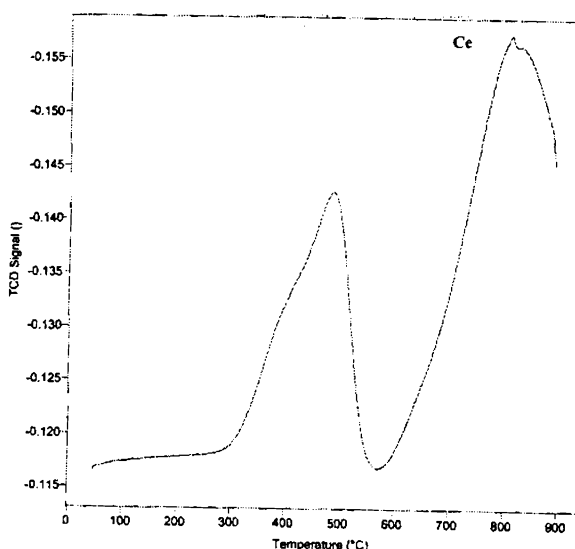


Figure 4.46

The TPR profile of ceria exhibits two reduction maxima, a low temperature (LT) peak with  $T_{\max 1}$  at 759 K, suggesting the reduction of surface-capping oxygen anions which attach to surface  $\text{Ce}^{4+}$  ions in an octahedral coordination and a high temperature peak (HT) at  $T_{\max 2}$  at 1084 K corresponding to the reduction of bulk oxygen ions<sup>190-192</sup>. The reduction profile of ceria is in agreement with previously reported data<sup>193</sup>. Since the intensity of low temperature peak is low majority of  $\text{H}_2$  consumption originates from the reduction of large ceria crystallites. The TPR profile of metal oxides as well as other solid materials is determined by factors like the thermodynamics and kinetics of reduction, the textural changes of the material and oxygen diffusion in the lattice structure.

Temperature programmed reduction profile of 4VC and 6VC recorded is depicted in Figure 4.47.

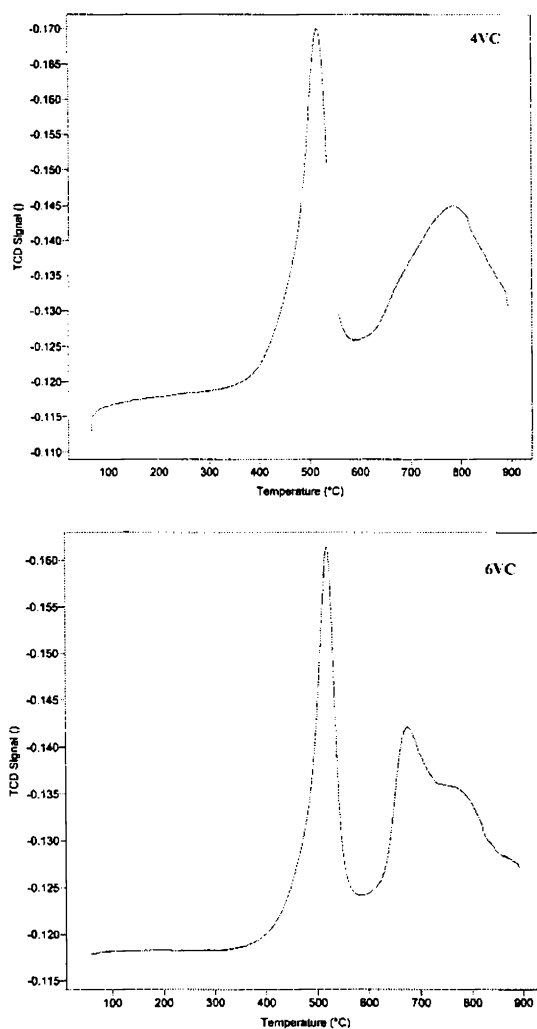


Figure 4.47

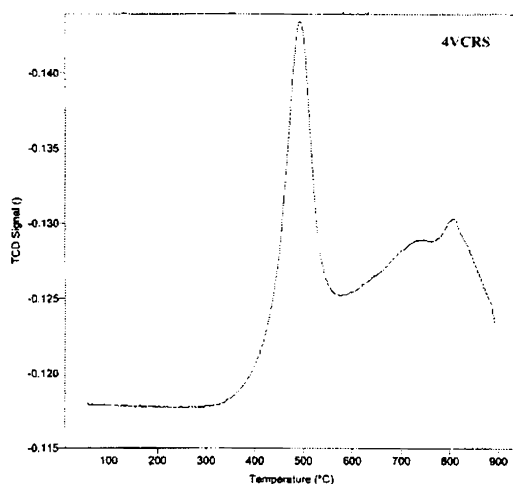
Analyzing the TPR spectra of 4VC and 6VC we may conclude that the change of  $T_{\max}$  positions in profiles of ceria supported catalysts suggests that vanadia interacts strongly with the supports<sup>194</sup>. In the case of supported catalysts the LT peak is shifted to significantly higher temperatures, while the

HT peaks shifted to lower temperatures. The TPR profile of 4VC is similar to that of ceria with low intense high temperature reduction peak. The fact that this TPR profile is similar to that of the ceria suggests that the  $\text{VO}_x$  species form a quite uniform layer over the support. Similar observation was reported by Munteanu et al.<sup>195</sup>. The  $\text{VO}_x$  species have, very probably, a similar structure to that of the ceria support being a kind of epitaxial  $\text{VO}_x$  layer on the surface of ceria. It is well known that the oxygen from the surface layers of ceria has a large mobility and this oxygen could reoxidize the  $\text{VO}_x$  species very quickly. This is in accordance with the findings of Andreeva et al.<sup>196</sup> which reported that in the case of  $\text{V}_2\text{O}_5/\text{TiO}_2$  and  $\text{V}_2\text{O}_5/\text{ZrO}_2$  catalysts an EPR signal specific of  $\text{V}^{4+}$  ions have evidenced, while in the case of  $\text{V}_2\text{O}_5/\text{CeO}_2$ , no such signal could be observed because when  $\text{CeO}_2$  is used as a support,  $\text{V}^{4+}$  cannot be preserved in this oxidation state due to the high mobility of the oxygen of the surface ceria layers. The TPR profile of 6VC exhibits the same pattern. The vanadia layer situated on ceria is thicker than that in the case of 4VC and consequently the processes become slower. This fact causes the shift of  $T_{\text{max}2}$  towards higher temperature.

The reduction pattern of  $\text{V}_2\text{O}_5$  exhibits multiple reduction peaks corresponding to the following reduction sequence:  $\text{V}_2\text{O}_5 \rightarrow \text{V}_6\text{O}_{13} \rightarrow \text{V}_2\text{O}_4 \rightarrow \text{V}_2\text{O}_3$ <sup>197</sup>. For the supported catalysts, depending on the support, a low temperature peak different in position and area was observed. This low temperature peak can be connected with the oxygen species around the vanadia particles as well as the reduction of the support on the border with vanadia. The reduction behaviour was different depending on the support and weight %  $\text{V}_2\text{O}_5$  loading. The impregnation of vanadia enhances the reduction of surface

layers. On the other hand, the reduction temperature of bulk layers decreases after  $V_2O_5$  impregnation in comparison to ceria. A synergistic effect between the vanadia and supports was established for the studied catalysts. Donka et al.<sup>198</sup> studied reduction behaviour of titania, zirconia and ceria supported gold-vanadia catalysts for complete benzene oxidation and concluded that, the highest activity and stability was established for the ceria supported catalysts, which can be connected with high oxygen storage capacity of ceria. The  $T_{max1}$  increased upon vanadia impregnation and increases with an increase in vanadia loading. This arises due to the formation of dispersed V oxides at higher loadings. Similar observation was found for Mn/CeO<sub>2</sub> catalysts<sup>199</sup>. As the vanadia loading increases, only a partial amount of V may get dissolved into the ceria matrix leaving excess amount residing as dispersed oxide on the surface of the ceria. It does not have a strong interaction, which in turn results in an increase in the reduction temperature.

The TPR spectra of VCRS series of catalysts are shown in Figure 4.48.



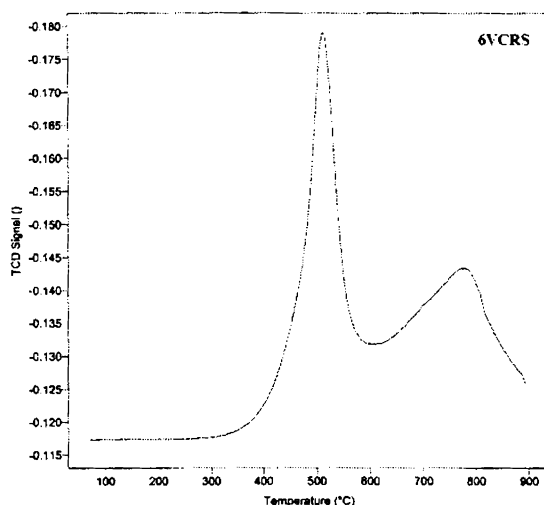


Figure 4.48

Various CRS supported catalysts also show the similar reduction behaviour as that of VC series of catalysts. The intensity of low temperature reduction peak is high than high temperature reduction peak. Recent findings suggested that incorporation of transition metal elements into ceria lattice could deeply influence reduction under hydrogen by promoting reduction of the bulk at lower temperature<sup>200</sup>. Recently, Rocchini et al.<sup>201</sup> reported that under specific conditions, silica positively affects the redox behaviour of ceria, resulting in an enhancement of its reduction properties even after a strong redox treatment, a condition that heavily inhibits reduction in pure ceria. The reduction behaviour in ceria-zirconia depends on structural perturbation in the lattice of ceria induced by the dopant<sup>202-204</sup>.

The temperatures of peak maxima are given in Table 4.9. This is graphically depicts in Figure 4.49.



Table 4.12

Catalyst	Temperature/K		
	$T_{\max 1}$	$T_{\max 2}$	
Ce	759	1084	325
4VC	787	1056	269
6VC	792	948	156
4VCRS	766	1079	313
6VCRS	785	1048	263

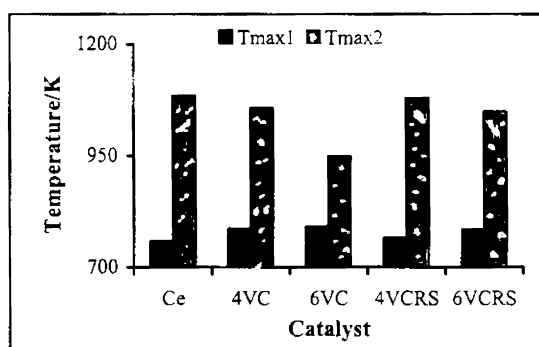


Figure 4.49

From the table it is shown that vanadia impregnation clearly modified the reduction behaviour of catalysts. The surface reduction peak has shifted to higher temperature for all the studied VC and VCRS series of catalysts. However, increase in temperature is more with VC series of catalysts than VCRS series. The bulk reduction peak shows a different behaviour. The temperature of reduction is high for 4VCRS and 6VCRS than 4VC and 6VC.

## **4.2 Acidity measurements**

The surface acidity of solid catalysts has been the subject of considerable study. It has been shown that the centers giving rise to surface acidity can be strongly acid, and they occupy only a small fraction of the total catalyst surface, but little is known regarding the acid strength distribution among such centers and how this distribution varies with the type of catalyst. The present studies were undertaken to obtain such information.

### **4.2.1 Temperature programmed desorption-NH<sub>3</sub>**

Temperature programmed desorption (TPD) has become a powerful tool for the characterization of catalysts. Ammonia is used frequently as a probe molecule because of its small molecular size, stability and strong basic strength<sup>205</sup>. Ammonia can be adsorbed on an oxide surface through hydrogen bonds or through dipolar interaction yielding the total acidity (Bronsted and Lewis type) of the system<sup>206</sup>. The total acidity measurements of catalysts have been carried out by step-wise temperature programmed desorption of NH<sub>3</sub>. The acid strength distribution is classified depending on the desorption temperature; region 373-473 K is for weak, 474-673 K is due to medium, and 674-873 K is due to strong acid sites<sup>207</sup>.

Acidity values obtained by TPD-NH<sub>3</sub> of VC series of catalysts are given in Table 4.13.

Table 4.13

Catalyst	Acidity Distribution (mmolg <sup>-1</sup> )			
	Weak	Medium	Strong #	Total
	373-473 (K)	474-673 (K)	674-873 (K)	373-873 (K)
Ce	0.34	0.12 (0.46)*	0.05	0.51
2VC	0.57	0.29 (0.86)*	0.19	1.04
4VC	0.81	0.08 (0.89)*	0.11	0.99
6VC	0.37	0.14 (0.51)*	0.02	0.53
8VC	0.34	0.17 (0.51)*	0.07	0.58
10VC	0.31	0.17 (0.48)*	0.09	0.58

\* Bronsted acid sites, # Lewis acid sites

Table 4.13 shows the acid strength distribution of ceria containing catalysts. The TPD results indicate that ceria possess less acidity since it is a basic oxide and acidity enhanced upon vanadia loading. Impregnation of vanadia increases the amount of ammonia desorbed at lower temperature region, whereas the amount is reduced at higher temperature region. The addition of vanadia onto non-acidic support may create both Lewis and, to a lesser extent some Bronsted acidity<sup>208</sup>. High loading over the support creates new Bronsted acid sites however; the number of Lewis acid sites may get reduced<sup>209</sup>. Among ceria supported catalysts, total acidity of 2VC is found to be more. Further increase in vanadia loading decreases the acidity. It could be due to masking of acidic sites by highly dispersed vanadium oxide phase on the surface of the support. The decrease in acidity is also attributed to the formation of orthovanadate type structure.

The TPD-NH<sub>3</sub> results of VCERS catalysts are given in Table 4.14.

Table 4.14

Catalyst	Acidity Distribution (mmolg <sup>-1</sup> )			
	Weak	Medium	Strong #	Total
	373-473 (K)	474-673 (K)	373-873 (K)	373-873 (K)
RS	1.13	0.17 (1.3)*	0.09	1.39
CRS	0.58	0.13 (0.71)*	0.07	0.79
2VCRS	0.59	0.19 (0.78)*	0.11	0.89
4VCRS	0.79	0.21 (1.0)*	0.13	1.13
6VCRS	0.92	0.24 (1.16)*	0.12	1.28
8VCRS	0.73	0.28 (1.01)*	0.09	1.11
10VCRS	0.67	0.29 (0.96)*	0.09	1.06
6VRS	0.23	0.22 (0.45)*	0.09	0.54
6VSG	0.81	- (0.81)*	-	0.81

\* Bronsted acid sites, # Lewis acid sites

Amorphous silica obtained from rice husk is very acidic. Acidity of ceria enhanced upon silica promotion. Acidity of VCRS catalysts was found to be higher in comparison with VC series. This is in agreement with high acidity of amorphous silica promoted ceria support. In this series, acidity decreases in 2VCRS and increases marginally with vanadia loading up to monolayer coverage of 6VCRS due to increase in active vanadia sites. Further increase causes decrease in acidity due to the formation of the orthovanadate type phase on the support<sup>210</sup>. The acidity generation is caused by an excess of a negative or positive charge in a model structure of binary oxide related to the coordination number of a positive element and a negative element. It is known

that bulk vanadia possesses both surface Lewis and Bronsted acidity and in dehydrated conditions no Lewis acid sites are present on SiO<sub>2</sub> surface, thus vanadia at higher loadings affects the number of Lewis acid sites<sup>211</sup>.

The TPD-NH<sub>3</sub> results of praseodymia catalysts are given in Table 4.15.

Table 4.15

Catalyst	Acidity distribution (mmolg <sup>-1</sup> )			
	Weak 373-473 (K)	Medium 474-673 (K)	Strong # 373-873 (K)	Total 373-873 (K)
Pr	0.65	0.23 (0.88)*	0.12	0.99
PRS	0.77	0.18 (0.95)*	0.09	1.03
2VP	0.36	0.12 (0.48)*	0.11	0.59
6VP	0.14	0.13 (0.27)*	0.08	0.35
10VP	0.24	0.14 (0.38)*	0.05	0.43
2VPRS	0.19	0.10 (0.29)*	0.02	0.32
6VPRS	0.44	0.19 (0.63)*	0.11	0.75
10VPRS	0.36	0.17 (0.53)*	0.11	0.63

\* Bronsted acid sites, # Lewis-type acid sites

Praseodymia exhibits higher number of acid sites in contrast to ceria. The total acidity of praseodymia increased upon silica promotion in accordance with high acidity of amorphous silica obtained from rice husk. In VP series catalysts, acidity of the support decreases with the addition of vanadium oxide due to masking of acidic sites of praseodymia by highly dispersed vanadium oxide phase. A similar behaviour related to ceria catalysts is observed for praseodymia catalysts. The acidity decreases in 2VP, increased

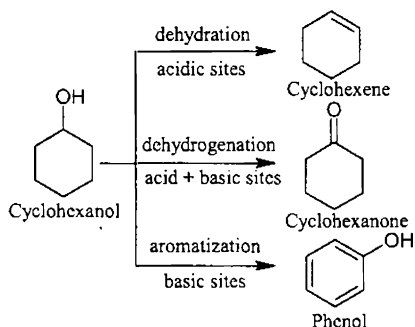
up to 6VP and then decreased. Higher loading results in an enhancement in Bronsted acid sites while Lewis acid sites are decrease to a large extent.

In VPRS series, total acidity found to be increased upon vanadia loading of 6 wt. % and then decreases. Bronsted acid sites increase upon 6 wt.% V<sub>2</sub>O<sub>5</sub> loading and further increase reduced the acidic sites.

It is reported that the evacuation of metal oxide surfaces at 673 K removes most of the probe molecules adsorbed on the Bronsted acid sites<sup>212,213</sup>. The amount of ammonia adsorbed at higher temperature region, is considered to be due to Lewis acid sites. Acid sites responsible for Lewis type acidity are coordinately unsaturated cations of the support<sup>214</sup>.

#### **4.2.2 Cyclohexanol decomposition**

The decomposition of cyclohexanol is an important industrial process since the products obtained are used as raw materials for the manufacture of fine chemicals in chemical industry<sup>215,216</sup>. Besides, this reaction is considered as a test reaction for acid-base properties of solid catalysts as well as a model reaction to determine the catalytic functionality of metal oxides<sup>217-221</sup>. Decomposition reaction of cyclohexanol to give cyclohexene and cyclohexanone as the main products has been used as a good model reaction in probing acid-base properties of metal oxide materials<sup>222</sup>. The amphoteric nature of the alcohol permits its interaction with acidic and basic sites, leading to the formation of cyclohexene and cyclohexanone. The process of cyclohexanol conversion leading to various products is depicted in scheme 4.1.



Scheme 4.1

It is generally accepted that the dehydration of cyclohexanol to cyclohexene occurs on acid sites, while dehydrogenation to cyclohexanone is associated with both acid/base and redox sites<sup>223-226</sup>. Accordingly, the product ratio of this conversion could be used to evaluate the surface acid-base properties of various oxide materials. Acid-base properties of metal oxides were dependent on a number of variables such as metal salt, method of preparation, precipitation agent, calcination temperature and the effect of promoters. Effect of a promoter in any reaction is to enhance the reaction rate with better product selectivity at lower temperatures<sup>227</sup>.

The dehydrogenation of cyclohexanol is a commercially important reaction and several papers have been widely reported for reactions in the gas-phase, liquid phase and solvent free conditions using a variety of solid catalysts<sup>228,229</sup>. Both acid and basic sites were responsible for the dehydration processes in the gas-phase conversion of alcohols<sup>230</sup>. Dehydrogenation activity over spinel type catalysts was suggested by the presence of both basic and redox properties<sup>231</sup>. Stronger acid sites are found to be responsible for the formation of methylcyclopentenes through the secondary reaction of

cyclohexene and aromatization of cyclohexanol produced phenol in small quantities<sup>232</sup>. Generally, dehydration takes place on acidic oxides such as  $V_2O_5$ ,  $SiO_2$ ,  $Al_2O_3$  and sulfated  $ZrO_2$  giving rise to cyclohexene as major product while on basic oxides such as  $MgO$ ,  $ZnO$  and  $CuO$ , dehydrogenation is favoured leading to the formation of cyclohexanone as major product. Small quantities of aromatized phenol have also been reported on  $Cu$  and  $Ni$  containing oxide catalysts<sup>233</sup>. The redox and acid-base properties of oxides can be tuned to produce surface acid-base and redox pair sites in mixed oxides to carry out organic reactions.

#### 4.2.2.1 Influence of reaction conditions

In order to check the influence of conditions, reaction was carried out by varying parameters such as temperature and flow rate of reactant with selected catalyst.

##### 1. Effect of Temperature

The effect of temperature on decomposition is shown in Figure 4.50.

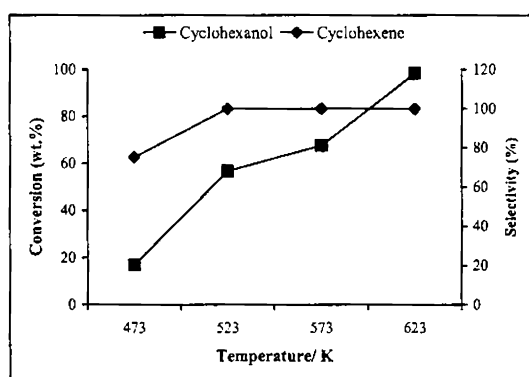


**Figure 4.50**

Reaction conditions:- 6VCRS-500 mg, Flow rate- 5 mlh<sup>-1</sup>,  
Time- 2 h and Nitrogen-20mlmin<sup>-1</sup>.



The overall conversion of cyclohexanol showed an increasing trend with an increase in reaction temperature. A maximum of 98.3 (wt. %) conversion was obtained at temperature of 623 K with cyclohexene as the only product, suggesting that active sites are not deactivated due to coke deposition. Small amount of benzene is formed at lower temperature.

## 2. Effect of Flow rate

Decomposition reaction carried out with different flow rate of reactant is presented in Figure 4.51.

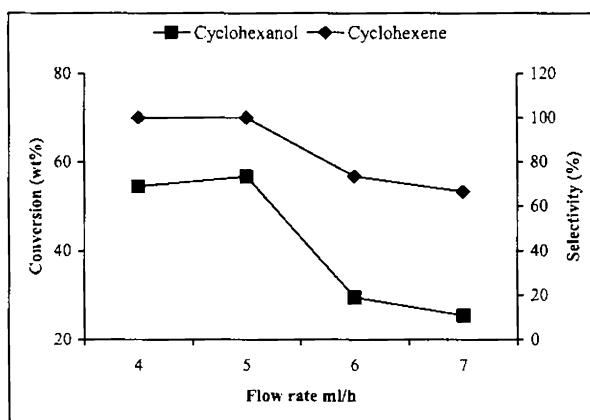


**Figure 4.51**

Reaction conditions:- 6VC-500 mg, Temperature- 523 K, Time- 2 h and Nitrogen-20mlmin<sup>-1</sup>.

The reaction with various cyclohexanol feed rate was carried out from 4 to 7 ml h<sup>-1</sup> at 523 K. It can be seen from figure 4.51 that the cyclohexanol conversion decreased with an increase in flow rate. Cyclohexene selectivity also showed some dependence on flow rate, it decreases upon increase in flow

rate. In general, a decrease in the conversion is observed at higher space velocities due to lesser contact time and thus kinetics gets modified<sup>234</sup>. For further reaction, flow rate of 5 mlh<sup>-1</sup> was selected.

#### 4.2.2.2 Cyclohexanol decomposition over catalysts

Cyclohexanol decomposition was carried out at 523 K in a conventional fixed-bed type reactor, with a continuous flow system at atmospheric temperature. By means of a glass syringe, a cyclohexanol stream with a feed rate  $F = 5 \text{ mlh}^{-1}$  was passed after dilution with dried nitrogen at a flow rate of 20 mlmin<sup>-1</sup> in 500 mg of catalyst weight. Reaction products collected after 2 h was analyzed by gas chromatograph.

The results of cyclohexanol decomposition obtained over VC catalysts are presented in Table 4.16.

Table 4.16

Catalyst	Conversion (wt.%)	Selectivity (%)	
		Cyclohexene	Cyclopentenes
Ce	12.5	72.5	27.5
2VC	3.4	51.6	23.3
4VC	6.3	76.7	48.4
6VC	56.7	100	0.0
8VC	43.0	99.4	0.6
10VC	41.1	98.8	1.2

Product analysis shows cyclohexene as the main reaction product along with small amounts of cyclopentenes. No cyclohexanone was formed over any catalysts under the reaction conditions studied. In accordance with Paula et al.

presence of nitrogen atmosphere throughout the reaction period can be a reason for the production of only cyclohexene<sup>235</sup>. Dehydrogenation of cyclohexanol occurs on basic/redox sites and vanadia-ceria combination catalysts are best known for its redox property<sup>236</sup>.

For ceria, cyclohexene along with small amount of cyclopentanes is obtained as the products. Impregnation of vanadia results an increase in conversion rate and cyclohexene selectivity up to loading of 6 wt. %  $V_2O_5$ . Further increase in vanadia loading decreased the conversion rate as well as cyclohexene selectivity. The dehydration activity observed under nitrogen stream is a typical acid-catalyzed reaction and it indicates that the catalyst possesses some surface acidity<sup>237</sup>. Isomerization and disproportionation reactions produce cyclopentenes, benzene and phenol due to the presence of strong acid sites<sup>238</sup>. In the present case, the low selectivity of ceria containing catalysts towards consecutive reaction products suggests that the acid sites are weak.

The results over VCRS catalysts are presented in Table 4.17.

**Table 4.17**

Catalyst	Conversion (wt.%)	Selectivity (%)	
		Cyclohexene	Cyclopentenes
RS	49.2	99.4	0.6
CRS	12.1	76.6	23.4
2VCRS	23.2	100	0.0
4VCRS	28.1	100	0.0
6VCRS	58.6	100	0.0
8VCRS	27.8	100	0.0

---

10VCRS	27.4	100	0.0
--------	------	-----	-----

---

Amorphous silica from rice husk produced cyclohexene with small amount of cyclopentenes as secondary oxidation products on strong acid sites. For silica promoted ceria, conversion rate and cyclohexene selectivity increased compared to ceria. However, activity and selectivity is lowered than that of silica due to the lowering of surface area and total acidity since ceria is well known as a basic oxide. Among supported vanadia catalysts, conversion rate increases up to 6 wt. % V<sub>2</sub>O<sub>5</sub> loading exclusively giving cyclohexene as the product. Higher loading above this reduced activity.

The results of cyclohexanol decomposition obtained over praseodymia containing catalysts along with different silica supported vanadia are presented in Table 4.18.

**Table 4.18**

Catalyst	Conversion (wt.%)	Selectivity (%)	
		Cyclohexene	Cyclopentenes
P	7.3	75.1	24.9
PRS	8.4	42.8	51.1
2VP	5.9	95.3	4.7
6VP	7.9	53.1	35.2
10VP	9.9	64.8	46.8
2VPRS	7.5	70.3	29.6
6VPRS	9.9	86.9	13.2
10VPRS	3.1	70.1	29.9
V	96.4	97.2	2.8
6VRS	52.7	98.7	1.3

6VSG

22.3

81.2

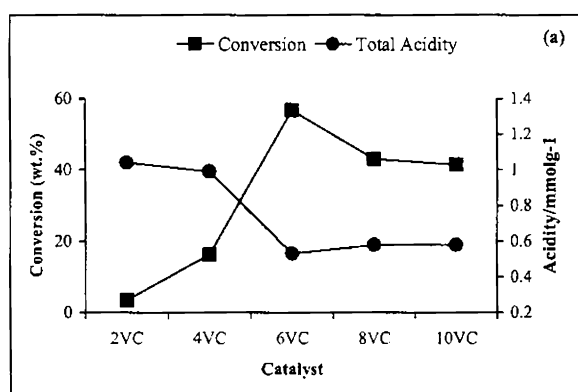
18.8

On the other hand, the praseodymia containing catalysts exhibit formation of isomerized products in high yield owing to the presence of some amount of strong acid sites in the catalysts. Conversion rate was found very low compared to ceria containing catalysts. Low cyclohexanol conversion rate and cyclohexene selectivity can be attributed to the difference in redox properties and low surface area compared to ceria catalysts.

#### 4.2.2.3 Cyclohexanol decomposition and acidity by TPD-NH<sub>3</sub>

To determine the role of physical properties on cyclohexanol decomposition over all of these catalysts, a correlation diagram developed using conversion rate, cyclohexene selectivity and acidity values.

Relation between % decomposition and acidic sites for VC catalysts is presented in Figure 4.52.



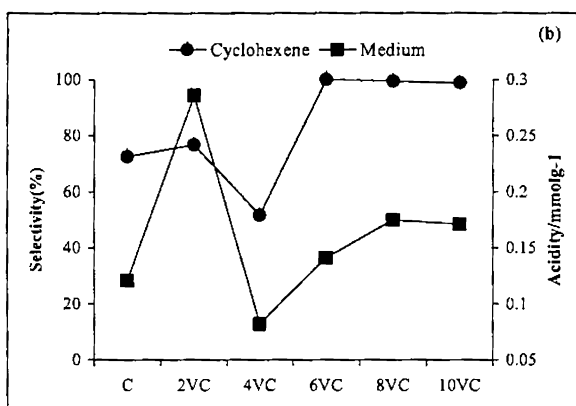


Figure 4.52

Figure 4.52 shows the effect of acidic sites on cyclohexanol decomposition. From Figure 4.52 (a) it is seen that activity increases as the loading of vanadia increases reaches a maximum and then decreases. However, acidity of the catalysts decreases upon low vanadia loading and then increases after the monolayer coverage of 6 wt. %  $V_2O_5$ . However, the cyclohexene selectivity shows a dependence on the medium acid sites of the VC catalysts obtained by TPD- $NH_3$  from figure 4.52 (b). The high conversion rate for low loading is due to highly dispersed smaller crystallites of vanadia over the support surface.

Relation between % decomposition rate and total acidity obtained for VCRS catalysts are presented in Figure 4.53.

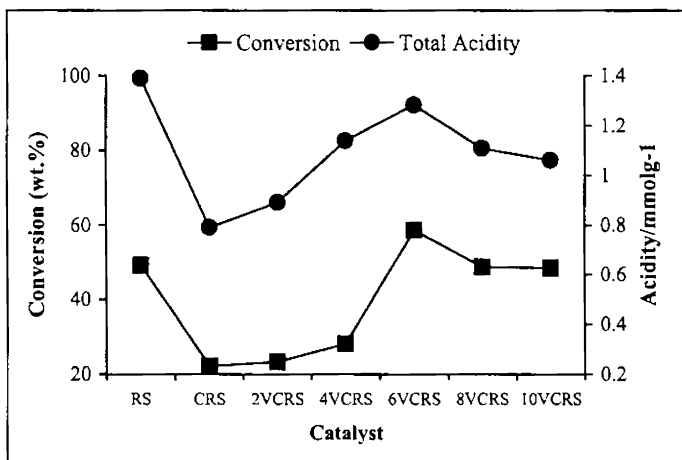


Figure 4.53

It could find a good correlation between decomposition activity and total acidity values obtained by TPD-NH<sub>3</sub> for CRS supported catalysts. Cyclohexanol conversion rate is in accordance with its total acidity obtained by ammonia desorption method for all these catalysts. For silica promoted ceria, activity and selectivity is lowered than silica due to the lowering of surface area and total acidity since ceria is well known as a basic oxide. In this case, the cyclohexanol dehydration to give cyclohexene is exclusively related to the total acidity of the oxides in accordance with several reports<sup>239</sup>. Formation of methyl cyclopentenes over the catalysts suggests that the isomerization activity must be associated with total acidity in agreement with Bautista et al.<sup>240</sup>. The influence of BET surface area of supported vanadia catalysts on catalytic activity is found to be negligible since impregnation of active phase over a support always reduces the surface area<sup>241</sup>.

Relation between decomposition and acidity obtained for VP catalysts is presented in Figure 4.54.

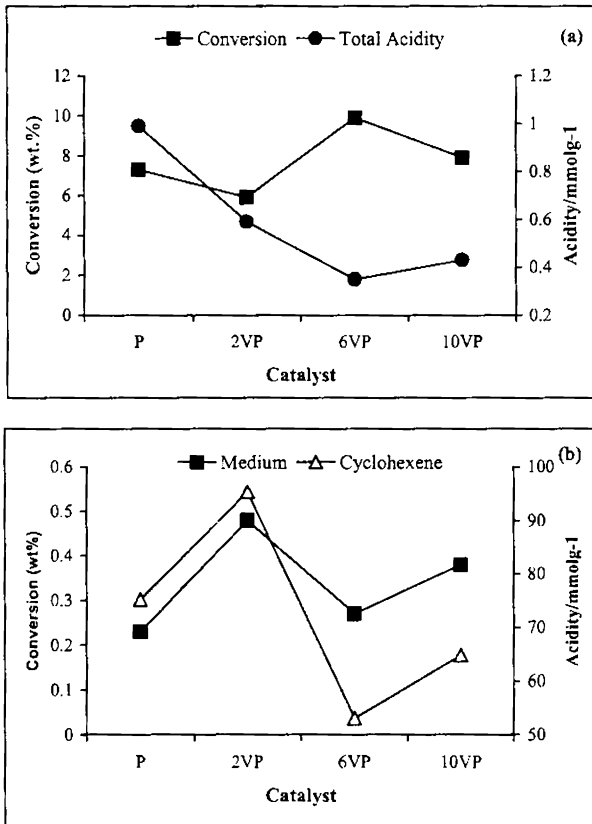


Figure 4.54

The VP catalysts show similar behaviour as that of VC series. Conversion rate was very low compared to ceria catalysts. It suggests the influence of surface area and redox properties on the cyclohexanol decomposition over these catalysts.

Relation between decomposition rate and total acidity for VPRS catalysts is presented in Figure 4.55.



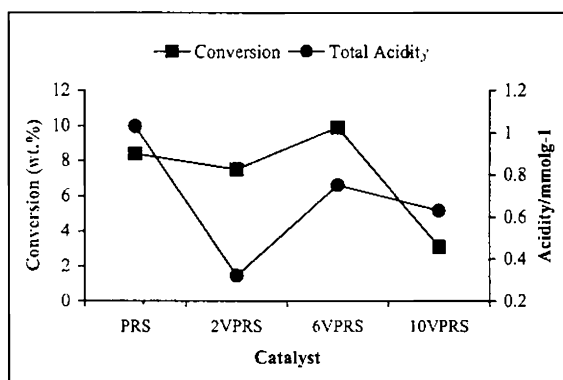


Figure 4.55

The effect of total acidity on conversion rate was similar to VCRS catalysts. Presence of amorphous silica makes these catalysts more acidic. Up to vanadia loading of 6 wt. % conversion and acidity increases and further increase reduced both acidity and total activity.

Decomposition of cyclohexanol over ceria and praseodymia supported vanadia catalysts suggest the dependence of properties such as surface area, amount of vanadia and acid site distribution upon loading. Cyclohexanol decomposition on silica promoted rare earth oxides should be associated with the total acidity from ammonia desorption measurements and the amount of vanadium loaded.

### 4.3 Discussion

Studies on the modification of vanadia based catalysts by addition of different promoting agents, usually metals or metal oxides, for selective hydrocarbon oxidations are extensive. However, studies on modified rare earth oxide-vanadia based catalysts are limited. Especially studies on rare earth

oxide praseodymia regarding the catalytic activity are rare in the literature. This work shows that the addition of vanadium to rice husk silica promoted rare earth oxides could significantly increases the catalytically important properties such as BET surface area, acidity, dispersion and reduction behaviour in comparison to rare earth oxide supported ones. This work has focused on a detailed catalyst characterization in order to probe the important characteristics for the enhanced catalytic activity.

For well-dispersed vanadia species on oxide supports, two types of surface vanadium oxide species are generally identified: isolated and polymeric vanadium oxide species. The ratio of polymerized to isolated surface vanadia species depends on the vanadia loading, the support surface area, and the specific nature of the support. Several properties of supported vanadium catalysts such as the role of the support, the vanadium loading, the strength of V=O bond, the reducibility of the V-O-Support, and the nature of active vanadium species in many industrial important reactions especially selective oxidation reactions. Characterization of various supported vanadia catalysts using different instrumental techniques in this study has helped to define the role these parameters.

#### **4.4 Conclusion**

Highly amorphous silica with high specific surface area could be prepared from an agrowaste rice husk and characterized using different techniques. Silica promoted ceria and praseodymia material exhibits reasonably high surface area and thermal stability. The combination of

different physicochemical techniques used in this study revealed presence of different vanadium oxide species on the supported catalysts.

Powder X-ray diffraction, a bulk characterization technique was used to study the crystallographic nature of the rare earth oxides and supported vanadium oxides. Analysis evidenced a fluorite type ceria and praseodymia and highly amorphous silica prepared from rice husk. It followed also from analysis that supported vanadia seems highly dispersed over the surface of the support for low loading and crystallization or compound formation occurs as the loading increases. Predominantly orthovanadate type formation observed at calcination temperature of 773 K on the nonpromoted oxides above 6 wt. %  $V_2O_5$  loading while no corresponding diffraction pattern observed for CRS supported catalysts owing to its amorphous nature. BET surface area analysis results high surface area for vanadia supported on silica promoted ceria and praseodymia. A gradual reduction of surface area was observed after vanadia incorporation over the supports as expected.

Thermal analysis of catalysts conducted before calcination procedure confirmed the removal of water molecules as well as oxalate species before 773 K, which was chosen as calcination temperature in order to produce oxides from precipitated hydroxides and impregnated solids. For praseodymia catalysts, exotherms in DTA pattern and corresponding TGA loss suggested the formation of praseodymia pyrovanadates.

The data obtained from UV-vis DRS spectroscopy confirm that it is an important tool for the characterization of supported vanadium oxide catalysts. The UV-vis spectra of ceria supported catalysts are characterized by charge

transfer transitions with low intense absorption pattern different from bulk  $V_2O_5$  suggesting a different coordination environment for supported catalysts. The peaks around 350-400 nm in the UV-vis spectra of the supported vanadia catalysts have been assigned to tetrahedrally coordinated  $V^{5+}$ . Reduced centers are present in supported catalysts. It has been reported that these reduced vanadyl centers, which allows easily the migration of electrons, are responsible for the selective oxidation reactions. Thus it is evident that the active sites for an oxidation catalyst working with a redox or Mars-van Krevelen mechanism need to be rapidly reoxidized by oxygen and the active sites be the  $V^{5+}=O$  species. Praseodymia catalysts appear black after calcination at 773 K and gave no absorption in the UV-vis range.

The analysis of Hamiltonian parameters provided g values corresponding to  $Ce^{3+}$  species in the ceria supported catalysts. The EPR measurements showed that the vanadium was mostly in the 5+ oxidation state.

The FT-IR spectra of the catalysts exhibited bands due to different vanadia species. Only isolated surface  $V=O$  species were observed for CRS supported catalysts suggesting high dispersion compared to ceria support alone. With increasing vanadia content the  $VO_4^{3-}$  species of orthovanadate structure observed. FT-IR spectra of praseodymia catalysts show formation of higher vanadates species.

A further confirmation of the presence of different vanadium oxide species in the catalysts is given by laser-Raman spectroscopy, applied to the calcined catalysts with the purpose of following the possible transformations of the vanadate species upon vanadia loading over various rare earth oxide supports and for amount of various vanadia loading.

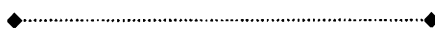
Solid state both  $^{29}\text{Si}$  and  $^{51}\text{V}$  MAS NMR techniques could helpfully complete the characterization of the local environment of Si and V in the surface species and was in good agreement with the other results. Ceria catalysts evidenced the presence of Si-O-Si ( $\text{Q}^4$ ) while the formation of silicate like Si-O-Pr configuration was observed for praseodymia catalysts.

$^{51}\text{V}$  MAS NMR spectra of VC catalysts exhibit presence of highly dispersed vanadia up to 4 wt.% and well defined shift corresponding to  $\text{CeVO}_4$  formation appeared on further loading. However, VCRS catalysts contain highly dispersed tetrahedral vanadia sites.

Scanning electron micrographs depicts the morphological change upon silica promotion and vanadia loading. Particles found agglomerated for higher vanadia loading.

TPR studies were used to evaluate the reducibility of the catalysts. All TPR profiles have two sharp peaks corresponding to low and high reduction temperature. The temperature and intensity ratio of the two peaks changed from sample to sample after vanadia loading.

Acidity of the catalysts were measured by temperature programmed desorption using ammonia as a probe molecule and also tested with gas-phase cyclohexanol dehydration. Conversion rate for cyclohexanol decomposition on ceria, silica and silica promoted ceria is associated with its surface area and total acidity. However, for supported catalysts, conversion should be associated with the total acidity from ammonia desorption and the amount of vanadia loading.



**REFERENCES**

- [1] H. Chen, A. Aleksandrov, Y. Chen, S. Zha, M. Liu, T.M. Orlando, *J. Phys. Chem. B* 109 (2005) 11257.
- [2] D.M. Lyons, K.M. Ryan, M.A. Morris, *J. Mater. Chem.* 12 (2002) 1207.
- [3] S. Sugunan, K. Sreejarani, C.S. Deepa, H. Suja, *React. Kinet. Catal. Lett.* 71 2 (2000) 307.
- [4] F.D. Smet, M. Devillers, C. Poleunis, P. Bertrand, *J. Chem. Soc., Faraday Trans.* 94 7 (1998) 941.
- [5] R. Long, H. Wan, *J. Catal.* 172 (1997) 471.
- [6] D.E. Keller, F.M.F. de Groot, D.C. Koningsberger, B.M. Weckhuysen, *J. Phys. Chem. B* 109 (2005) 10223.
- [7] X. Gao, S.R. Bare, J.L. Fierro, I.E. Wachs, *J. Phys. Chem. B* 103 (1999) 618.
- [8] M. Calatayud, C. Minot, *J. Phys. Chem. B* 108 (2004) 15679.
- [9] C.L. Pieck, M.A. Banares, J.L.G. Fierro, *J. Catal.* 224 (2004) 1.
- [10] M.A. Banares, M.V.M. Huerta, X. Gao, J.L.G. Fierro, I.E. Wachs, *Catal. Today* 61 (2000) 295.
- [11] I.E. Wachs, J.M. Jehng, G. Deo, B.M. Weckhuysen, V.V. Guliants, J.B. Benziger, S. Sundaresan, *J. Catal.* 170 (1997) 75.
- [12] C. Real, M.D. Alcalá, J.M. Criado, *J. Am. Ceram. Soc.* 79 8 (1996) 2012.
- [13] B.M. Reddy, A. Khan, Y. Yamada, T. Kobayashi, S. Loricant, J.C. Volta, *J. Phys. Chem. B* 106 (2002) 10964.
- [14] F. Zhang, S.W. Chan, J.E. Spanier, E. Apak, Q. Jin, *Appl. Phys. Lett.* 80 (2002) 127.
- [15] L.J. Kennedy, J.J. Vijaya, G. Sekaran, *Indian Eng. Chem. Res.* 43 (2004) 1832.
- [16] L. Kepinski, M. Wolcyrz, *Catal. Lett.* 15 (1992) 329.
- [17] K. Asami, K.I. Kusakabe, N. Ashi, Y. Ohtsuka, *Appl. Catal. A: Gen.* 156 (1997) 43.
- [18] A. Fissel, J. Dabrowski, H.J. Osten, *J. Appl. Phys.* 91 11 (2002) 8986.
- [19] F.R. Merritt, H. Guggenheim, C.G.B. Garrett, *Phys. Rev.* 145 1 (1996) 188.
- [20] G.D. Nero, G. Cappelletti, S. Ardizzone, P. Fermo, S. Gilardoni, *J. Eur. Ceram. Soc.* 24 14 (2004) 3603.

- [21] Y. Kaneko, S. Mori, J. Yamanaka, *Solid State Ionics* 151 (2002) 35.
- [22] J.C. Badot, A. Mantoux, N. Baffier, O. Dubrunfaut, D. Lincot, *J. Mater. Chem.* 14 (2004) 3411.
- [23] B.M. Reddy, P. Lakshmanan, A. Khan, *J. Phys. Chem.* 108 43 (2004) 16855.
- [24] G.S. Wong, J.M. Vohs, *Surf. Sci.* 498 (2002) 266.
- [25] G.S. Wong, M.R. Concepcion, J.M. Vohs, *J. Phys. Chem. B* 106 (2002) 6451.
- [26] B.M. Reddy, I. Ganesh, E.P. Reddy, *J. Phys. Chem. B* 101 (1997) 1769.
- [27] K. Sohlberg, S.T. Pantelides, S.J. Pennycook, *J. Am. Chem. Soc.* 123 (2001) 6609.
- [28] B.M. Reddy, P. Lakshmanan, A. Khan, C.L. Cartes, T.C. Rojas, A. Fernandez, *J. Phys. Chem. B* 109 (2005) 1781.
- [29] B. Murugan, A.V. Ramaswamy, D. Srinivas, C.S. Gopinath, V. Ramaswamy, *Chem. Mater.* 17 15 (2005) 3983.
- [30] J.Z. Colina, R.M. Nix, H. Weiss, *J. Phys. Chem. B* 109 (2005) 10978.
- [31] R. Cousin, M. Dourdin, E. Abi-Aad, D. Courcot, S. Capelle, M. Guelton, A. Aboukais, *J. Chem. Soc., Faraday Trans.* 93 21 (1997) 3863.
- [32] U.O. Krasovec, B. Orel, A. Surca, N. Bukovec, R. Reisfeld, *Solid State Ionics* 118 (1999) 195.
- [33] J. Matta, D. Courcot, E. Abi-Aad, A. Aboukais, *Chem. Mater.* 14 (2002) 4118.
- [34] G.D. Nero, G. Cappelletti, S. Ardizzone, P. Fermo, S. Gilardoni, *J. Europ. Ceram. Soc.* 25 6 (2005) 911.
- [35] M. Ocana, A. Caballero, A.R. Gonzalez-Elipe, P. Tartej, C. Serna, R.I. Merino, *J. Eur. Ceram. Soc.* 19 (1999) 641.
- [36] F. De Smet, P. Ruiz, B. Delmon, M. Devillers, *Appl. Catal. A: Gen.* 172 (1998) 333.
- [37] U.G. Nielsen, H.J. Jakobsen, J. Skibsted, P. Norby, *J. Chem. Soc., Dalton Trans.* (2001) 3214.
- [38] I.D. Brown, C. Calvo, *J. Solid State Chem.* 1 (1970) 173.  
S. Lutkehoff, M. Neumann, A. Slebarski, *Phys. Rev. B* 52 (1995) 13808.
- [39] G.M. Clark, R. Morley, *J. Solid State Chem.* 16 (1976) 429.
- [40] G.D. Wilk, R.M. Wallace, J.M. Anthony, *J. Appl. Phys.* 89 (2000) 5243.

- [41] H. Ono, T. Katsumata, *Appl. Phys. Lett.* 78 (2001) 1832.
- [42] S. Rossignol, C. Descorme, C. Kappenstein, D. Duprez, *J. Mater. Chem.* 11 (2001) 2587.
- [43] A.B. Corradi, F. Bondioli, A.M. Ferrari, *Chem. Mater.* 13 (2001) 4550.
- [44] C.B. Wang, G. Deo, I.E. Wachs, *J. Catal.* 178 (1998) 640.
- [45] A. Khodakov, B. Olthof, A. Bell. E. Iglesia, *J. Catal.* 181 (1999) 205.
- [46] F.E. Massoth, *Adv. Catal.* 27 (1978) 265.
- [47] J. Matta, D. Courcot, E. Abi-Aad, A. Aboukais, *Chem. Mater.* 14 (2002) 4118.
- [48] G.C. Bond, S.F. Tahir, *Appl. Catal.* 71 (1991) 1.
- [49] T.H. Liou, *Mater. Sci. Eng.* 364 1-2 (2004) 314.
- [50] M.M. Mohamed, S.M.A. Katib, *Appl. Catal. A: Gen.* 287 (2005) 236.
- [51] F.M. Bautista, J.M. Campelo, A. Garcia, D. Luna, J.M. Marins, R.A. Quiros, A.A. Romero, *Appl. Catal. A. Gen.* 243 (2003) 93.
- [52] I.A. Rahman, J. Ismail, H. Osman, *J. Mater. Chem.* 7 8 (1997) 1505.
- [53] E. Abi-Aad, R. Bechara, J. Grimblot, A. Aboukais, *Chem. Mater.* 5 (1993) 793.
- [54] B.M. Reddy, A. Khan, Y. Yamada, T. Kobayashi, S. Loidant, J.C. Volta, *J. Phys. Chem. B* 106 (2002) 10964.
- [55] M. Ponzi, C. Duschatzky, A. Carrascull, E. Ponzi, *Appl. Catal. A: Gen.* 169 (1998) 373.
- [56] M. Taniguchi, T.R. Ingraham, *Canad. J. Chem.* 42 (1964) 2467.
- [57] M. Gotic, S. Popovic, M. Ivanda S. Musiv, *Mater. Lett.* 57 (2003) 3186.
- [58] J. Matta, D. Courcot, E. Abi-Aad, A. Aboukais, *J. Therm. Anal. Calorim.* 66 (2001) 717.
- [59] G.C. Bond, A.J. Sarkani, G.O. Parfitt, *J. Catal.* 57 (1979) 476.
- [60] R.E. Ferguson, E. Daniel Guth, L. Eyring, "Praseodymium Oxides. I. Phase Study by Dissociation Pressure Measurements" 76 (1953) 3890.
- [61] M. Rajendran, K.K. Mallick, A.K. Bhattacharya, *J. Mater. Sci.* 33 20 (1998) 5001.
- [62] M.J. Holgado, S. San Roman, P. Malet, V. Rives, *Mat. Chem. Phys.* 89 (2005) 49.
- [63] J.D. McCullough, *J. Amer. Ceram. Soc.* 72 (1950) 1386.



- [64] F. Bondioli, A.M. Ferrari, L. Lusvardi, T. Manfredini, S. Nannarone, L. Pasquali, G. Selvaggi, *J. Mater. Chem.* 15 (2005) 1061.
- [65] G.R. Rao, B.G. Mishra, *Mater. Chem. Phys.* 89 (2005) 110.
- [66] E. Nakazawa, *J. Luminescence* 100 (2002) 89.
- [67] D.C.M. Dutoit, M. Schneider, P. Fabrizioli, A. Baiker, *J. Mater. Chem.* 7 2 (1997) 271.
- [68] P. Brandao, A. Philippou, N. Hanif, P.R. Claro, A. Ferreira, M.W. Anderson, J. Rocha, *Chem. Mater.* 14 (2002) 1053.
- [69] R.G. Toro, G. Malandrino, I.L. Fragala, R.L. Nigro, M. Losurdo, G. Bruno, *J. Phys. Chem. B* 108 (2004) 16357.
- [70] J.M. Coronado, A.J. Maria, A. Martinez-Arias, J.C. Conesa, J. Soria, *J. Photochem. Photobio. A: Chem.* 150 (2002) 213.
- [71] C. Ho, J.C. Yu, T. Kwong, A.C. Mak, S. Lai, *Chem. Mater.* 17 (2005) 4514.
- [72] G. Catana, R.R. Rao, B.M. Weckhuysen, P. van der Voort, E. Vansant, R.A. Schoonheydt, *J. Phys. Chem. B* 102 (1998) 8005.
- [73] C. Resini, M. Panizza, F. Raccogli, M. Fadda, M.M. Carnasciali, G. Busca, E.F. Lopez, V.S. Escribano, *Appl. Catal. A: Chem.* 251 (2003) 29.
- [74] X. Gao, M.A. Banares, I. Wachs, *J. Catal.* 188 (1999) 325.
- [75] D.C.M. Dutoit, M. Schneider, P. Fabrizioli, A. Baiker, *J. Mater. Chem.* 7 2 (1997) 271.
- [76] M.A. Larrubia, G. Busca, *Mater. Chem. Phys.* 72 (2001) 337.
- [77] F. Arena, F. Frusteri, A. Parmaliana, *Appl. Catal. A* 176 (1999) 189.
- [78] L.J. Burcham, I.E. Wachs, *Catal. Today* 49 (1999) 467.
- [79] P. Ciambelli, L. Lisi, G. Russo, J.C. Volta, *Appl. Catal. B: Environ.* 7 (1995) 1.
- [80] S. Shylesh, A.P. Singh, *J. Catal.* 228 2 (2004) 333.
- [81] C.T. Au, W.D. Zhang, *J. Chem. Soc., Faraday Trans.* 93 6 (1997) 1195.
- [82] L.B. Asprey, T.K. Keenan, *J. Inorg. Nucl. Chem.* 16 (1961) 260.
- [83] G. De, A. Licciulli, M. Nacucchi, *J. Non-Cryst. Solids* 201 (1996) 153.
- [84] J.A. Badenes, J.B. Vincent, M. Llusar, M.A. Tena, G. Monros, *J. Mater. Sci.* 37 7 (2002) 1413.

- [85] N.C. Wu, E.W. Shi, Y.Q. Zheng, W.J. Li, *J. Am. Ceram. Soc.* 85 (2002) 2462.
- [86] J. George, S. Shylesh, A.P. Singh, *Appl. Catal. A: Gen.* 290 1-2 (2005) 148.
- [87] K. Mori, A. Miyamoto, Y. Murakami, *J. Chem. Soc., Faraday Trans. 1* 83 (1987) 3303.
- [88] J.R. Sohn, I.J. Doh, Y.I. Pae, *Langmuir* 18 (2002) 6280.
- [89] M. Kantcheva, *Phys. Chem. Chem. Phys.* 2 (2000) 3043.
- [90] H. E. Rast, H. H. Caspers, S. A. Miller, *Phys. Rev.* 169 (1968) 705.
- [91] J.R. Sohn, K.C. Seo, Y. II Pae, *Bull. Korean Chem. Soc.* 24 3 (2003) 311.
- [92] I.E. Wachs, B.M. Weckhuysen, *Appl. Catal. A* 157 (1997) 67.
- [93] N. Das, E. Hellmut, H. Hu, I.E. Wachs, J.F. Walzer, F.J. Feher, *J. Phys. Chem.* 97 (1993) 8240.
- [94] G. Deo, I.E. Wachs, J. Haber, *J. Crit. Rev. Surf. Chem.* 94 (1994) 141.
- [95] J.M. Jehng, H. Hu, X. Gao, I.E. Wachs, *Catal. Today* 28 (1996) 335.
- [96] I.E. Wachs, *Catal. Today* 27 (1996) 437.
- [97] G. Busca, G. Centi, L. Marchetti, F. Trifiro, *Langmuir* 2 (1986) 568.
- [98] J.A. Gadsen, *IR Spectra of Minerals and Related Compounds* (1975).
- [99] G. Deo, I.E. Wachs, *J. Phys. Chem.* 95 (1991) 5889.
- [100] S. Shylesh, T. Radhika, K. Sreejarani, S. Sugunan, *J. Mol. Catal. A: Chem.* 236 (2005) 250.
- [101] L.D. Frederickson Jr., D.M. Hausen, *Anal. Chem.* 35 (1963) 818.
- [102] J.K. Bartley, C.J. Kiely, R.P.K. Wells, G.J. Hutchings, *Catal. Lett.* 72 1-2 (2001) 99.
- [103] F. Javier, C. Sanchez, R.P.K. Wells, C. Rhodes, J.K. Bartley, C.J. Kiely, G.J. Hutchings, *Phys. Chem. Chem. Phys.* 3 (2001) 4122.
- [104] J.K. Bartley, I.J. Ellison, A. Delimitis, C.J. Kiely, A.Z. Isfahani, C. Rhodes, G.J. Hutchings, *Phys. Chem. Chem. Phys.* 3 (2001) 4606.
- [105] M. Gotic, S. Popovic, M. Ivanda, S. Music, *Mater. Lett.* 57 (2003) 3186.
- [106] T. Garcia, B. Solsona, D.M. Murphy, K.L. Antcliff, S.H. Taylor, *J. Catal.* 229 (2005) 1.
- [107] P. Kornelk, F. Mizukami, A.W. Birczynska, L. Proniewicz, G.D. Mariadassou, A. Bialas, M. Najbar, *Catal. Today* 90 (2004) 103.
- [108] J. Keranen, A. Auroux, S. Ek, L. Niinisto, *Appl. Catal. A: Gen.* 228 (2002) 213.

- [109] D.A. Bulushev, L.K. Minsker, F. Rainone, A. Renken, *J. Catal.* 205 (2002) 115.
- [110] J.M. Stencel, *Raman Spectroscopy for Catalysis*, Van Nostrand Reinhold Catalysis Series, New York (1990).
- [111] J. Twin, C.F. Shih, T.H. Guo, K. Hsien, *J. Mater. Chem.* 7 11 (1997) 2273.
- [112] V. Briois, D.L. Hecht, F. Villain, E. Fonda, S. Belin, B. Griesebock, R. Frahm, *J. Phys. Chem. A.* 109 (2005) 320.
- [113] N. Sergent, J.F. Lamonier, A. Aboukais, *Chem. Mater.* 12 (2000) 3830.
- [114] K. Nagaveni, M.S. Hegde, G. Madras, *J. Phys. Chem. B.* 108 (2004) 20204.
- [115] V.S. Escribano, E.F. Lopez, M. Panizza, C. Resini, J. Manuel, G. Amores, G. Busca, *Solid State Sciences* 5 (2003) 1369.
- [116] T. Feng, J.M. Vohs, *J. Phys. Chem. B* 109 (2005) 2120.
- [117] N. Ballarini, F. Cavani, M. Ferrari, R. Catani, U. Cornaro, *J. Catal.* 213 (2003) 95.
- [118] X. Gao, J.M. Jehng, I.E. Wachs, *J. Catal.* 209 (2002) 43.
- [119] M.V.M. Huerta, J.M. Coronado, M.F. Garcia, A.I. Juez, G. Deo, J.L.G. Fierro, M.A. Banares, *J. Catal.* 225 (2004) 240.
- [120] Z. Wu, H.S. Kim, P.C. Stair, S. Rugmini, S.D. Jackson, *J. Phys. Chem. B* 109 (2005) 2793.
- [121] V. Luca, D.J. MacLachlan, R. Bramley, *Phys. Chem. Chem. Phys.* 1 (1999) 2597.
- [126] D.A. Bulushev, L. Kiwi-Minsker, F. Rainone, A. Renken, *J. Catal.* 205 (2002) 115.
- [127] D. Wolfframm, M. Ratzke, S.K. Arguirova, J. Reif, *Mater. Sci. Semiconductor Processing* 5 (2003) 429.
- [128] B.A. Weinstein, G. Piermarini, *J. Phys. Rev. B* 12 (1975) 1172.
- [129] A. Adamski, Z. Sojka, K. Dyrek, M. Che, G. Wendt, S. Albrecht, *Langmuir* 15 (1999) 5733.
- [130] D. Wolf I, *Semicond. Sci. Technol.* 11 (1996) 139.
- [131] M.F. Garcia, A.M. Arias, A. I. Juez, C. Belver, A.B. Hungria, J.C. Conesa, J. Soria, *J. Catal.* 194 (2000) 385.
- [132] M. Hunger, J. Weitkamp, *Angew. Chem. Int. Ed.* 40 (2001) 2954.
- [133] Z. Sojka, M. Che, *Appl. Mag. Reson.* 20 (2001) 433.

- [134] A.M. Arias, M.F. Garcia, C. Belver, J.C. Conesa, J. Soria, *Catal. Lett.* 65 (2000) 197.
- [135] T. Lopez, F. Tzompantzi, J. Navarrete, R. Gomez, J.L. Boldu, E. Munoz, O. Novaro, *J. Catal.* 181 (1999) 285.
- [136] A. Aboukas, A. Bennani, C.F. Aissi, G. Wrobel, M. Guelton, *J. Chem. Soc., Faraday Trans.* 88 (1992) 1321.
- [137] E. Abi-Aad, R. Bechara, J. Grimblot, A. Aboukas, *Chem. Mater.* 5 (1993) 793.
- [138] M. Che, M. Fournier, J.P. Launay, *J. Chem. Phys.* 71 (1979) 1954.
- [139] A.M. Arias, J.M. Coronado, J.C. Conesa, J. Soria, *Rare Earths*, R.S. Puche, P. Caro (Eds.) Complutense, Madrid (1997) 299.
- [140] M. Che, J.F.J. Kibblewhite, A.J. Tench, M. Dufaux, C. Nacache, *J. Chem. Soc., Faraday Trans.* 169 (1973) 857.
- [141] A.M. Arias, M.F. Garcia, C. Belver, J.C. Conesa, J. Soria, *Catal. Lett.* 65 (2000) 197.
- [142] A.M. Venezia, G. Pantaleo, A. Longo, G. Dicarlo, M.P. Casaletto, F.L. Liotta, G. Deganello, *J. Phys. Chem. B* 109 (2005) 2821.
- [143] S.K. Misra, S.I. Andronenko, *J. Phys. Chem. B* 108 (2004) 9397.
- [144] J.W. Wiench, C.J. Fontenot, J.F. Woodworth, G.L. Schrader, M. Pruski, S.C. Larsen, *J. Phys. Chem. B* 109 (2005) 1756.
- [145] V.M. Orera, R.I. Merino, F. Pena, *Solid State Ionics* 72 (1994) 224.
- [146] M. Hartmanova, M. Jergel, I. Thurzo, F. Kundracik, K. Gmucova, S. Chromik, L. Ortega, *Russ. J. Electrochem.* 39 (2003) 478.
- [147] C. Force, J.P. Belzunegui, J. Sanz, A.M. Arias, J. Soria, *J. Catal.* 197 (2001) 192.
- [148] E. Abi-Aad, A. Bennani, J.P. Bonnelle, A. Aboukais, *J. Chem. Soc., Faraday Trans.* 91 (1995) 99.
- [149] A. Werich, L.A. Kappers, O.R. Gilliam, R.H. Bartram, I. Foldvari, L. Korecz, *Nucl. Instrum. Method Phys. Res. B* 191 (2002) 261.
- [150] J.L.G. Fierro, J. Soria, J. Sanz, M.J. Rojo, *J. Solid State Chem.* 66 (1987) 154.
- [151] A. Aboukais, A. Bennani, C.L. Dulongpont, E. Abi-Aad, G. Wrobel, *Colloids Surf. A: Physicochemical and Engineering Aspects* 115 (1996) 171.
- [152] X.S. Zhao, Max G.Q. Lu, C. Song, *J. Mol. Catal. A: Chem.* 191 (2003) 67.
- [153] M. Bhaiyalakshmi, K. Shanmugapriya, M. Palanichamy, B. Arabindoo, V. Murugesan, *Appl. Catal. A: Gen.* 1-2 (2004) 77.

- [154] P. Selvam, S.E. Dapurkar, *J. Catal.* 229 (2005) 64.
- [155] A. Sakthivel, S.E. Dapurkar, P. Selvam, T. White, D. Sun (Eds.), *Advances in Environmental Materials, Pollution Control Materials, Materials Research Society, Singapore 1* (2001) 67.
- [156] S.S. Shevade, B.S. Rao, *J. Mater. Chem.* 9 (1999) 2459.
- [157] M. Copel, M. Cartier, F.M. Ross, *Appl. Phys. Lett.* 78 (2001) 1607.
- [158] M. Gurvitch, L. Manchanda, J.M. Gibson, *Appl. Phys. Lett.* 51 (1987) 919.
- [159] M. Shoyama, H. Nasu, K. Kamiya, *J. Ceram. Soc. Jpn. Int. Ed.* 106 (1998) 289.
- [160] S. de Val, M.L. Granados, J.G. Fierro, J.S. Gonzalez, A.J. Lopez, T. Blasco, *J. Catal.* 204 (2001) 466.
- [161] X. Yu, S. Cai, Z. Chen, *Spectrochimica Acta Part A* 60 (2004) 391.
- [162] K.V.R Chary, C.P. Kumar, A. Murali, A. Tripathi, A. Clearfield, *J. Mol. Catal. A: Chem.* 216 (2004) 139.
- [163] B. Solsona, T. Blasco, J.M. Lopez Nieto, M.L. Pena, F. Rey, A. Vidal-Moya, *J. Catal.* 203 (2001) 443.
- [164] C. Martin, D. Klissurski, J. Rocha, V. Rives, *Phys. Chem. Chem. Phys.* 2 (2000) 1543.
- [165] A.G.S. Filho, O.P. Ferreira, E.J.G. Santos, J.M. Filho, O.L. Alves, *Nano Lett.* 4 11 (2004) 2099.
- [166] U.G. Nielsen, A. Boisen, M. Brorson, C.J.H Jacobsen, H.J. Jakobsen, J. Skibsted, *Inorg. Chem.* 41 (2002) 6432.
- [167] C.J. Fontenot, J.W. Wiench, M. Pruski, G.L. Schrader, *J. Phys. Chem. B* 104 (2001) 11622.
- [168] O.B. Lapina, A.A. Shubin, D.F. Khabibulin, V.V. Terskikh, P.R. Bodart, J. P. Amoureux, *Catal. Today* 78 (2003) 91.
- [169] E.H. Park, M.H. Lee, J. R. Sohn, *Bull. Korean Chem. Soc.* 21 9 (2000).
- [170] B. Olthof, A. Khodakov, A.T. Bell, E. Inglesia, *J. Phys. Chem. B* 104 (2000) 1516.
- [171] R. Cousin, D. Courcot, E. Abi-Aad, S. Capelle, J.P. Amoureux, M. Dourdin, A. Aboukais, *Colloids Surf. A.* 158 (1999) 43.
- [172] M.L. Occelli, R.S. Maxwell, H. Eckert, *J. Catal.* 137 (1992) 36.
- [173] U.G. Nielsen, H.J. Jakobsen, J. Skibsted, *J. Phys. Chem. B* 105 (2001) 420.
- [174] J.A.L. Sanchez, J.K. Bartley, R.P.K. Wells, C. Rhodes, G. Hutchings, *New J. Chem.* 26 (2002) 1613.
- [175] K.V. Narayana, A. Venugopal, K.S.R. Rao, S.K. Masthan, V.V. Rao, P.K. Rao, *Appl. Catal. A: Gen.* 167 (1998) 11.

- [176] Y.H. Kim, H.I. Lee, *Bull. Korean Chem. Soc.* 20 12 (1999) 1457.
- [177] Q. Fu, A. Weber, M.F. Stephanopoulos, *Catal. Lett.* 77 1-3 (2001).
- [178] D. Andreeva, T. Tabakova, V. Idakiev, A. Naydenov, *Gold Bull.* 31 (1998) 105.
- [179] A. Jones, B. McNicol (Eds.), *Temperature-Programmed Reduction for solid Materials Characterization*, Marcel Dekker, New York (1986).
- [180] M. Boaro, M. Vicario, C. de Leitenburg, G. Dolcetti, A. Trovarelli, *Catal. Today* 77 (2003) 407.
- [181] E. Rocchini, M. Vicario, J. Llorca, C. de Leitenburg, G. Dolcetti, A. Trovarelli, *J. Catal.* 211 (2002) 407.
- [182] D.A. Bulushev, L.K. Minsker, F. Rainone A. Renken, *J. Catal.* 205 (2002) 115.
- [183] S. Besselmann, C. Freitag, O. Hinrichsen, M. Muhler, *Phys. Chem. Chem. Phys.* 3 (2001) 4633.
- [184] A. Piras, A. Trovarelli, G. Dolcetti, *Appl. Catal. B* 28 (2000) L77.
- [185] K.V.R Chary, G. Kishan, C.P. Kumar, G.V. Sagar, *Appl. Catal. A: Gen.* 246 (2003) 335.
- [186] M.L. Ferreira, M. Volpe, *J. Mol. Catal. A: Chem.* 184 (2002) 349.
- [187] M.L. Ferreira, M. Volpe, *J. Mol. Catal. A: Chem.* 164 (2000) 281.
- [188] S.T. Oyama, G. Went, K. Lewis, A. Bell, G. Somorjai, *J. Phys. Chem.* 93 (1989) 6786.
- [189] S. Bernal, G. Blanco, J.M. Pintado, J.M.R. Izquierdo, M.P. Yeste, *Catal. Commun.* 6 (2005) 582.
- [190] D. Andreeva, R. Nedyalkova, L. Ilieva, M.V. Abrashev, *Appl. Catal. A: Gen.* 246 (2003) 29.
- [191] D. Terribile, A. Trovarelli, C. de Leitenburg, A. Primavera, G. Dolcetti, *Catal. Today* 47 (1999) 133.
- [192] H.C. Yao, Y.F.Y. Yao, *J. Catal.* 86 (1984) 254.
- [193] A. Trovarelli, *Catal. Rev. Sci. Eng.* 38 (1996) 439.
- [194] R. Sasikala, N.M Gupta, S.K Kulshreshtha, *Catal. Lett.* 71 1-2 (2001) 81.
- [195] G. Munteanu, L. Ilieva, R. Nedyalkova, D. Andreeva, *Appl. Catal. A: Gen.* 277 (2004) 31.
- [196] D. Andreeva, T. Tabakova, L. Ilieva, A. Naydenov, D. Mehanjiev, M.V. Abrashev, *Appl. Catal. A: Gen.* 209 (2001) 291.
- [197] A. Bielaski, J. Haber, *Cat. Rev. Sci. Eng.* 19 (1979) 1.
- [198] D. Andreeva, V. Idakiev, T. Tabakova, L. Ilieva, P. Falaras, B. Travlos, *Catal. Today* 72 (2002) 51.

- [199] J. Zarraga-Colina, R.M. Nix, H. Weiss, *J. Phys. Chem. B* 109 (2005) 10978.
- [200] J. Kaspar, P. Fornasiero, M. Graziani, *Catal. Today* 50 (1999) 285.
- [201] E. Rocchini, A. Trovarelli, J. Liorca, G.W. Graham, W.H. Weber, M. Maciejewski, A. Baiker, *J. Catal.* 194 (2000) 461.
- [202] R.T Baker, S. Bernal, G. Blanco, A.M. Cordon, J.M. Pintado, J.M.R. Izquierdo, F. Fally, V. Perrichon, *Chem. Commun.* (1999) 149.
- [203] A. Trovarelli, *App. Catal. B: Environ.* 52 3 (2004) 225.
- [204] L. F. Liotta, A. Macaluso, A. Longo, G. Pantaleo, A. Martorana, G. Deganello, *Appl. Catal. A: Gen.* 240 1-2 (2003) 295.
- [205] H. A. Benesi, *J. Am. Chem. Soc.* 78 (1956) 5490.
- [206] S. Sugunan, N.K. Renuka, *Bull. Chem. Soc. Jpn.* 75 (2002) 463.
- [207] S. Sugunan, N.K. Renuka, A.R. Koshy, S.M. Varghese, C.G Ramankutty, *React. Kinet. Catal. Lett.* 67 2 (1997) 267.
- [208] J. Datka, A. Turek, J. Jehng, I. Wachs, *J. Catal.* 135 (1992) 186.
- [209] I.E. Wachs, B. Weckhuysen, *Appl. Catal. A* 157 (1997) 67.
- [210] K.V.R Chary, C.P. Kumar, A. Murali, A. Tripathi, A. Clearfield, *J. Mol. Catal. A: Chem.* 216 (2004) 139.
- [211] J. Keranen, A. Auroux, S. Ek, L. Niinisto, *Appl. Catal. A: Gen.* 228 (2002) 213.
- [212] A. Auroux, A. Gervasini, *J. Phys. Chem.* 94 (1990) 6371.
- [213] F. Hatayama, T. Ohno, T. Maruoka, T. Ono, H. Miyata, *J. Chem. Soc., Faraday Trans.* 87 (1991) 2629.
- [214] M.M. Kantcheva, K.I. Hadjiivanov, D.G. Klissurski, *J. Catal.* 134 (1992) 299.
- [215] B.M. Nagaraja, V.S. Kumar, V. Shashikala, A.H. Padmasri, S.S. Reddy, B.D. Raju, K.S.R. Rao, *J. Mol. Catal. A: Chem.* 223 (2004) 339.
- [216] M.A. Aramendia, V. Borau, C. Jimenez, J.M. Marinas, F.J. Romero, *J. Colloid Interface Sci.* 179 (1996) 290.
- [217] H.J.M. Bosman, E.C. Kruissink, J. van der Spoel, F. van den Brink, *J. Catal.* 148 (1994) 660.
- [218] D. Duprez, D. Martin *J. Mol. Catal. A: Chem.* 118 (1997) 113.
- [219] D.A. Cesar, C.A. Perz, V.M.M. Salim, M. Schmal, *Appl. Catal. A: Gen.* 176 (1999) 205.
- [220] R.A.W. Jonstone, J. Liu, D. Whittaker, *J. Mol. Catal. A* 174 (2001) 159.

- [221] R. Jothiramalingam, B. Viswanathan, T.K. Varadarajan, *Catal. Commun.* 6 (2005) 41.
- [222] B.G. Mishra, G. Ranga Rao, *Bull. Mater. Sci.* 25 2 (2002) 155.
- [223] A. Valente, Z. Lin, P. Brandao, I. Portugal, M. Anderson, J. Rocha, *J. Catal.* 200 (2001) 99.
- [224] C.P. Bezouhanova, M.A. Al-Zihari, *Catal. Lett.* 11 (1991) 245.
- [225] J.L. Colon, D.S. Thakur, C.Y. Yang, A. Clearfield C.R. Martin, *J. Catal.* 124 (1990) 148.
- [226] R.A.W. Jonstone, J. Liu, D. Whittaker, *J. Chem. Soc., Perkin Trans.* (1998) 1287.
- [227] M.A. Aramendia, V. Borau, C. Jimenez, J.M. Marinas, A. Porras, F.J. Urbano *J. Mater. Chem.* 9 (1999) 819.
- [228] V.Z. Fridman, A.A. Davydov, *J. Catal.* 195 (2000) 20.
- [229] M. Ilyas, Ikramullah, *Catal. Commun.* 5 (2004) 1.
- [230] H. Nur, H. Hamdan. *Mater. Res. Bull.* 36 (2001) 315.
- [231] M.A. Aramendia, V. Borau, C. Jimenez, J.M. Marinas, F.J. Romero, J.A. Navio, J. Barrios, *J. Catal.* 157 (1995) 97.
- [232] B. M. Reddy, A. Khan, Y. Yamada, T. Kobayashi, S. Loridant, Jean-Claude Volta, *J. Phys. Chem. B* 106 (2002) 10964.
- [233] F.M.T. Mendes, Martin Schmal, *App. Catal. A: Gen.* 151 (1997) 393.
- [234] R.M. Koros, E.J. Novak, *Chem. Eng. Sci.* 22 (1967) 470.
- [235] P. Brandao, A. Valente, A. Ferreira, V.S. Amaral, J. Rocha, *Micro. Meso. Mater.* 69 (2004) 209.
- [236] F.M. Bautista, J.M. Campelo, A. Garcia, D. Luna, J.M. Marinas, R.A. Quiros, A.A. Romero, *Appl. Catal. A: Gen.* 243 (2003) 93.
- [237] P.E. Hathaway, M.E. Davis, *J. Catal.* 116 (1989) 263.
- [238] J. Datka, B. Gil, O. Vogt, J. Rakoczy, in: I. Kiricsi, G. PalBorbely, J. B. Nagy, H.G. Karge (Eds.), *Porous Materials in Environmentally Friendly Processes*, Elsevier, Amsterdam 125 (1999) 409.
- [239] U.O. Krasovec, B. Orel, A. Surca, N. Bukovec, R. Reisfeld, *Solid state Ionics* 118 (1999) 195.
- [240] F.M. Bautista, J.M. Campelo, A. Garcia, D. Luna, J.M. Marinas, R.A. Quiros, A.A. Romero, *Appl. Catal. A: Gen.* 243 (2003) 93.
- [241] J. Datka, B. Gil, O. Vogt, J. Rakoczy, in: I. Kiricsi, G. Pal, Borbely, J. B. Nagy, H.G. Karge (Eds.), *Porous Materials in Environmentally Friendly Processes*, Elsevier, Amsterdam, 125 (1999) 409.



## CHAPTER 5

### OXIDATION OF BENZENE

#### Abstract

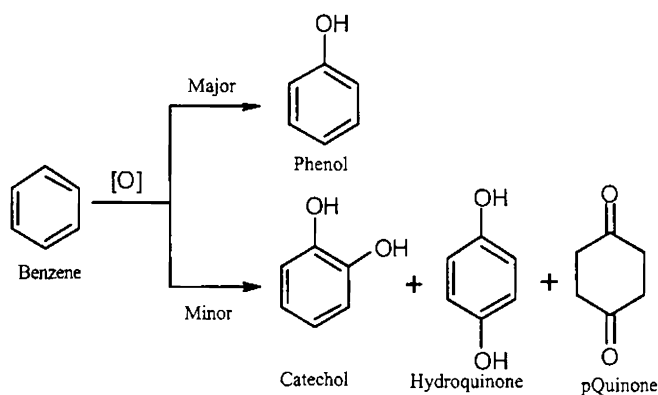
---

*Direct oxidation of benzene with  $H_2O_2$  to form phenol is a very promising tool for the chemical industry, since the commonly employed 'cumene' process being of uncertain profitability and technologically complex. Due to the high stability of benzene, the direct oxygenation of benzene has been thought to be one of the most difficult oxidation reactions but also to be one of the most challenging oxidation from the point of view of synthetic organic chemistry. Phenol has been known to be a versatile intermediate for the manufacture of various petrochemicals such as phenolic resins, adipic acid, caprolactum, bisphenol, nitro and chlorophenols, phenol sulfonic acid, and is mainly produced by 'cumene' process. However, this process consists of three steps, and has many disadvantages. Hence, finding a one-step process for the production of phenol by direct oxidation of benzene, which is one of the most challenging tasks in oxidation catalysis, attracts much attention in recent years.*

---

## 5.1. INTRODUCTION

At the present time, phenol an important intermediate for the manufacture of petrochemicals, agrochemicals and plastics is commercially produced via the so-called "Cumene Process" which accounts for more than 90% of the world output with only 5% of phenol yield. The advantage of "Cumene Process" (Hock Process) is that it take two inexpensive starting materials, benzene and propylene, and converts them into two expensive useful products, phenol and acetone, just using air<sup>1</sup>. However, the marketability of acetone by-product and the need of a high capital investment due to its characteristic multi-step process are disadvantages. For these reasons, a process is desired whereby phenol can be formed in one step<sup>2</sup>. The reaction pathways involved in one step production of phenol from benzene is shown in Scheme 5.1.



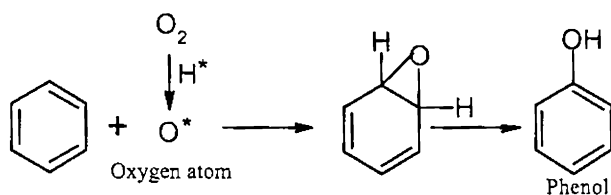
Scheme 5.1

It is not easy to get the relatively higher conversion of benzene oxidation due to the difficulty of overcoming its resonance energy. Nowadays,



the selective insertion of the hydroxyl group onto the aromatic ring, to manufacture phenols and naphthols is a very promising tool for the chemical industry. A one-step production of phenol through the direct oxygenation of benzene has so far been attempted using various catalytic systems by many researchers<sup>3-7</sup>. The practical development of one step production of phenol will have advantages in cost reduction and energy saving.

The direct oxygenation of benzene formally includes insertion of an oxygen atom between the C-H bonds to form phenol. The oxygen insertion for benzene oxidation is shown in Scheme 5.2.



Scheme 5.2

Many approaches have been reported in the literature for the oxidation of benzene to produce phenol<sup>8,9</sup>. Classical system such as Fenton's reagent ( $Fe^{2+}$ - $H_2O_2$ ), Udenfriend's reagent ( $Fe^{2+}$ -EDTA- $O^{2-}$ -L-ascorbic acid), and Hamilton's reagent ( $Fe^{2+}$ -catechol- $H_2O_2$ ) has been known to yield phenol from benzene. Recently, iron- and chromium-containing phosphotungstate salts were reported as efficient catalysts for benzene hydroxylation<sup>10</sup>.

Direct benzene to phenol oxidation over iron modified zeolites of MFI structures using  $N_2O$  as an oxidant has been developed for the last 10 years, which resulted in commercialization of new technology for phenol production

at Solutia<sup>11</sup>. In recent years, a new class of commercial oxidation catalysts, Fe-ZSM5 has emerged for phenol production from benzene using nitrous oxide as oxidizing agent<sup>12-14</sup>. Influence of acidity, both the Bronsted acid sites and the Lewis ones on benzene to phenol hydroxylation over iron modified zeolite ZSM-5, was discussed extensively in the literature<sup>15</sup>. At the beginning, the acidic centers were believed to be responsible for this reaction. However, Panov and co-workers<sup>16</sup> have shown that benzene to phenol oxidation does not occur according to acidic mechanism and they proved the exceptional role of iron complexes for this reaction. After the finding that benzene can be selectively oxidized to phenol over ZSM-5 type zeolites using N<sub>2</sub>O as an oxidant, several research groups have investigated the mechanism of such a reaction, reaching different conclusions<sup>17,18</sup>. The presence of Bronsted acid sites on the catalyst surface was demonstrated to be necessary but, according to Burch and Howitt, not sufficient for assuring high activity and selectivity, while Lewis acid sites should be inactive<sup>19</sup>. Liang et al.<sup>20</sup> reported that heterogeneous modified mesoporous SBA-15 catalyst by the covalent grafting of ferrocene complex show high catalytic activity for benzene oxidation with hydrogen peroxide as the oxygen source and the excellent stability of these catalysts is attributed to the covalent grafting between the organic ligand and the inorganic meosporous material.

Molecular oxygen is an ideal oxidant, but aerobic oxidation is often difficult to control and only one oxygen atom has been used in most reactions (50 % atom efficiency) thus oxidation requires reducing agents<sup>21,22</sup>. H<sub>2</sub>O<sub>2</sub> is considered as an ideal oxidant due to its high oxidizing ability and lack of toxic by-products since it produces water as the only by-product<sup>23</sup>. The catalytic

hydroxylation of aromatics with aqueous  $\text{H}_2\text{O}_2$  has been widely investigated with catalysts such as iron complexes, silica-supported iron salts, titanosilicates and V-substituted polyoxometalates<sup>24-29</sup>. In recent years, many efforts have also been published in the field of cheaper  $\text{H}_2\text{O}_2$  production since it is too expensive compared to the frequently applied air and/or oxygen. Several researchers reported very cheap and clean  $\text{H}_2\text{O}_2$  technology, in which  $\text{H}_2\text{O}_2$  is produced in situ and reacts in one pot with an organic substrate. In 'Niwa concept' with the oxidation of benzene to phenol as the model reaction consists of a  $\text{H}_2$ -permeable Pd based membrane through which  $\text{H}_2$  is transported as an active hydrogen atom towards the reaction side of the membrane reactor containing oxygen and benzene<sup>32,31</sup>. Takahiro et al.<sup>32</sup> reported the liquid-phase oxidation of benzene by various supported Cu catalysts using molecular oxygen as an oxidant and ascorbic acid as a reductant. A Fenton-type reaction scheme was suggested by the accumulation of  $\text{H}_2\text{O}_2$  during the benzene oxidation. According to Feng-Shou Xiao et al.<sup>33</sup> benzene oxidation with  $\text{H}_2\text{O}_2$  on Cu catalysts produced phenol selectively with high conversion rate in comparison with TS-1 catalyst. The high catalytic activity is related to the intensity of hydroxyl radicals resulting from the interaction of Cu-OH with  $\text{H}_2\text{O}_2$  from EPR analysis.

Noble metal-vanadium (V) oxide catalysts supported on  $\text{SiO}_2$  have been reported to be active for benzene oxidation to phenol in the presence of both gaseous oxygen and hydrogen under a pressurized atmosphere<sup>34</sup>. Vanadium catalysts supported on  $\text{SiO}_2$  and  $\text{Al}_2\text{O}_3$ , have also been utilized for the benzene oxidation using gaseous oxygen as an oxidant and ascorbic acid as a reducing agent<sup>35</sup>. Kenji Nomiya et al.<sup>36</sup> studied the catalytic hydroxylation of

benzene using mono-vanadium (V) substituted heteropolymolybdate as single species in presence of  $\text{H}_2\text{O}_2$ . They have summarized the requirement of one vanadium center acting in cooperation with the Mo(VI) atom constructed on the A-site of the  $\alpha$ -Keggin polyoxoanion structure in contrast to the bimetallic vanadium species with the corner-shared octahedra. John et al.<sup>37</sup> reported that  $\text{V}_2\text{O}_5/\text{TiO}_2$  can be used to achieve the oxidation of monochlorobenzene at moderate temperatures and the higher catalytic activity is due to the crystalline vanadia species on the surface of the catalyst. Vanadium containing mesoporous materials such as VMCM-41 showed good catalytic activity for the oxidation of benzene over biocatalytic system with Pd-metal catalysts<sup>38,39</sup>. In complete benzene oxidation, the promoting effect of Pd and Ag over supported vanadium oxide has been related to the activation of oxygen on the metal particles, which enables the reverse oxidation of  $\text{V}^{4+}$  and leads to an equilibrium in the redox process<sup>40,41</sup>. The complete benzene oxidation over titania, zirconia and ceria supported gold-vanadia catalysts have shown that the highest activity and stability was established for the ceria supported catalysts, which can be connected with high oxygen storage capacity of ceria<sup>42-45</sup>.

## 5.2 INFLUENCE OF REACTION CONDITION

Influence of reaction conditions is essential for a chemical reaction to occur with high percentage conversion and selectivity for products. The influence of different reaction parameters was analyzed in order to maximize the product yield and selectivity. Effect of reaction conditions for benzene oxidation with  $\text{H}_2\text{O}_2$  was initially assayed in non-optimized conditions with

6VC as the catalyst. No phenol was produced when the reaction is carried out without catalyst and in the absence of either oxidant or solvent.

### 5.2.1 Effect of Temperature

The dependence of phenol production on the reaction temperature was studied by varying the temperature between 298 and 373 K while other parameters were kept constant. Results are presented in Figure 5.1.

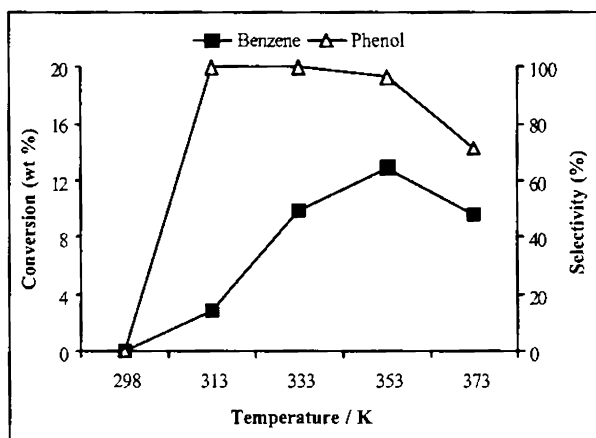


Figure 5.1

Reaction conditions:- 6VC-100 mg, Benzene-34 mmol, Acetonitrile-191 mmol,  $H_2O_2$ -88 mmol and Time-5 h.

No reaction occurs at room temperature. However, when temperature was increased from 313 to 333 K, conversion rate increased drastically with phenol as the only product. Further increase in reaction temperature increased the conversion rate with decreased phenol selectivity. At higher temperature, the self-decomposition of  $H_2O_2$  to molecular oxygen proceeds faster and it could not participate efficiently for the oxidation process<sup>46</sup>. Temperature above 353 K produced small quantities of catechol and hydroquinone as secondary

oxidation products of phenol. Evaporation of the solvent at higher temperature may also result in reduced conversion. The decreased conversion with increasing temperature suggests that the activation energy for  $\text{H}_2\text{O}_2$  decomposition is lower than that for the oxidation reaction<sup>47</sup>. For the present reaction the temperature selected was 333 K in order to get phenol selectively.

### 5.2.2 Effect of Solvent

In order to investigate the role of solvent, the oxidation of benzene was carried out in water, acetone, acetic acid and acetonitrile. The influence of these solvents on phenol production is shown in Figure 5.2.

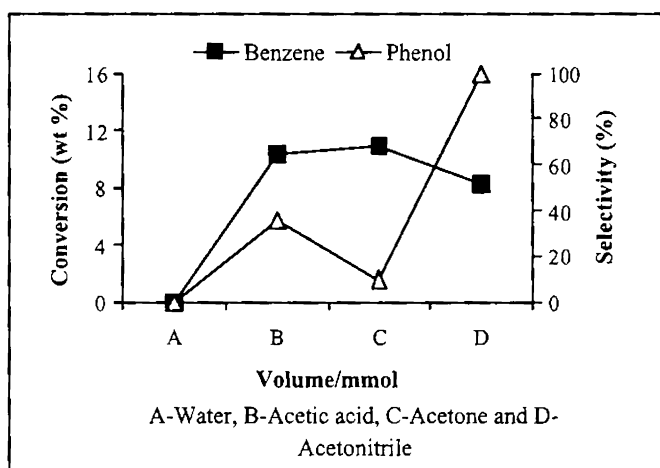


**Figure 5.2**

Reaction conditions:- Temperature-333 K, 6VC-100 mg, Benzene-34 mmol, Solvent-191 mmol,  $\text{H}_2\text{O}_2$ -88 mmol and Time-4 h.

The choice of solvent is crucial in the case of liquid phase oxidation reactions and it is known that solvent had a great influence on the catalytic activity and selectivity since they can affect the mass transfer and diffusional problems with heterogeneous solid catalysts. It is clear that water does not act



as a good solvent for the system. Acetic acid and acetone gave profound conversion but phenol selectivity was low. The presence of acidic component strongly affected the catalytic activity of hydroxylation with  $\text{H}_2\text{O}_2$  as oxidant<sup>48</sup>. Acetonitrile is found to be best solvent for the reaction system with high phenol selectivity and it could be due to its polarity. It has a comparatively good solubility power for both the organic substrate as well as the aqueous  $\text{H}_2\text{O}_2$ . In this aprotic solvent, activity of the catalyst increased since the phase separation between the aromatic substrate and the aqueous oxidant is greatly reduced which enables easy transport of the active oxygen species for the oxidation<sup>49</sup>. It was reported that the double phase system composed by water-acetonitrile-benzene is an efficient solvent system for the hydroxylation of benzene<sup>50</sup>. In this biphasic reaction medium, the resulting phenol was extracted into the organic phase and the catalyst was soluble in the aqueous phase. It could enhance the selectivity of the benzene hydroxylation by reducing the contact between phenol and the catalyst. While acetone and methanol can be used as solvents, it has been found that the hydroxylation of benzene without any organic solvent, i.e., in a triphase system, is 20 times faster than when using acetone or acetonitrile as solvents. It is evident that for this reaction the hydrophobic/hydrophilic properties of the catalyst should be of paramount importance. Thus a more hydrophobic catalyst should favor the adsorption of organophilic reagents (benzene) toward other more polar ones ( $\text{H}_2\text{O}_2$ , acetone)<sup>51</sup>.

### 5.2.3 Effect of Catalyst weight

The dependence of the amount of the catalyst on the production of phenol is presented in Figure 5.3.

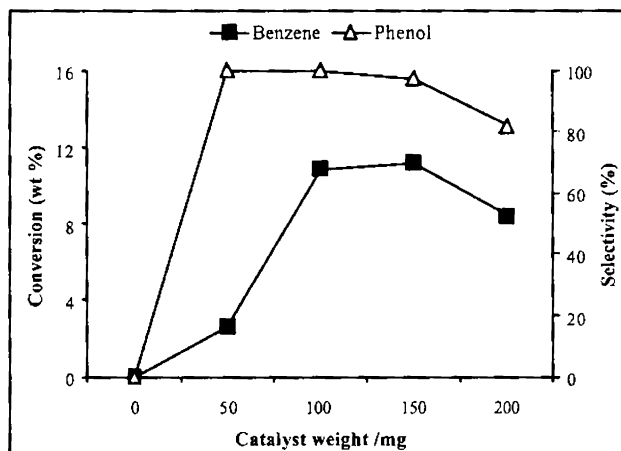


Figure 5.3

Reaction conditions:-6VC, Temperature-333 K, Benzene-34 mmol, Acetonitrile-191 mmol,  $H_2O_2$ -88 mmol and Time-5 h.

The influence of catalyst amount is studied by taking different weight of catalyst while keeping other parameters constant. No oxidation occurs in the absence of catalyst. The oxidation rate sharply increased from 2.3 to 10.9 % as the amount of the catalyst increased from 50 to 100 mg. Further increase of catalyst amount caused a decline in the selectivity and production rate of phenol. Lowering of selectivity with more catalyst can be attributed to further oxidation of phenol. Amount of catalyst is crucial in heterogeneous reactions. The dependence of product formation on the amount of catalyst suggests that the reaction proceeds purely in a heterogenic fashion<sup>52</sup>. The catalyst amount selected for the present reaction is 100 mg for the selective production of phenol.

#### 5.2.4 Effect of Acetonitrile volume

The effect of the volume of acetonitrile on the production of phenol is illustrated in Figure 5.4.

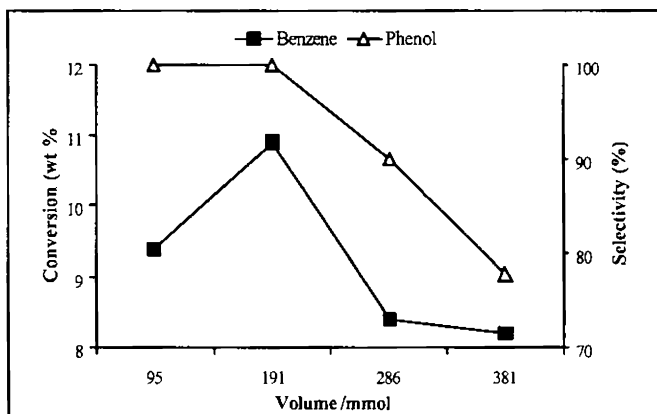


Figure 5.4

Reaction conditions:- 6VC-100 mg, Temperature-333 K,  
Benzene-34 mmol,  $\text{H}_2\text{O}_2$ -88 mmol and Time -5 h.

In order to study the effect of amount of solvent present in the reaction, the oxidation was conducted as a function of acetonitrile concentration. The conversion increased with increase in acetonitrile volume and passed through a maximum value at a volume corresponding to 191 mmol with maximum phenol selectivity. Further increase in acetonitrile volume causes a reduction to both conversion and phenol selectivity. The acetonitrile with the concentration of 191 mmol was thus found to be an optimum solvent to yield phenol selectively with high conversion rate. This can be attributed to different concentrations of benzene or catalyst between the organic and aqueous phase, which is dependent upon the added solvent and  $\text{H}_2\text{O}_2$ . When the solvent was excess, the benzene or catalyst concentration at the interface may be lower, thus resulting in a decreased conversion rate.

### 5.2.5 Effect of Benzene volume

The effect of the benzene concentration for the oxidation was investigated and the results are shown in Figure 5.5.

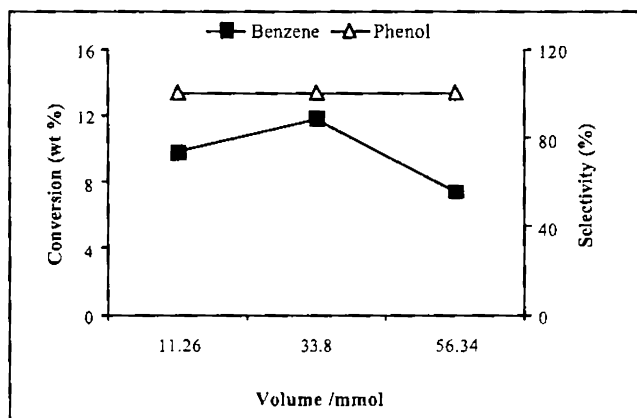


Figure 5.5

Reaction conditions:- 6VC-100 mg, Temperature-333 K,  
Acetonitrile-191 mmol,  $H_2O_2$ -88 mmol and Time-5 h.

It is seen that the oxidation rate increases with an increase in benzene concentration reaches a maximum and then decreases. Phenol selectivity remains the same. When the substrate concentration is high, an enhanced poisoning effect may arise from the strong adsorption of the products formed on the catalyst surface. This restricts further adsorption of the reactant molecules on the active sites and thus reduces the total conversion rate<sup>53</sup>.

### 5.2.6 Effect of $H_2O_2$ volume

The effect of the amount of  $H_2O_2$  on the oxidation reaction was investigated and the results are presented in Figure 5.6.

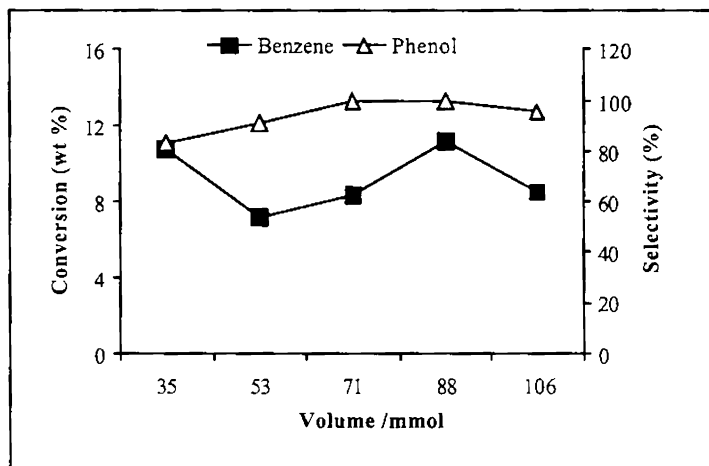


Figure 5.6

Reaction conditions:- 6VC-100 mg, Temperature-333 K,  
Acetonitrile-191 mmol, Benzene-34 mmol and Time-5 h.

With small amount of  $\text{H}_2\text{O}_2$ , the solution becomes completely miscible and conversion and selectivity was low. An increase in the amount of  $\text{H}_2\text{O}_2$  resulted in a decrease of conversion initially while conversion rate increases gradually with high phenol selectivity and reaches a maximum at 88 mmol. A decrease in both conversion and selectivity was observed with further increase of the amount of  $\text{H}_2\text{O}_2$ . This can result from either the oxidation of phenol formed or can be explained by the negative effect due to the production of  $\text{H}_2\text{O}$  as a byproduct<sup>54</sup>. The water and oxidant compete for complexation to the vanadium center, therefore excess water relative to  $\text{H}_2\text{O}_2$  inhibits the reaction. Small amounts of hydroquinone and catechol are produced besides the main product. The stoichiometric ratio of  $\text{H}_2\text{O}_2$  to benzene for the oxidation reaction is 1:1. However the results show that the  $\text{H}_2\text{O}_2$  needed for the favourable oxidation is about double its stoichiometry. Generally, the benzene oxidation

catalysis is accompanied by the self-decomposition of  $\text{H}_2\text{O}_2$ . The amount of  $\text{H}_2\text{O}_2$  consumed in self-decomposition was much more than that consumed in the oxidation reaction. This may be why more than stoichiometric amount of  $\text{H}_2\text{O}_2$  is needed<sup>55</sup>.

### 5.2.7 Effect of Time

The formation and selectivity of products always depends upon the reaction time in heterogeneous catalysis. Effect of time on benzene oxidation is shown in Figure 5.7.

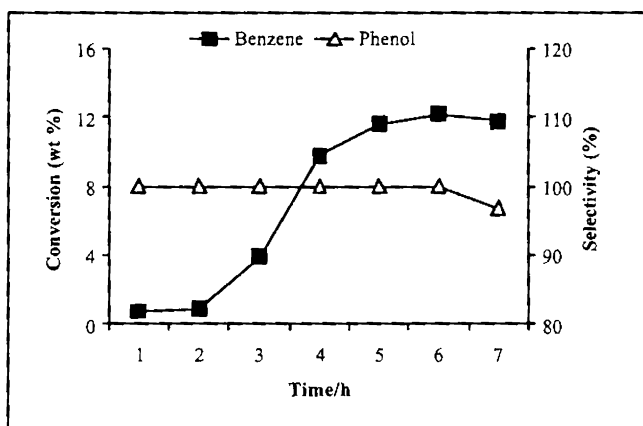


Figure 5.7

Reaction conditions:- 6VC-100 mg, Temperature-333 K,  
Acetonitrile-191 mmol, Benzene-34 mmol and  $\text{H}_2\text{O}_2$ -88 mmol.

The conversion rate increased with the reaction time up to around 5-6 h, but the extent of the increase in the oxidation rate and phenol selectivity declined beyond reaction times of around 7 h. Literature reports support the present information that much longer reaction times would cause less phenol

yield<sup>56</sup>. This is attributed to the poisoning of the surface sites by the reaction products, which in turn block the active sites<sup>57</sup>. Lowering of phenol selectivity after 7 h indicates the further conversion of phenol to other products with long time of reaction. The optimized reaction time was 6 h.

### 5.3 BENZENE OXIDATION OVER PREPARED CATALYSTS

The above observations reveal that in the liquid-phase oxidation of benzene using hydrogen peroxide as oxidant on supported vanadia catalysts, the reaction parameters play a decisive role in determining the oxidation rate and phenol selectivity. The oxidation of benzene reaction was carried out over all the prepared catalysts under the selected reaction conditions (Table 5.1) in order to produce phenol more selectively.

Table 5.1

Parameters	Selected condition
Temperature/K	333
Acetonitrile/mmol,	191
Benzene/mmol	34
H <sub>2</sub> O <sub>2</sub> /mmol	88
Time/h	6

Table 5.2 shows the activity for benzene oxidation over VC series of catalysts along with silica supported V<sub>2</sub>O<sub>5</sub>.

Table 5.2

Catalyst	Conversion (wt.%)	Selectivity (%)	
		Phenol	Hydroquinone
Ce	-	-	-
2VC	2.0	100	-
4VC	6.5	100	-
6VC	14.0	100	-
8VC	15.6	98.5	1.5
10VC	8.3	92.4	7.6
V	22.0	88.9	11.1
6VRS	20.4	96.1	3.9
6VSG	42.0	45.6	54.4

No oxidation reaction occurs with ceria. The oxidation products formed over VC catalysts suggest the presence of vanadium in the reaction. Phenol is produced as the main product over VC series of catalysts. Small amount of hydroquinone is detected as secondary oxidation products with high vanadia loading. The production of phenol increases rapidly with increasing vanadia loading until 8 wt.%  $V_2O_5$ . An increase in vanadium content beyond this results in reduced conversion rate and phenol selectivity.  $V_2O_5$  show conversion of 22 % with phenol selectivity of 88.9 %. Among silica supported vanadia 6VRS gave 20.4 % benzene conversion with 98.2 % phenol. Eventhough, 6VSG could convert 42 % benzene, the phenol selectivity is found to be only 45.6 %.

Table 5.3 shows result of benzene oxidation over VCRS series of catalysts.



**Table 5.3**

Catalyst	Conversion (wt.%)	Phenol (%)
RS	-	-
CRS	-	-
2VCRS	1.8	100
4VCRS	5.9	100
6VCRS	18.8	100
8VCRS	20.1	100
10VCRS	13.5	100

Only phenol was detected as the oxidation product for all VCRS catalysts. These catalysts exhibit higher activity in comparison to the VC series of catalysts. Amount of phenol generated increases rapidly with increasing vanadia loading until a plateau is reached. An increase in vanadia content beyond this point, results in decreased phenol production. Catalytic activity increases up to 8 wt. %  $V_2O_5$  while further increase to 10 wt.% reduces the conversion.

Table 5.4 shows result of benzene oxidation over praseodymia catalysts.

**Table 5.4**

Catalyst	Conversion (wt.%)	Phenol (%)
P	-	-
PRS	-	-
2VP	1.0	100
6VP	3.5	100
10VP	1.6	100
2VPRS	1.2	100
6VPRS	5.2	100
10VPRS	1.7	100

Benzene oxidation over praseodymia containing catalysts show that the activity was very low compared to that of ceria containing catalysts. Only phenol was produced on supported vanadia catalysts while no product formed with Pr and PRS supports. Catalysts with 6 wt. % vanadia exhibit higher activity than the 10 wt.% vanadia loading.

#### 5.4 EFFECT OF LEACHING

Leaching of the supported metal ion into the reaction solution during the catalytic reaction is a concomitant concern whenever a supported metal catalyst is utilized in a liquid-phase reaction with organic hydroperoxides or H<sub>2</sub>O<sub>2</sub>. The influence of leaching of V species from the catalyst into the reaction solution during the production of phenol was investigated using the filtrate and the used catalyst, respectively, separated by filtration while hot after the first benzene oxidation. According to Sheldon et al.<sup>58</sup> the heterogeneity of a catalyst can be better understood only if the catalyst applied under reaction conditions will be removed after half an hour of the run and carrying out the reaction with filtrate under similar reaction conditions. The benzene oxidation with the catalyst in acetonitrile/hydrogen peroxide mixture was stirred at 333 K. The catalyst was removed from the reaction mixture after ½ h by filtration while hot. The filtrate was refluxed under same reaction conditions for 2 h. Filtered catalyst was again used for the reaction after washing, drying and calcination process.

Table 5.5 shows the effect of V leaching into the reaction solution during oxidation.

Table 5.5

Catalyst	Conversion (wt%)	Phenol (%)
4VC	2.4	100
Filtrate	4.5	93.4
6VC	6.3	100
Filtrate	8.4	92.6
4VCRS	2.8	100
Filtrate	3.8	97.8
6VCRS	7.9	100
Filtrate	8.6	96.7

Accordingly, resubmission of the filtrate under the reaction conditions (for 4VC,6VC and 4VCRS,6VCRS) shows an enhancement in conversion rate, pointing out that some of the vanadium atoms on the surface are leached out during the run and thus the observed enhanced activity of the filtrate may result from the leached vanadia species. When the filtrate was further studied for reaction without catalyst after half an hour reaction the amount of phenol was decreased due to further oxidation. Water is a best known solvent for phenol oxidation and the leached V species can oxidize phenol easily under the reaction conditions<sup>59</sup>. However, VCRS catalysts showed high stability against leaching of the active species into the liquid phase under the set reaction conditions than VC catalysts. This is achieved by the presence of silica on the support, which makes highly dispersed species over the surface.  $\text{H}_2\text{O}_2$  is an aggressive oxidant and can leach metal cation from framework of mesoporous silicas. This was observed in V-, Co-, Fe-, and Ti-containing mesoporous catalysts<sup>60-63</sup>. Acetonitrile is sufficiently coordinating and the V-O-Si bonds are

sufficiently labile for the formation of soluble vanadium oxides in acetonitrile<sup>64</sup>. In the present case the leaching observed correlates with these factors.

### 5.5 REGENERATION AND STABILITY

After 2 h reaction, the catalysts was recovered by hot filtration, washed several times with acetone, dried at 383 K overnight and calcined for 5 h at 773 K. The recovered catalysts were reused for benzene oxidation under the same reaction conditions.

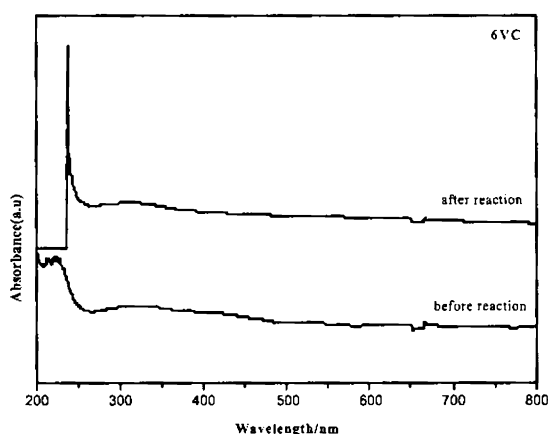
The catalytic behaviour in the reuse of the catalysts during oxidation is reported in Table 5.6.

**Table 5.6**

Catalyst	Cycle	Conversion (wt%)	Phenol (%)
4VC	1	4.9	100
	2	3.4	97.6
	3	1.8	96.5
6VC	1	9.2	100
	2	7.9	98.7
	3	3.2	95.3
4VCRS	1	6.0	100
	2	4.7	100
	3	2.1	98.5
6VCRS	1	13.0	100
	2	11.6	100
	3	10.4	98.2

The production of phenol over the recovered catalysts was obviously lower than that over the corresponding fresh catalysts. Results indicated a decrease in conversion rate from 4.9 to 1.8 (wt %) for 4VC and 9.2 to 3.2 (wt %) for 6VC after third cycle of use. After second recycling itself phenol selectivity of these catalysts was found decreasing. Activity drop-off is less for 4 and 6VCRS catalysts and phenol selectivity decreased only during the third cycle of use.

The recovered catalysts were characterized by UV-vis DRS. Spectra are depicted in Figure 5.7.



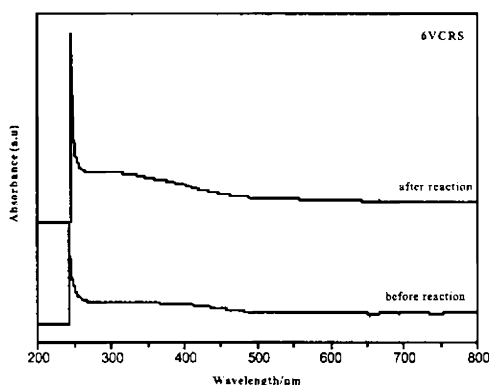


Figure 5.7

The UV-vis spectra of 6VC and 6VCRS are characterized by charge transfer (CT) transitions between central vanadium atoms and oxygen ligands. The absorption band at  $\sim 350$  nm can be assigned to  $V^{5+}$  species in a tetrahedral environment characterized by a V=O bond<sup>65</sup>. The absorption bands around  $\sim 600$  nm is assigned to the d-d transitions of  $V^{4+}$  which are not observed for catalysts after reaction<sup>66</sup>. The absence of absorption in the 600-800 nm suggests that catalysts contain only  $V^{5+}$ . The UV-vis spectra obtained for 6VC and 6VCRS after reaction time of 6 h were similar to the fresh one suggesting no change of coordination site for vanadium during oxidation reaction.

## 5.6 DISCUSSION

The catalytic activity observed in the present study and structural analysis studies in previous section allow a better understanding of the influence of catalyst characteristics on the catalytic activity. It seems that the parameters, which influences the catalytic activities are the dispersion of

supported vanadia species and the characteristic of the active species over the support surface.

Selective oxidation reactions of aromatics are known to follow a Mars-van Krevelen mechanism<sup>67</sup>. As lattice oxygen is inserted into the molecule, the reaction can occur in the absence of gas-phase O<sub>2</sub>. The capability of oxygen insertion is associated with the presence of reducibility and reoxidizability of the supported catalysts. Active centers convert sufficiently fast between two boundary oxidation states to keep their population constant in a steady state of the catalytic reaction. Sachtler et al.<sup>68,69</sup> reported that the activity and selectivity in oxidation reactions are determined by the intrinsic activity of lattice oxygen and their availability.

In the case of V<sub>2</sub>O<sub>5</sub>/CeO<sub>2</sub> catalysts, we have observed that the catalysts with a lower vanadia loading up to 6 wt. % V<sub>2</sub>O<sub>5</sub> exhibit higher catalytic activity and phenol selectivity in comparison to the series loading up to 10 wt.% V<sub>2</sub>O<sub>5</sub>. Phenol selectivity decreased with 8 wt. % while conversion rate reduced only for 10 wt. % V<sub>2</sub>O<sub>5</sub> loading. VCRS series of catalysts selectively produced phenol with high conversion rate. Conversion decreased after 8 wt. % V<sub>2</sub>O<sub>5</sub> loading. Praseodymia containing catalysts show very low catalytic activity than ceria catalysts.

The XRD analysis of VC catalysts evidenced that supported vanadia seems highly dispersed over the surface of the support for low loading and crystallization or compound formation occurs as the loading increases. Predominantly CeVO<sub>4</sub> formation observed at calcination temperature of 773 K in the V<sub>2</sub>O<sub>5</sub>/CeO<sub>2</sub> catalysts above 6 wt. % V<sub>2</sub>O<sub>5</sub> loading. UV-vis spectral

analysis indicates tetrahedral  $V^{5+}$  species for highly dispersed VC series of catalysts at lower loading. As the loading increases to 10 wt. %  $V_2O_5$ , agglomeration of vanadia particles envisaged from SEM pictures could reduce the number of active surface monolayer species, which results in polyvanadate species formation. A gradual reduction of surface area was observed after vanadia incorporation over ceria. This observation is parallel to the increased crystallite size observed from XRD data.  $^{51}V$  MAS NMR and FT-Raman of the prepared catalysts exhibit features corresponding to  $CeVO_4$ . This trend becomes more evident as vanadium loading increases. These catalysts exhibit a change in the structure and catalytic performance during benzene oxidation, which is related to the deactivation of the catalysts with fall in phenol selectivity. During alkane oxidation reactions, the conversion decreases due to deactivation, due to the formation of  $CeVO_4$ , which is already reported<sup>70,71</sup>.

Various studies have been attempted to understand the mechanism of aromatic oxidation over vanadium containing molecular sieves. Tetrahedral vanadium species ( $V^{5+}$ ) with redox properties are the only active phase<sup>72</sup>. The presence of vanadium must play a critical role in the oxidation reactions. However, the formation of bridged vanadia groups most likely represents the inactive catalyst form and these species, which are presumably responsible for the decrease in activity under high catalyst loading<sup>73</sup>.

In ceria containing catalysts, a redox mechanism can be fairly operative at low loading since vanadia is highly dispersed over the support. Increasing vanadia content to submonolayer coverage causes the formation of  $CeVO_4$  in which Ce is 3+ and V is 5+. It can possess oxygen insertion capacity through the redox pairs  $Ce^{3+/4+}$  and  $V^{5+/4+}$ . However, high concentration at higher



loading, results in the formation of crystallites of  $\text{CeVO}_4$ , which makes availability of the active sites for redox mechanism difficult which in turn reduces the total activity. It has been related to the surface modification of vanadia/ceria catalysts through the facile oxygen vacancies creation since no indication of  $\text{V}^{4+}$  could be obtained from the characterization of catalysts. Mohamed et al.<sup>74</sup> studied the CO oxidation over  $\text{MoO}_3/\text{CeO}_2$  catalysts and inferred that surface molybdate that permits the formation of  $\text{Mo}^{6+}$  in highly dispersed state beside the  $\text{Ce}^{3+}/\text{Ce}^{4+}$  redox couples were responsible for the revealed catalytic activity. Higher conversion rate at low loaded catalysts can arise from the presence of monovanadate species as Ce-V-O however, the decrease in activity and phenol selectivity can be attributed to the presence of V-O-V species formed at higher loading. Phenol formed can be quickly oxidized to dihydroxyl benzene at the set conditions<sup>75</sup>. According to Ayusman et al.<sup>76</sup> over vanadia containing catalysts the drop-off in activity was attributed to equilibrium between the catalytically active monomeric vanadium species and an inactive dimer. The oxidation states in  $\text{CeVO}_4$  are  $\text{V}^{5+}$  and  $\text{Ce}^{3+}$  and UV-vis analysis after reaction show no reduction of  $\text{V}^{5+}$  during oxidation reaction. It is assumed that the catalytic redox cycle on ceria-supported vanadia may be due to the redox cycle of cerium near vanadium; unlike the most supported vanadia catalysts, which work on the redox cycle of vanadium sites. A similar observation was reported for ceria supported chromia catalysts<sup>76</sup>. The EPR data also favour this interpretation. The interaction of ceria with vanadia stabilizes surface  $\text{Ce}^{3+}$  sites, which in turn moderates the valence change ability of the  $\text{Ce}^{3+}/\text{Ce}^{4+}$  pair, as well as block the corresponding V redox pairs. Vanadium would moderate the liability of ceria oxygen sites.

In VCRS series of catalysts, conversion is found higher compared to VC series of catalysts. BET surface area and pore volume analysis shows high values for VCRS catalysts. Silica helps to form highly dispersed vanadia species by providing high surface area. Powder XRD suggested more dispersion of vanadia over CRS support than ceria alone. As evidenced from  $^{29}\text{Si}$  MAS NMR, no compound formation occurs between  $\text{SiO}_2$  and supported  $\text{V}_2\text{O}_5$ . TPD- $\text{NH}_3$  analysis results a higher number of acid sites for VCRS catalysts than VC series of catalysts. Highly selective formation of phenol over VCRS catalysts is attributed to highly dispersed tetrahedral  $\text{V}^{5+}$  surface species. Silica promotion of ceria makes the supported vanadia to be in amorphous state with the help of large number of silanol groups present in silica. According to Park et al.<sup>77</sup> mesoporous molecular sieves make benzene molecule favourable to move easily towards active sites due to its large pore size and could provide more active sites because of very high surface area. Lower activity of microporous molecular sieves was attributed to lower number of silanol defect sites on the surface, where the vanadium ions can be anchored, in comparison with the mesoporous materials. The more surface vanadium species of V-MCM-41 resulted in higher catalytic activity. An important condition for the achievement of catalyst capable of activating  $\text{H}_2\text{O}_2$  is site isolation to avoid extensive  $\text{H}_2\text{O}_2$  radical decomposition<sup>78</sup>. It was reported that titania based amorphous solids fail to promote oxidations with  $\text{H}_2\text{O}_2$  because of its hydrophilic properties compared to the hydrophobic silicalites. According to Klein et al.<sup>79</sup> hydrophilic sol-gel  $\text{TiO}_2$ - $\text{SiO}_2$  amorphous solids with more number of surface silica could enhance surface polarity which in turn could achieve good oxidation rates with  $\text{H}_2\text{O}_2$ . They also documented

that surface polarity can affect not only the reaction rate and selectivity but also the overall conversion and catalyst lifetime. According to Chiara et al.<sup>80</sup> in oxidation of olefins the activity and selectivity of the catalyst and the extent of H<sub>2</sub>O<sub>2</sub> decomposition seem to be controlled by an appropriate polarity of the medium, by the polarity/acidity of the surface, and by the possibility to carry out the reaction at lower temperatures where the acidity effects of H<sub>2</sub>O<sub>2</sub> and the silica matrix could be minimized.

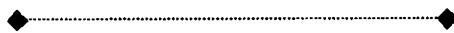
A good catalyst for partial oxidation must have two redox couples, one of which should have a reduction potential higher than the other one, in order to facilitate an efficient electron transfer and promoting the reoxidation of oxygen-inserting sites<sup>81</sup>. The separation of the reduction temperatures observed in the TPR-H<sub>2</sub> experiments, which is related to the difference in the reduction potentials present in the supported catalyst, could correlate to the higher activity of VCRS catalysts than VC catalysts.

The X-ray diffraction pattern of praseodymia supported vanadia catalysts correspond to Pr<sub>x</sub>V<sub>2</sub>O<sub>7</sub> type pyrovanadate structure formation as the vanadia loading increases. Pyrovanadates contain two tetrahedrally coordinated vanadium atoms connected by bridging oxygen in a V<sub>2</sub>O<sub>7</sub><sup>4-</sup> unit, which consists mainly V-O-V bonds. BET measurements resulted low surface area compared to ceria containing catalysts. Supported VP and VPRS catalysts presents endotherm corresponding to pyrovanadate type formation, Pr<sub>6</sub>V<sub>2</sub>O<sub>7</sub> depending upon the vanadia loading. The formation of silicate like Si-O-Pr configuration was evidenced from <sup>29</sup>Si MAS NMR studies for VPRS catalysts. The observed low activity of VP and VPRS catalysts can be attributed to the low oxygen storage property of praseodymia. Under reaction conditions the

redox behaviour of praseodymia is different from that of ceria. Ceria is relatively easy to reoxidise while with praseodymia the reoxidation is too slow to provide the necessary oxygen storage properties under reaction conditions. The oxidation of CO over Pd/praseodymia catalysts exhibited a similar behaviour<sup>82</sup>. If  $\text{Pr}_6\text{O}_{11}$  once reduced to  $\text{Pr}_2\text{O}_3$  the reoxidation by exposure to  $\text{O}_2$  is difficult<sup>83</sup>.

## 5.7 CONCLUSION

Investigation of the one step liquid-phase oxidation of benzene to phenol by hydrogen peroxide on various rare earth oxide supported vanadia is described. Ceria containing catalysts are found to catalyze the oxidation with higher conversion rate than praseodymia catalysts. Among ceria catalysts VCRS series of catalysts exhibits higher conversion rate and phenol selectivity in comparison to VC catalysts. Praseodymia supported vanadia catalysts show negligible oxidation activity. Studies on influence of reaction parameters such as temperature, solvent, time and volume of oxidant, substrate and solvent suggests that these are crucial in determining catalytic efficiency in heterogeneous catalytic systems. The catalytic activity of the ceria containing catalysts was presumably related to the strong interaction between the support and vanadia as emphasized by means of FT-IR (V=O and V-O-Support linkages), UV-vis DRS (dispersed tetrahedral  $\text{V}^{5+}$ ), XRD (crystallite size), EPR ( $\text{Ce}^{3+}/\text{Ce}^{4+}$ ) and MAS NMR ( $\text{V}^{5+}$ ) techniques. Comparatively very low activity of VP and VPRS catalysts can be attributed to the formation of poly vanadate species of the type V-O-V and Si-O-Pr species.



REFERENCES

- [1] K. Weissermehi, H.J. Arpe, *Industrial Organic Chemistry*, VCH, New York (1993) 344.
- [2] R. Hamada, Y. Shibata, S. Nishiyama, S. Tsuruya, *Phys. Chem. Chem. Phys.* 5 (2003) 956.
- [3] S. Yamaguchi, S. Sumimoto, Y. Ichihashi, S. Nishiyama, S. Tsuruya, *Ind. Eng. Chem. Res.* 44 (2005) 1.
- [4] K. Nomiya, H. Yanagibayashi, C. Nozaki, K. Kondoh, E. Hiramatsu, Y. Shimizu, *J. Mol. Catal. A: Chem.* 114 (1996) 25.
- [5] L.C. Passoni, A.T. Cruz, R. Buffon, U. Schuchardt, *J. Mol. Catal. A: Chem.* 120 (1997) 117.
- [6] L.C. Passoni, F.J. Luna, M. Wallau, R. Buffon, U. Schuchardt, *J. Mol. Catal. A: Chem.* 134 (1998) 229.
- [7] J.M. Brégeault, *Dalton Trans.* (2003) 3289.
- [8] M. Bonchio, V. Conte, F.D. Furia, G. Modena, S. Moro, *J. Org. Chem.* 59 (1994) 6262.
- [9] L. Li, J.I. Shi, J.N. Yan, X.G. Zhao, H.G. Chen, *J. Mol. Catal.* 263 (2004) 213.
- [10] L.I. Kuznetsova, L.G. Detusheva, M.A. Fedotov, V.A. Likholobov, *J. Mol. Catal.* 111 (1996) 81.
- [11] A.K. Uriarte, M.A. Rodkin, M.J. Gross, A.S. Kharitonov, G.I. Panov, *Stud. Surf. Sci. Catal.* 110 (1997) 857.
- [12] A.A. Ivanov, V.S. Chernyavsky, M.J. Gross, A.S. Kharitonov, A.K. Uriarte, G.I. Panov, *Appl. Catal. A: Gen.* 249 (2003) 327.
- [13] J. Jia, K.S. Pillai, Wolfganag, M.H Sachtler, *J. Catal.* 221 (2004) 119.
- [14] J. Okamura, S. Nishiyama, S. Tsuruya, M. Masai, *J. Mol. Catal. A: Chem.* 135 (1998) 133.
- [15] E. Selli, I. Rossetti, D. Meloni, F. Sini, L. Forni, *Appl. Catal A: Gen.* 262 (2004) 131.
- [16] G. I. Panov, A.K. Uriarte, M.I. Rodkin, V.I. Sobolev, *Catal. Today* 41 (1998) 365.
- [17] E.J.M. Hensen, Q. Zhu, R.A. van Santen, *J. Catal.* 233 (2005) 136.

- [18] A. Waclaw, K. Nowinska, W. Schwieger, *Appl. Catal. A: Gen.* 270 (2004) 151.
- [19] E. Selli, A. Isernia, L. Forni, *Phys. Chem. Chem. Phys.* 2 (2000) 3301.
- [20] L. Li, J.L. Shi, J.N. Yan, X.G. Zhao, H.G. Chen. *Appl. Catal. A: Gen.* 263 (2004) 213.
- [21] R. Noyori, M. Aoki, K. Sato, *Chem. Commun.* (2003) 1977.
- [22] E. Battistel, R. Tassinari, M. Fornaroli, L. Bonoldi, *J. Mol. Catal. A: Chem.* 202 (2003) 107.
- [23] J.E. Remias, T.A. Pavlosky, A. Sen, *J. Mol. Catal. A: Chem.* 203 (2003) 179.
- [24] D. Bianchi, M. Bertoli, R. Tassinari, *J. Mol. Catal. A: Chem.* 200 (2003) 111.
- [25] T. Tagawa, Y-J. Seo, S. Goto, *J. Mol. Catal.* 78 (1993) 201.
- [26] J. Peng, F. Shi, Y. Gu, Y. Deng, *Green Chem.* 5 (2003) 224.
- [27] R. Kumar, P. Mukharjee, A. Bhaumik, *Catal. Today* 49 (1999) 185.
- [28] K. Nomiya, K. Hashino, Y. Nemoto, M. Watnabe, *J. Mol. Catal. A: Chem.* 176 (2001) 79.
- [29] G. Strukul (Ed.), *Catalytic Oxidations with Hydrogen Peroxide as Oxidant*, Kluwer Academic Publishers, Dordrecht (1992).
- [30] G.D. Vulpescu, M. Rutenbeek, L.L. van Lieshout, L.A. Correia, D. Meyer, P.P.A.C. Pex, *Catal. Commun.* 5 (2004) 347.
- [31] S. Niwa, M. Eswaramoorthy, N. Jalajakumari, R. Anuj, I. Naotsugu, S. Hiroshi, N. Takemi, M. Fujio, *Sci.* 295 (2002) 105.
- [32] T. Miyahara, H. Kanzaki, R. Hamada, S. Kuroiwa, S. Nishiyama, S. Tsuruya, *J. Mol. Catal. A: Chem.* 176 (2001) 141.
- [33] F.S. Xiao, J. Sun, X. Meng, R. Yu, H. Yuan, D. Jiang, S. Qiu, R. Xu, *Appl. Catal. A: Gen.* 207 (2001) 267.
- [34] M.A. Ishida, Y. Masumoto, R. Hamada, S. Nishiyama, S. Tsuruya, M. Masai, *J. Chem. Soc., Perkin Trans. 2* (1999) 847.
- [35] H. Kanzaki, T. Kitamura, R. Hamada, S. Nishiyama, S. Tsuruya, *J. Mol. Catal. A: Chem.* 208 (2004) 203.
- [36] K. Nomiya, K. Yagishita, Y. Nemoto, T.A. Kamataki, *J. Mol. Catal. A: Chem.* 126 (1997) 43.

- [37] J.L. Graham, C.B. Almquist, S. Kumar, S. Sidhu, *Catal. Today* 88 (2003) 73.
- [38] C.W. Lee, W.J. Lee, Y.K. Park, S.E. Park, *Catal. Today* 61 (2000) 137.
- [39] S.E. Park, J.W. Yoo, W.J. Lee, *Proceedings of the 12<sup>th</sup> IZC, Baltimore, USA, II* (1999) 1253.
- [40] M. Vassileva, A. Andreeva, S. Dancheva, N. Kotzev, *Appl. Catal.* 49 (1989) 125.
- [41] M. Vassileva, A. Andreeva, S. Dancheva, *Appl. Catal.* 69 (1991) 221.
- [42] D. Andreeva, T. Tabakova, V. Idakiev, A. Naydenov, *Gold Bull.* 31 (1998) 105.
- [43] D. Andreeva, T. Tabakova, L. Ilieva, A. Naydenov, D. Mehanjiev, M.V. Abrashev, *Appl. Catal. A: Gen.* 209 (2001) 291.
- [44] D. Andreeva, T. Tabakova, A. Naydenov, F. Verport, *Proc. 9<sup>th</sup> Intern. Symp. Heter. Catal. Varna* (2000) 731.
- [45] F. Boccuzzi, A. Chiorino, M. Manzoli, D. Andreeva, T. Tabakova, *Proc. 9<sup>th</sup> Intern. Symp. Heter. Catal. Varna* (2000) 725.
- [46] G. Strukul, *Angew. Chem., Int. Ed. Engl.* 37 (1998) 1199.
- [47] R. Yu, F. Xiao, D. Wang, T. Sun, Y. Liu, G. Pang, S. Feng, S. Qui, R. Xu, C. Fang, *Catal. Today* 51 (1999) 39.
- [48] F. Gao, R. Hua, *App. Catal. A: Gen.* 270 (2004) 223.
- [49] S. Shylesh, A.P. Singh, *J. Catal.* 228 (2004) 333.
- [50] D. Bianchi, R. Bortolo, R. Tassinari, M. Ricci, R. Vignola, *Angew. Chem. Int. Ed.* 39 (2000) 4321.
- [51] R. Kumar, A. Bhaumik, *Micropor. Mesopor. Mat.* 21 (1998) 497.
- [52] A.P. Singh, B. Jacob, S. Sugunan, *Appl. Catal. A: Gen.* 174 (1998) 51.
- [53] D. Rohan, C. Canaff, E. Romeafin, M. Guismet, *J. Catal.* 177 (1998) 2743.
- [54] R. Yu, F. Xiao, D. Wang, G. Pang, S. Feng, S. Qui, R. Xu, *Catal. Lett.* 49 (1997) 49.
- [55] J. Zhang, Y. Tang, G. Li, C. Hu, *Appl. Catal. A: Gen.* 278 (2005) 251.
- [56] K. Nomiya, H. Yangibayashi, C. Nozaki, K. Kondoh, E. Hiramatsu, Y. Shimizu, *J. Mol. Catal.* 114 (1996) 181.
- [57] C.B. Lui, Z. Zhang, X.G. Yang, Y. Wu, *J. Chem. Soc. Commun.* (1996) 1019.

- [58] R.A. Sheldon, M. Wallau, I.W.C.E. Arends, U. Schuchardt, *Acc. Chem. Res.* 31 (1998) 485.
- [59] Z. Ziolek, I. Sobezak, I. Nowak, P. Decyk, A. Lewandowska, J. Kujawa, *Micro. Meso. Mater.* 35-36 (2000) 195.
- [60] V. Parvulescu, C. Dascalescu, B.L. Su, *Stud. Surf. Sci. Catal.* 135 (2001) 4772.
- [61] V. Parvulescu, B.L. Su, *Catal. Today* 69 (2001) 315.
- [62] A. Tuel, *Micro. Meso. Mater.* 27 (1999) 151.
- [63] R. Neumann, M.L. Elad, *Appl. Catal. A: Gen.* 122 (1995) 85.
- [67] P. Mars, D.W. van Krevelen, *Chem. Eng. Sci.* 3 (1954) 41.
- [68] W.M.H. Sachtler, N.H. De Boer, *Proc. 3<sup>d</sup> Int. Con. on Catal.* Amsterdam, 1964, Wiley, New York (1965) 240.
- [69] W.M.H. Sachtler, G.J.H. Dorgelo, J. Fahrenfort, R.J.H. Voorhoev, *Proc. 4<sup>th</sup> Int. Con. Catal.* Moscow, 1968, B.A. Kazanski, Adler (eds.) New York (1968) 454.
- [70] J.M. Vohs, T. Feng, G.S. Wong, *Catal. Today* 85 (2003) 303.
- [71] W. Daniell, F. Anderle, A. Ponchel, S. Kuba, D.H. Gregory, H. Knozinger, *Top. Catal.* 8 (1999) 45.
- [72] D.A. Bulushev, L.K. Minsker, F. Rainone, A. Renken, *J. Catal.* 205 (2002) 115.
- [73] M.L. Ferreira, M. Volpe, *J. Mol. Catal. A: Chem.* 164 (2000) 281.
- [74] M.M. Mohamed, S.M.A. Katib, *Appl. Catal. A: Gen.* 287 (2005) 236.
- [75] P. Chipurici, R. Avram, L. Papahagi, A.I. Gavrilla, 12<sup>th</sup> Romanian Int. Conf. Chem. Chem. Eng. Bucuresti, Romania (2001).
- [76] J.E. Remias, T.A. Pavlosky, A. Sen, *J. Mol. Catal. A: Chem.* 203 (2003) 179.
- [77] B. Notari, *Catal. Today* 18 (1993) 63.
- [78] U. Schuchardt, D. Cardoso, R. Sercheli, R. Pereira, R.S. Cruz, M.C. Guerreiro, D. Mandelli, E.V. Spimace, E.L. Pires, *Appl. Catal.* 211 (2001) 1.
- [79] S. Klein, W.F. Maier, *Angew. Chem. Int. Ed. Engl.* 35 (1996) 2230.
- [80] C. Palazzi, L. Oliva, M. Signoretto, G. Strukul, *J. Catal.* 194 (2000) 286.



## CHAPTER 6

### OXIDATION OF ETHYLBENZENE

#### Abstract

---

---

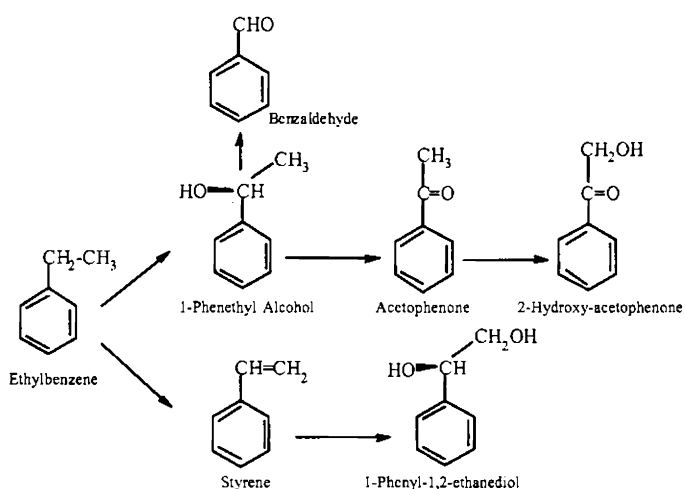
*The selective oxidation of alkylaromatics is one of the main processes since the reaction products are important as intermediates in numerous industrial organic chemicals. Side-chain oxidation of alkyl aromatic compounds catalyzed by heterogeneous catalysts using cleaner peroxide oxidants is an especially attractive goal since classical synthetic laboratory procedures preferably use permanganate or acid dichromate as stoichiometric oxidants. In spite of many studies, there are very few which use hydrogen peroxide as a source of oxygen in the C-H activation of alkanes. Effective utilization of ethylbenzene, available in the xylene stream of the petrochemical industry to more value added products is a promising one in chemical industry. The oxidation products of ethylbenzene are widely employed as intermediates in organic, steroid and resin synthesis.*

---

---

## 6.1 INTRODUCTION

The oxidation of alkylbenzenes is an important transformation in chemical synthesis usually conducted with corrosive, toxic or carcinogenic materials and the desired products are obtained with low selectivity accompanied by environmentally harmful by-products<sup>1</sup>. Metal oxides catalyzed oxidation of aromatics with atom efficient oxidants such as O<sub>2</sub> or H<sub>2</sub>O<sub>2</sub> is rapidly gaining attention as a viable alternative to the environmentally hazardous metal promoted stoichiometric oxidations. Side-chain oxidation of alkyl aromatics using cleaner peroxide oxidants catalyzed by heterogeneous catalysts has been interested much<sup>2</sup>. The oxidation pathways of ethylbenzene are presented in scheme 6.1.



Scheme 6.1

A broad variety of catalytic systems have been described in the literature for the oxidation of alkylaromatics. Copper tri- and tetraaza macrocyclic complexes encapsulated in zeolite-Y exhibit good catalytic

performance in the oxidation of ethylbenzene using TBHP as oxidant<sup>3</sup>. Acetophenone was the major product with small amounts of *o*- and *p*-hydroxyacetophenones indicating that C-H bond activation takes place both at benzylic and aromatic ring carbon atoms. Soluble acetylacetonate-nickel(II) complexes have been used for ethylbenzene oxidation with quaternary ammonium salts and macrocyclic polyethers<sup>4</sup>. The catalytic oxidation of ethylbenzene to ethylbenzene hydroperoxide with air in liquid phase using Ni(II) complexes results mainly reaction byproducts as acetophenone and phenol<sup>5</sup>. Ethylbenzene oxidation with TBHP by polynuclear Mn Schiff base complexes produced acetophenone and 1-phenyl ethanol with small amounts of peroxy compounds<sup>6</sup>. Selective oxidation of ethylbenzene with air produced 1-phenyl ethanol and acetophenone over dimeric metalloporphyrins<sup>7</sup>.

The oxidation of organic substrates using H<sub>2</sub>O<sub>2</sub> as oxidant has been well documented<sup>8-10</sup>. According to Yusuff et al.<sup>11</sup> Y Zeolite encapsulated Co(II), Ni(II) and Cu(II) complexes gave acetophenone as the only partial oxidation product during ethylbenzene oxidation with H<sub>2</sub>O<sub>2</sub>. The catalytic activity is attributed to the geometry of encapsulated complexes. Titanosilicates mainly catalyze ring hydroxylation of arenes with H<sub>2</sub>O<sub>2</sub>, whereas vanadium and chromium substituted zeolites and aluminophosphate molecular sieves has been known to favour side chain oxidation selectively<sup>12</sup>. Cavaleiro et al.<sup>13</sup> studied the oxidation of alkylaromatics with H<sub>2</sub>O<sub>2</sub> over Mn(III) porphyrins in the presence of ammonium acetate as co-catalyst. The catalysts produced acetophenone as the major product with 1-phenylethanol, 2-ethyl-1,4-benzoquinone and styrene. Mainly oxidation takes place in the benzylic positions with these catalysts. Products arising from further oxidation

of acetophenone were not detected. The oxidation of alkylbenzenes with  $\text{H}_2\text{O}_2$  over  $\text{Cu(II)}$  complexes took place selectively at the benzylic C-H bond without any oxidation in the remaining C-H bonds<sup>14</sup>. During liquid-phase oxidation of ethylbenzene with molecular oxygen over quaternary ammonium compounds ethylbenzene hydroperoxide is obtained as the main product<sup>15,16</sup>.

## 6.2 INFLUENCE OF REACTION CONDITION

The influence of different reaction parameters was analyzed in order to maximize the product yield and selectivity. Effect of reaction conditions for ethylbenzene oxidation with  $\text{H}_2\text{O}_2$  was initially assayed in non-optimized conditions with 6VC as the catalyst.

### 6.2.1 Effect of Temperature

The effect of temperature on the rate and selectivity of the ethylbenzene oxidation is shown in the Figure 6.1.

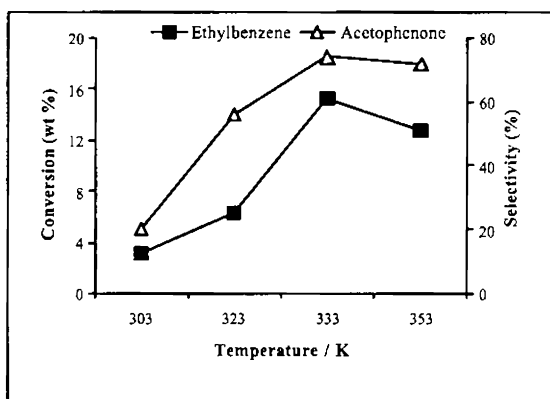


Figure 6.1

Reaction conditions:- 6VC-100 mg, Ethylbenzene-8 mmol, Acetonitrile-95 mmol and  $\text{H}_2\text{O}_2$ -26 mmol and Time-3 h.

The effect of the temperature on the rate of oxidation is very important. Oxidation of ethylbenzene (EB) using  $H_2O_2$  in acetonitrile produced acetophenone (Acph) as the major product. Benzaldehyde and other products such as 1-phenyl ethanol and 2-hydroxyacetophenone are also formed in small quantities depending on the reaction conditions. Four temperatures have been tested and found that as the temperature rises, there is an increase in the oxidation until 333 K while further increase caused decrease in rate. Lower conversion rate at 353 K might be attributed to decomposition of  $H_2O_2$ <sup>17</sup>. The selectivity to acetophenone increases as the temperature rises from 303 to 333 K and decreased at 353 K. This can result by further oxidation of acetophenone to hydroxy products. The temperature of choice for further reaction was 333 K.

### 6.2.2 Effect of Solvent

The influence of various solvents on oxidation is shown in Figure 6.2.

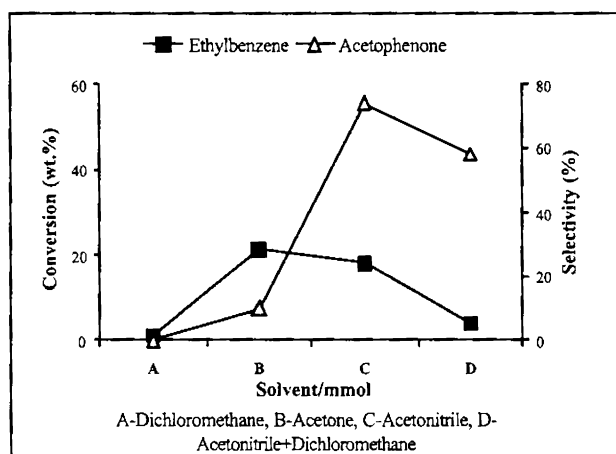


Figure 6.2

Reaction conditions:- 6VC-100 mg, Ethylbenzene-8 mmol, Solvent-95 mmol,  $H_2O_2$ -26 mmol, Temperature-333 K and Time -3 h.

Generally the role of solvent on the liquid-phase reaction is very complex, especially on the product distribution. The use of polar solvents favours oxidation at the double bond, whereas the non-polar solvents lead to allylic oxidation<sup>18</sup>. Reaction conducted without any solvent and with dichloromethane not resulted in oxidation. When acetonitrile and dichloromethane was used in 1:1 mole ratio conversion and selectivity increased. Acetonitrile as solvent gave acetophenone selectively in high conversion rate. Acetonitrile being an aprotic solvent initiates side chain oxidation at the interface with high conversion rate<sup>19</sup>. Acetonitrile is known to activate  $\text{H}_2\text{O}_2$  by forming a perhydroxyl anion, which in turn produces a good oxygen transfer intermediate<sup>20</sup>. Eventhough conversion is more in acetone, the acetophenone produced was very small. This can arise from side reactions between acidic solvent and  $\text{H}_2\text{O}_2$  yielding peroxy or hydroperoxy products, causing a lower concentration of free  $\text{H}_2\text{O}_2$  at or near the active sites<sup>21</sup>.

### 6.2.3 Effect of Catalyst weight

The effect of catalyst amount on oxidation is presented in Figure 6.3.

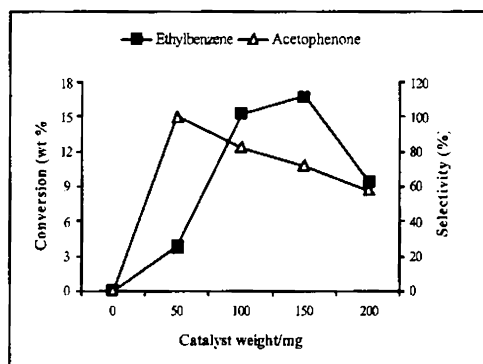


**Figure 6.3**

Reaction conditions: 6VC, Ethylbenzene-8 mmol, Acetonitrile-95 mmol,  $\text{H}_2\text{O}_2$ -26 mmol, Temperature-333 K and Time-3 h.

The oxidation reaction was not observed in the absence of any catalyst indicating that  $\text{H}_2\text{O}_2$  alone is unable to oxidize the substrate to a significant extent and reaction can occur only when a catalyst is present. It can be seen from the figure that the ethylbenzene conversion rate improves as the catalyst amount is increased reaches a maximum at 150 mg. Further increase to 200 mg decreases the conversion rate. High metal concentration can inhibit the autooxidation reactions<sup>22</sup>. However acetophenone selectivity displays a different pattern. With 50 mg 6VC catalyst, acetophenone was produced as the main product while selectivity drops greatly as the catalyst amount increases to 200 mg. At lower catalyst concentration acetophenone was obtained as major product while at higher catalyst amount selectivity decreases at the cost of hydroxyacetophenone<sup>23,24</sup>.

#### 6.2.4 Effect of Acetonitrile volume

The effect of concentration of the solvent (acetonitrile) on ethylbenzene oxidation is shown in Figure 6.4.

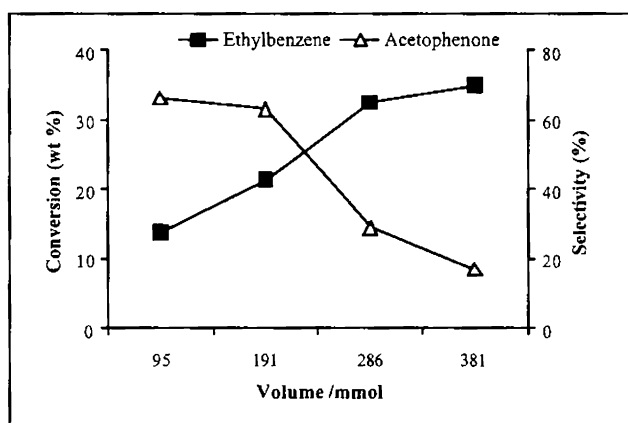


**Figure 6.4**

Reaction conditions:- 6VC-100 mg, Ethylbenzene-8 mmol,  $\text{H}_2\text{O}_2$ - 26 mmol, Temperature- 333 K and Time-3 h.

Ethylbenzene oxidation conducted with various concentration of acetonitrile shows that solvent concentration affects the activity and selectivity in liquid phase reaction. An increase in acetonitrile concentration from 91 to 381 mmol leads to a marginal decrease of the acetophenone selectivity even though conversion rate increases. An effect of solvent dilution on the product distribution was thus observed<sup>25</sup>.

### 6.2.5 Effect of Ethylbenzene volume

The effect of ethylbenzene volume for oxidation is shown in Figure 6.5.

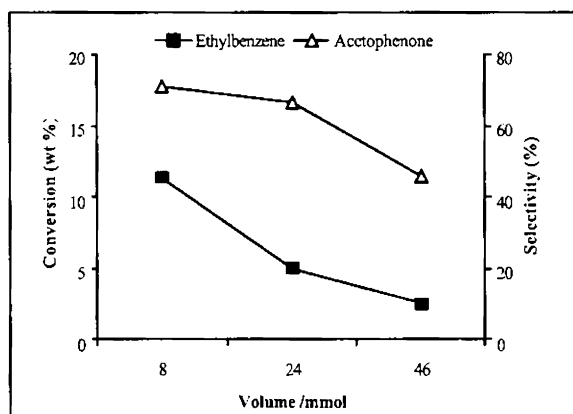


Figure 6.5

Reaction conditions:- 6VC-100 mg, Acetonitrile-191 mmol,  
 $H_2O_2$ -88 mmol, Temperature-333 K and Time-3 h.

As shown in figure, conversion rate and acetophenone selectivity decreases with increase in ethylbenzene volume from 8 to 24 (mmol). An increase in substrate to catalyst ratio can cause unavailability of active sites for the reaction reducing activity and selectivity<sup>26</sup>.



### 6.2.6 Effect of H<sub>2</sub>O<sub>2</sub> volume

The effect of oxidant volume on oxidation is illustrated in Figure 6.6.

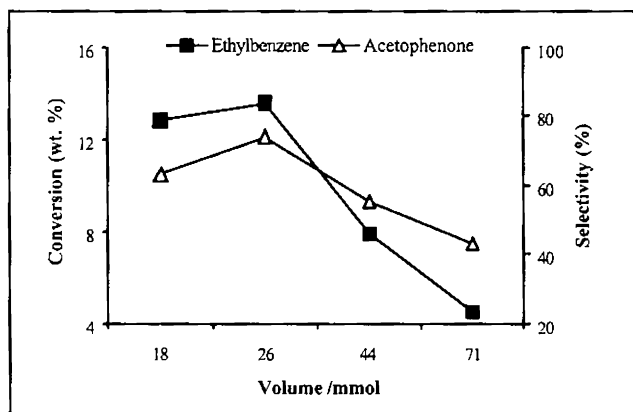


**Figure 6.6**

Reaction conditions:- 6VC-100 mg, Ethylbenzene- 8 mmol, Acetonitrile- 191 mmol, Temperature- 333 K and Time-3 h.

No oxidation is observed when reaction was done without oxidant under the set conditions. The rate of oxidation was found to increase with the H<sub>2</sub>O<sub>2</sub> concentration up to 26 mmol, thereafter decreasing. The oxidation with different concentration of oxidant shows that the catalytic activity and acetophenone product selectivity was maximum at lower concentration. The “active oxygen” content of H<sub>2</sub>O<sub>2</sub> is 47 % of its weight and water is the only byproduct. The higher concentration of H<sub>2</sub>O<sub>2</sub> favours secondary oxidation of the acetophenone thus formed. It indicates that a high oxidant concentration can inhibit the reaction with nonselective peroxide decomposition<sup>27</sup>.

### 6.2.7 Effect of Time

The effect of time on ethylbenzene oxidation is illustrated in Figure 6.7.

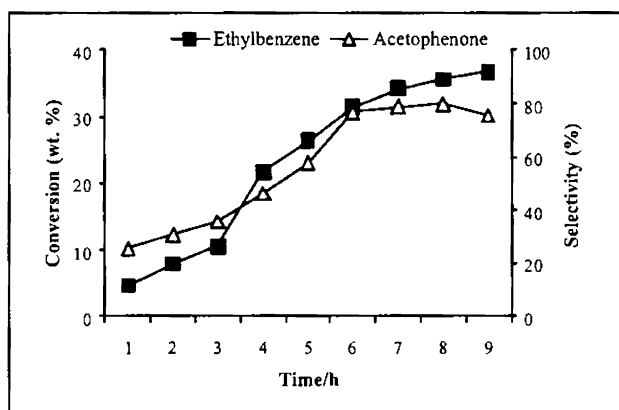


**Figure 6.7**

Reaction conditions:- 6VC-100 mg, Ethylbenzene-8 mmol, Acetonitrile-191 mmol, Temperature-333 K and  $\text{H}_2\text{O}_2$ -26 mmol.

Acetophenone was the main product with lesser concentration of benzaldehyde and 2-hydroxyacetophenone. Conversion rate and selective formation of acetophenone increases with time up to 6 h. After 7 h of reaction conversion rate remains more or less constant while acetophenone selectivity decreases indicating further oxidation to form hydroxyl product under the reaction conditions. Acetophenone could be formed directly or by the oxidation of 1-phenylethanol formed as an intermediate<sup>28</sup>. The polar oxidation and transformation products formed during reaction cover the surface of the solid oxide, which can also lead to catalyst inactivation<sup>29</sup>.

### 6.3 ETHYLBENZENE OXIDATION OVER PREPARED CATALYSTS

The studies on various reaction parameters show that oxidation rate and product selectivity in the liquid-phase oxidation of ethylbenzene is greatly dependent on a cooperative effect of the substrate, solvent, oxidant, time and

temperature. The ethylbenzene oxidation reaction was carried out with all the catalysts prepared under the reaction conditions shown in Table 6.1.

Table 6.1

Parameters	Selected condition
Temperature/K	333
Acetonitrile/mmol	191
Ethylbenzene/mmol	8
H <sub>2</sub> O <sub>2</sub> /mmol	26
Time/h	6

Table 6.2 compares the activity of ethylbenzene oxidation over VC series of catalysts.

Table 6.2

Catalyst	Conversion (wt.%)	Selectivity (%)		
		Acph	2-OH Acph	Bald
Ce	4.4	13.2	-	86.8
2VC	4.8	69.3	-	30.6
4VC	9.9	73.8	-	26.2
6VC	16.8	75.6	16.2	11.7
8VC	18.7	78.9	13.2	7.7
10VC	20.5	72.2	21.1	6.7

Acph-Acetophenone and Bald-Benzaldehyde

The catalytic activity of VC series of catalysts was evaluated for the oxidation of ethylbenzene with H<sub>2</sub>O<sub>2</sub> in acetonitrile solvent at 333 K. The oxidation reaction carried out over ceria has exhibited only negligible

conversion with benzaldehyde as the major product. Supported vanadia catalysts were found to be active in the ethylbenzene oxidation with acetophenone as the major product. Benzaldehyde and 2-hydroxyacetophenone are also detected in minor quantities indicating that C-H bond activation takes place only at benzylic position. For a series of ceria supported vanadia catalysts, activity increases with increase in loading up to 10 V<sub>2</sub>O<sub>5</sub> wt. % at which it gave a conversion of 20.5 %. However, acetophenone selectivity decreases for 10VC with more amounts of 2-hydroxyproduct. The formation of alcohols by the interaction of the intermediate, benzylic carbocation with the solvent water was observed for Ce(IV)/BrO<sub>3</sub><sup>-</sup> systems<sup>46</sup>.

Table 6.3 shows the activity of VCRS series of catalysts towards ethylbenzene oxidation.

Table 6.3

Catalyst	Conversion (wt.%)	Selectivity (%)		
		Acph	2-OH Acph	Bald
RS	3.0	-	-	100
CRS	4.0	18.6	8.8	72.4
2VCRS	9.6	66.7	-	34.3
4VCRS	11.3	71.3	12.1	28.6
6VCRS	23.9	82.9	13.7	3.4
8VCRS	29.7	94.2	5.8	2.9
10VCRS	34.6	82.4	14.4	-

The oxidation of ethylbenzene over VCRS series of catalysts shows higher conversion and selectivity in comparison to VC series. Silica and ceria-silica were quite active towards oxidation while acetophenone is produced only with low selectivity. Benzaldehyde and hydroxyacetophenones are also observed during the oxidation reaction. For supported vanadia catalysts conversion increases upon vanadia loading reaches maximum of 34.6 % conversion for 10VCRS. Acetophenone selectivity decreased for 10VCRS at the expense of hydroxyproduct.

Table 6.4 shows the activity of ethylbenzene oxidation over praseodymia and various silica supported vanadia catalysts.

Table 6.4

Catalyst	Conversion (wt. %)	Selectivity (%)		
		Acph	2-OH Acph	Bald
P	1.8	-	-	100
PRS	2.5	-	-	100
2VP	4.8	25.8	1.4	74.7
6VP	6.8	15.2	9.8	74.8
10VP	5.0	11.0	9.3	79.6
2VPRS	9.9	49.4	15.9	34.7
6VPRS	17.6	48.3	12.9	41.0
10VPRS	9.5	43.2	3.9	39.8
V <sup>s</sup>	42.1	43.9	19.6	76.5
6VRS <sup>#</sup>	28.1	15.4	64.1	28.1
6VSG <sup>#</sup>	41.3	8.4	90.1	41.3

\* - \$ -5 min, # - 2 h

The activity and selectivity of praseodymia containing catalysts along with various silica supported vanadia catalysts are reported. No acetophenone is observed with praseodymia and PRS. However, VP and VPRS series of catalysts produced acetophenone to some extent. As the vanadia loading increases catalytic activity increases to 6 wt.%  $V_2O_5$  while decreased thereafter for 10 wt.% loading. Major amount of benzaldehyde was produced over VP series of catalysts. However VPRS catalysts was more selective towards acetophenone production. Vanadium pentoxide gave 42.1 % conversion within 5 minutes with 43.9 %, 76.9 % acetophenone and benzaldehyde respectively. The oxidation rate of 6VRS was lower than that of 6VSG while acetophenone selectivity was found higher.

#### **6.4 EFFECT OF LEACHING**

Leaching of metal ions if any during the reaction can cause serious errors in the activity of catalysts. The influence of leaching of V species from the catalyst into the reaction solution during ethylbenzene oxidation was investigated using the filtrate and the used catalyst, respectively, separated by filtration while hot after the first oxidation. In representative tests, the ethylbenzene in acetonitrile/hydrogen peroxide mixture was stirred at 333 K. The catalyst was filtered out after ½h of the reaction while hot. The filtrate was kept under same reaction conditions for long time to check the experiment for further reaction. Table 6.5 displays the results of leaching studies conducted with representative catalysts.

Table 6.5

Catalyst	Conversion (wt.%)	Acph (%)
6VC	3.1	41.6
Filtrate	4.2	83.4
8VC	6.8	56.7
Filtrate	8.2	82.6
6VCRS	13.8	77.9
Filtrate	14.0	79.3
8VCRS	15.8	74.6
Filtrate	16.6	86.7
6VP	1.2	-
Filtrate	1.3	-
6VPRS	3.5	-
Filtrate	3.8	-

Analysis of filtrate after 1 h reaction shows enhancement in activity with some of the catalysts. An interesting observation could be made that analysis of reaction mixture at  $\frac{1}{2}$ h exhibits production of acetophnone in lower selectivity. However, after 1h reaction filtrates test of VC and VCRS series of catalysts shows an enhancement in acetophnone selectivity suggesting the formation of acetophnone through an intermediate 1-phenyl ethanol as reported<sup>31</sup>. Lack of further reaction with 6VP and 6VPRS catalysts shows the absence of any catalytic species into the solution during this liquid-phase reaction conditions. Generally use of 30%  $\text{H}_2\text{O}_2$  and acetonitrile as solvent results considerable leaching<sup>32</sup>.

**6.5 REGENERATION AND STABILITY**

Filtering off the catalyst from one batch of experiment and subsequently using it for another batch of experiment under the similar reaction conditions was done to test the catalyst regeneration ability. The catalyst after reaction of 2 h was recovered by hot filtration, washed several times with acetone, dried at 383 K overnight and calcined for 5 h at 773 K. The recovered catalysts were reused for ethylbenzene oxidation under the same reaction conditions. Reaction was continuously run for 2 cycles and the results are presented in Table 6.6.

**Table 6.6**

Catalyst	Cycle	Conversion (wt.%)	Acph (%)
6VC	1	5.6	68.1
	2	3.9	67.5
10VC	1	9.9	54.5
	2	5.2	52.8
6VCRS	1	7.5	71.5
	2	5.6	72.8
10VCRS	1	12.5	62.7
	2	10.4	58.9
6VP	1	2.1	-
	2	2.0	-
6VPRS	1	5.2	-
	2	5.4	-



Regeneration and stability studies show that the recovered catalysts are less effective as expected in comparison to fresh ones owing to leaching of vanadium ions under the reaction conditions. Leaching studies already resulted enhanced activity of filtrate suggesting the leaching of some active metal ions to the solution. This is generally observed with all liquid-phase reactions more predominantly with peroxide catalyzed reaction in acetonitrile solvent<sup>33</sup>. Interestingly, no activity loss observed with VP and VPRS catalysts and these have not produced any acetophenone by the oxidation.

## 6.6 DISCUSSION

It is believed that the selective oxidation reactions of aromatics are known to follow a Mars-van Krevelen mechanism<sup>34</sup>. The reaction pathways of arenes observed with supported vanadia catalysts are dependent on the catalyst, substrate and all other reaction parameters. The structural relationship of supported vanadia catalysts and behaviour in benzene oxidation was already discussed in chapter 5. The catalytic redox cycle on ceria-supported vanadia may be due to the redox cycle of cerium near vanadium; unlike the most supported vanadia catalysts, which work on the redox cycle of vanadium sites in accordance with a report for ceria supported chromia catalysts<sup>35</sup>.

In the case of VC catalysts, the observation shows that as the vanadia loading increases to 10 wt. %  $V_2O_5$ , catalytic activity increases while acetophenone selectivity drops. Benzaldehyde was also produced over these catalysts. When vanadia loading is higher above 6 wt. %  $V_2O_5$  could oxidize the acetophenone formed to produce hydroxyl acetophenone as observed by the product analysis.

The VCRS series of catalysts exhibit higher conversion as well as acetophenone selectivity in comparison to VC catalysts. For 10VCRS eventhough conversion is more selectivity to acetophenone drops.

Praseodymia catalysts exhibit very low activity and acetophenone selectivity. Benzaldehyde was obtained as the major product over these catalysts.

The structural characterization of supported catalysts by various technique such as XRD, FT-IR, FT-Raman, UV-vis DRS etc show the presence of highly dispersed vanadia on lower loading and formation of  $\text{CeVO}_4$  as the vanadia loading increases to 10 wt.%  $\text{V}_2\text{O}_5$ . Lower loading consists vanadia as tetrahedral  $\text{V}=\text{O}$  species while higher loading can lead to formation of V-O-V species on the support surface. The EPR data of ceria containing catalysts show that the interaction of  $\text{CeO}_2$  with vanadia stabilizes surface  $\text{Ce}^{3+}$  sites, which in turn moderating the valence change ability of the  $\text{Ce}^{4+}/\text{Ce}^{3+}$  pair, as well as blocking the corresponding V redox interplay. Vanadium would moderate the liability of ceria oxygen sites.  $^{29}\text{Si}$  and  $^{51}\text{V}$  MAS NMR studies suggest the formation of  $\text{CeVO}_4$  even with 6 wt.% vanadia on ceria. However for CRS supported catalysts support envisages highly dispersed  $\text{V}=\text{O}$  species up to 10 wt.%  $\text{V}_2\text{O}_5$  loading. VP and VPRS catalysts contain pyrovanadate,  $\text{Pr}_x\text{V}_2\text{O}_7$  groups as observed by powder XRD analysis. The formation of silicate like Si-O-Pr configuration was evidenced from  $^{29}\text{Si}$  MAS NMR studies for VPRS catalysts.

Several mechanisms have been proposed for oxidation of ethylbenzene over redox catalysts. According to Singh et al.<sup>36</sup> the ethylbenzene oxidation

over MeAPO-11 using TBHP involves an intermolecular mechanism, where the redox metal sites are catalytically active sites, which change its oxidation states after the reaction. They also observed that among framework substituted MeAPO-11s, VAPO-11 has maximum redox behaviour and is most active with higher acetophenone selectivity. With vanadium silicates (VS-1 and VS-2) Ramaswamy et al.<sup>37,38</sup> proposed a peroxy radical intermediate capable of the side chain oxidation in aromatic substrates and oxyfunctionalization of primary carbon atoms in alkane oxidation. Ethylbenzene oxidation with Sn-Sil-1 is also reported through a peroxy radical ion intermediate giving acetophenone in major amount<sup>39</sup>. The formation of such an intermediate and its ability to attack the carbon of the substrate is influenced to a great extent by the solvent molecules. The presence of defect silanol groups makes the redox pair to be more stable during the reaction. They also observed that VS-1 and Sn-Sil-1 exhibit a greater ability to oxidize 1-phenylethanol to acetophenone by the contribution of surface V and Sn species. The higher catalytic activity of aromatic oxidation over zeolite Cu(II) complexes are related to tetrahedrally distorted square planar geometrics as they easily provide the vacant coordination sites for oxygen binding, however the octahedral symmetries of Co(II) and Ni(II) complexes are weakly active<sup>40</sup>. According to Yang et al.<sup>41</sup> mechanism for oxidation of methanol involves the abstraction of methyl hydrogen by catalytic surface oxygen, followed by rapid intramolecular rearrangement and desorption of formaldehyde and other products. Therefore, coordinatively unsaturated V-oxide sites are considered as the locations for the initial dissociative adsorption of ethylbenzene following the mentioned mechanism. It is also reported that coordinatively unsaturated V-oxides are the

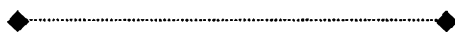
location for initial dissociative adsorption of methanol<sup>42,43</sup>. The studies of Varma et al.<sup>44</sup> indicated that oxygen vacancies are the active sites. These active sites or oxygen vacancies are greatly influenced by geometric and electronic factors and are responsible for the formation of different products. Acetophenone and benzaldehyde are produced on terminal oxygen vacancy (M=O) sites while bridged oxygen vacancy sites are responsible for the formation of more oxygenated products. The side-chain oxidation of alkylbenzenes by cerium(IV) ammonium nitrate with bromate salt in acetic acid involves via an electron-transfer mechanism leading to the formation of radical cations as reaction intermediates<sup>45</sup>. In the presence of cerium(IV) ammonium nitrate, while the Ce(IV) and bromate salts acts as efficient oxidants, the bromate salts act as a reoxidant for the Ce(III) ion. This reports that the Ce(IV) salts are catalysts for selective oxidation of alkylbenzenes<sup>46</sup>.

In the present case the oxidation takes place mainly in the benzylic position, show a higher preference for the oxidation of the aromatic ring. Aromatic ring hydroxylation was not observed when the reactions were conducted using the prepared catalysts at the set conditions. The high oxidation activity associated with lower loaded vanadia catalysts attributed to the presence of highly dispersed tetrahedral V=O species on the support surface. Abstraction of an alcoholic OH hydrogen and the CH hydrogen by the active oxygen yields acetophenone while similar abstraction of OH hydrogen of 1-phenylethanol by the active oxygen forms benzaldehyde. The CeVO<sub>4</sub> formation associated with increased concentration of vanadia causes a reduction in acetophenone selectivity in the ethylbenzene oxidation studied. High activity and enhanced acetophenone selectivity associated with VCRS

series of catalysts attributed to the presence of silica in amorphous form, which can help the surface vanadia to be more dispersed and redox pair more stable during the reaction. In contrary to benzene oxidation, praseodymia catalysts possess some activity to ethylbenzene oxidation. Major product benzaldehyde formation may be occurring via the benzylic oxidation of ethylbenzene. The observed low activity of VP and VPRS catalysts can be attributed to the low oxygen storage capacity of praseodymia. In praseodymia catalysts there is no evidence for the presence of highly dispersed tetrahedral vanadia sites. Under reaction conditions the redox behaviour of praseodymia is different from that of ceria. Ceria is relatively easy to reoxidise while with praseodymia the reoxidation is too slow to provide the necessary oxygen storage properties under reaction conditions.

## 6.7 CONCLUSION

The various supported vanadia catalysts exhibit efficient catalytic activity in the selective oxidation of ethylbenzene using  $\text{H}_2\text{O}_2$ . The oxidation with ceria catalysts afforded acetophenone as the main product. The VCRS series of catalysts exhibit enhanced activity and selectivity in the oxidation reaction. A direct relationship between the structural characteristics and oxidation behaviour is observed. Highly dispersed tetrahedral vanadia species evidenced by various spectroscopic techniques are highly active and selective for acetophenone production. The type of the active centers formed on the support catalysts determines the product selectivity. Low activity and acetophenone selectivity of praseodymia catalysts can be attributed to different structural and redox properties.



**REFERENCES**

- [1] S.C. Kim, *J. Hazardous Mater. B* 91 (2002) 285.
- [2] S.E. Dapurkar, A. Sakthivel, P. Selvam, *New J. Chem.* 27 (2003) 1184.
- [3] T.H. Bennur, D. Srinivas, S. Sivasankar, *J. Mol. Catal. A: Chem.* 207 (2004) 163.
- [4] L.I. Matienko, L.A. Molosova, *Russ. Chem. Bull.* 46 (1997) 658.
- [5] R. Alcantara, L. Canoira, P.G. Joao, J.M. Santos, I. Vazquez, *Appl. Catal. A: Gen.* 203 (2000) 259.
- [6] G.L. Tembe, P.A. Ganeshpure, S. Satish, *J. Mol. Catal. A: Chem.* 121 (1997) 17.
- [7] C. Guo, Q. Peng, Q. Liu, G. Jiang, *J. Mol. Catal. A: Chem.* 192 (2003) 295.
- [8] B. Notari, *Stud. Surf. Sci. Catal.* 60 (1991) 343.
- [9] N.K. Mal, V. Ramaswamy, S. Ganapathy, A.V. Ramaswamy, *Appl. Catal. A.* 125 (1995) 233.
- [10] R. Neumamm, M.L. Elad, *Appl. Catal. A: Gen.* 122 (1995) 85.
- [11] K.O. Xavier, J. Chako, K.K.M. Yusuff, *Appl. Catal. A: Gen.* 258 (2004) 251.
- [12] P. Kumar, R. Kumar, B. Pandey, *Synlett* (1995) 289.
- [13] S.L.H. Rebelo, M.M.Q. Simoes, M. Graca, P.M.S. Neves, J.A.S. Cavaleiro, *J. Mol. Catal. A: Chem.* 201 (2003) 9.
- [14] S. Velusamy, T. Punniyamurthy, *Tetrahedron Lett.* 44 (2003) 8955.
- [15] P.P. Toribio, J.M.C. Martin, J.L.G. Fierro, *Appl. Catal. A: Gen.* 294 2 (2005) 290.
- [16] L. Barrio, P.P. Toribio, J.M.C. Martin, J.L.G. Fierro, *Tetrahedron* 60 50 (2004) 11527.
- [17] R. Yu, F. Xiao, D. Wang, T. Sun, Y. Liu, G. Pang, S. Feng, S. Qui, R. Xu, C. Fang, *Catal. Today* 51 (1999) 39.
- [18] G. Cainielli, G. Cardillon, *Chromium Oxidation in Organic Chemistry*, Springer-Verlag, New York (1984).
- [19] S. Shylesh, A.P. Singh, *J. Catal.* 228 (2004) 333.
- [20] U.R. Pillai, E.S. Demessie, *J. Mol. Catal. A: Chem.* 191 (2003) 93.
- [21] U. Wilkenhoner, G. Langhendries, F. van Laar, G.V. Baron, D.W. Gammon,

- P. A. Jacobs, E. van Steen, *J. Catal.* 203 (2001) 201.
- [22] L.C.W. Baker, V.W. Simons, *J. Am. Chem. Soc.* 81 (1959) 4744.
- [23] J.M. Thomas, *Angew. Chem. Int. Ed. Engl.* 33 (1994) 913.
- [24] J.M. Thomas, R. Raja, *Chem. Commun.* (2001) 675.
- [25] R. Kumar, A. Bhaumik, *Micropor. Mesopor. Mat.* 21 (1998) 497.
- [26] D. Rohan, C. Canaff, E. Romeafin, M. Guismet, *J. Catal.* 177 (1998) 2743.
- [27] G. Strukul, *Angew. Chem., Int. Ed. Engl.* 37 (1998) 1199.
- [28] P.P. Toribio, J.M.C. Martin, J.L.G. Fierro, *J. Mol. Catal. A: Chem.* 227 (2005) 101.
- [29] O.T. Kasaikina, V.D. Kortenska, Z.S. Kartasheva, G.M. Kuznetsova, T.V. Maximova, T.V. Sirota, N.V. Yanishlieva, *Colloids Surf. A. Physicochem. Eng. Aspects* 149 (1999) 29.
- [30] E. Ganin, I. Amer, *J. Mol. Catal. A: Chem.* 116 (1997) 323.
- [31] B.B. Wentzel, M.P.J. Donners, P.L. Alsters, M.C. Feiters, R.J.M. Nolte, *Tetrahedron* 56 39 (2000) 7797.
- [32] J.D. Chen, R.A. Sheldon, *J. Catal.* 153 (1995) 1.
- [33] Y. Deng, C. Lettmann, W.F. Maier, *Appl. Catal. A: Gen.* 214 (2001) 31.
- [34] P. Mars, D.W. van Krevelen, *Chem. Eng. Sci.* 3 (1954) 41.
- [35] J.E. Remias, T.A. Pavlosky, A. Sen, *J. Mol. Catal. A: Chem.* 203 (2003) 179.
- [36] P.S. Singh, K. Kosuge, V. Ramaswamy, B.S. Rao, *Appl. Catal. A: Gen.* 177 (1999) 149.
- [37] P.R.H.P. Rao, A.V. Ramaswamy, *J. Chem. Soc., Chem. Commun.* (1992) 1245.
- [38] P.R. Hari Prasad Rao, A.V. Ramaswamy, P. Ratnaswamy, *J. Catal.* 143 (1993) 275.
- [39] N.K. Mal, A.V. Ramaswamy, *Appl. Catal. A: Gen.* 143 (1996) 75.
- [40] C.R. Jacob, S.P. Varkey, P. Ratnaswamy, *Appl. Catal. A* 182 (1999) 91.
- [41] T.J. Yang, J.H. Lunsford, *J. Catal.* 103 (1987) 55.
- [42] K.R. Reddy, A.V. Ramaswamy, P. Ratnaswamy, *J. Catal.* 143 (1993) 275.
- [43] B.M Reddy, E.P. Reddy, B. Manohar, S. Mehdi, *Adv. Catal. Design* 2 (1993) 193.
- [44] E.P Reddy, R.S. Varma, *J. Catal.* 221 (2004) 93.
- [45] E. Baciocchi, L. Mandolini, C. Rol, *Tetrahedron Lett.* (1976) 3343.
- [46] E. Ganin, I. Amer, *J. Mol. Catal. A: Chem.* 116 (1997) 323.

### OXIDATION OF NAPHTHALENE

#### Abstract

---

---

*Polycyclic aromatic hydrocarbons are carcinogenic substances to which humans are exposed from the environment. The major exhausts of the diesel vehicles are particulates and polycyclic aromatic hydrocarbons, which are emitted from diesel engines and can be much higher than those of Otto engines. Naphthalene, a constituent of diesel and jet fuel is the most volatile member of this class of pollutants. The industrial production of naphthalene and its application as an intermediate can contribute to the environmental naphthalene burden, it is widely accepted that the major part comes from burning processes such as residential, industrial and natural sources. Common methods applicable for naphthalene elimination from the waste stream include biodegradation, adsorption, absorption, high-energy electron beam, ozonization and catalytic oxidation. Among them, the catalytic oxidation has been demonstrated as one of the cost effective and efficient technologies to destroy the troublesome volatile organic compounds.*

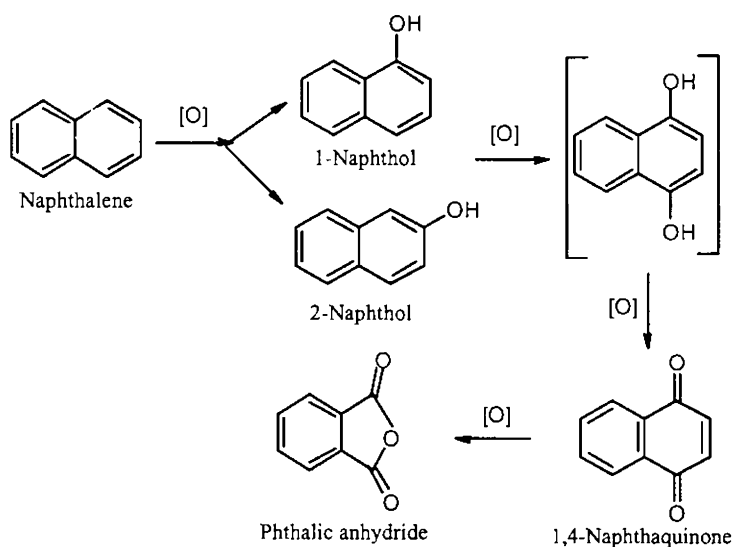
---

---



## 7.1 INTRODUCTION

Polycyclic aromatic compounds (PACs) have been found special concern because these are among the most toxic pollutants and can be transported by small particles deep into human lungs. Therefore, it is desired that new formulations of metal-based catalysts, which are effective in controlling  $\text{NO}_x$  problems, be utilized to satisfactorily mitigate PACs toxicity in diesel emissions. Naphthalene (Nap) consists of a basic aromatic structure and is the simplest and least toxic poly aromatic hydrocarbon. It is one of the most stable tar compounds and it is difficult to decompose<sup>1</sup>. The oxidation reaction pathways are depicted in Scheme 7.1.



Scheme 7.1

In the last decade certain success has been achieved in the resolution of oxidation of aromatic compounds in nuclei. The main product of naphthalene oxidation is phthalic anhydride (PAN). Generally phthalic anhydride

production is by catalytic oxidation of *o*-xylene or naphthalene using  $V_2O_5$  operated at 340 to 385 °C<sup>2</sup>. Of the current production of phthalic anhydride obtained by naphthalene and *o*-xylene oxidation, 50 percent is used for plasticizers, 25 percent for alkyl resins, 20 percent for unsaturated polyester resins, and 5 percent for miscellaneous and exports. Because emission factors are intended for future as well as present application, utilization of highly carcinogenic feedstock naphthalene for phthalic anhydride production is very desirable.

Several groups investigated the activities of metal catalysts in decomposing naphthalene. Decomposition of naphthalene with  $O_2$  is reported by Zhang et al.<sup>3</sup> over supported catalysts like Pt, Pd, Ru, Co, Mo and W on  $\gamma$ - $Al_2O_3$ . Xiao et al.<sup>4</sup> investigated the intermediates generated during catalytic oxidation of naphthalene over 1%Pt/ $\gamma$ - $Al_2O_3$  and 5%Co/ $\gamma$ - $Al_2O_3$  catalysts and were identified as naphthalene-decomposed by-products, naphthalene derivatives, and polymerized PACs. They also conclude that the weaker adsorption on Co catalysts allowed more direct and complete oxidation of naphthalene. Other catalysts, which have been utilized to oxidize polyaromatic hydrocarbons including volatile organic compounds, are Pt/Al-MCM-41,  $V_2O_5$ - $WO_3$ / $TiO_2$ ,  $Fe_2O_3$  and  $MoO_3$ - $V_2O_5$ , Pd-Ce/ $Al_2O_3$ , Pd-Ba/ $Al_2O_3$  and Pd-Zr/Y zeolite<sup>5-12</sup>. Li et al. studied the influence of Pt on catalytic activity of Ni/ $Al_2O_3$  by using naphthalene as a model compound<sup>13</sup>. Cr(VI) oxide catalyzed oxidation of arenes with periodic acid as the terminal oxidant in acetonitrile produced quinone as the main product and naphthalene was oxidized to 1,4-naphthaquinone<sup>14</sup>. The effect of protic and aprotic solvents on naphthalene oxidation over cytochrome P-450 was studied by Safari et al.<sup>15</sup> and reported a

mechanism based upon the electrophilic addition with a carbocation intermediate which is consistent with peroxy iron intermediate. The formation of phthalic anhydride by further oxidation of 1,4-dihydroxy naphthalene from 1-naphthol was observed on mesoporous vanadosilicates. The active sites were the tetrahedral vanadium sites inside the pore channels of MCM-41<sup>16</sup>. The steam reforming of naphthalene have been studied over Ni and Co/MgO catalysts, in which Co/MgO catalyst pre calcined at 873 K exhibited the best performance<sup>17-20</sup>.

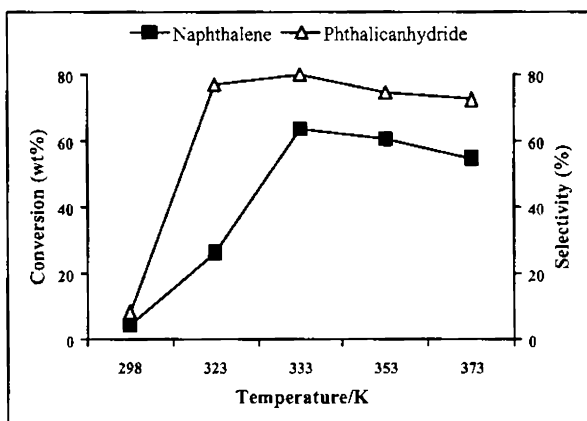
This chapter deals with the oxidation of naphthalene in order to develop an abatement technique of polyaromatic hydrocarbons emitted into the atmosphere. The relationship between conversion efficiency, operating parameters and relevant factors such as treatment temperatures, catalyst weight, solvent effect and oxidant volume etc are examined in detail.

## **7.2 INFLUENCE OF REACTION CONDITION**

The influence of reaction condition was analyzed in order to maximize the product yield and selectivity. Influence of reaction parameters on naphthalene oxidation with H<sub>2</sub>O<sub>2</sub> was initially studied in non-optimized conditions with 8VC as the catalyst.

### **7.2.1 Effect of Temperature**

The effect of temperature on naphthalene oxidation was studied by varying the temperature between 298 and 373 K while other parameters were kept constant. Results are presented in Figure 7.1.

**Figure 7.1**

Reaction conditions:-8VC-100 mg, Naphthalene-1.56 mmol, Acetonitrile-191 mmol,  $\text{H}_2\text{O}_2$ -44 mmol and Time-4 h.

Temperature variation on naphthalene oxidation shows that as the temperature increases from room temperature conversion and phthalic anhydride selectivity increases reaches a maximum and then decrease. At 333 K, a maximum conversion (63.5 %) with high phthalic anhydride selectivity (79 %) is observed. Further increase in reaction temperature cause decrease in conversion as well as phthalic anhydride selectivity. Low activity is attributed to the competitive thermal decomposition of  $\text{H}_2\text{O}_2$  at higher temperatures without being involved in the reaction<sup>21</sup>.

### 7.2.2 Effect of Solvent

The oxidation activity of the catalyst obtained for a series of solvents with different polarities is depicted in Figure 7.2.

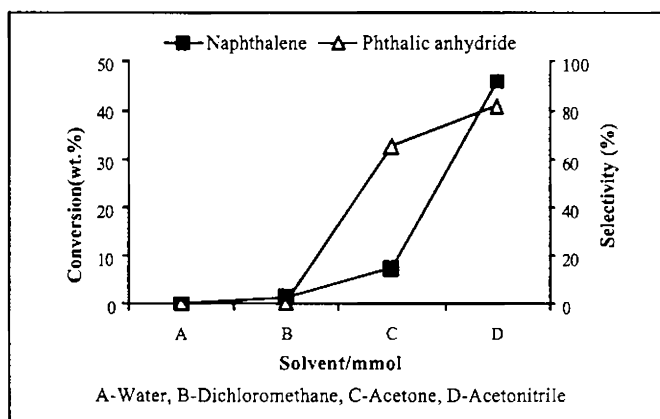


Figure 7.2

Reaction conditions:- 8VC-100 mg, Naphthalene-1.56 mmol, Solvent -191 ml,  $H_2O_2$  -44 mmol, Temperature- 333 K and Time-2 h.

The reaction media have a strong influence on the activity of the catalyst. Absence of any solvent didn't activate the reaction. Water was inactive in the oxidation. Acetone and acetonitrile acts positively giving phthalic anhydride as the main product. The enhanced activity and selectivity of the catalysts in acetonitrile can be explained on the basis of polarity of these solvents. In organic solvent the reaction is initiated by electron transfer at the interface leading to the radical cation of the substrate and superoxide anion while in the aqueous solution, the actual active species are assumed to be hydroxyl radicals formed by oxidation of solvent<sup>22,23</sup>. Acetonitrile is an aprotic solvent. The activity of the catalysts is found to increase with the solvent polarity and acetonitrile having more polar nature always enhances the activity. In this solvent, the phase separation between the aromatic substrate and the aqueous oxidant is greatly decreased thereby allows an easy transport of the active oxygen species for the oxidation<sup>24</sup>. According to Federica et al.<sup>25</sup> the

oxidation of naphthalene in acetonitrile gave only traces of dialdehydes with significant amount of 1,4-naphthaquinone (Napqone) and the main product was phthalic anhydride.

### 7.2.3 Effect of Catalyst weight

The influence of amount of the catalyst on the naphthalene oxidation is presented in Figure 7.3.

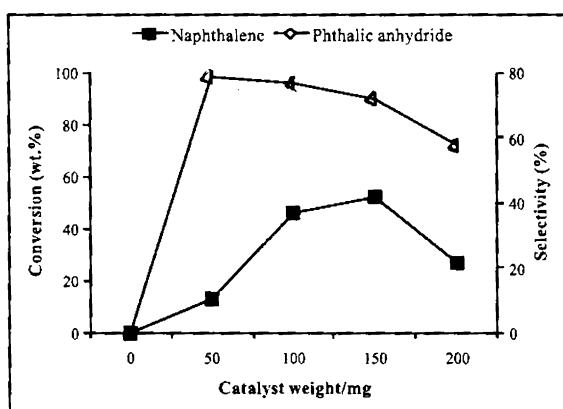


**Figure 7.3**

Reaction conditions:-8VC, Naphthalene-1.56 mmol, Acetonitrile-191 mmol, H<sub>2</sub>O<sub>2</sub>-44 mmol, Temperature-333 K and Time-2 h.

Absence of catalyst resulted no oxidation. As the amount of catalyst increases, an increase in the activity and phthalic anhydride selectivity was noted to a certain extent and decreased with a further increase in the catalyst amount. Very high concentration of catalyst amount can inhibit the autooxidation reactions, which in turn results in lower activity with nonselective products<sup>26</sup>.

### 7.2.4 Effect of Acetonitrile volume

The effect of concentration of the acetonitrile on naphthalene oxidation is shown in Figure 7.4.

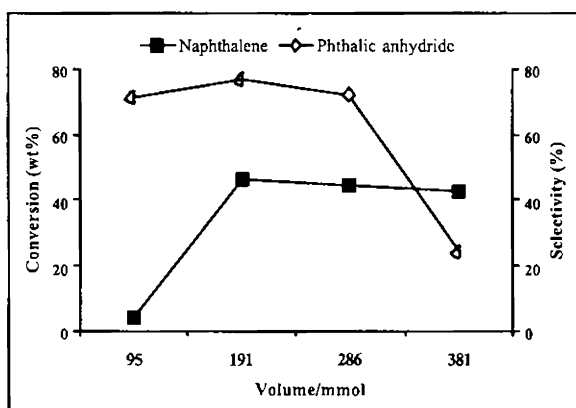


Figure 7.4

Reaction conditions:- 8VC-100 mg, Temperature-333 K,  
Naphthalene-1.56 mmol,  $H_2O_2$  -44 mmol and Time-2 h.

Taking different volumes of solvent while keeping other parameters constant, influence of solvent concentration on oxidation reaction was tested. The conversion increased with increase in acetonitrile volume and reaches a maximum value and then decreases thereafter. Too much of acetonitrile concentration reduces conversion as well as acetophenone selectivity. The acetonitrile with the concentration of 191 mmol was thus found to be optimum. When the solvent was excess, the benzene or catalyst concentration at the interface may be lower, thus resulting in a decreased conversion rate and nonselective oxidation of alcohols formed<sup>27</sup>.

### 7.2.5 Effect of Naphthalene volume

The effect of volume of naphthalene during oxidation is shown in Figure 7.5.

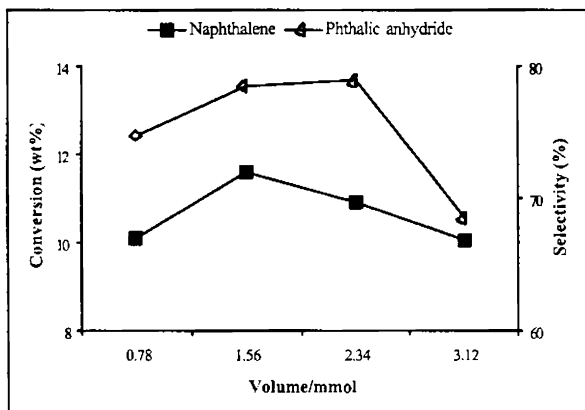


Figure 7.5

Reaction conditions:- 8VC-100 mg, Temperature-333 K, Acetonitrile-95 mmol,  $H_2O_2$  - 44 mmol and Time-4 h.

Polarity of the reactant and products formed play an important role in the oxidation of naphthalene. The substrate naphthalene is nonpolar while the primary products formed are polar. An increase in activity and selectivity was observed to a certain extent and then decreased with further increase in substrate to catalysts ratio. This could be probably due to the decrease in the number of active centers for the reaction. Selectivity decline can be due to further oxidation of phthalic anhydride thus formed under the reaction conditions<sup>28</sup>.

### 7.2.6 Effect of $H_2O_2$ volume

The effect of oxidant volume on naphthalene oxidation is illustrated in Figure 7.6



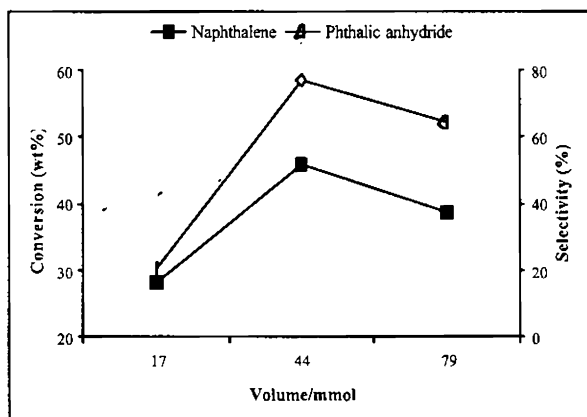


Figure 7.6

Reaction conditions:- 8VC-100 mg, Acetonitrile-191 mmol,  
Naphthalene- 156 mmol, Temperature-333 K and Time-2 h.

No oxidation takes place in the absence of oxidant. An increase in the amount of oxidant resulted an increase in rate together with phthalic anhydride selectivity reaches a maximum and then decrease. This can arise from the negative effect due to the production of  $\text{H}_2\text{O}$  as a byproduct<sup>29</sup>. The water and oxidant compete for complexation to the vanadium center, therefore excess water relative to  $\text{H}_2\text{O}_2$  inhibits the reaction. The amount of  $\text{H}_2\text{O}_2$  consumed in self-decomposition was much more than that consumed in the oxidation reaction. This may be why more than stoichiometric amount of  $\text{H}_2\text{O}_2$  is needed<sup>30</sup>.

### 7.2.7 Effect of Time

The influence of reaction time on naphthalene oxidation is illustrated in Figure 7.6.

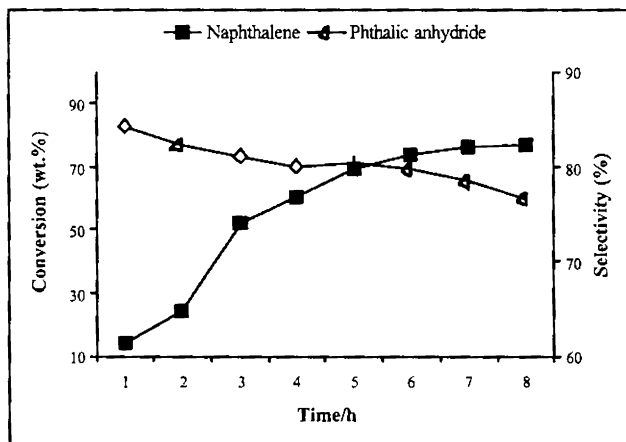


Figure 7.6

Reaction conditions:- Temperature-333 K, 8VC-100 mg, Acetonitrile - 191 mmol, Naphthalene- 156 mmol and  $H_2O_2$  -44 mmol.

As observed from the figure, variation of time intervals on reaction indicated that around 74 % of the conversion was achieved at a time of 6 h, while further increase in reaction time did not significantly enhance the conversion. Phthalic anhydride of about 88 % was obtained selectively in the initial period of time. Further oxidation of this to acid can cause drop off in selectivity with time. Similar observation was reported for benzene oxidation and attributed to the poisoning of the surface sites by the reaction products which in turn block the active sites with long time of reaction run<sup>31</sup>.

### 7.3 NAPHTHALENE OXIDATION OVER PREPARED CATALYSTS

The reaction parameters play an important role in determining the oxidation rate and product selectivity in the liquid-phase oxidation of naphthalene using hydrogen peroxide as oxidant. The naphthalene oxidation

was carried out over all the prepared catalysts under the selected reaction conditions as shown in Table 7.1.

Parameters	Selected condition
Temperature/K	333
Acetonitrile/mmol	191
Naphthalene/mmol	1.56
H <sub>2</sub> O <sub>2</sub> /mmol	44
Time/h	6

Table 7.2 shows the results of naphthalene oxidation over VC series of catalysts.

Catalyst	Conversion (wt. %)	Selectivity (%)		
		PAN	2-Naphthol	1,4-Napqone
Ce	-	-	-	-
2VC	1.0	-	100	-
4VC	25.0	73.6	26.3	-
6VC	71.3	86.4	7.2	6.4
8VC	73.1	89.4	6.6	3.8
10VC	69.3	90.7	4.2	5.1

The ceria is completely inactive towards naphthalene oxidation under the reaction conditions studied. Addition of vanadia enhances the activity and phthalic anhydride selectivity. Conversion increases up to 8VC while it decreases for 10VC. Phthalic anhydride production was increased with vanadia

loading. Small amounts of 2-naphthol and 1,4-naphthaquinone were also observed.

Table 7.3 shows the results of naphthalene oxidation over VCRS series of catalysts.

**Table 7.3**

Catalyst	Conversion (wt.%)	Selectivity (%)	
		PAN	1,4-Napqone
RS	-	-	-
CRS	-	-	-
2VCRS	1.2		100
4VCRS	25.9	92.7	7.3
6VCRS	84.6	94.5	5.5
8VCRS	89.7	96.5	4.0
10VCRS	76.9	96.7	3.2

Silica and CRS support gave no oxidation products under the set reaction conditions. Interestingly, only phthalic anhydride and 1,4-naphthaquinone were obtained with VCRS series of catalysts. Conversion increased up to 8VCRS and further increase in vanadia loading to 10 wt.%  $V_2O_5$  reduced the conversion rate. However, phthalic anhydride selectivity was found to be the same with 8 and 10VCRS.

Table 7.4 shows the results of naphthalene oxidation over praseodymia containing catalysts along with various silica supported vanadia catalysts.

Table 7.4

Catalyst	Conversion (wt. %)	Selectivity (%)		
		PAN	2-Naphthol	1,4-Napqone
P	-	-	-	-
PRS	1.3	-	100	-
2VP	1.23	-	100	-
6VP	17.8	-	100	-
10VP	1.2	-	82.4	17.6
2VPRS	-	-	-	-
6VPRS	-	-	-	-
10VPRS	2.3	-	58.1	41.8
V <sup>s</sup>	53.6	11.3	-	88.6
6VRS <sup>#</sup>	77.9	91.9	-	11.9
6VSG <sup>#</sup>	78.2	94.7	-	5.3

§ - 5 min, # - 4 h

Praseodymia catalysts exhibit a very different behaviour during oxidation of naphthalene. P, 2 and 6VPRS did not respond to the oxidation reaction under the set conditions. Any of the catalysts of VP and VPRS series produced no phthalic anhydride during naphthalene oxidation. Among VP series activity increased with vanadia loading to 6VP and then decreases for 10VP. 2 and 6 VP produced only 2-naphthol while small amount of 1,4-naphthaquinone was observed with 10VP. 10VPRS produced 2-naphthol and 1,4-naphthaquinone as the oxidation products. V<sub>2</sub>O<sub>5</sub> (V) oxidized 53.6 % naphthalene within 5 minutes of reaction and gave 11.3 % phthalic anhydride and 88.6 % 1,4-naphthaquinone. Various silica (6VRS and 6VSG) supported

vanadia catalysts show higher oxidation activity to produce phthalic anhydride in high amount within 4 h of the reaction.

#### 7.4 EFFECT OF LEACHING

In order to attain a better insight into the catalyst behaviour it is important to check the heterogeneity during the reaction conditions<sup>32</sup>. Leaching of active metal sites may occur during reactions and the enhanced catalytic activity can arise from the presence of such homogeneous leached metal species. The leaching of vanadium ions under reaction conditions from the catalysts was verified by carrying out filtrate experiments. After 1 h of reaction, the catalyst was filtered off while hot and the filtrate solution was again used for the reaction without any further addition of the oxidant. Table 7.5 shows the results of leaching studies conducted with representative catalysts.

**Table 7.5**

Catalyst	Time/h	Conversion (wt.%)	PAN (%)
8VC	½	12.6	80.2
Filtrate	1	14.8	81.2
8VCRS	½	17.6	88.8
Filtrate	1	19.3	89.5

An enhancement observed for the filtrate reaction indicates some of the active vanadia sites may leach into the reaction during oxidation condition thus enhancing the conversion rate. The use of 30 % H<sub>2</sub>O<sub>2</sub> and acetonitrile as solvent results considerable leaching in liquid phase reactions<sup>33</sup>. However the phthalic anhydride selectivity remains more or less the same.

## 7.5 REGENERATION AND STABILITY

The stability of the catalysts was tested by recycling experiments with regenerated catalysts. The recycling experiments were carried out as follows. After 2 h reaction, the catalyst was recovered by hot filtration, washed several times with acetone, dried at 383 K overnight and calcined for 5 h at 773 K. The recovered catalysts were reused for naphthalene oxidation under the same reaction conditions. Table 7.6 displays the results obtained with regenerated catalysts.

Table 7.6

Catalyst	Cycle	Conversion (wt.%)	PAN (%)
8VC	1	26.2	82.3
	2	23.3	81.2
8VCRS	1	28.7	95.4
	2	26.4	93.8

The activity of the reused catalyst was found to be lower than the fresh catalyst as expected. It is attributed to the leaching of vanadium ions under the reaction conditions thus reducing the catalytic activity. This is generally observed with all liquid-phase reactions more predominantly with peroxide catalyzed reaction in acetonitrile solvent<sup>34</sup>.

## 7.6 DISCUSSION

Selective oxidation reactions of aromatics are known to follow a Mars-van Krevelen mechanism<sup>35</sup>. The reaction pathways of arenes observed with supported vanadia catalysts are dependent on the catalyst, substrate and all

other reaction parameters. The structural relationship of supported vanadia catalysts and behaviour in benzene and ethylbenzene oxidation was already discussed in chapters 5 and 6. The catalytic redox cycle on ceria-supported vanadia may be due to the redox cycle of cerium near vanadium; unlike the most supported vanadia catalysts, which work on the redox cycle of vanadium sites in accordance for ceria supported chromia catalysts<sup>36</sup>.

In naphthalene oxidation reaction, support materials shows completely inactive nature. Hence, the activity enhancement reveals that the nature of vanadium species and its different site isolations/coordination environments may be responsible for the differences in the conversion/selectivity behaviour. Catalytic activity of VC and VCRS series of catalysts exhibits the same pattern while phthalic anhydride selectivity was more with VCRS catalysts. Small amount of 2-naphthol was also produced with VC catalysts and selectivity to this decrease as the vanadia loading increases. Among praseodymia catalysts, VP series only exhibits considerable activity towards oxidation but no phthalic anhydride was observed with these catalysts.

The structural characterization of supported catalysts by various techniques such as XRD, FT-IR, FT-Raman and UV-vis DRS shows the presence of highly dispersed vanadia on lower loading and formation of  $\text{CeVO}_4$  as the vanadia loading increases to 10 wt.%  $\text{V}_2\text{O}_5$ . Lower loading consists vanadia as tetrahedral  $\text{V}=\text{O}$  species while higher loading can lead to formation of V-O-V species on the support surface. The EPR data of ceria containing catalysts shows that the interaction of  $\text{CeO}_2$  with vanadia stabilizes surface  $\text{Ce}^{3+}$  sites, which inturn moderating the valence change ability of the



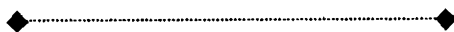
Ce<sup>4+</sup>/Ce<sup>3+</sup> pair, as well as blocking the corresponding V redox interplay. Vanadium would moderate the liability of ceria oxygen sites. <sup>29</sup>Si and <sup>51</sup>V MAS NMR studies suggest the formation of CeVO<sub>4</sub> even with 6 wt.% vanadia on ceria. However for CRS supported catalysts support envisages highly dispersed V=O species up to 10 wt.% vanadia loading. VP and VPRS catalysts contain pyrovanadate, Pr<sub>x</sub>V<sub>2</sub>O<sub>7</sub> groups as observed by powder XRD analysis. The formation of silicate like Si-O-Pr configuration was evidenced from <sup>29</sup>Si MAS NMR studies for VPRS catalysts.

As reported, hydrocarbon hydroxylation can occur via either H atom abstraction or the insertion of an oxygen atom of metallo-oxene into the C-H bond with the intermediate formation of a penta coordinated carbon atom<sup>37,38</sup>. Scheme 7.1 shows that 1,4-naphthaquinone was produced without requiring naphthalene ring destruction while phthalic anhydride was subsequently produced with ring rupture as reported by Bruckner et al.<sup>39</sup> over vanadia catalysts. Alternatively, Linstromberg et al.<sup>40</sup> reported that naphthalene could be directly oxidized to phthalic anhydride during oxidation over vanadium pentoxide catalyst, and can be easily converted to phthalic acid ester. They also argued that naphthalene followed the similar pathways undertaken by benzene during selective gas-phase oxidation. The catalytic activity of benzene and naphthalene oxidations conducted in this work also results the same behaviour. Present catalytic systems of ceria supported ones shows higher concentration of phthalic anhydride suggesting that ring rupture route was most probable over these catalysts. This is possible with the highly dispersed tetrahedral vanadia species on the supports. Formation of CeVO<sub>4</sub> at higher vanadia loading results lower activity suggesting deactivation of catalysts. We have already

shown that nature of solvent have an important role in oxidation reaction. The presence of aprotic solvent may yield the naphthol products. According to Khavasi et al.<sup>41</sup> in protic solvents, high oxo intermediate produced quinonic compounds but in aprotic solvent, phenolic compounds were produced from peroxy active oxidant. Production of no phthalic anhydride with praseodymia catalysts suggests these are not able to cause ring rupture thereby oxidizing the aromatic ring. This low activity can be attributed to the difference in redox property of praseodymia and ceria supported vanadia catalysts.

### 7.7 CONCLUSION

The liquid phase oxidation of naphthalene in acetonitrile is conducted with  $\text{H}_2\text{O}_2$  as oxidant. All the ceria supported vanadia catalyst prepared was considerably active towards the oxidation, which produced phthalic anhydride as the main product while praseodymia was less active and not produced phthalic anhydride in any catalysts. High activity and phthalic anhydride selectivity of ceria supported vanadia can arise from the presence of tetrahedral vanadia species as evidenced in the case of benzene oxidation. Low activity and no phthalic anhydride production over praseodymia catalysts suggest different redox behaviour from that of ceria.



**REFERENCE**

- [1] T. Furusawa, A. Tsutsumi, *Appl. Catal. A: Gen.* 278 (2005) 207.
- [2] G. Golinelli, F. Trifiro, *Catal. Today* 20 1 (1994) 153.
- [3] X. W. Zhang, S.C. Shen, L.E. Yu, S. Kawi, H. Hidajat, K.Y.S. Ng, *Appl. Catal. A: Gen.* 250 (2003) 341.
- [4] X.W. Zhang, S.C. Shen, K. Hidajat, S. Kawi, L.E. Yu, K.Y Simon Ng, *Catal. Lett.* 1-2 (2004) 96.
- [5] K.M Reddy, C. Song, *Catal. Today* 31 (1996) 137.
- [6] R. Weber, T. Sakurai, H. Hagenmaier, *Appl. Catal. B: Environ.* 20 (1999) 249.
- [7] R. Weber, T. Sakurai, *Appl. Catal. B: Environ.* 34 (2001) 113.
- [8] K. Everaert, J. Baeyens, *J. Hazard Mater. B* 109 (2004) 113.
- [9] K. Everaert, M. Mathieu, J. Baeyens, E. Vansent, *J. Chem. Technol. Biotechnol.* 78 (2003) 167.
- [10] F. Klingstedt, A.K. Neyestanaki, R. Byggningsbacka, L.E. Lindfors, M. Lunden, M. Petersson, P. Tengstrom, T. Ollonquist, J. Vayrynen, *Appl. Catal. A: Gen.* 209 (2001) 301.
- [11] F. Klingstedt, H. Karhu, A.K. Neyestanaki, L.E. Lindfors, T. Salmi, J. Vayrynen, *J. Catal* 206 (2002) 248.
- [12] F. Klingstedt, A.K. Neyestanaki, L.E. Lindfors, T. Salmi, T. Heikkila, E. Laine, *Appl. Catal. A: Gen.* 239 (2003) 229.
- [13] Z.X. Li, X.R. Chen, *Chin. J. Catal.* 24 (2003) 253.
- [14] S. Yamazaki, *Tetrahedron Lett.* 42 (2001) 3355.
- [15] H.R. Khavasi, N. Safari, *J. Mol. Catal. A: Chem.* 220 (2004) 127.
- [16] S. Shylesh, S.P. Mirajkar, A.P. Singh, *J. Mol. Catal. A: Chem.* 239 (2005) 57.
- [17] D.N. Bangala, N. Abatzoglou, E. Chornet, *AlChE J.* 44 (1998) 937.
- [18] H. Zhao, D.J. Draelants, G.V. Baron, *Ind. Eng. Chem. Res.* 39 (2000) 3195.
- [19] R. Coll, J. Salvado, X. Farriol, D. Montane, *Fuel Process. Tech.* 74 (2001) 19.
- [20] T. Furusawa, A. Tsutsumi, *Appl. Catal. A: Gen.* 283 (2005) 75.
- [21] U. Schuchdart, D. Cardoso, R. Sercheli, R. Pereira, R.S. Cruz, M.C. Guerreiro, D. Mandelli, E.V. Spimace, E.L. Pires, *Appl. Catal.* 211 (2001) 1.

- [22] A. Mills, S. Le Hunte, J. Photochem. Photobio. A: Chem. 108 (1997) 1.
- [23] M.A. Fox, Top. Curr. Chem. 142 (1987) 71.
- [24] N. Radic, B. Grbic, A.T. Baricevic, Appl. Catal. B: Environ. 50 (2004) 153.
- [25] F. Soana, M. Sturini, L. Cermenati, A. Albini, J. Chem. Soc., Perkin Trans. 2 (2000) 699.
- [26] A.P Singh, B. Jacob, S. Sugunan, Appl. Catal. A: Gen. 174 (1998) 51.
- [27] R. Kumar, A. Bhaumik, Micropor. Mesopor. Mat. 21 (1998) 497.
- [28] A. Dubey, S. Kannan, S. Velu, K. Suzuki, Appl. Catal. A: gen. 238 (2003) 319.
- [29] R. Yu, F. Xiao, D. Wang, G. Pang, S. Feng, S. Qui, R. Xu, Catal. Lett. 49 (1997) 49.
- [30] J. Zhang, Y. Tang, G. Li, C. Hu, Appl. Catal. A: Gen. 278 (2005) 251.
- [31] C.B. Lui, Z. Zhang, X.G. Yang, Y. Wu, J. Chem. Soc. Commun. (1996) 1019.
- [32] Y. Deng, C. Lettmann, W.F. Maier, Appl. Catal. A: Gen. 214 (2001) 31.
- [33] E. Ganin, I. Amer, J. Mol. Catal. A: Chem. 116 (1997) 323.
- [34] R. Neumann, M. Levin-Elad, Appl. Catal. A: Gen. 148 (1996) 7.
- [35] P. Mars, D.W. van Krevelen, Chem. Eng. Sci. 3 (1954) 41.
- [36] Z. Li, M. F. Stephanopoulos, Ind. Eng. Chem. Res. 36 (1997) 187.
- [37] T. Nakano, N. Agatsuma, S. Kodama, H. Kakuda, D. Dolphin, Bull. Chem. Soc. Jpn. 69 (1996) 3513.
- [38] A.F. Shestakov, A.E. Shilov, J. Mol. Catal. A: Chem. 105 (1996) 1.
- [39] A. Bruckner, M. Baerns, Appl. Catal. A: Gen. 157 (1997) 311.
- [40] W.W. Linstromberg, H.E. Baumgarten, Organic Chemistry, D.C Health and Company, Toronto (1983) 117.
- [41] H.R. Khavasi, S.S.H. Davarani, N. Safari, J. Mol. Catal. A: Chem. 188 (2002) 115.

### OXIDATIVE DEHYDROGENATION OF ETHYLBENZENE

#### Abstract

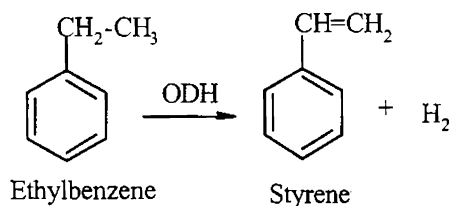
---

*The production of light olefins from alkanes separated from natural gas, today largely available and cheap, is a desirable option to limit the dependence from oil. This can be obtained through endothermic reactions such as steam cracking and thermal catalytic dehydrogenation or through an exothermic reaction such as oxidative dehydrogenation. However, several problems still remain, such as the formation of coke on the catalyst, thermodynamic constraints, and a large amount of wasted energy in the form of excess steam. Energy saving and more economical dehydrogenation processes are therefore desirable. For styrene synthesis, one of the ten most important industrial processes, the exothermic oxidative dehydrogenation of ethylbenzene is an elegant and promising reaction. Oxidative dehydrogenation has attracted much since it can be operated at low temperatures and it is free from equilibrium limitations. Oxidative dehydrogenation reactions also receive great attention in the synthesis of valuable alkenes but, the finding of efficient catalysts with good olefin production is still a critical point and these processes are still far from being widely used at industrial-scale.*

---

## 8.1 INTRODUCTION

The utilization of relatively abundant and cheap alkanes in the chemical industry is always desirable. In the transformation of alkanes into valuable chemicals, selective oxidation is considered to be important. Styrene, one of the most important basic chemicals mainly used as the monomer for the production of different synthetic polymers, such as polystyrene, styrene-acrylonitrile and acrylonitrile-butadiene-styrene is produced commercially by dehydrogenation of ethylbenzene, using Fe-Cr-K as catalyst in the presence of a large amount of superheated steam as a diluent and heat carrier at high temperature of 550-650 °C. Small amounts of elements such as V, Mo, Ce, Co, and Ca were added to improve catalyst performance. The schematic representation of the ethylbenzene dehydrogenation is shown in scheme 8.1.



**Scheme 8.1**

This commercial process is equilibrium limited and has high energy consumption. Thus an alternative way is still being pursued. The advantage of an oxidative dehydrogenation process in the presence of oxygen is that, reaction is exothermic and it can be operated at lower temperatures<sup>1</sup>. Since the reaction would not be equilibrium limited and energy intensive, there is a strong incentive for the development of an oxidative dehydrogenation process<sup>2</sup>.

Oxidative dehydrogenation process (ODH) is promising due to its exothermic reaction, but such a process requires an active and selective

oxidation stable catalyst. Among the catalysts reported for the ODH of ethylbenzene includes metal oxides, supported oxides, phosphates and organic polymers<sup>3-6</sup>. An extensive body of work has been published, aiming at the nature of the active phase and the role of promoters. Alumina is reported to be an active catalyst for the ODH of ethylbenzene and other alkylbenzenes. Moderate acid strength of silica-alumina, tin oxides and phosphates are reported to be the key factor for the ODH reaction<sup>7</sup>. Among various metal oxide incorporated alumina, the introduction of  $\text{Fe}_2\text{O}_3$  and  $\text{Cr}_2\text{O}_3$  considerably enhanced the dehydrogenation activity<sup>8</sup>. According to Sugunan et al.<sup>9</sup> the ODH of ethylbenzene over rare earth promoted sulfated oxides exhibits better activity compared to non-sulfated and sulfated tin oxide systems. Nicolas et al.<sup>10</sup> reported the catalytic use of onion-like carbon materials for styrene synthesis by oxidative dehydrogenation of ethylbenzene.

Oxidative dehydrogenation of alkanes has been studied with various vanadia based catalysts in presence of oxygen<sup>11,12</sup>. VMgO was first reported to be active and selective in the ODH of ethylbenzene<sup>13</sup>. For silica supported vanadia catalysts, the very high activity at low surface coverage is attributed to the highly dispersed species of  $(\text{Si-O})_3\text{V=O}$  formed on the  $\text{SiO}_2$  surface<sup>14-16</sup>. This suggested that the redox properties are operative during ODH of lower alkanes since these surface species are more easily reducible than bulk phase. Kung and co-workers<sup>17-20</sup> attributed magnesium orthovanadate ( $\text{Mg}_3\text{V}_2\text{O}_8$ ) as the active phase in the ODH of propane, n-butane, and cyclohexane over VMgO catalyst. Several metal orthovanadates have also been tested and found to be quite active and studies have also focused on vanadia supported alumina and titania<sup>21</sup>. Three factors, viz. (a) the presence of tetrahedral  $\text{VO}_4$ , (b) the

absence of V=O double bonds and (c) the difference in metallic vanadates, were pointed out to be responsible for the oxidative dehydrogenation properties of VMgO catalysts. According to Albonetti et al.<sup>22</sup> vanadium is a key element for performing the oxidative dehydrogenation of propane to propene. N<sub>2</sub>O was used as an oxidizing agent by Lopez Nieto et al.<sup>23</sup> for the oxidative dehydrogenation of n-butane and found higher selectivity for olefins compared with molecular oxygen. Unsupported and alumina supported NiO-V<sub>2</sub>O<sub>5</sub> are known as rather efficient catalysts for oxidative and non-oxidative dehydrogenation of various hydrocarbons<sup>24</sup>. According to Petrov et al.<sup>25</sup> the catalytic activity of binary NiO-V<sub>2</sub>O<sub>5</sub> catalysts for ethylbenzene dehydrogenation is due to predominantly V<sub>2</sub>O<sub>5</sub> phase while other phases catalyze mostly cracking and dealkylation reactions. The dehydrogenation activity of supported vanadia catalysts is dependent upon both the nature of the support and dispersion of the vanadium component on that support. Su et al.<sup>26</sup> reported the first application of carbon nanotubes in the ODH of ethylbenzene. Report stated that the catalytic activity shows only a minor dependence on the oxygen concentration and activity and selectivity of the sp<sup>2</sup> carbon is related to the optimized distribution of sites required for the oxygen activation and basic centers, where ethylbenzene adsorption takes place. Suzuki and coworkers<sup>27</sup> reported that active carbon supported vanadium catalysts exhibit high catalytic activity in ODH of ethylbenzene to give styrene in the presence of carbon oxide. Oxidative dehydrogenation, ODH, of alkanes is a subject of an ever-growing interest as a source of cheap olefins for industrial applications and supported vanadium oxides are suitable catalysts for the ODH of alkanes<sup>28-30</sup>.



## 8.2 INFLUENCE OF REACTION CONDITION

To get an idea about the influence of reaction conditions on the dehydrogenation activity and selectivity, the reaction was conducted by varying different properties. 10VCRS was taken as a representative catalyst to study the effect of properties viz. temperature, flow rate, air flow and time.

### 8.2.1 Effect of Temperature

The dependence of ethylbenzene dehydrogenation activity and selectivity on the reaction temperature for the catalysts is shown in Figure 8.1.

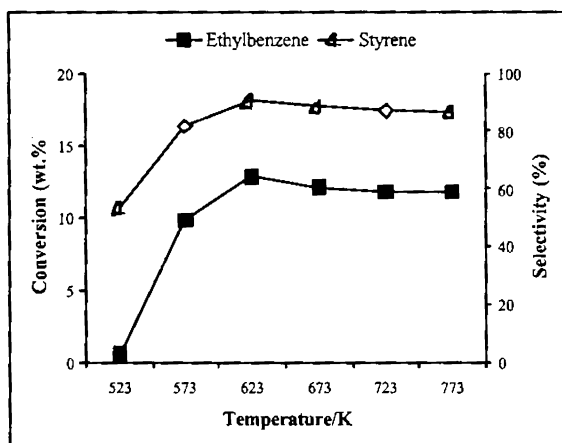


Figure 8.1

Reaction conditions:- 10VCRS-500 mg, Flow rate- 4 ml/h, Airflow- 120 ml/min and Time-3 h.

The ODH of ethylbenzene was conducted with air at temperature range 523-723 K over 10VCRS catalyst. Ethylbenzene conversion and styrene selectivity increases with increase in temperature from 523 to 623 K. Further increases in reaction temperature slightly reduced ethylbenzene conversion and remain more or less constant throughout a period of 673-773 K. The decrease in conversion can be attributed to the blocking of active sites of catalyst by

coke formation. The rate of coke deposition during ethylbenzene ODH depends on many factors among which reaction temperature is the crucial one. Indeed, an excessively high operation temperature enhances the cracking side reactions occurring on the acidic surface sites of the catalyst<sup>31,32</sup>. The selectivity of styrene increases with rise in temperature up to 623 K and decreases thereafter. Since the formation of styrene by direct dehydrogenation of ethylbenzene is an endothermic reaction ( $\Delta H = 124.9 \text{ KJ/mol}$ ), it is more favoured with high temperature<sup>33</sup>. Cracking products formation and deep oxidation with increase in temperature could result in reduced styrene selectivity at high temperature. From the study, 623 K was chosen for further performance of the reaction.

### 8.2.2 Effect of Air flow

The variations of dehydrogenation activity and selectivity of catalyst with air flow is presented in Figure 8.2.

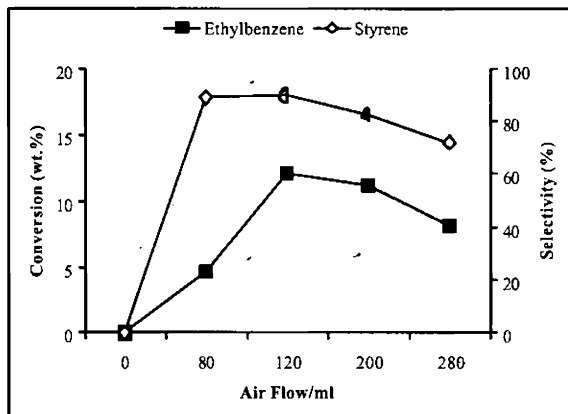


**Figure 8.2**

Reaction conditions:-10VCRS-500 mg, Temperature-623 K, Flow Rate-  $4\text{mlh}^{-1}$  and Time-3 h.

Dehydrogenation conducted in the absence of any air flow produced no styrene. The conversion rate and styrene selectivity was found increasing with increase in air flow rate reaches a maximum and then decreases. Supply of air helps the reaction by supply of oxygen needed for H abstraction by reoxidizing the catalyst. The surface adsorbed oxygen can improve the combustion of hydrocarbon<sup>35</sup>. Increase in oxygen supply may result in complete oxidation products and thus yield of liquid products decreases along with styrene selectivity. In the supported vanadia catalysts, lattice oxygen is taking part in dehydrogenation. Activity and selectivity towards ODH decided by the average number of oxygen molecules that reacts with each hydrocarbon<sup>36</sup>. Increase in air flow result in reduced oxygen molecules for reaction and decreases conversion rate and selectivity considerably.

### 8.2.3 Effect of Feed flow rate

The results of effect of flow rate on ODH are shown in Figure 8.3.

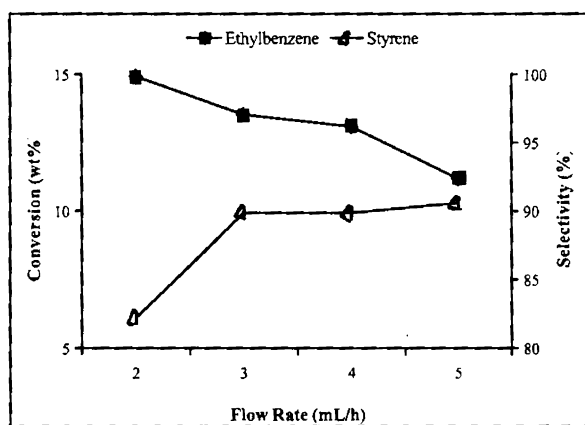


**Figure 8.3**

Reaction conditions:- 10VCRS-500 mg, Temperature-623 K,  
Air flow- 120mlmin<sup>-1</sup>, and Time-3 h.

From Figure 8.3 it is shown that the conversion decreases with an increase in the flow rate of ethylbenzene from 2 to 5 ml/h since the contact time of the reactants with the catalyst surface reduces as the flow rate increases. At small flow rate the contact time of the reactant on the catalyst surface should be more. At higher flow rate of reactant, it will not get enough time to adsorb on the catalyst surface and which results in reduced conversion rate. High rate of ethylbenzene dehydrogenation at small flow rate (higher contact time) results due to the higher probability of reactive adsorption. Selectivity of styrene was increased with an increase in flow rate from 2 to 3 ml/h and maximum selectivity is observed for flow rate of 5 ml/h. At lower flow rate, the possibility of product readsorption and the production of more oxygenated products are probable which leads to less selectivity of styrene since more amounts of byproducts toluene and benzene are produced with increasing contact time<sup>37,38</sup>. Small styrene selectivity at low flow rate could also be accounted for the thermal decomposition of ethylbenzene and styrene<sup>39</sup>. Prevention of readsorption of styrene on catalyst surface can prevent the formation of oxygenated products at high flow rate giving rise to styrene selectively. The 3 ml/h was selected as the optimal flow rate for further reaction to obtain high conversion rate with styrene selectively.

#### **8.2.4 Effect of Time**

Effect of time on reaction is an important factor in vapour phase reactions. In figure 8.4 the conversion of ethylbenzene is plotted as a function of time-on-stream.

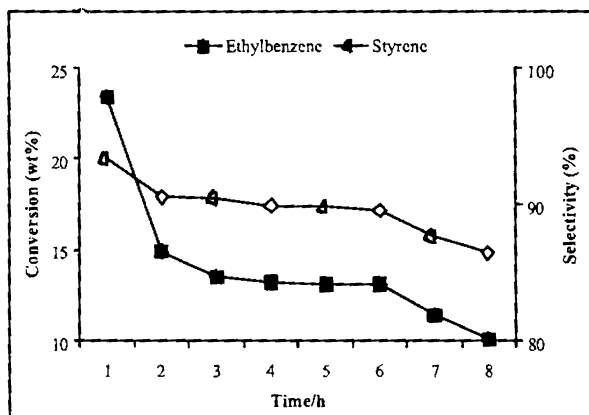


Figure 8.4

Reaction conditions:- 10VCRS-500 mg, Temperature-623 K,  
Air flow-120mlmin<sup>-1</sup> and Flow rate -3mlh<sup>-1</sup>.

Under the reaction conditions studied, the initial conversion rate and styrene selectivity was high. Conversion is almost constant after an initial period. However, with an increasing reaction period, the dehydrogenation rate and styrene selectivity decreased gradually. After 6 h run, the conversion rate and styrene selectivity was decreased considerably. The maximum styrene selectivity obtained is 89.6%. The yellow coloured catalysts turned black after the reaction period and could be regenerated after treatment at 773 K for 6h. Reduction of metal ions on the catalysts surface can cause deactivation in reaction<sup>40</sup>. The deposition of carbon on the catalyst surface also seems to be a major cause of deactivation of the catalyst. Deposited carbon can be burned off by high temperature treatment<sup>41</sup>.

### 8.3 OXIDATIVE DEHYDROGENATION OVER CATALYSTS

The catalytic performances of all the catalysts prepared were monitored in the oxidative dehydrogenation of ethylbenzene and the results are discussed

below. The selected conditions for the reaction to carry out are presented in Table 8.1.

**Table 8.1**

Parameter	Selected condition
Catalyst/mg	500
Temperature/K	623
Air flow/mlmin <sup>-1</sup>	120
Flow rate/mlh <sup>-1</sup>	3
Time/h	3

Table 8.2 shows the results of the catalytic performance during the dehydrogenation of ethylbenzene over VC series of catalysts.

**Table 8.2**

Catalyst	Conversion (wt.%)	Selectivity (%)	
		Styrene	Benzene+Toluene
C	19.9	49.1	50.9
2VC	7.4	85.9	17.1
4VC	9.6	82.8	14.2
6VC	10.0	72.4	27.6
8VC	8.8	77.6	22.4
10VC	8.4	79.2	20.8

The main product obtained by ethylbenzene dehydrogenation is styrene with small amounts of by-products such as benzene and toluene over all catalysts. Mass balance calculation showed that the formation of total oxidation products CO and CO<sub>2</sub> under the studied reaction conditions is negligible. This is attributed to the formation of stable dehydrogenated product

styrene during the oxidation reaction of ethylbenzene. This phenomenon already reported by Centi et al.<sup>42</sup>. The styrene preferentially adsorbed through its C=C bond and oxygen is chemisorbed over Lewis acid sites. The interaction of the olefinic double bond with the Lewis acid sites inhibits the oxygen adsorption and reduces the oxygen availability on the surface. As a consequence, the selectivity to carbon oxides is reduced.

Table 8.3 gives the catalytic performance during the dehydrogenation of ethylbenzene over VCRS series of catalysts.

Table 8.3

Catalyst	Conversion (wt.%)	Selectivity (%)	
		Styrene	Benzene+Toluene
RS	0.9	40.0	60.0
CRS	26.7	95.1	4.8
2VCRS	13.0	85.6	14.4
4VCRS	16.3	84.0	16
6VCRS	16.6	82.6	17.4
8VCRS	16.7	86.3	13.7
10VCRS	16.8	89.4	10.6

Compared to ceria, CRS support exhibited higher conversion rate and styrene selectivity. The supported vanadia catalysts exhibited higher styrene selectivity than ceria. Among supported catalysts, CRS supported vanadia exhibited higher conversion rate and styrene selectivity. As the vanadia loading is increased, the conversion of ethylbenzene on VC series catalysts first increases and then decreases. However, selectivity to styrene at the maximum

conversion of 6VC is 72.3 %, which is low compared to other loading. The activities of the CRS supported vanadia catalysts are higher than those of VC series with higher styrene selectivity. Among these, initially the ethylbenzene conversion increases slightly with the vanadia loading and remains the same thereafter.

Table 8.4 shows the results of the catalytic activity during the dehydrogenation of ethylbenzene with praseodymia containing catalysts.

**Table 8.4**

Catalyst	Conversion (wt.%)	Selectivity (%)	
		Styrene	Benzene+Toluene
P	15.9	78.5	21.5
PRS	12.2	93.8	6.3
2VP	26.5	87.6	12.4
6VP	19.0	83.6	16.4
10VP	21.2	91.2	8.9
2VPRS	10.9	94.8	5.2
6VPRS	16.8	90.2	9.8
10VPRS	9.2	96.8	4.2
V	37.4	21.8	78.2
6VRS	29.6	71	29.0
6VSG	19.7	71.4	28.6

The relation of the conversion of ethylbenzene on praseodymia containing catalysts shows a different pattern. PRS produced styrene selectively than praseodymia. When praseodymia was promoted with SiO<sub>2</sub>, these catalysts exhibited higher conversion rate and styrene selectivity than



ceria containing catalysts. Further more, styrene selectivity reached nearly 90 % with these supported vanadia catalysts. Among VP series catalysts, dehydrogenation rate decreases from 2VP to 6VP and then increases for 10VP. Styrene selectivity decreases up to 6VP and then enhanced for 10VP.

For comparison, the reaction was conducted also with  $V_2O_5$  and various silica supported vanadia.  $V_2O_5$  exhibits high conversion rate while styrene selectivity is very low. It produced more amounts of oxygenated products. Among 6VRS and 6VSG, VRS shows high conversion rate with similar styrene selectivity as that of 6VSG.

#### 8.4 REGENERATION AND STABILITY

Regeneration and stability of the catalyst were tested over selected catalysts. Coke deposition must be the reason for the deactivation of catalysts under vapour phase reaction conditions. Other reasons include promoter's loss or redistribution, ion reduction and physical degradation<sup>43</sup>. Influence of time on dehydrogenation reaction show that after 6 h the catalytic activity along with styrene selectivity is reduced. Procedure for the stability study was chosen as follows. After dehydrogenation reaction for 6 h at 623 K, flow of reactant feed and air were stopped. Catalyst was allowed to stay in the reactor itself. Temperature was increased to 773 K, the calcination temperature of the catalyst. Under this condition, catalyst was allowed to stay within the reactor for 10 h in the presence of nitrogen flow. ODH of ethylbenzene conducted later show the same activity as that of fresh catalysts suggesting that catalysts can be regenerated without loss in activity.

## 8.5 DISCUSSION

There are two different kinds of oxidation reactions such as oxygen insertion reaction and oxidative dehydrogenation. In the case of oxides of vanadium, they possess catalytic activity for both oxidation reactions. However it is very difficult to control the selectivity between these two reactions since in some cases, they promote oxygen insertion and in other cases promote oxidative dehydrogenation. The selectivity varies according to the nature of reactants and products. Oxidation is performed by a redox cycle of metal oxide catalysts and, as a result, the oxidation activity is dependent on the redox action, that is, a pair of reducibility and reoxidizability of metal oxide<sup>44</sup>. However, it is hard to understand satisfactorily the selectivity of catalysts in an oxidation reaction only by the redox properties. It has long been postulated that the catalytic activity and selectivity of an oxide in selective oxidation is related to the reduction rate of the oxide. Over an oxide, which is very difficult to reduce, the activity will be low for an oxide, which is very easy to reduce the activity is high but the selectivity low. An active and selective catalyst should have an intermediate ease of reduction<sup>45</sup>.

It is known that surface acidity and basicity of a catalyst play an important role in partial oxidation and oxidative dehydrogenation<sup>46</sup>. This was reviewed by Corma et al.<sup>47</sup> It has been reported that the activation of olefins in partial oxidation and ODH occurs on acid sites of a catalyst surface. The strength of acid sites influences the strength of binding of a reagent to an active site. According to Tsybukh et al.<sup>48</sup> the surface acidity of catalysts play an important role in the ODH of ethylbenzene over Fe-Bi-Mo-O catalysts. Supported vanadium oxides are among the most important heterogeneous

catalysts for the vapor-phase oxidation of alkylaromatics, alcohols, and alkenes. In this type of catalysts the nature of metal oxide support plays an important role modulating the nature of V species and the catalytic behavior for oxidation reactions. Vanadium dispersion (related to the loading and the nature of the support) and acidity of the catalyst are the main factors to be considered. A correlation between the isoelectric point (acid-base character) of the support and the photoluminescence of V=O groups has been recently found. Acidity determination evidenced that vanadia addition could impart more number of acid sites for ceria containing catalysts while number of acid sites was reduced for praseodymia catalysts. Thus a correlation between ODH activity and acid-base properties is very difficult. The physical and chemical characteristics are reflected in the catalytic performance of catalysts.

Characterization of the prepared catalysts by various complimentary techniques such as XRD, EDX, TG/DTG/DTA, FT-IR, FT-Raman, UV-vis DRS, solid state MAS NMR and TPR are presented in chapter 4. Studies show that structure of VO<sub>x</sub> species on the supports are different and depends on the nature of the support and amount of vanadia loading. The variation of ethylbenzene dehydrogenation activity with vanadia loading in the presence of air in tables 8.1 and 8.2 reveals that the impregnated vanadia phase on the support is positively affecting the reaction. The CRS supported catalysts gives better performance for the reaction than the ceria supported catalyst with the same vanadia content, since vanadia is more homogeneously distributed over the high surface area amorphous CRS support. High conversion in activity observed for VCRS series catalysts can be attributed to the high dispersion of

vanadia on the support. In these catalysts conversion rate remains more or less constant while styrene selectivity found decreasing initially and then increases.

For VC catalysts, the activity initially increases with vanadia loading and then decreases. The maximum activity appears at a vanadia loading of 6 wt.%, corresponding to monolayer surface coverage of vanadia on the ceria support, whereas the activity of the catalysts levels off at higher loading attributed to the formation of orthovanadate crystallites. This indicates that structure and dispersion of supported phase is related to the dehydrogenation reactivity. Initially styrene selectivity decreased up to 6 wt. % loading and then increased. Juarez Lopez et al.<sup>49</sup> concluded that the presence of free vanadium and nickel oxides in the alumina supported MVSb catalysts negatively influenced the selectivity over the dehydrogenation of ethane. According to Daniell et al.<sup>50</sup> in the study of catalytic activity of  $\text{VO}_x\text{-CeO}_2$  catalysts for ODH of propane, 6 wt.%  $\text{VO}_x\text{-CeO}_2$  displayed highest activity and selectivity towards propene. It is attributed to amorphous  $\text{VO}_x$  surface species and higher loadings displayed deactivation due to  $\text{CeVO}_4$  phase formation with reduced surface area. Lopez Nieto et al.<sup>51</sup> have summarized that the coordination number, the aggregation state of vanadium oxide surface species and the presence of acid-base sites are important factors in the selectivity of ODH reactions over vanadia catalysts. It was reported for V-Sb catalysts that reoxidation is the rate-limiting step and both metals in the bulk participate in the solid reoxidation mechanism<sup>52</sup>. It is also reported in the literature that limiting step in alkane oxidation or ODH is the H-abstraction<sup>53</sup>.

In the present case, X-ray diffraction pattern of VC series of catalysts show that the formation of orthovanadate starts with 6 wt.% loading and results

in high aggregated crystallites with further increase in vanadia loading. VCRS catalysts also exhibited the similar behaviour from NMR studies. BET surface area measurements displayed a lowering in surface area with increasing vanadia loading. UV-vis spectroscopy suggests that vanadia exists as monomeric vanadium (V) species with tetrahedral coordination at lower loading and indicates progressive condensation of vanadia species with increasing vanadia loading. Spectroscopic techniques evidenced the formation of orthovanadate structure for higher vanadia loading on the ceria support. The reducibility of the ceria containing catalysts show a shift in  $T_{\max}$  to lower temperature ( $T_{\max 2}$ ) with an increase in vanadia loading from 2 to 6 wt. %. Various characterization results suggests that monomeric tetrahedral  $\text{VO}_x$  species are predominant on the  $\text{V}_2\text{O}_5/\text{CeO}_2$  catalysts at lower loading, while complete consumption of  $\text{V}_2\text{O}_5$  occurs to form  $\text{CeVO}_4$  as the loading increases to 10 wt. %  $\text{V}_2\text{O}_5$ .

The relationship observed between dehydrogenation rate and vanadia loading of VC catalysts can be explained on the basis of dispersion and aggregation of vanadia species. The activity for the catalysts with lower loading is the lowest since monomeric vanadia species predominant on this catalyst, are less active. Generally, an oxidation reaction involves the oxidation-reduction cycles of easily reducible centers.  $\text{V}_2\text{O}_5/\text{CeO}_2$  catalysts consists of two redox centers viz.  $\text{Ce}^{3+}/\text{Ce}^{4+}$  and  $\text{V}^{4+}/\text{V}^{5+}$ . The V-O-Support species appear to be more difficult to reduce than V-O-V or V=O sites in polymeric species. Thus reducibility of the catalysts increases with an increase in vanadia loading up to a limit of monolayer coverage. The activity decreases when a multilayer of polymerized  $\text{V}^{5+}$  species is formed on the support surface

at higher vanadia loading, which prevents the accessibility of the reactants to all of the active vanadium sites. Hence the maximum conversion rate is observed at intermediate surface densities corresponding to highly dispersed vanadia on the support. It was already reported that the activity for the ODH of ethane and propane over vanadia catalysts supported on MgO, Al<sub>2</sub>O<sub>3</sub>, and ZrO<sub>2</sub> depend on the structure of the VO<sub>x</sub> overlayer<sup>54</sup>. The observed selectivity also reveals that monomeric V<sup>5+</sup> species are better suited for the dehydrogenation of ethylbenzene since the maximum styrene selectivity is observed at the lower vanadia loading. Styrene selectivity decreases with increase in vanadia loading. The more reducible the catalyst, less selective the supported system. For all the supported vanadium oxide catalysts, the vanadium loading is a parameter of paramount importance in the catalytic activity of the solid. As the vanadium loading increases, aggregation occurs, thus, varying the nature of the vanadium species and their catalytic properties. For instance, for the catalytic behavior of  $\gamma$ -alumina supported vanadium oxide for the oxidative dehydrogenation of ethane and *n*-butane, it has been observed that the activity for dehydrogenation increases as the vanadium loading, while the selectivity toward alkene formation reaches a maximum at 3-4 wt %. Apparently, the highest propene yields require of a solid containing redox sites of adequate potential combined with strong Lewis acid sites and mild basic sites<sup>55</sup>. These findings seem to be in agreement with the operation of a Mars and van Krevelen mechanism, that requires the combination of these three types of sites. Vislovskiy et al. reported high activity and selectivity over various vanadia-alumina catalysts in dehydrogenation of EB to styrene with CO<sub>2</sub>. Redox behavior of V<sub>2</sub>O<sub>5</sub> played a key role in the dehydrogenation. Among several additives, antimony oxide has

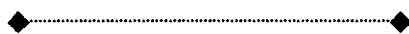
been observed to improve catalyst stability as well as catalytic activity to produce styrene. Characterization revealed that the addition of the antimony oxide led to an easier redox cycle between fully oxidized and reduced vanadium species<sup>56</sup>.

Praseodymia containing catalysts exhibited high conversion rate as well as styrene selectivity under the reaction conditions studied. According to Ruiqiang et al.<sup>57</sup> high C<sub>2</sub> selectivity and yield were observed with SrF<sub>2</sub>/Pr<sub>6</sub>O<sub>11</sub> catalysts than Pr<sub>6</sub>O<sub>11</sub> in oxidative coupling of methane at high temperature. This is correlated to the decrease in secondary deep oxidation due to reduced mobility of lattice oxygen and the surface concentration of Pr<sup>+4</sup> ion as well as the dispersion of F<sup>-</sup> on the surface of the SrF<sub>2</sub> promoted Pr<sub>6</sub>O<sub>11</sub> catalysts. Influence of lanthana, ceria, praseodymia and neodymia incorporation into molybdena-alumina systems were studied towards ODH activity by Kim et al.<sup>58</sup>. They concluded that praseodymia has the maximum effect among these lanthanide oxides. Among various rare earth orthovanadates (PrVO<sub>4</sub>, ErVO<sub>4</sub>, GdVO<sub>4</sub>, DyVO<sub>4</sub>, NdVO<sub>4</sub>, TbVO<sub>4</sub>, LuVO<sub>4</sub> and HoVO<sub>4</sub>) studied towards ODH of propane, PrVO<sub>4</sub>, ErVO<sub>4</sub>, GdVO<sub>4</sub>, DyVO<sub>4</sub>, NdVO<sub>4</sub> gave high propene selectivity. The difference in catalytic activities of the orthovanadates is related to its redox properties. Higher propene selectivity of the latter catalysts indicated easier reducibility by TPR analysis<sup>59</sup>. In VP and VPRS series catalysts, the amount of V obtained from EDX measurements show high values compared to ceria containing catalysts. BET surface area values of the former were found to be lower. Thus formation of polymeric V-O-V species is predominant with these catalysts. According to Sakurai et al.<sup>60</sup> at low loadings, only isolated VO<sub>4</sub> species were dispersed over the MgO support, whereas for higher loading,

polymeric species with bridging V-O-V oxide ions forming  $\text{MgV}_2\text{O}_6$  and  $\text{MgV}_2\text{O}_7$  are formed. The degree of polymerization of vanadate species increases with loading over praseodymia catalysts, which results in high styrene selectivity. The praseodymia catalysts produced styrene selectively than ceria containing ones. However, among catalysts, CRS supported vanadia exhibits comparatively higher activity than PRS supported vanadia catalysts. Solid state MAS NMR studies reveal that, only  $\text{CeVO}_4$  formation is favourable with CRS support while compounds of  $\text{SiO}_2$  and  $\text{Pr}_x\text{O}_y$  is formed over PRS support. Thus  $\text{Pr}_x\text{V}_2\text{O}_5$  can easily replace Si in place of Pr. Such species result in non reducible phases which in turn decrease the dehydrogenation activity<sup>61</sup>.

## 8.6 CONCLUSION

The catalytic behaviour of rare earth oxides supported vanadia catalysts in the oxidative dehydrogenation ethylbenzene has been studied with air as the oxidant. Styrene was produced as the main product and styrene selectivity of all the supported catalysts found to be above 75%, but the activity of the catalysts differs from one another. The adsorption of styrene in the ODH of ethylbenzene inhibits the oxygen chemisorption at surface Lewis active sites, thus total oxidation of hydrocarbon molecule is controlled and the selectivity to total oxidation products decreases. The ethylbenzene dehydrogenation activity depends on the vanadia loading, nature of vanadia over the supports etc. The different catalytic activities of the rare earth supported catalysts can be related to their redox properties as well as to the surface properties of the catalysts. Presence of easily reducible polymeric vanadia species in praseodymia catalysts results in higher styrene selectivity than ceria supported catalysts.





## REFERENCES

- [1] X. Ye, W. Hua, Y. Yue, W. Dai, C. Miao, Z. Xie, Z. Gao, *New. J. Chem.* 28 (2004) 373.
- [2] N.R. Shiju, M. Anilkumar, S.P. Mirajkar, C.S. Gopinath, B.S. Rao, C.V. Satyanarayana, *J. Catal.* 230 (2005) 493.
- [3] W.W. Kaeding, *Catal. Rev.* 8 (1973) 307.
- [4] E.H. Lee, *Catal. Rev.* 8 (1973) 285.
- [5] G. Emig, H. Hofmann, *J. Catal.* 84 (1983) 15.
- [6] E. Vriel, P.G. Menon, *Appl. Catal.* 77 (1999) 1.
- [7] T. Tagawa, T. Hattori, Y. Murakami, K. Iwayama, Y. Ishida, H. Uchida, *J. Catal.* 75 (1982) 56.
- [8] W. Kania, K. Jurczyk, *Appl. Catal.* 61 (1990) 35.
- [9] T.M. Jyothi, K. Sreekumar, M.B. Talwar, A.A. Behelkar, B.S. Rao, S. Sugunan, *Bull. Chem. Soc. Jpn.* 73 (2000) 1.
- [10] N. Keller, N.I. Maksimova, V.V. Roddatis, M. Schur, G. Mestl, Y.V. Butenko, V.L. Kuznetsov, R. Schlogl, *Angew. Chem. Int. Ed.* 41 11 (2002) 1811.
- [11] T.G. Alkhazhov, A.F. Lisovskoi, *Oxidative Dehydrogenation of Hydrocarbons*, (in Russian) Khimia, Moscow (1980).
- [12] F. Cavani, F. Trifiro, *Appl. Catal. A.* 88 (1992) 115.
- [13] J. Hanuza, B.J. Trzeblatowska, W. Oganowski, *J. Mol. Catal.* 29 (1985) 109.
- [14] S.T. Oyama, G.A. Somorjai, *J. Phys. Chem.* 94 (1990) 5022.
- [15] L. Owens, H.H. Kung, *J. Catal.* 144 (1993) 202.
- [16] J.L. Bars, J.C. Vedrine, A. Auroux, S. Trautmann, M. Baerns, *Appl. Catal. A.* 88 (1992) 179.
- [17] M.A. Chaar, D. Patel, M.C. Kung, H.H. Kung, *J. Catal.* 105 (1987) 483.
- [18] C.S. Chen, H.W. Chen, *Appl. Catal. A: Gen.* 260 (2003) 207.
- [19] H. K. Kung, *Adv. Catal.* 40 1 (1994).
- [20] D. Patel, P.J. Anderson, H.H. Kung, *J. Catal.* 125 (1990) 132.
- [21] C. Resini, F. Milella, G. Busca, *Phys. Chem. Chem. Phys.* 2 (2000) 2039.
- [22] S. Albonetti, F. Cavani, F. Trifiro, *Catal. Rev. Sci. Eng.* 38 (1996) 413.

- [23] J.M.L. Nieto, A. Dejoz, M.I. Vazquez, W. O'Leary, J. Cunningham, *Catal. Today* 40 (1998) 215.
- [24] B. Zhaorigeta, Q. Ge, W. Li, M. Jia, C. Yu, H. Xu, C.X. Chin, *J. Catal.* 21 (2000) 332.
- [25] I.Y. Petrov, O.V. Zolotaryov, B.G. Tryasunov, *Catalysis and Adsorption in Fuels Processing and Environmental Protection*, Wroclaw (1999) 219.
- [26] D.S. Su, N. Maksimova, N. Keller, G. Mestl, M.J. Ledoux, R. Schlogl, *Catal. Today* (2005) 102.
- [27] N. Ikenaga, T. Tsuruda, K. Senma, T. Yamaguchi, Y. Sakurai, T. Suzuki, *Ind. Eng. Chem. Res.* 39 (2000) 1228.
- [28] P. Moriceau, B. Grzybowska, Y. Barbaux, G. Wrobel, G. Hecquet, *Appl. Catal. A: Gen.* 168 (1998) 269.
- [29] J. Keranen, A. Auroux, S. Ek, L. Niinisto, *Appl. Catal. A: Gen.* 228 (2002) 213.
- [30] W.S. Chang, Y.Z. Chen, B.L. Yang, *Appl. Catal. A: Gen.* 124 (1995) 221.
- [31] F. Trifiro, I. Pasaquon, *J. Catal.* 12 (1968) 412.
- [32] R. Neumann, M.L. Elad, *Appl. Catal. A: Gen.* 122 (1995) 85.
- [33] W.M.H. Sachtler, N.H. de Boer, *Proc. 3<sup>rd</sup> Int. Con. on Catal.* Amsterdam, Wiley, New York (1965) 240.
- [34] S. Vetrivel, A. Pandurangan, *Appl. Catal.* 264 (2004) 243.
- [35] C. Doornkamp, M. Clement, X. Gao, G. Deo, I.E. Wachs, V. Ponc, *J. Catal.* 185 (1999) 415.
- [36] H.H. Kung, M.C. Kung, *Appl. Catal. A: Gen.* 157 (1997) 105.
- [37] R. Raja, P. Ratnaswamy, *Appl. Catal.* 143 (1996) 145.
- [38] M. Ai, 7<sup>th</sup> Sanka-Banno, *Oxidation Meeting*, Noyaga (1973) 98.
- [39] Y. Sakurai, T. Suzaki, N. Ikenaga, T. Suzuki, *Appl. Catal. A: Gen.* 192 (2000) 281.
- [40] F. Matsuda, K. Inoue, K. Kato, *Jap. Pat.* H06-116187 (1994).
- [41] R. Yu, F. Xiao, D. Wang, T. Sun, Y. Liu, G. Pang, S. Feng, S. Qui, R. Xu, C. Fang, *Catal. Today* 51 (1999) 39.
- [42] G. Centi, S. Perathoner, *Catal. Today* 41 (1998) 457.
- [43] I. Rossetti, E. Bencini, L. Trentini, L. Forni, *Appl. Catal. A: Gen.* 292 (2005) 118.

- [44] P. Mars, D.W. Van Krevelan, *Chem. Eng. Sci.* 3 (1954) 41.
- [45] R. Long, H. Wan, *J. Catal.* 172 (1997) 471.
- [46] G.K. Boreskov, *Kinet. Catal.* 115 1 (1977) 5.
- [47] A. Corma, H. Garcy, *Chem. Rev.* 102 (2002) 3837.
- [48] V.M. Zhynevskiy, R.D. Tsybukh, V.V. Gumenetskiy, V.V. Kochubeiy, *Appl. Catal. A: Gen.* 238 (2003) 19.
- [49] R.J. Lopez, N.S. Godjayeva, V.C. Corberan, J.L.G. Fierro, E.A. Mamedov, *Appl. Catal. A: Gen.* 124 (1995) 281.
- [50] W. Daniell, F. Anderle, A. Ponchel, S. Kuba, D.H. Gregory, H. Knozinger, *Top. Catal.* 8 (1999) 45.
- [51] T. Blasco, J.M. Lopez Nieto, *Appl. Catal. A: Gen.* 127 (1997) 117.
- [52] S. Larrondo, G. Alvaro, B. Irigoyen, N. Amadeo, *Catal. Today* 107 (2005) 444.
- [53] G. Centi, *Catal. Today* 16 (1993) 5.
- [54] C. Pak, A.T. Bell, T. Don Tilley, *J. Catal.* 206 (2002) 49.
- [55] A. Pantazidis, A. Auroux, J.M. Herrmann, C. Mirodatos, *Catal. Today* 32 (1996) 81.
- [56] V.P. Vislovskiy, J.S. Chang, M.S. Park, S.E. Park, *Catal. Commun.* 3 (2002) 227.
- [57] V.D. Sokolovskii, *Catal. Rev. Sci. Eng.* 32 (1990) 1.
- [58] J.J. Kim, S.W. Weller, *Appl. Catal.* 33 (1987) 15.
- [59] C.T. Au, W.D. Zhang, *J. Chem. Soc., Faraday Trans.* 93 (6) (1997) 1195.
- [60] Y. Sakurai, T. Suzuki, K. Nakagawa, N. Ikenaga, H. Aota, T. Suzuki, *J. Catal.* 209 (2002) 16.

## CHAPTER 9

### SUMMARY AND CONCLUSION

#### **Abstract**

---

---

*Heterogeneous catalysis is one of the most important processes in the petroleum and the chemical industries. Today, almost 70% of all chemicals that are produced have been in contact with a catalyst somewhere in their synthesis process. This number stresses the importance of the role of catalysis in the chemical industry. Without a catalyst, processes are less clean and sometimes impossible to perform. To be able to screen catalysts at high throughput will dramatically improve performance and reduce costs. With this background the main building blocks of the present venture includes preparation, characterization and catalytic activity of supported vanadia catalysts. Rare earth oxides ceria and praseodymia were used as the support material. Silica synthesized from rice husk has been used as a promoter for the support materials in order to enhance the surface and catalytic properties. Catalysts were successfully utilized in industrially important oxidation of aromatics after a detailed investigation of physico-chemical characteristics by various instrumental techniques.*

---

---

## 9.1 SUMMARY

Selective oxidation is a very important industrial process that is used to manufacture a variety of chemicals. Vanadium pentoxide catalysts are widely used as the selective catalysts for the oxidation of aromatic hydrocarbons. Various promoters are frequently added to vanadium pentoxide to improve the selectivity and activity to produce the desired products. In search of active catalysts one starts with simple oxides and looks for possible in terms of composition and sample preparation methods. The utilization of silica from an agrowaste rice husk in catalysis is very promising in the era of green chemical world. The development for ecologically friendly technologies is certainly one of the major present goals of research in chemistry. This is especially true in the field of oxidation of organic compounds where there is an urgent need to replace highly effective but wasteful and toxic stoichiometric oxidants with a more preferred technology based on catalytic oxygen transfer using 'clean' oxygen donors such as hydrogen peroxide.

Chapter 1 dealt with a brief literature review on catalysis by supported vanadia oxides and rare earth oxides. The role played by vanadia catalyst in chemical transformation processes is described. The attempts for the production of silica from an agrowaste rice husk and its current application are also discussed in detail.

In chapter 2 the importance of heterogeneous catalytic oxidation together with various mechanisms are discussed. It also envisages the redox behaviour of ceria and praseodymia due to its lattice defect structure and the importance of redox catalysis played by vanadia.

Chapter 3 focused on the building block chemicals of present thesis work and the various instrumental techniques adopted for the characterization of all the catalysts prepared. The preparation methods of catalysts are discussed in detail. The experimental procedures used for the oxidation activity of aromatics along with gas chromatograph analysis conditions are also presented in the same chapter.

Chapter 4 described in detail the results of various characterization methods applied for the surface as well as bulk characterization of supports and supported vanadia catalysts. Surface characterization was done by BET surface area and pore volume analysis, crystal nature by X-ray diffraction and chemical composition from energy dispersive X-ray analysis. Thermal analysis, TGA/DTA was confirmed the thermal stability. Surface morphology was collected on scanning electron microscope. Information regarding the coordination and oxidation state of the vanadia and rare earth metal ions is obtained from UV-vis DRS. Various spectroscopic technique have been applied to discriminate between the surface and bulk structures on the supported oxides. Vibrational absorption by FT-IR helped to confirm the structure assignments together with FT-Raman spectroscopy which was used to identify changes in the structure of dispersed  $V_2O_5$  in dependence on its loading and the nature of the support. EPR measurements investigated the influence of vanadia loading on the coordination geometry of vanadium oxide structures and the electron delocalization of rare earth oxides supported vanadia catalysts under room and liquid nitrogen temperatures. Solid-state nuclear magnetic resonance methods ( $^{29}\text{Si}$  and  $^{51}\text{V}$  MAS NMR) illustrated the difference in local environment of a nucleus under study and suited for the

structural analysis of various Si-O-Si units and surface vanadium oxide phases mainly the existence of  $\text{CeVO}_4$  respectively. Redox behaviour of the catalysts was examined by TPR using hydrogen. TPD of ammonia together with cyclohexanol decomposition gave surface acidic properties.

Chapter 5 dealt with the activity of the catalysts tested towards liquid-phase benzene oxidation reaction. The oxidation was conducted under a condition after checking the influence of various reaction parameters such as temperature, catalyst weight, solvent and volumes of substrate, solvent and oxidant in order to get product selectively with high yield. The activity and selectivity of the supported catalysts was correlated to the difference in structural species as observed by characterization techniques.

In chapter 6 the activity of the catalysts tested towards liquid-phase ethylbenzene oxidation reaction is presented. Reaction was conducted in a selected condition after verifying the influence of reaction parameters in detail. The product formation and selectivity could correlate with the difference in structural properties associated with vanadia catalysts supported on various support materials.

Chapter 7 describes the oxidation activity of catalysts for naphthalene as substrate in liquid phase. Influence of reaction parameters like temperature, solvent, catalyst weight and volume of acetonitrile,  $\text{H}_2\text{O}_2$  and naphthalene were also tested. Catalytic activity was correlated with the structural environment of by various species obtained by characterization techniques.

In chapter 8 the activity of the catalysts in oxidative dehydrogenation of ethylbenzene done was explained. Catalytic activity and selectivity of all the

catalysts were conducted at selected conditions after optimization of reaction conditions in order to get products selectively with high conversion rate.

Chapter 9 illustrates the summary, conclusion and future outlook of the present thesis work.

## **9.2 CONCLUSION**

The major conclusions that can be drawn from the present thesis work are the following;

High surface area amorphous silica with high purity could be prepared from rice husk by an acid leaching process. Application of this silica as promoter of rare earth oxides ceria and praseodymia improved the surface area and dispersion properties.

Supported vanadia prepared with various wt. % of  $V_2O_5$  (2-10) on silica promoted rare earth oxides and rare earth oxides.

Structural and physico-chemical characterization of catalysts were carried out with different techniques like XRD, EDAX, BET SA, TGA/DTG/DTA, SEM as well as spectroscopic techniques such as UV-vis DRS, FT-IR, FT-Raman, EPR,  $^{29}\text{Si}$  and  $^{51}\text{V}$  MAS NMR. Acidity obtained by TPD- $\text{NH}_3$  and vapour phase cyclohexanol decomposition and redox behaviour by TPR- $\text{H}_2$ .

Catalytic activity of catalysts was tested towards oxidation of aromatics such as benzene, ethylbenzene and naphthalene in liquid phase with  $\text{H}_2\text{O}_2$  as oxidant and  $\text{CH}_3\text{CN}$  as solvent. Oxidative dehydrogenation of ethylbenzene tested in vapour phase with air as the oxidant.



Silica promoted rare earth oxides and vanadia on those supports exhibited relatively high surface area. Chemical composition gave an idea about the atom % of V loaded. XRD pattern results cubic form of ceria and praseodymia.

For low vanadia loading, highly dispersed vanadia species on the support surface obtained. As vanadia loading exceeds monolayer coverage, formation of orthovanadate type structure evidenced for ceria support alone while this phase is highly dispersed over the silica promoted supports owing to its higher surface area and peaks obtained only after high temperature treatment.

In praseodymia containing catalysts, higher loading introduced the formation of pyrovanadate type structure.

Coordinatively unsaturated V-oxides sites and oxygen vacancies are the locations for oxidation of aromatics. High oxidation activity of ceria containing catalysts can be related to the high reducibility and structure of vanadia on the support. Higher dispersion provides the necessary isolation of active sites, which is one fundamental factor in selective oxidation.

Lower oxidative dehydrogenation activity of ceria systems is caused by the progressive formation of ceriumorthovanadate.

The activity behaviour of praseodymia containing catalysts in oxidation reactions is found very different from that of ceria supported vanadia.

Rice husk can pose as a potential alternative for supported catalysts systems since it has high silica content and replace the conventional silica due to its enhanced properties like small particle size and high specific surface area.

## **FUTURE OUTLOOK**

Structural properties and catalytic activity studies of rare earth oxides need more insight. Other transition metal oxides supported rare earth oxides can be studied in the same way. Application of rice husk silica to other metal oxides as a promoter is an interesting and promising approach since it can impart an amorphous nature and high surface area. Since the activity of few oxidations of aromatics were only estimated, further research is needed to obtain the more accurate catalytic route into the mechanism of reaction over the studies on supported vanadia catalysts. The study can be extended to other metal oxides especially to redox centre oxides.

